Bioactive trace metals and their isotopes as paleoproductivity proxies: An assessment using GEOTRACES-era data

T.J. Horner[1,2,*], S.H. Little[3,*], T.M. Conway[4,*], J.R. Farmer[5,6,*], J.E. Hertzberg[7,†], D.J. Janssen[8], A.J.M. Lough[9,‡], J. McKay[10], A. Tessin[11], S.J.G. Galer[6], S.L. Jaccard[8,§], F. Lacan[12], A. Paytan[13], K. Wuttig[14, ‖], and GEOTRACES–PAGES Biological Productivity Working Group Members[15].

[1]NIRVANA Labs, [2]Department of Marine Chemistry & Geochemistry, Woods Hole Oceanographic Institution, Woods Hole, MA, USA; [3]Department of Earth Sciences, University College London, London, GBR; [4]College of Marine Science, University of South Florida, FL, USA; [5]Department of Geosciences, Princeton University, Princeton, NJ, USA; [6]Max-Planck Institute for Chemistry, Mainz, DEU; [7]Department of Ocean, Earth & Atmospheric Sciences, Old Dominion University, Norfolk, VA, USA; [8]Institute of Geological Sciences and Oeschger Center for Climate Change Research, University of Bern, Bern, CHE; [9]University of Southampton, National Oceanography Centre, Southampton, GBR; [10]College of Earth, Ocean, and Atmospheric Sciences, Oregon State University, Corvallis, OR, USA; [11]Department of Geology, Kent State University, Kent, OH, USA; [12]LEGOS, University of Toulouse, CNRS, CNES, IRD, UPS, Toulouse, FRA; [13]Institute of Marine Sciences, University of California Santa Cruz, Santa Cruz, CA, USA; [14]Antarctic Climate and Ecosystems Cooperative Research Centre, University of Tasmania, Hobart, AUS; [15]A full list of working group members and their affiliations appears at the end of the manuscript.

*To whom correspondence should be addressed: T.J.H. (Tristan.Horner@whoi.edu), S.H.L. (susan.little@ucl.ac.uk), T.M.C. (tmconway@usf.edu), or J.R.F. (jesse.farmer@princeton.edu).

[†]Now at: International Ocean Discovery Program, Texas A&M University, College Station, TX, USA; [‡]Now at: School of Geography, University of Leeds, Leeds, GBR; [§]Now at: Institute of Earth Sciences, Université de Lausanne, Lausanne, CHE; [‖]Now at: Federal Maritime and Hydrographic Agency (BSH), Hamburg, DEU.

Key Points

- Distributions, drivers, and depositional archives described for iron, zinc, copper, cadmium, molybdenum, barium, nickel, chromium, & silver
- Cadmium, barium, nickel, and chromium isotopes offer the most promise as paleoproductivity tracers, but key uncertainties remain
- Future priorities include quantification of ‘missing’ flux terms, constraining circulation influences, and identifying sedimentary archives

Keywords: biological pump; marine chemistry; biogeochemical cycles; micronutrients; phytoplankton; paleoceanography

This article has been accepted for publication and undergone full peer review but has not been through the copyediting, typesetting, pagination and proofreading process, which may lead to differences between this version and the Version of Record. Please cite this article as doi: 10.1029/2020GB006814.

Abstract

Phytoplankton productivity and export sequester climatically significant quantities of atmospheric carbon dioxide as particulate organic carbon through a suite of processes termed the biological pump. How the biological pump operated in the past is therefore important for understanding past atmospheric carbon dioxide concentrations and Earth's climate history. However, reconstructing the history of the biological pump requires proxies. Due to their intimate association with biological processes, several bioactive trace metals and their isotopes are potential proxies for past phytoplankton productivity, including: iron, zinc, copper, cadmium, molybdenum, barium, nickel, chromium, and silver. Here we review the oceanic distributions, driving processes, and depositional archives for these nine metals and their isotopes based on GEOTRACES-era datasets. We offer an assessment of the overall maturity of each isotope system to serve as a proxy for diagnosing aspects of past ocean productivity and identify priorities for future research. This assessment reveals that cadmium, barium, nickel, and chromium isotopes offer the most promise as tracers of paleoproductivity, whereas iron, zinc, copper, and molybdenum do not. Too little is known about silver to make a confident determination. Intriguingly, the elements that are least sensitive to productivity may be used to trace other aspects of ocean chemistry, such as nutrient sources, particle scavenging, organic complexation, and ocean redox state. These complementary sensitivities suggest new opportunities for combining perspectives from multiple proxies that will ultimately enable painting a more complete picture of marine paleoproductivity, biogeochemical cycles, and Earth's climate history.

1. Introduction

The ocean plays host to three carbon ‘pumps’ that redistribute climatically significant quantities of carbon dioxide (CO_2) from the atmosphere to the ocean interior and seafloor (Volk & Hoffert, 1985). These ocean carbon pumps—biological, carbonate, and solubility—influence Earth’s climate over timescales ranging from decades to millions of years (e.g., Volk & Hoffert, 1985; Sigman et al., 2010; Khatiwala et al., 2019). The biological pump refers specifically to the production of particulate organic carbon (POC) within the sunlit surface ocean (euphotic zone) and export of POC to the intermediate and deep ocean, where POC is largely (but not wholly) regenerated. The biological pump is of particular interest as it connects the cycles of C to those of dissolved O_2, nutrients, and marine biology, and today accounts for as much as 70 % of the carbon concentration gradient between the euphotic zone and the deep ocean (Sarmiento & Gruber, 2006).

The biological pump acts to redistribute CO_2 from the atmospheric/surface ocean carbon reservoir to the deep ocean and sediment carbon reservoirs via two steps. First, phytoplankton, photoautotrophic microbes, use sunlight (represented here by *hv*) to transform ambient DIC (dissolved inorganic carbon) into POC (particulate organic carbon), represented here by CO_2 and a simple sugar (CH_2O), respectively, by the simplified reaction:

$$\mathbf{CO_2 + H_2O + \mathit{hv} \rightarrow CH_2O + O_2} \qquad \textbf{[1]}$$

The second step requires that some fraction of the newly formed POC sinks into the ocean interior through a combination of biological and physical aggregation processes (e.g., Alldredge & Silver 1988), where ultimately some POC may be buried in marine sediments. The resulting surface ocean DIC deficit promotes dissolution of atmospheric CO_2 into seawater to maintain air–sea CO_2 equilibrium, driving an overall reduction in the partial pressure of atmospheric CO_2 (pCO_2). Note that this definition of the biological pump neglects dissolved organic carbon export, which is comparatively understudied, though may account for as much as one-third of C export (e.g., Carlson et al., 2010; Giering et al., 2014). Importantly, Reaction [1] requires sunlight and can only occur in the euphotic zone of the ocean. In contrast, aerobic heterotrophic respiration can occur wherever POC and O_2 are present:

$$\mathbf{CH_2O + O_2 \rightarrow CO_2 + H_2O} \qquad \textbf{[2]}$$

(There are also a number of O_2-independent respiration pathways that are reviewed in detail elsewhere; e.g., Froelich et al., 1979.)

While the representation of all POC as a simple sugar (CH_2O) is instructive for illustrating an important biotic transformation in the ocean, it is also simplistic; microbial biomass consists of dozens of bioactive elements that serve many essential functions (e.g., da Silva & Williams, 1991). The elemental stoichiometry of POC can thus be expanded to include a number of major and micronutrient elements, as illustrated by the extended Redfield ratio reported by Ho et al. (2003):

$$\mathbf{C_{124,000}N_{16,000}P_{1,000}S_{1,300}K_{1,700}Mg_{560}Ca_{500}Sr_{5.0}Fe_{7.5}Zn_{0.8}Cu_{0.38}Co_{0.19}Cd_{0.21}Mo_{0.03}} \quad \mathbf{[3]}$$

With this extended stoichiometry in mind, it is clear that Reactions [1] and [2]—the production and regeneration of organic matter, respectively—will not only generate gradients in the dissolved concentration of DIC and O_2, but also for many other bioactive elements associated with POC cycling. These gradients will be steepest for those elements possessing shorter residence times and where biological uptake and regeneration are the most important processes driving their vertical distributions. Likewise, such gradients may be almost absent for elements that possess long residence times or are primarily cycled by processes other than productivity.

For those bioactive metals where biological processes are important, the implication of Reactions [1] and [2] is that many of the elements listed in [3] may, in turn, be used as proxies of POC cycling and, potentially, paleoproductivity. Indeed, aspects of past ocean productivity that impact carbon and nutrient cycling are routinely reconstructed using the stable isotope compositions of carbon and macronutrient elements (N and Si; see Farmer et al., *this issue*). It thus follows that the abundance and isotopic compositions of bioactive trace metals cycled along with POC could also provide valuable information on past ocean productivity. However, in order to use systems of trace elements and their isotopes as proxies for productivity, it is necessary to develop a comprehensive understanding of the marine behavior of these elements, including: mapping their distribution in the ocean; elucidating the drivers of the distribution; characterizing sources, sinks, and transformations associated with biological, physical and chemical (notably redox) reactions; and, recognizing if (and how) a given element is incorporated and preserved in marine sediments.

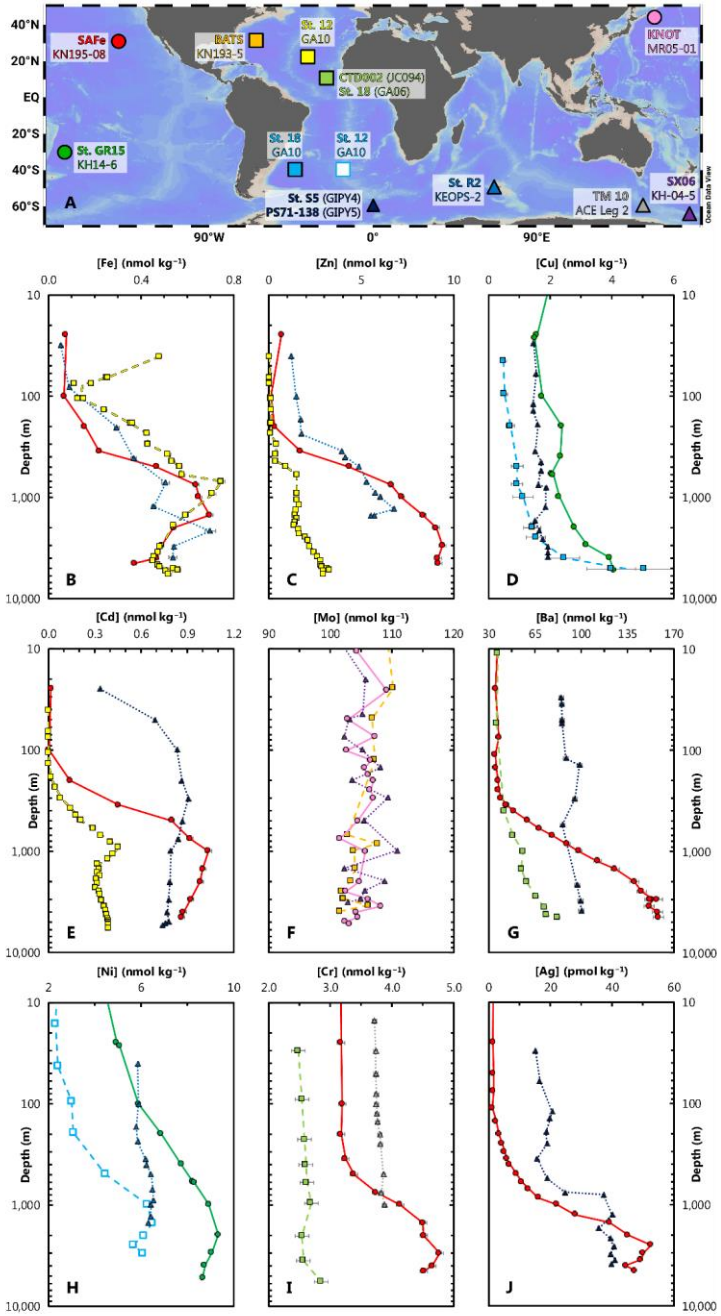

Figure 1 | Overview of bioactive dissolved trace metal concentration distributions discussed in this review. A Map showing locations of the representative depth profiles shown in both the lower panels and discussed throughout this review (Sec. 3–11). The specific station (bold) and cruise identifier are given for each location; circles, squares, and triangles denote stations in the Pacific, Atlantic, and Southern Oceans, respectively. The lack of exemplar stations from the Indian Ocean reflects the current paucity of GEOTRACES-compliant campaigns in this basin. Two stations sampled from the Atlantic Sector of the Southern Ocean share the same symbol (St. S5 of GIPY4 at 57.55 S, 0.04 W; PS71-138 of GIPY5 at 61.00 S on the Zero Meridian), as do two stations from the Eastern Tropical North Atlantic (St. 18 of GA06 at 12.03 N, 28.98 W and CTD002 of JC09 at 9.28 N, 21.63 W). **B–J** Depth profiles of bioactive trace metal concentrations for Fe (B), Zn (C), Cu (D), Cd (E), Mo (F), Ba (G), Ni (H), Cr (I), and Ag (J). Profiles are shown in semi-log space to illustrate variations in the epi- and mesopelagic realm. Originators are cited in the Data Sources section. Map created using Ocean Data View (Schlitzer, R., https://odv.awi.de, 2018).

The wealth of new TEI (trace element and isotope) data from the GEOTRACES program (e.g., Fig. 1) now permits an assessment of whether certain bioactive TEI metals are promising proxies for past ocean productivity. This contribution represents such an assessment. Our study synthesizes what is known about the processes governing the cycling of nine bioactive metal in seawater, explores the level of development and readiness of each isotope system to inform on aspects of past ocean productivity, and identifies areas where further research is most needed to improve our understanding of the geochemistry of trace metals in the past and present ocean. We base our assessment on publicly available results from the international GEOTRACES programme (e.g., Mawji et al. 2015; Schlitzer et al., 2018). Our study is not intended to be a thorough review of all available techniques used to reconstruct paleoproductivity. Instead, we focus on bioactive metal isotope systems that are either recognized as micronutrients (such as those in Eq. [3]) or exhibit nutrient-like dissolved profiles in seawater, regardless of their nutritional status to phytoplankton (e.g., Ba, Cr, Ag). This will not be the last word on the topic; our understanding of many of these metal isotope systems has rapidly evolved in recent years, and will continue to evolve as new data are generated.

2. Key concepts

In this section we introduce several key concepts to which we refer throughout the review. First, we provide definitions for reporting bioactive metal concentrations and isotope variations, and for the concept of paleoproductivity (Sec. 2.1.). Second, we describe an idealized framework for reconstructing paleoproductivity based on the coupled cycling of bioactive trace metals and their isotopes (Sec. 2.2.). Finally, we introduce a number of additional trace metal cycling processes that are important considerations in the application of bioactive trace metal isotope systems to reconstruct paleoproductivity (Sec. 2.3.). The review of each metal system follows.

The review sections are structured such that each bioactive metal isotope system is described similarly and systematically. The order in which metals are reviewed follows the extended Redfield ratio—Fe (Sec. 3.), Zn (Sec. 4.), Cu (Sec. 5.), Cd (Sec. 6.), and Mo (Sec. 7.)—before describing the nonessential elements Ba (Sec. 8.), Ni (Sec. 9.), Cr (Sec. 10.) and Ag (Sec. 11.) in order of decreasing dissolved concentration in seawater. The review of each metal isotope system is organized around four questions:

1. What is the modern marine distribution of this trace metal isotope system?
2. Which biological, chemical, and physical processes are most important for maintaining this distribution?
3. In what form is this trace metal isotope system incorporated into sediments?
4. What are the priorities for improving the utility of this trace metal isotope system to track paleoproductivity?

This structure results in some repetition of the main distributions, drivers, and sedimentary archives between individual isotope systems. This redundancy is deliberate: each section can be read independently without reference to the other bioactive trace metals. We close our review by assessing the 'maturity' of each system based on a comparison to more established productivity proxies, offer suggestions for future studies, and discuss prospects for paleoproductivity reconstructions using bioactive trace metal isotope systems.

2.1. Definitions

2.1.1. Data reporting conventions

The isotope literature abounds with isotope notations (e.g., ε, δ), reference materials (e.g., IRMM, JMC, NIST), and isotope ratio pairs (e.g., ^{57}Fe/^{54}Fe versus ^{56}Fe/^{54}Fe; ^{137}Ba/^{134}Ba versus ^{138}Ba/^{134}Ba). There are merits to each of these choices and we do not intend to review these here. However, we believe that the sheer number of ways in which trace metal isotope data have been reported can be confusing to scientists in other disciplines and this ultimately diminishes the reach and utility of isotope-based research. To avoid furthering this confusion, we have adopted a number of conventions that apply throughout this review, regardless of how literature data were originally reported. First, we use a single isotope notation throughout (‘δ’; i.e., the delta notation). Second, we express all data relative to the most widely accepted standard for each isotope system. For many isotope systems, the most widely accepted standard may have since been exhausted (e.g., JMC-Lyon for Zn). In those cases, there are usually cross-calibrated secondary materials that can be used to report new isotope data in terms of ‘legacy’ materials (e.g., AA-ETH for Zn, Archer et al., 2017). Third, we report trace metal isotope data using the same isotope ratio pairs and reference materials as used in the GEOTRACES data products (e.g., Mawji et al., 2015; Schlitzer et al., 2018). We note that isotope data are a unitless ratio quantity (Coplen, 2011), though are commonly reported with ‘units’ of ‰ (i.e., parts per one thousand):

$$\boldsymbol{\delta^{i}\mathrm{Me} = R_{sample} / R_{standard} - 1} \qquad \textbf{[4]}$$

where δ^{i}Me and R are listed for each element in Table 1. For clarity, all isotopic data reviewed here have been calculated using notation in Eq. 4, and renormalized to the standards listed in Table 1, regardless of how the data originators reported their results.

We denote the concentrations of different species using square brackets (i.e., [ ]). Unless specifically stated, all concentrations refer to dissolved species; for example, [Fe] denotes dissolved Fe concentrations, and [Me] denotes the concentration of a metal (‘Me’) in a general case. Salient features of each trace metal isotope system are summarized in Table 1.

Table 1 | Summary of oceanic dissolved concentrations, isotope notation, standards, and isotopic compositions, and mean ocean residence times for trace metals discussed in this review. Superscripts denote references listed in the Data Sources section.

Element	Dissolved concentration range (nmol kg^{-1})	δ^iMe and R	Standard used for δ^iMe	Mean Upper Continental Crust δ^iMe (‰)	Mean deep ocean δ^iMe (‰)	Range of deep ocean δ^iMe (‰)	Residence time estimates (kyr)
Fe	0.01–100^{a}	δ^{56}Fe, ^{56}Fe/^{54}Fe	IRMM-014^{e}	+0.1^{m}	Variable^{t}	−2.4 to +1.5^{t}	0.004–0.6^{aa}
Zn	0.01–10^{a}	δ^{66}Zn, ^{66}Zn/^{64}Zn	JMC-Lyon^{f}	+0.3^{f}	≈+0.5^{u}	-0.2 to +0.6^{u}	1–11^{aa}
Cu	0.5–4^{a}	δ^{65}Cu ^{65}Cu/^{63}Cu	NIST SRM 976^{f}	+0.1^{f}	≈+0.7^{v}	+0.6 to +0.8^{v}	2–5^{aa}
Cd	0.00003–1.2^{a}	δ^{114}Cd ^{114}Cd/^{110}Cd	NIST SRM 3108^{g}	0.0^{n}	≈+0.3^{w}	+0.2 to +0.4^{w}	22–105^{aa}
Mo	100^{b}	δ^{98}Mo ^{98}Mo/^{95}Mo	NIST SRM 3134 + 0.25‰^{h}	≤0.4^{o}	≈+2.3^{x}	Homogeneous^{x}	440^{ab}
Ba	35–160^{a}	δ^{138}Ba ^{138}Ba/^{134}Ba	NIST SRM 3104a^{i}	0.0^{p}	≈+0.3^{y}	+0.2 to +0.4^{y}	8^{ac}
Ni	1.5-11^{a}	δ^{60}Ni ^{60}Ni/^{58}Ni	NIST SRM 986^{j}	+0.1^{q}	≈+1.3^{z}	+1.2 to +1.5^{z}	10–30^{ad}
Cr	1-7 ^{c}	δ^{53}Cr ^{53}Cr/^{52}Cr	NIST SRM 979^{k}	-0.12^{r}	≈+0.8^{c}	0.6-1.2^{c}	6^{ae}
Ag	0.0002–0.1^{d}	δ^{109}Ag ^{109}Ag/^{107}Ag	NIST SRM 978a^{l}	0.0^{s}	Unknown	Unknown	0.4^{af}

2.1.2. Paleoproductivity

We define paleoproductivity as the productivity of an ecosystem that contributes to the sequestration of atmospheric CO$_2$ as POC in the ocean interior and on the seafloor. Our definition of paleoproductivity is therefore analogous to that of NEP (net ecosystem productivity), which is defined as gross primary production minus autotrophic and heterotrophic respiration and where gross primary production is the total autotrophic production of POC (or O_2; Eq. 1; Sigman & Hain, 2012). If considering only the euphotic zone, NEP is equivalent to export production, which is an important component of the biological carbon pump (Boyd et al., 2019); indeed, changes in export production have been implicated as a major driver of variations in glacial–interglacial $p\mathrm{CO}_2$ and hence climate (e.g., Broecker, 1982; Boyle, 1988a; Berger et al., 1989; Paytan, 2009). Many of these changes in past export production were inferred on the basis of variations in the cycling of major nutrients and their isotopes (e.g., N, Si; Farmer et al., *this volume*). The net consumption of nutrients can be interpreted in terms of export production by assuming a fixed proportionality between the major nutrients and C. This proportionality therefore allows the connection of major nutrient cycles to the sequestration of atmospheric CO_2 via biological productivity. In the next section, we outline how such a framework can be similarly applied to interpret the distributions of bioactive metals and their isotopes in terms of export productivity.

2.2. From nutrients to productivity

The cycling of nutrients is intimately connected with productivity; along with sunlight, nutrients are the fuel that powers the biological pump. In turn, the biological pump renders systematic changes in the concentration and isotopic composition of nutrients throughout the oceans. Assuming that these changes follow certain known rules, we can use bioactive metals and their isotopes as tracers of biological productivity in Earth's past. In this section we describe how nutrient uptake can generate isotope variations in seawater and develop a framework for linking nutrients with productivity that applies to several of the isotope systems reviewed here.

2.2.1. The isotope reactor model

Here we use an example whereby an hypothetical micronutrient metal ('Me') is supplied to, and consumed within, an isotope reactor (Fig. 2). Though a simple, non-dimensional representation of myriad oceanographic processes, isotope reactor models have found utility in describing the marine behaviors of macro- (e.g., N; Sigman et al., 1999; Si, Reynolds et al., 2006) and micronutrients (e.g., Ba, Horner et al., 2015; Cd, Abouchami et al., 2011; Cr, Scheiderich et al., 2015; Ni, Yang et al., 2020). Reactor models assume that a Me is only consumed within the reactor, and that consumption is modeled as a single reaction with a fixed isotope separation factor, $\Delta_{\mathrm{P-R}}$, defined as:

$$\mathbf{\Delta_{P\text{–}R} \equiv \delta^{i}Me_{P} - \delta^{i}Me_{R}} \qquad \textbf{[5]}$$

where $\delta^{i}Me_{P}$ and $\delta^{i}Me_{R}$ are the stable isotope compositions of the product (phytoplankton) and reactant (dissolved nutrient), respectively (see Eq. 4.).

Following reaction, there may be a fraction of the initial micronutrient Me that remains unused, which we term *f*:

$$\boldsymbol{f} \textbf{ = Unused nutrient / Nutrient supplied} \qquad \textbf{[6]}$$

where the nutrient terms represent quantities and *f* is unitless. (It follows that the fraction of nutrient consumed by phytoplankton equals $1 - f$.) In systems where most nutrients are consumed, *f* will be close to zero. However, when productivity is limited by some other resource, such as another nutrient (e.g., Fe, Co) or light, systems will exhibit *f* that can approach the theoretical maximum of one.

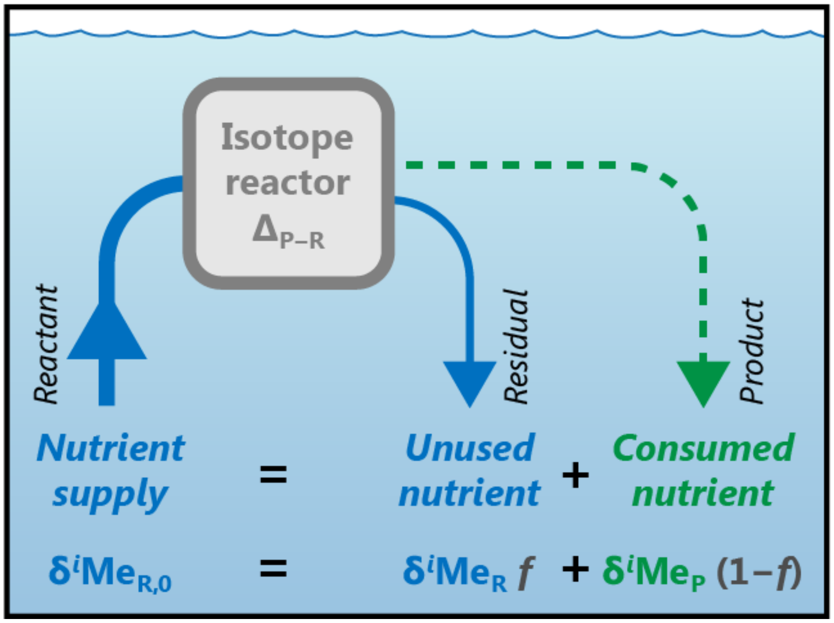

Figure 2 | Overview of a single-process reactor with an isotope separation factor $\Delta_{P\text{–}R}$. The reactor is assumed to follow the principles of isotope mass balance, in that the isotope composition of the residual unused nutrient ($\delta^{i}Me_{R}$) and consumed nutrient ($\delta^{i}Me_{P}$) sum to the isotope composition of metal initially supplied to the reactor ($\delta^{i}Me_{R,0}$)

The isotope composition of the residual nutrients and product phytoplankton will evolve over the course of a reaction. The precise nature of their evolution depends on three factors: the progress of the reaction, quantified in terms of the fraction of the initial reactant remaining (i.e., *f*); the magnitude and sign of $\Delta_{P\text{–}R}$; and, whether the system is 'open' or 'closed.' If the system remains open during the course of reaction, with the addition of new reactants balanced by the removal of product plankton and residual reactant, the system will follow Steady State behavior (SS). Alternatively, if the system is closed before and during the reaction, the system will follow Rayleigh Distillation (RD). We illustrate the effect of open- versus closed-system behavior using an example in which a reactant metal, possessing an initial isotope composition, $\delta^i\mathrm{Me}_{R,0}$, of +0.3 ‰ is reacted to form a product assuming $\Delta_{P\text{–}R} = -0.5$ ‰ (Fig. 3).

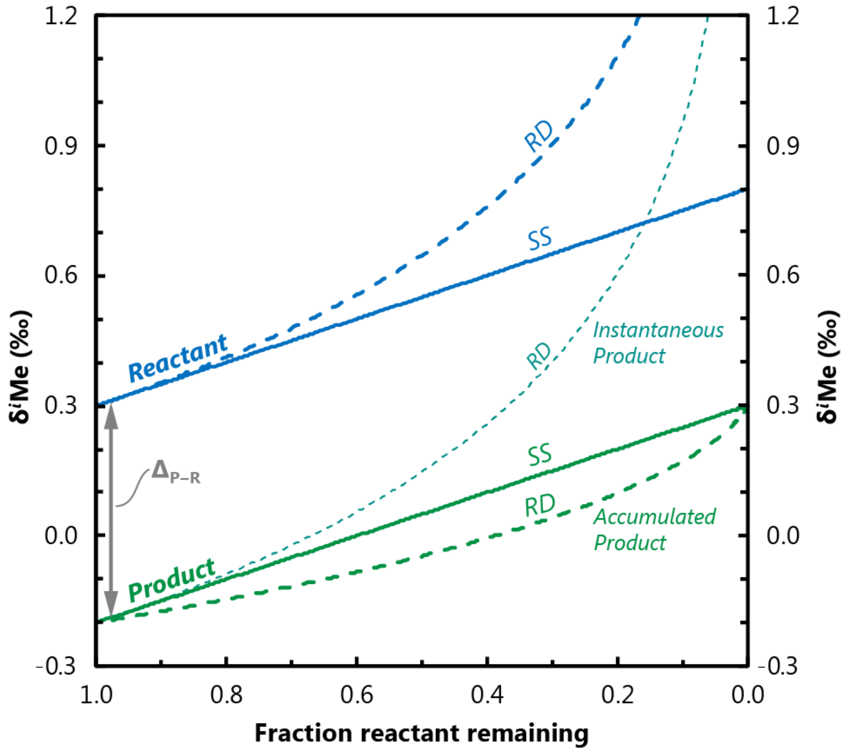

Figure 3 | Isotopic evolution of an hypothetical metal (Me) in a reactor as a function of initial reactant remaining. The metal is supplied to a reactor with an initial composition, $\delta^i\mathrm{Me}_{R,0}$, of +0.3 ‰, where it is reacted with an isotope separation factor, $\Delta_{P\text{–}R}$, of −0.5 ‰. The evolution of the reactants and products are shown for open-system behavior at SS (Steady State, solid lines; Eqs. 7, 8) and closed-system RD (Rayleigh Distillation, dashed lines) for both the Instantaneous (Eq. 10) and Accumulated Products (Eq. 11). This example illustrates that the isotope evolution of the residual reactant is strongly dependent on whether the system is open or closed during the course of the reaction.

If Me supply and removal from the system are continuous, the system is considered open and will follow the lines marked SS (Fig. 3). The SS scenario applies if the residual reactant Me is exported along with Me consumed by plankton, and that the sum of these removal terms are exactly balanced by Me resupply to the reactor. To define SS behavior, we draw on the simplifying approximations described by Johnson et al. (2004), whereby the the isotope composition of the SS product follows:

$$\boldsymbol{\delta^{i}\mathrm{Me}_{\mathrm{P}} \approx \delta^{i}\mathrm{Me}_{\mathrm{R,0}} + f\,\Delta_{\mathrm{P-R}}} \qquad [7]$$

Because of this simplification, the isotope composition of the SS reactants, $\delta^{i}\mathrm{Me}_{\mathrm{R}}$, at a given value of *f* is simply:

$$\boldsymbol{\delta^{i}\mathrm{Me}_{\mathrm{R}} \approx \delta^{i}\mathrm{Me}_{\mathrm{P}} - \Delta_{\mathrm{P-R}}} \qquad [8]$$

and thus the reactant isotope composition will not exceed $\delta^{i}\mathrm{Me}_{\mathrm{R,0}} - \Delta_{\mathrm{P-R}}$.

If the reactor is closed before and during reaction, the system will follow the lines marked RD (Fig. 3). We define RD using the simplifying approximations of Mariotti et al. (1981). These approximations are unlikely to introduce significant systematic errors for the metals discussed here since they exhibit modest isotope variations (see Hayes, 2004). Unlike SS, the RD residual reactant isotope composition can evolve to extremely fractionated isotope compositions under as $f \to 0$:

$$\boldsymbol{\delta^{i}\mathrm{Me}_{\mathrm{R}} \approx \Delta_{\mathrm{P-R}} \ln f + \delta^{i}\mathrm{Me}_{\mathrm{R,0}}} \qquad [9]$$

The RD product formed at any point in the reaction is always offset from the reactant by −0.5 ‰. This is termed the instantaneous product, $\delta^{i}\mathrm{Me}_{\mathrm{IP}}$ (Fig. 3), defined as:

$$\boldsymbol{\delta^{i}\mathrm{Me}_{\mathrm{IP}} \approx \delta^{i}\mathrm{Me}_{\mathrm{R}} + \Delta_{\mathrm{P-R}}} \qquad [10]$$

The RD Accumulated Product, $\delta^{i}\mathrm{Me}_{\mathrm{AP}}$, represents the integration of the instantaneous products formed up until that point in the reaction, given by:

$$\delta^{i}\mathrm{Me}_{\mathrm{AP}} \approx \frac{\Delta_{\mathrm{P-R}}\, f \ln f}{f-1} + \delta^{i}\mathrm{Me}_{\mathrm{R,0}} \qquad [11]$$

Regardless of whether the system follows SS or RD behavior, the first product formed will exhibit $\delta^{i}\mathrm{Me}_{\mathrm{P}}$ offset from $\delta^{i}\mathrm{Me}_{\mathrm{R,0}}$ by $\Delta_{\mathrm{P-R}}$ (double-ended arrow in Fig. 3). Likewise, at $f = 0$, $\delta^{i}\mathrm{Me}_{\mathrm{P}} = \delta^{i}\mathrm{Me}_{\mathrm{R,0}}$.

2.2.2. From reactors to relative nutrient utilization

The isotope reactor models may be used to interpret metal isotope variations in the geological record in terms of Me supply and demand in the surface ocean. This is possible if one considers the reaction progress term in the reactors as being analogous to the fraction of initially supplied nutrient left unconsumed by phytoplankton (i.e., f). A major benefit of this approach is that it does not require that the initial concentration of metal ($[\mathrm{Me}_{\mathrm{R},0}]$) supplied to the reactor be known, only its initial isotope composition, $\delta^{i}\mathrm{Me}_{\mathrm{R},0}$. However, the models do require assuming that the isotope separation factor during Me removal from seawater, $\Delta_{\mathrm{P-R}}$, has remained constant over time and that $\delta^{i}\mathrm{Me}_{\mathrm{R},0}$ does not vary. If these assumptions are justified, the reactor framework enables estimation of f from the Me isotope composition of either the residual reactants (seawater) or products (exported Me). For example, if a sedimentary archive were to accurately capture $\delta^{i}\mathrm{Me}_{\mathrm{R}}$, the isotope composition of a metal following reaction, f can be calculated assuming RD using:

$$\ln f \approx (\delta^{i}\mathrm{Me}_{\mathrm{R}} - \delta^{i}\mathrm{Me}_{\mathrm{R},0}) / \Delta_{\mathrm{P-R}} \qquad [12]$$

or, if the reaction follows SS, using:

$$f \approx (\delta^{i}\mathrm{Me}_{\mathrm{R}} + \Delta_{\mathrm{P-R}} - \delta^{i}\mathrm{Me}_{\mathrm{R},0}) / \Delta_{\mathrm{P-R}} \qquad [13]$$

Likewise, f can be estimated from the isotope composition of exported products, $\delta^{i}\mathrm{Me}_{\mathrm{P}}$, assuming SS behavior using:

$$f \approx (\delta^{i}\mathrm{Me}_{\mathrm{P}} - \delta^{i}\mathrm{Me}_{\mathrm{R},0}) / \Delta_{\mathrm{P-R}} \qquad [14]$$

(There is no equivalent approximation for computing f from $\delta^{i}\mathrm{Me}_{\mathrm{P}}$ assuming Rayleigh Distillation.)

Equations 12–14 illustrate how metal isotope compositions can be used to calculate f. However, f is a measure of the relative utilization of nutrients in a system, and does not confer direct information about the size and thus total productivity of that system. This point is illustrated in the example shown in Fig. 4, where we plot the demand for a nutrient by phytoplankton in a reactor against the initial quantity of nutrient supplied to the reactor (i.e., both axes represent quantities), with contours representing various f. These lines illustrate that a wide range of possible nutrient consumptions—and thus net ecosystem production—

are possible for any value of *f*. Put another way, if all that was known about a system was *f*, it would be difficult to determine the productivity of that system.

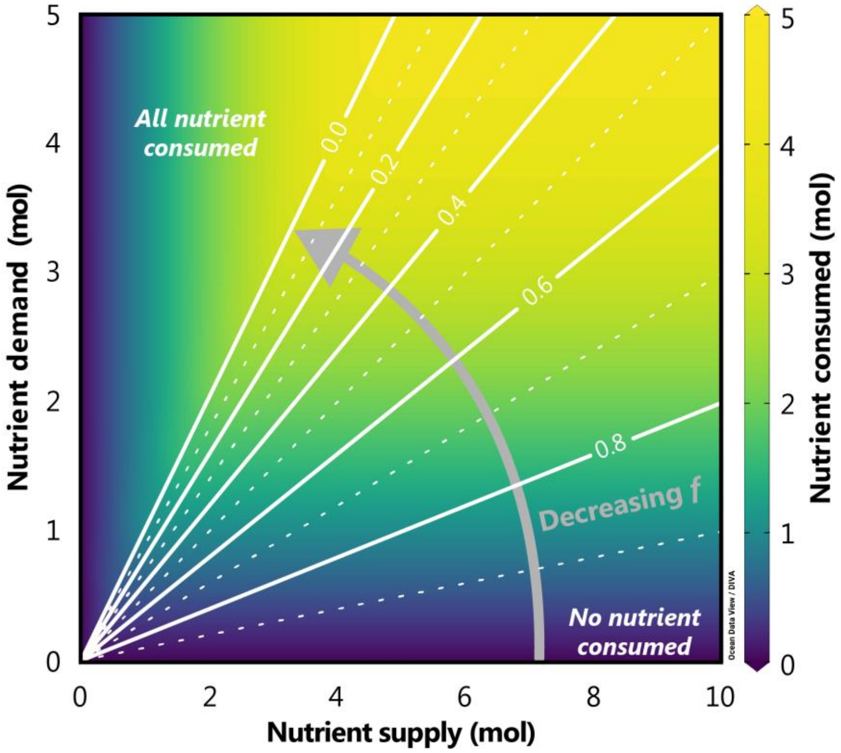

Figure 4 | Relationships between nutrient demand, supply, and consumption. The *y*- and *x*-axes represent combinations of nutrient demand and supply, respectively. The total nutrient consumed by phytoplankton for each combination is illustrated by the shading; productive systems exist in the upper-right portion of the figure, where nutrient supply and demand are high, and unproductive systems are found close to the figure axes, where supply and demand are mismatched. Between these two extremes are moderately productive systems. The fraction of nutrients unused in these systems, *f*, is shown by the contour lines. This figure illustrates that *f* cannot be used in isolation to estimate productivity.

Interpreting *f* in terms of ocean productivity requires an independent constraint on the nutrient supply, unused nutrient, or consumed nutrient (Fig. 4). A common and powerful approach is to use the flux of bioactive metals to sediments as an indicator of past nutrient consumption (e.g., Eagle et al., 2003; Brumsack, 2006; Tribovillard et al., 2006). By assuming a fixed Me:C stoichiometry, bioactive metal fluxes can then be interpreted in terms of C export productivity. The isotope composition of Me is then used as an indicator of the balance between supply and demand for Me in that system (i.e., *f*), which is sensitive to factors such as ocean circulation and ecosystem structure (e.g., François et al., 1997). These approaches are especially powerful when the constraints on export and *f* are derived from the same Me system—barite mass accumulation rates and δ^{138}Ba (e.g., Bridgestock et al., 2019), [Cd] and δ^{114}Cd (e.g., Georgiev et al., 2015), [Zn] and δ^{66}Zn (e.g., Kunzmann et al., 2013)—since this minimizes potential confounding influences from other metal cycling processes, discussed next.

2.3. Other trace metal cycling processes

The framework outlined in Sec. 2.2. represents an idealized situation that implicitly assumes that phytoplankton productivity dominates the marine cycling of a trace metal. As we show in subsequent sections, many other processes cycle the bioactive trace metals and their isotopes in the marine realm; indeed, depending on the metal and the type of process, other factors—not directly related to productivity—may even dominate the cycling of that metal. Below we introduce a number of these processes, which we group into three broad categories: biological, chemical, and physical. While these three categories of cycling processes may appear as insurmountable obstacles to the reliable application of a metal isotope system to reconstruct paleoproductivity, there are two reasons to be optimistic. First, that so many cycling processes are now recognized highlights how far our understanding of trace metal geochemistry has evolved in recent years. Second, the multiple sensitivities of these metal systems to various ocean processes means that bioactive metals and their isotopes may be applied in concert to constrain multiple aspects of past ocean chemistry. Multi-proxy approaches are a familiar feature of the paleoredox landscape and are likely to become increasingly common for constraining paleoproductivity (e.g., Cd and Zn, John et al., 2017, Sweere et al., 2020; Cd and Cr, Frei et al., 2021).

2.3.1. Biological

Biological processes exclusive of productivity can play an important role in marine trace metal behavior. The example described above assumes that organisms exhibit inflexible Me:C stoichiometries, whereas in reality many marine microbes appear to have wide tolerances for the intracellular proportions of certain trace elements compared to those of C, N, and P. The physiological mechanisms enabling these wide tolerances, and the feedback interactions that drive them, are beyond the scope of this review, and are discussed in detail elsewhere (e.g., Sunda, 2012; Morel et al., 2020). From a proxy perspective, this flexibility may cause uncertainty in paleoproductivity estimates; the more variable the Me:C stoichiometry of organisms within an ecosystem, the more uncertain the paleoproductivity estimate derived from that Me. (The corollary being that the more rigid the stoichiometry, the more robust the paleoproductivity estimate.) An extreme example concerns nonessential elements (e.g., Ag), or metals that are only essential for certain groups of organisms within an ecosystem (e.g., Mo for nitrogen fixers). Productivity estimates derived from the export of these nonessential elements are potentially most susceptible to decoupling from productivity cycles as their export is not intrinsically tied to the overall functioning of an ecosystem.

Similarly, the reactor models assume that nutrient uptake is well described by a single and fixed isotope separation factor, $\Delta_{\text{P–R}}$. A number of studies showed that this assumption is violated for Zn; different phytoplankton (e.g., Köbberich & Vance, 2017; 2019) and—depending on environmental conditions—even a single organism (e.g., John et al., 2007; Köbberich & Vance, 2017) can an exhibit a range of $\Delta_{\text{P–R}}$. Whether such behavior is also seen for other metal isotope systems is unknown, but could be important given that calculation of f is dependent on $\Delta_{\text{P–R}}$ (Eqs. 12–14).

Biological processes can potentially exert an additional control on bioactive metal isotope distributions through remineralization—the regeneration of POC to inorganic nutrients. In the case of a scarce nutrient, such as Fe, individual organisms (e.g., Saito et al., 2011) and even entire ecosystems (e.g., Rafter et al., 2017) may have evolved mechanisms to retain certain nutrients. Likewise, macro- and micronutrients may be regenerated by heterotrophic organisms at different rates (e.g., Twining et al., 2014; Ohnemus et al., 2019), which could affect the Me:C stoichiometry of exported POC and thus the accuracy of Me-derived C export fluxes. Even less is known about the role of heterotrophs in fractionating POC-associated metal isotope compositions, which could be significant for some metals (e.g., Cd, Janssen et al., 2019).

Lastly, many of the metals reviewed here form complexes with organic ligands. Indeed, for some metals, such as Fe and Cu, almost the entire oceanic inventory is bound to organic ligands. The effect of ligands on trace metal cycling is an area of active research, and is potentially important from the perspective of modulating isotope fractionation during uptake by plankton and into secondary Me sinks. Where known, these effects are discussed in the relevant sections.

2.3.2. Chemical

There are several chemical transformations that can modulate marine trace metal distributions without affecting C, such as scavenging and precipitation–dissolution reactions. Scavenging, meaning adsorption and desorption, can alter Me:C relationships by redistributing metals, but not C. Originally developed in the context of dissolved and particulate thorium isotopes (Bacon & Anderson, 1982), reversible scavenging is now suggested to play a role in the vertical cycling of other metals, including Cu (e.g., Little et al., 2013), Fe (e.g., Abadie et al., 2017), and Zn (e.g., Weber et al., 2018). Reversible scavenging is a continuous process that occurs between particle surfaces and dissolved species. While this process can occur at any depth, scavenging intensity is positively correlated with the quantity of particles, and so is most important in the upper water column. Likewise, while dissolved metals may be scavenged by any class of particle (e.g., opal, lithogenics), certain particle types may preferentially scavenge certain elements (e.g., Lerner et al., 2018). Scavenging can even affect trace metals cycled predominantly by organic matter; secondary phases may scavenge metals during remineralization, which can affect trace metal distributions in the upper water column (e.g., Zn, John & Conway, 2014; Co, Hawco et al., 2018; Fe, Tagliabue et al., 2019).

Precipitation and dissolution of minerals is also a consideration for certain trace metals discussed here. However, the relative importance of mineral cycling depends on the metal and the redox environment. For example, Ba is primarily cycled by the mineral barite, rather than POC, and the thermodynamics of precipitation vary throughout the ocean (e.g., Rushdi et al., 2000). Changes in the ambient redox environment, such as in an oxygen minimum zone (OMZ), may even enhance dissolved–particulate transformations for certain trace metals. Some metals, such as Fe, may have large sources in OMZs associated with the reductive dissolution of particulate Fe–Mn oxides. Other metals may experience enhanced removal via precipitation into sulfide minerals (e.g., Zn, Cu, Cd, Mo, Ni, Ag; Helz et al., 1996; McKay & Pedersen, 2008; Kramer et al., 2011; Janssen et al., 2014; Vance et al., 2016; Bianchi et al., 2018; Guinoiseau et al., 2019). The net effect of these non POC-associated transformations is that processes other than POC cycling may redistribute trace metals, but not C, within the ocean interior. If significant, these processes could drive the ocean to a different Me:C stoichiometry and/or dissolved metal isotope composition that could impact calculations of export and *f*, respectively, when using the nutrient utilization framework described in Sec. 1.3.

2.3.3. Physical

The physical circulation of the ocean exerts a major control on many oceanic TEI distributions and we describe this influence on our 9 trace metals in detail in later sections. In addition to circulation, there are also scale dependencies that can affect trace metal based productivity estimates at both small and large scales, as well as other, non-productivity metal sinks. At the local to regional scale, Me point sources may be significant if they mask any POC-related Me drawdown. Though perhaps less significant for C, point sources—rivers, dust, desorption from particles, sediments, and hydrothermalism—may be significant terms in local and regional trace metal budgets if the magnitude is comparable to the dissolved supply from ocean circulation. Examples include dust-derived Cu to surface planktonic communities (e.g., Paytan et al., 2009) and hydrothermal-derived Fe to the deep ocean (e.g., Resing et al., 2015). Consideration of these external sources is particularly important when productivity estates are derived close to such point sources and for metals with residence times that are less than or similar to the mixing time of the ocean (~1 kyr).

At larger scales, the location of a site and the assumption of steady state can influence the calculation of *f*. The importance of location is illustrated using the examples in Fig. 4. Close to an upwelling source of metal, such as in the modern Southern Ocean, *f* is, by definition, close to one and decreases downstream into the low latitudes. Given this dependence, it follows that a change in ocean circulation geometry could influence the spatial pattern of *f* without any net changes in productivity. This is particularly important to consider from a paleoceanographic perspective, since records are typically generated from fixed locations (i.e., sediment cores), making it challenging to determine if variations in *f* originated from overlying changes in ocean circulation or productivity. One solution to this challenge is to obtain an independent constraint on ocean circulation, such as from another isotope system or using a model. Alternatively, the spatial pattern of *f* could be discerned from multi-site reconstructions of Me distributions.

On a global scale, the assumption of steady state can affect how productivity is estimated from Me reactor models. The input and output fluxes of a metal through the ocean should balance, regardless of productivity. Likewise, the flux-weighted metal isotope composition of inputs and outputs should also balance. Thus, at large scales, the isotopic composition of a sedimented Me should reflect the average input δ^{i}Me, regardless of mean ocean *f*. Such a situation is possible because the flux terms interact. As an example, we return to the metal in Fig. 3. We will assume that this metal follows SS behavior and that biological productivity is the only sink of this metal from seawater. If the mean marine input of this metal possessed $\delta^{i}\mathrm{Me} = -0.1$ ‰, the system would only be in steady state if, on a global basis, $f = 0.8$. However, if mean global *f* were to decrease to 0.2 (i.e., a smaller fraction of this nutrient Me is left unused), mean global $\delta^{i}\mathrm{Me}_{\mathrm{P}}$ would increase from −0.1 to +0.2 ‰, which no longer matches the input δ^{i}Me of −0.1 ‰. Such an imbalance cannot be sustained indefinitely, since the ocean would be losing more ‘heavy’ Me than is being added. As such, the ocean would gradually compensate by a lowering of $\delta^{i}\mathrm{Me}_{\mathrm{R,0}}$ to 0.0 ‰. In turn, mean ocean $\delta^{i}\mathrm{Me}_{\mathrm{P}}$ would return to values ≈ −0.1 ‰, even if *f* remained at 0.2. This example illustrates how ocean-scale processes can influence the relationship between trace metals and productivity, even if productivity is the main sink of a metal from a system.

Lastly, the relationship between Me and productivity—$\delta^{i}\mathrm{Me}_{\mathrm{R,0}}$, and potentially, $[\mathrm{Me}_{\mathrm{R,0}}]$—can also be influenced by non-productivity Me sinks. Indeed, non-productivity sink terms are of considerable significance for many of the trace metals reviewed here. The significance of these terms may offer another, indirect means to constrain paleoproductivity: if non-productivity Me sinks possess different $\Delta_{\mathrm{P-R}}$ and/or Me:C to productivity-related sinks, mean deep ocean δ^{i}Me and/or [Me] will be sensitive to the relative balance of Me burial between the various sink terms, analogous to the canonical C cycle mass balance (e.g., Berner et al., 2000). For example, if assuming fixed Me inputs over time and that whole-ocean productivity abruptly decreased, the relative significance of non-productivity Me sinks would increase to compensate for the decrease in productivity. This compensation could drive deep ocean δ^{i}Me and/or [Me] to new values that are sensitive to the balance between productivity and Me burial by other sinks. This multi-sink framework similarly underpins the use of many TEI-based redox proxies (e.g., Tl, Owens et al., 2017; U, Montoya-Pino et al., 2010), though this approach is relatively underexplored in the context of reconstructing paleoproductivity.

3. Iron

Iron plays a key role within phytoplankton as an electron carrier for photosynthesis and respiration processes, as well as within enzymes necessary for photosynthesis and nitrogen fixation (Morel & Price, 2003). However, in oxygenated seawater, Fe(II) is rapidly oxidized to Fe(III), which is highly insoluble (Liu & Millero, 2002). Intense biological demand coupled to low solubility results in generally sub-nanomolar [Fe] throughout the oceans, approaching the low picomolar range in some surface regions far from Fe sources, such as the vast Southern Ocean and North Pacific (e.g., Fig. 5; Chever et al., 2010; Klunder et al., 2011; Schlitzer et al., 2018). Consequently, biological production in about 30 % of the modern surface ocean is thought to be limited primarily by Fe (Moore et al., 2013), principally in upwelling regions where deep water is depleted in Fe relative to the macronutrients nitrate (NO_3^-) and phosphate (PO_4^{3-}; e.g., Moore, 2016; Boyd et al., 2017). In these regions, termed 'High Nutrient Low Chlorophyll' (HNLC), Fe supply can limit primary productivity (e.g., Martin & Fitzwater, 1988) and potentially the exchange of carbon between the ocean and atmosphere. Furthermore, a changing supply of Fe from sources such as atmospheric dust, hydrothermal venting, or sedimentary release to the surface oceans through geological time can exert a significant control on both the distribution of primary productivity in the oceans and, through this, the global carbon cycle. Changes in supply of dust to the Fe-limited Southern Oceans has been shown to correlate with climate variability on millennial time scales and has also been invoked to explain the dramatic sawtooth glacial–interglacial shifts in atmospheric carbon dioxide (Martin, 1990; Sigman & Boyle, 2000; Martínez-Garcia et al., 2011; 2014).

The strong link between Fe supply and primary productivity suggests that ratios of Fe to other elements and/or Fe isotope ratios (δ^{56}Fe) might be useful proxies for paleoproductivity. However, in the vast majority of settings, δ^{56}Fe and Fe flux records do not reflect paleoproductivity; the influence of the major Fe sources and their redox-driven cycling exert far stronger controls over marine Fe geochemistry compared to biological productivity. Thus, a simple reactor framework, as outlined in Sec. 2.2.1, cannot be applied to δ^{56}Fe. However, we note that there are a number of promising archives of paleo Fe isotope chemistry, particularly for the deep ocean, and we anticipate that these records will prove most valuable as context for interpreting other proxy records, or for generating novel hypotheses regarding the connections between Fe sources, biological productivity, and global climate.

3.1. Marine distribution

The distribution of dissolved Fe in seawater is driven by a mixture of competing processes, including: biological uptake and regeneration; distinct sources of Fe at shallow, intermediate, and deep depths; adsorption–desorption processes onto organic and lithogenic particles; dissolution and precipitation processes; and, complexation to organic ligands (Fig. 6; e.g., Boyd & Ellwood, 2010; Labatut et al. 2014; Tagliabue et al., 2017). As a result, [Fe] displays what has historically been termed as a hybrid-type depth profile in the open ocean, which exhibits a number of similarities between different ocean basins (Fig. 5). Surface Fe is drawn down in surface waters by biological uptake, and [Fe] can even be as low as 0.01 nmol kg^{-1} in Fe limited regions (Schlitzer et al., 2018). However, some areas of the oceans, such as the 'dusty' North Atlantic, surface [Fe] can be driven as high as 2 nmol kg^{-1} as a result of dust deposition events (Sedwick et al., 2005). Below the surface mixed layers, regeneration of biogenic material, reversible particle scavenging, and complexation by organic ligands all act to keep the background deep ocean [Fe] at around 0.4–0.6 nmol kg^{-1} (e.g., Lauderdale et al., 2020). Against this background, it has been known for decades that [Fe] in deeper waters are elevated near point sources such as sedimentary margins (Johnson et al., 1999). Recently, however, a range of studies including those conducted as part of the GEOTRACES program, have illuminated this picture, showing that deep sources of Fe—such as sedimentary and hydrothermal release—are widespread, may have distinct traceable δ^{56}Fe source signatures, and that this Fe can be transported over large distances through the ocean interior (e.g., Radic et al. 2011; Saito et al., 2013; Conway and John, 2014; Resing et al., 2015; Nishioka et al., 2020). Despite exhibiting well-defined deep maxima close to point sources, [Fe] distributions at shallow and intermediate depths are much more variable and models have struggled to reproduce these variations (e.g., Tagliabue et al., 2016). The extent to which deeply sourced Fe is supplied to surface seawater is thus equivocal (e.g., Tagliabue et al., 2010; Roshan et al., 2020).

The origin of [Fe] variability in the shallow and intermediate ocean is thought to reflect local differences in the competition between uptake, regeneration, sources, and scavenging. The same processes influence δ^{56}Fe; however, unlike variations in [Fe], δ^{56}Fe exhibits dramatic variability between—and even within—ocean basins (Fig. 5; Schlitzer et al., 2018). Such water column variability in δ^{56}Fe, from isotope compositions as light as −4 ‰ (Charette et al., 2020), to as heavy as +2 ‰ (Ellwood et al., 2020), is thought to be driven by Fe source signatures and therefore also oceanic circulation, and a combination of biological uptake, Fe complexation to organic ligands in surface waters, and non-reductive release of dissolved Fe from particles (notably lithogenic particles) during desorption and/or ligand-promoted dissolution (e.g., Conway and John, 2014; Abadie et al. 2017; Ellwood et al., 2020; Fig. 6). These processes can render remarkably different δ^{56}Fe profiles, even when profiles of [Fe] are similar, such as in the examples from the Northeast Pacific, Eastern Tropical North Atlantic, and the Weddell Sea of the Southern Ocean (Fig. 5). In the North Pacific and North Atlantic examples, the deep distribution of δ^{56}Fe is considered to be most strongly influenced by the dominant regional Fe source—dust in the Atlantic and Fe released from continental margins in the Pacific (Conway and John, 2014; Conway and John, 2015b). In the Weddell Sea, the deep δ^{56}Fe distribution has been attributed to regeneration of biogenic light Fe at depth (Abadie et al., 2017), or, more recently, to addition of light Fe from regional sedimentary release (Sieber et al., 2021). Thus, δ^{56}Fe may provide insight to the contribution of Fe sources at the basin scale (e.g., Conway & John, 2014a), as well as for Fe cycling processes such as uptake and regeneration.

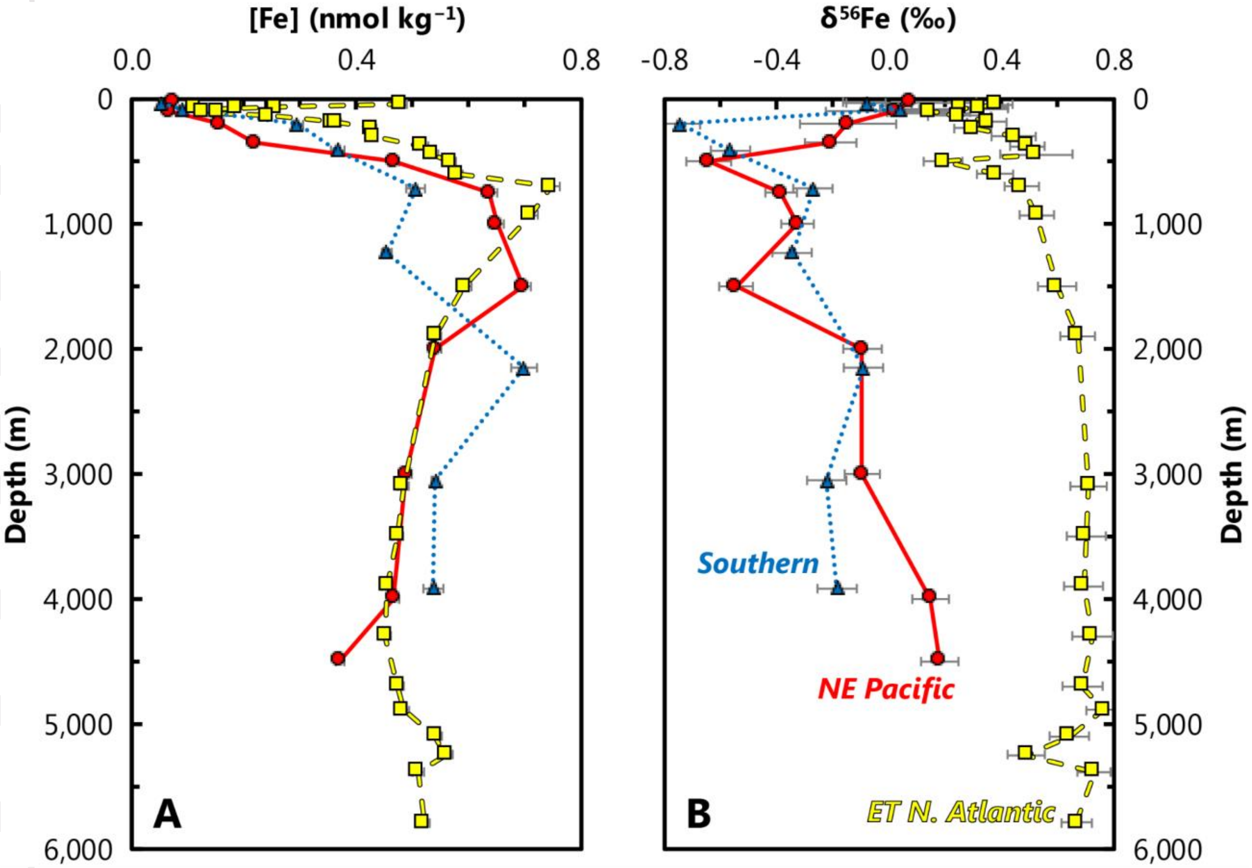

Figure 5 | Representative profiles of dissolved Fe concentrations ([Fe]; A) and Fe isotopic compositions (δ^{56}Fe; B). Data from the Eastern Tropical North Atlantic (squares, dashed line; Conway & John, 2014a), Northeast Pacific (circles, solid line; Conway & John, 2015a), and Southern Oceans (triangles, dotted line; Abadie et al., 2017). Station locations as per Fig. 1. This comparison illustrates that despite possessing similar dissolved concentration profiles, the isotopic behavior of Fe is markedly different between basins.

Despite synthesis of numerous studies of both small- (e.g., Martin et al., 1990; Coale, 1991; Coale et al., 2003) and large-scale iron fertilization events (e.g., de Baar et al., 2005; Boyd et al., 2007; Boyd & Ellwood, 2010; Urban et al., 2020), there are still uncertainties in how changing Fe supply to the surface ocean may affect phytoplankton growth in Fe-limited regions, and/or nitrogen fixers under NO_3^- limitation, leading to gaps in our understanding of linking Fe cycling directly to climate change (Misumi et al., 2014). One major challenge is assessing what portion of the dissolved Fe pool is available for uptake by different microbes, termed 'bioavailable' Fe. Such uncertainties on Fe supply, speciation, and bioavailability in the surface ocean are compounded by limitations in our ability to constrain the supply of dissolved Fe in upwelled deep waters. For example, while the ratio of C to macronutrients such N and P in the deep ocean is well known and the residence time and distribution can be accurately reproduced using apparent oxygen utilization (AOU), this is not the case for Fe. Only around 10–15 % of cellular Fe (Fe:C = 18–33 µmol:mol) appears to be regenerated in the deep ocean (Fe:C 4–6 µmol:mol; Twining & Baines, 2013), leading to a weaker correlation between [Fe] and AOU, even in regions away from Fe sources (Rijkenberg et al., 2014) and upwelling deep waters that are depleted in dissolved Fe relative to macronutrients. Since incubation experiments show that Fe associated with sinking organic matter from the subsurface is effectively regenerated (Velasquez et al., 2016), much of the released Fe must be rapidly scavenged (Tagliabue et al., 2019). Despite this scavenging, vertical transport is still thought to be the major source of dissolved Fe for phytoplankton in most Fe-limited regions, indicating that additional research into the interplay between Fe supply (sources, stabilization, and transport) and demand (biological uptake, scavenging) are required.

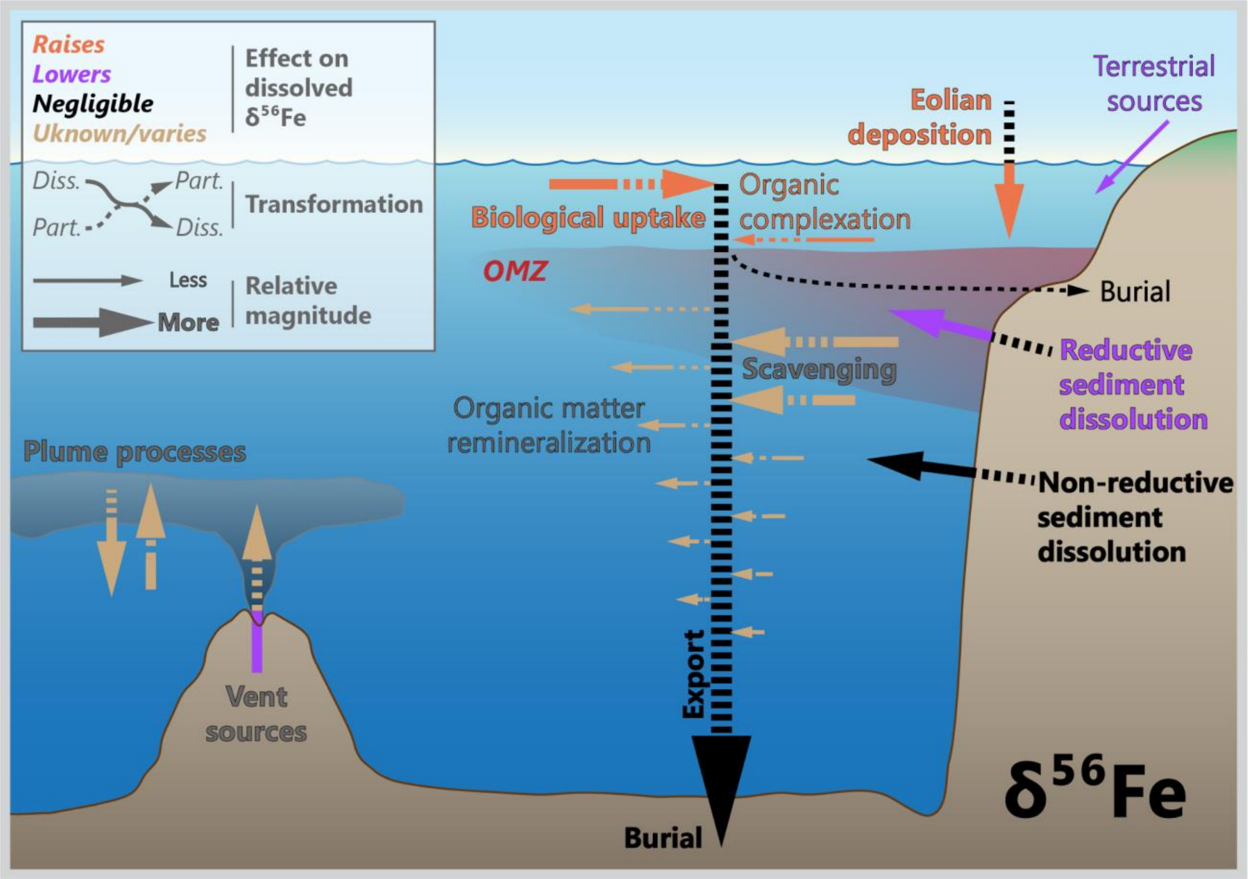

Figure 6 | Processes driving Fe isotope variations in modern seawater. The oceans' internal cycle of Fe is perhaps the most complex of the trace metals discussed here, exhibiting several significant sources, sinks, and transformations not directly associated with biological productivity.

3.2. Driving processes

3.2.1. Biological

Initial studies of processes that fractionate Fe isotopes were optimistic that δ^{56}Fe would make for a powerful proxy of physiological 'biosignatures' (Beard et al., 1999), especially once measurement of δ^{56}Fe was extended to seawater by Lacan et al. (2008). However, much of this early optimism faded once it was found that other factors were also important in setting dissolved δ^{56}Fe, such as external Fe sources (e.g., Radic et al., 2011; John et al., 2012; Sec. 2.2.3.). Moreover, organisms exhibit significant variability in Fe:C ratios (e.g., Twining & Baines, 2013), suggesting that Fe cycling may be partially decoupled from ecosystem productivity. Despite the more nuanced picture, there is a growing body of evidence suggesting that phytoplankton probably preferentially incorporate light Fe isotopes from seawater and, in some circumstances, can render detectable changes in dissolved δ^{56}Fe (Fig. 6). For example, studies from isolated eddies, the Mertz Polynya, and the open Southern Ocean showed that surface δ^{56}Fe at picomolar [Fe] are isotopically heavy (>+1‰), which has been attributed to the combination of surface uptake, regeneration, and organic complexation (Ellwood et al., 2015; 2020; Sieber et al., 2021). Estimates for the magnitude of fractionation due to biological uptake, Δ_{P-R}, range between −0.1 (Radic et al., 2011) and −1.0 ‰ (Ellwood et al., 2020; Sieber et al., 2021). The magnitude and direction of any Fe isotope fractionation during uptake may depend on the phytoplankton species, uptake mechanism, and Fe species consumed. Thus, additional research is required on all three fronts.

Below the surface mixed layer, dissolved δ^{56}Fe compositions appear to be primarily a reflection of the isotope signature of Fe sources, rather than reflecting a dominant influence from the biological processes of remineralization (Fig. 6; e.g., Abadie et al., 2017; Conway & John, 2014a; John et al., 2018a; Labatut et al., 2014; Sieber et al., 2021). Accordingly, there remains the possibility for δ^{56}Fe of surface seawater to be linked to productivity in some oceanographic settings, though the relative role of other Fe-cycling processes and the degree to which they erase any diagnostic productivity signatures requires further investigation.

3.2.2. Chemical

The chemical behavior of Fe in seawater is complex and has the potential to decouple Fe cycling from macronutrients and thus productivity. Unlike the macronutrients, which are present as aqueous ions in solution, Fe is scarcely soluble in seawater, and much of what constitutes ‘dissolved’ Fe—operationally defined as that which can pass through a 0.2 or 0.4 μm filter—is in actuality a ‘soup’ containing organic complexes, nanoparticles, colloids, and a small fraction of truly ionic Fe. The controls governing, and the extent to which exchange occurs between these forms of dissolved Fe, are areas of focused interest (e.g., Fitzsimmons & Boyle, 2014; Fitzsimmons et al., 2015). Additionally, dissolved Fe is subject to strong removal via scavenging, which lowers the Fe:macronutrient ratio of waters returned to the surface via upwelling (Moore, 2016). Chemical processes can also exert a significant influence over the isotopic composition of Fe in seawater, such as through redox transformations, exchange reactions (e.g., complexation, particle interactions), and by authigenic precipitation, discussed below.

Redox transformations drive large Fe isotope effects (e.g., Johnson et al., 2002; Skulan et al., 2002; Welch et al., 2003; Anbar et al., 2005). Indeed, much of the Fe isotope variation in Earth’s ancient, more-reducing past likely derives from fractionations associated with redox transformations (see e.g., Rouxel et al., 2005; Johnson et al., 2008 and references therein). While the role of redox relative to other processes is somewhat diminished in today’s largely oxygenated ocean, it remains an important mediator of Fe isotope source compositions, particularly within the ocean interior. This is neatly illustrated using the example of sediment dissolution, which can occur with or without a change in the redox state of Fe (Fig. 6). Bulk marine sediments typically possess a composition similar to the crustal composition of +0.1 ‰ (Beard et al., 2003; Poitrasson, 2006). However, dissolved Fe(II) derived from bacterially mediated reductive dissolution in sediments has been characterized by δ^{56}Fe between −1 and −3 ‰ (Berquist & Boyle, 2006; Severmann et al., 2006; 2010; Homoky et al., 2009; 2013; Klar et al., 2017a; Henkel et al., 2018), whereas Fe derived from non-reductive dissolution processes is thought to be considerably heavier, between +0.1 to +0.3‰, and also likely to be present in the colloidal phase (Homoky et al., 2009; 2013; 2021; Radic et al., 2011). Further modification of reductive endmember compositions is possible upon contact with oxidizing seawater, potentially masking true source signatures. Oceanic water column dissolved δ^{56}Fe compositions attributed to either non-reductive (+0.1 to +0.4 ‰) or reductive (−0.3 to −4 ‰) release of Fe from sediments have now been observed globally (Radic et al., 2011; John et al., 2012; Staubwasser et al., 2013; Conway & John, 2014a; Labutut et al., 2014; Conway & John 2015a; Chever et al., 2015; Fitszimmons et al., 2016; Klar et al., 2017a; Abadie et al., 2017; Klar et al., 2018; Rolison et al., 2018; John et al., 2018a; Charette et al., 2020).

Exchange reactions can also fractionate primary Fe isotope compositions. For example, natural lithogenic dust is thought to possess a relatively narrow range of Fe isotope compositions (i.e., δ^{56}Fe ≈ +0.1±0.2‰; Waeles et al., 2007; Mead et al., 2013; Conway et al., 2019; Chen et al., 2020), reflecting the overall homogeneity of the upper continental crust. However, dissolved Fe in seawater attributed to dissolving dust particles is isotopically heavy, around +0.7 ‰ (Fig. 6; Conway & John, 2014a). This fractionation is thought to reflect dissolution in concert with, and complexation by, strong organic ligands (Fishwick et al., 2014), which have been experimentally shown to preferentially bind heavy Fe isotopes (Dideriksen et al., 2008; Morgan et al., 2010). Fractionation effects may also arise during exchange of Fe between dissolved and particulate forms, though the magnitude of the effect depends on whether the exchange is primarily physical (negligible fractionation; e.g., Fitzsimmons et al., 2017) or chemical (from ≈+0.3 up to +1‰; Labutut et al., 2014; Fitzsimmons et al., 2015).

Lastly, authigenic precipitation can control the isotopic composition of Fe released by large point sources, such as hydrothermal vents and margin sediments (Fig. 6). Iron in hydrothermal vent fluids possesses endmember compositions ranging from −0.7 to +0.1‰ (Sharma et al., 2001; Beard et al., 2003; Severmann et al., 2004; Rouxel et al., 2008; Bennett et al., 2009; Rouxel et al., 2016; Nasemann et al., 2018; Rouxel et al., 2018). However, precipitation of Fe into authigenic minerals can render significant changes in dissolved δ^{56}Fe (e.g., Severmann et al., 2004; Bennett et al., 2009). The direction of fractionation depends on—and may thus be diagnostic of—the specific transformations occurring (e.g., Horner et al., 2015b; Lough et al., 2017): Fe sulfides and oxides preferentially incorporate isotopically light and heavy Fe, respectively (e.g., Skulan et al. 2002; Rouxel et al., 2008). Mineral precipitation can drive δ^{56}Fe of residual Fe stabilized in seawater to values ranging between −2.4 to +1.5 ‰, depending on the authigenic mineral produced (Conway & John, 2014a; Ellwood et al., 2015; Fitzsimmons et al., 2016; 2017; Klar et al., 2017b; Lough et al., 2017; Rouxel et al., 2018). Analogous processes appear to operate along continental margins, whereby 'light' Fe, mobilized by reductive dissolution, encounters oxidizing seawater and forms precipitates that are heavier than the source Fe (though overall still considerably lighter than background seawater; e.g., Marsay et al., 2018; Fig. 6).

Additionally, the importance of local point sources on dissolved δ^{56}Fe continue to emerge, including from anthropogenic aerosol dust (e.g., Mead et al., 2013; Kurisu et al., 2016a,b; Conway et al., 2019; Pinedo-González et al., 2020), glaciers and meltwater (e.g., Zhang et al., 2015; Stevenson et al., 2017), and rivers (e.g., Fantle & DePaolo, 2004; Bergquist & Boyle, 2006; Ingri et al., 2006; Escoube et al., 2009; Ilina et al., 2013; Akerman et al., 2014; Chen et al., 2014; Poitrasson et al., 2014; Escoube et al., 2015; Mullholland et al., 2015). These local point sources can vary dramatically over short spatial and temporal scales and with *in situ* chemical conditions. The net effect of the dominance of Fe sources on dissolved δ^{56}Fe in seawater means that any signal from biological uptake in the Fe-depleted mixed layer, even if could be recorded in an archive, may be easily overprinted by even a small addition of new Fe from either above or below.

3.2.3. Physical

The residence time of Fe in seawater is substantially less than the mixing time of the global ocean (Table 1). Local and regional Fe sources can thus drive large differences in [Fe] and dissolved δ^{56}Fe between ocean basins (Fig. 5). Local source signatures—[Fe], δ^{56}Fe, and perhaps Fe speciation—can be transported and retained over the scale of individual ocean basins (Fig. 7; Conway & John, 2014a; Abadie et al., 2017).

This is arguably one of the marquee findings of the GEOTRACES program, and underpins the utility of sedimentary δ^{56}Fe to reconstruct past marine Fe sources, discussed next.

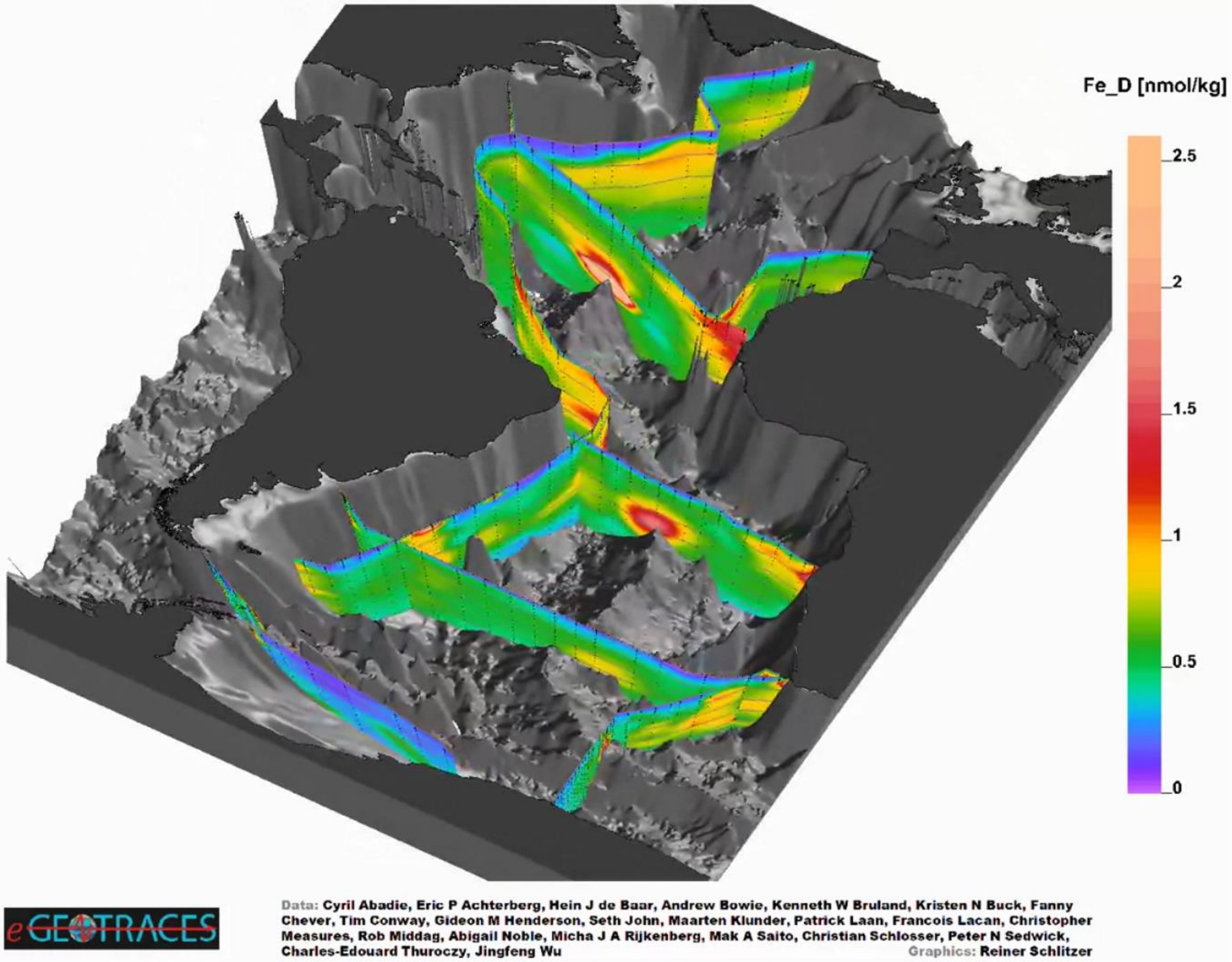

Data: Cyril Abadie, Eric P Achterberg, Hein J de Baar, Andrew Bowie, Kenneth W Bruland, Kristen N Buck, Fanny Chever, Tim Conway, Gideon M Henderson, Seth John, Maarten Klunder, Patrick Laan, Francois Lacan, Christopher Measures, Rob Middag, Abigail Noble, Micha J A Rijkenberg, Mak A Saito, Christian Schlosser, Peter N Sedwick, Charles-Edouard Thuroczy, Jingfeng Wu

Graphics: Reiner Schlitzer

Figure 7 | Three-dimensional scene depicting dissolved Fe concentrations in the Atlantic Ocean (Schlitzer, 2017). This perspective illustrates the density of GEOTRACES data in the region as well as the influence of multiple Fe ‘hot spots’, such as mid-ocean ridges and continental margins. Data are available in the GEOTRACES Intermediate Data Product 2017 (Schlitzer et al., 2018); names of data originators appear in the figure. Three-dimensional scenes for other TEIs are available from https://eGEOTRACES.org/.

3.3. Marine archives

3.3.1. Surface ocean

A requirement of the application of any paleoproxy is the availability of suitable sedimentary archives. These archives must have both a high fidelity for the signal of interest and be robust to post-depositional alteration. Archives most relevant to reconstructing paleoproductivity should capture surface ocean δ^{56}Fe;

however, there are few—if any—reliable archives. The lack of surface water archives reflects two related challenges. First, most archives for surface seawater are derived from biominerals, such as foraminifera, diatoms, sponges, and corals. These archives possess vanishingly low Fe content compared to Ca or Si, such that Fe isotopic analysis of these substrates has proven difficult. Second, following burial, many biominerals will act as substrates for authigenic mineral formation. These authigenic minerals, such as clays (e.g., Badaut & Risacher, 1983) and Fe–Mn oxides (e.g., Boyle, 1981), possess Fe contents far in excess of those in the underlying biomineral, necessitating significant physical and chemical cleaning (e.g., Cheng et al., 2000).

Despite these obstacles, there are three positive signs that reconstructing past surface seawater δ^{56}Fe is possible. First, biogenic opal may contain Fe at concentrations in the μg g^{-1} range (Ellwood & Hunter, 2000; Lal et al., 2006; Shemesh et al., 1988; Sun et al., 2016), which is tractable for δ^{56}Fe analysis. Second, the Fe content of diatoms is correlated with ambient [Fe] (Twining & Baines, 2013). Lastly, the positive relationship between the Fe content of diatoms and corresponding seawater appears to hold through sinking and sedimentation (Pichevin et al., 2014), indicating that diatoms are a potential window into past surface ocean Fe chemistry. Whether these relationships also extend to δ^{56}Fe remains to be seen, and will require additional coretop calibrations, incubation experiments, and detailed assessment of the efficacy of chemical cleaning.

3.3.2. Deep ocean

There are several studies examining Fe sources and fluxes in the meso- and bathypelagic ocean using sedimentary archives. Given the considerable spatial variability in modern δ^{56}Fe, it is likely that sedimentary reconstructions will reflect, at most, a regional view of the past Fe cycle. This means that multiple, contemporaneous records will be required to diagnose whole-ocean changes in Fe cycling, but that individual records will still have utility in offering basin-scale perspectives. To constrain Fe sources, researchers have examined the Fe isotope composition of Fe-rich sediments, including red clays (Dunlea et al., 2021), polymetallic nodules (Marcus et al., 2015), and Fe–Mn crusts (Zhu et al., 2000; Levasseur et al., 2004; Chu et al., 2006; Horner et al., 2015b; Liu et al., 2020). Ferromanganese crusts are currently the best studied for Fe isotopes (Fig. 8); Fe–Mn crusts are slowly accumulating deposits (~mm Myr^{-1}) that record ambient seawater δ^{56}Fe with a spatially invariant offset of -0.77 ± 0.06 ‰ (Levasseur et al., 2004; Horner et al., 2015b). The constancy of the offset between crusts and seawater implies that the Fe isotope composition of individual Fe–Mn crust layers can be interpreted in terms of past dissolved δ^{56}Fe, and thus past Fe sources. Iron is effectively immobile in Fe–Mn crusts, with a calculated effective diffusivity $<10^{-12}$ cm^2

yr^{-1} (Henderson & Burton, 1999), implying that post-depositional diffusion of Fe is unlikely to reset primary $\delta^{56}Fe$ (Horner et al., 2015b; Marcus et al., 2015). Curiously, however, the Fe isotopic variability of Fe–Mn deposits recovered from the central Pacific—particularly layers formed before ~20 Ma—exceed the range of modern deep ocean $\delta^{56}Fe$ (though only in the positive direction; Fig. 8). The reasons for elevated $\delta^{56}Fe$ in the past are debated. Horner et al. (2015b) report that heavy $\delta^{56}Fe$ could arise through widespread secondary modification of large Fe sources through authigenic reactions, such as sulfide precipitation. In contrast, Johnson et al. (2020) contend that the elevated $\delta^{56}Fe$ reflects extensive biological modification of dissolved Fe, driven by large-scale Fe fertilization. Regardless, the variation in these records points to a dynamic and enigmatic Fe cycle in Earth's past, and indicates that Fe–Mn crusts have a largely untapped potential to reconstruct spatiotemporal variations in this cycle.

Other approaches are also showing promise to study Fe fluxes to the deep ocean through time. For example, researchers have constrained the rate of sedimentary accumulation of hydrothermally derived Fe and Cu using constant flux proxies such as extraterrestrial helium-3 (e.g., Middleton et al., 2016) or thorium-230 (Costa et al., 2017). These studies report that hydrothermal activity may be coherent with sea level changes on Quaternary glacial–interglacial cycles, suggesting a potentially remarkable set of connections between the solid Earth, ocean chemistry, and global climate (e.g., Cullen & Coogan, 2017). Reconstruction of hydrothermal metal fluxes over million-year timescales may also be possible using the geochemistry of pelagic clays (e.g., Dunlea et al., 2015), though such approaches are still in their infancy.

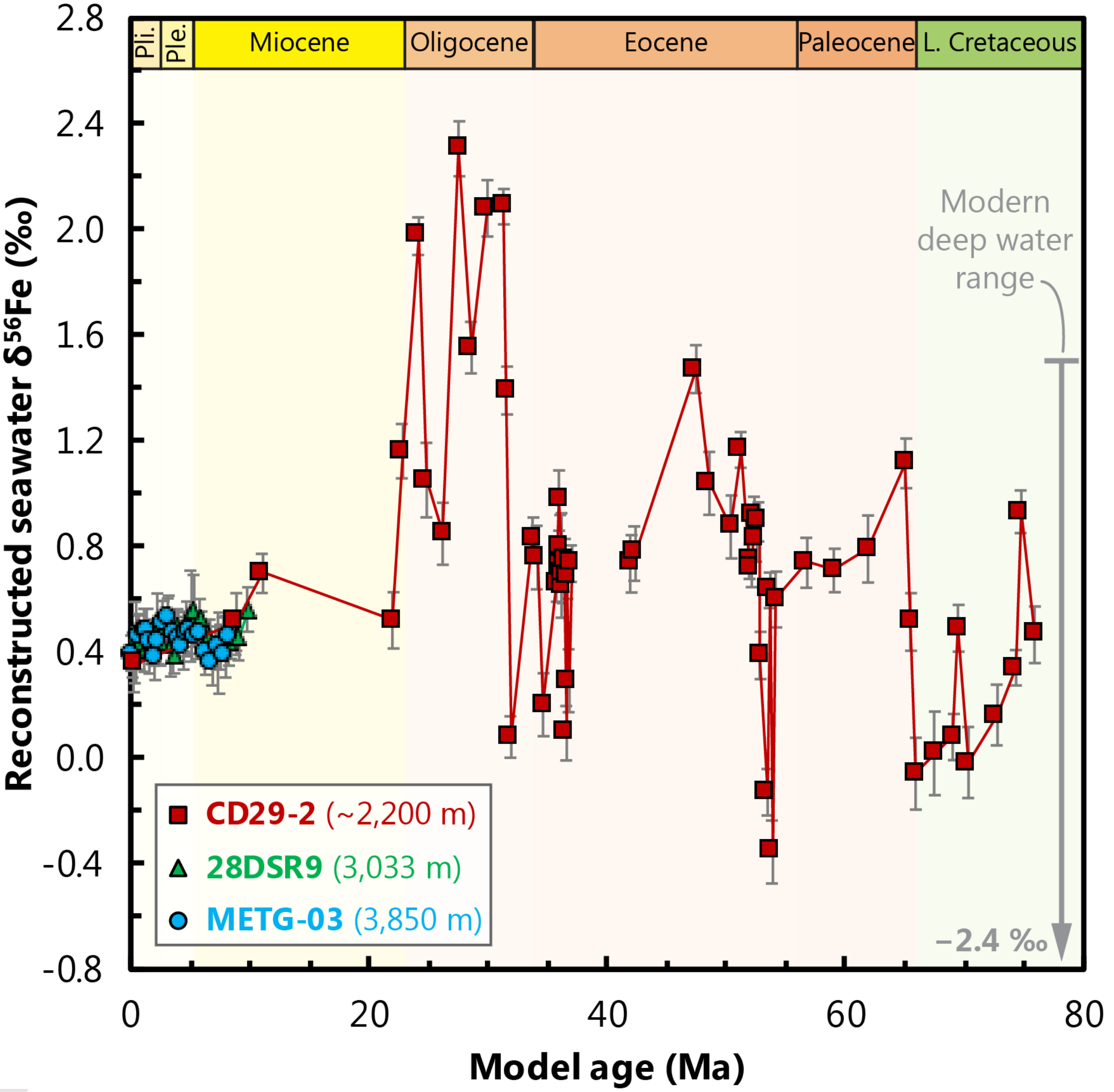

Figure 8 | Ferromanganese crust records of central Pacific δ^{56}Fe since the Late Cretaceous. Records from CD29-2, 28DSR9, and METG-03 from Horner et al. (2015b), Chu et al. (2006) and Liu et al. (2020), respectively. The record from CD29-2 was interpreted by Horner et al. (2015b) as evidencing the importance of deep (non-eolian) Fe sources to central Pacific Fe budgets throughout much of the Cenozoic and Late Cretaceous. In contrast, the δ^{56}Fe recorded by three central Pacific Fe–Mn crusts have been similar since the late Miocene, consistent with a regional Fe source derived largely from non-reductive sediment dissolution and/or eolian deposition.

3.4. Prospects

While the marine Fe cycle is complex, Fe isotopes are proving to be a valuable tool for untangling the many processes that are involved. Detailed study of the Fe cycle reveals that it is driven by a multitude of biological, physical and chemical processes, amongst which productivity is but one small part. In our view, this means that there is no clear path to using δ^{56}Fe as a paleoproductivity tracer. However, this does not preclude δ^{56}Fe from emerging as a powerful tracer for studying the dynamics of the Fe cycle in the modern and paleo oceans. Such a tracer would be especially powerful given the proximal connection between Fe supply and the biological productivity of the ocean.

Exploiting δ^{56}Fe will require resolving and refining several ambiguities. First, there is a clear need to better constrain the Fe isotope fractionation factor associated with biological uptake (in variable conditions and from different species) and to diagnose locations where dissolved δ^{56}Fe is most affected by productivity. Second, the fractionation factors for remineralization and scavenging are essentially unknown, though field data suggests that the net result of these effects is relatively small (e.g., Radic et al., 2011; Labutut et al., 2104). Constraining these fractionation factors will be particularly important for developing novel archives of the paleo Fe cycle, such as pelagic clays (e.g., Dunlea et al., 2021). Third, any sedimentary reconstruction of past Fe isotope chemistry will need to consider the high degree of spatial variability in modern δ^{56}Fe. This will necessitate spatially distributed core sampling, similar to the approach used to constrain basin-scale patterns of dust deposition over glacial–interglacial timescales (e.g., Costa et al., 2016; Winckler et al., 2016). Addressing these priorities will provide valuable constraints on the extent to which the Fe cycle has influenced primary productivity over recent geological history, and provide key insights into the potential sensitivity of Earth’s climate to perturbations in marine trace element cycles.

4. Zinc

After Fe, Zn is the second most abundant transition metal in marine phytoplankton (e.g., Twining & Baines, 2013) and is involved in many cellular processes ranging from RNA synthesis to nutrient acquisition (e.g., Maret, 2001). Consistent with its importance to organisms, [Zn] exhibits a nutrient-type distribution in the ocean most similar to that of [Si] (e.g., Bruland et al., 1978). Additionally, there are some sedimentary archives that faithfully capture variations in ambient [Zn], particularly for the deep ocean (e.g., Marchitto et al., 2000). In contrast, there remains considerable debate surrounding the influence of biological productivity on dissolved δ^{66}Zn compared to other processes such as scavenging, ligand binding, non-productivity sinks, and anthropogenic contamination. This complexity prevents the simple modelling of Zn uptake via a simple reactor framework (as outlined in Sec. 2.2.1.), and at present, it seems unlikely that there is a direct link between δ^{66}Zn and paleoproductivity. That said, there are a number of promising sedimentary archives of past seawater δ^{66}Zn that may inform on the myriad other processes that cycle Zn in seawater.

4.1. Marine distribution

Typical surface ocean [Zn] are 0.01 to 0.5 nmol kg^{-1}, compared to deep water [Zn] of ~2.5 nmol kg^{-1} in the north Atlantic and ~10 nmol kg^{-1} in the north Pacific (Fig. 9). The [Zn] distribution in the ocean closely follows that of the macronutrient Si (Bruland, 1980), at least partially due to the similar behaviour of both elements in the Southern Ocean (Vance et al., 2017; de Souza et al., 2018; Weber et al., 2018; Roshan et al., 2018; Middag et al., 2019). The largest decouplings of [Zn] from [Si] are observed in regions remote from Southern Ocean influence, such as the North Pacific (Janssen & Cullen, 2015; Vance et al., 2019) or North Atlantic (Conway and John, 2014b).

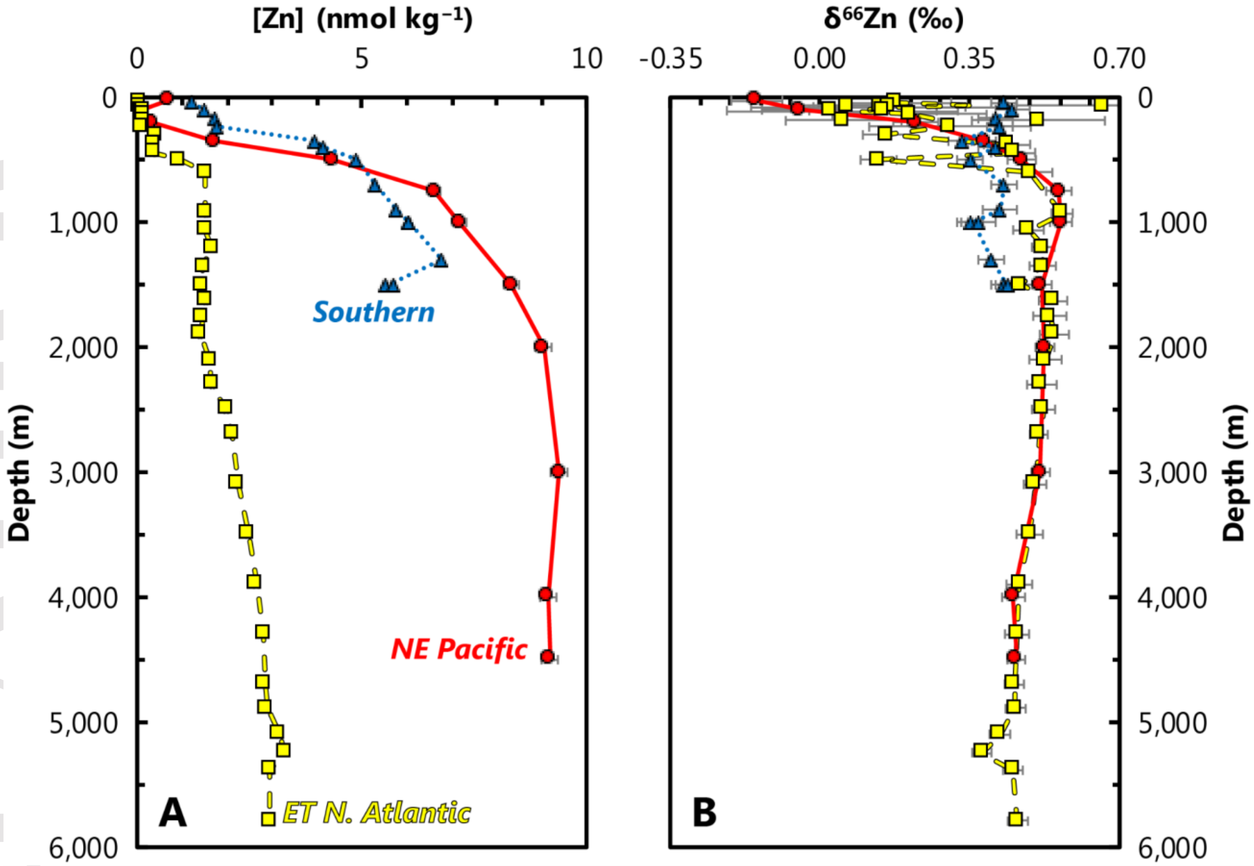

Figure 9 | Representative profiles of dissolved Zn concentrations ([Zn]; A) and Zn isotopic compositions (δ^{66}Zn; B). Data from the Eastern Tropical North Atlantic (squares, dashed line; Conway & John, 2014b), Northeast Pacific (circles, solid line; Conway & John, 2015a) and Southern Oceans (triangles, dotted line; Wang et al., 2019a). Station locations as per Fig. 1. This comparison illustrates that despite possessing distinct dissolved concentration profiles, the isotopic behavior of Zn is similar between basins.

Given the apparent importance of biological uptake to [Zn] distributions, it was initially expected that Zn isotope ratios would be similarly sensitive to biological processes. Indeed, culture studies consistently showed that phytoplankton assimilated isotopically light Zn from their environment (e.g., John et al., 2007; Köbberich and Vance, 2017; Samanta et al., 2018). It was therefore expected that dissolved profiles of δ^{66}Zn would exhibit similar features to those of the macronutrients (e.g., δ^{13}C, δ^{15}N, δ^{30}Si; Farmer et al., *this issue*) and certain micronutrient metals (e.g., δ^{114}Cd, δ^{138}Ba; Secs. 6., 8.), whereby Zn-depleted surface waters would exhibit isotopically heavy compositions relative to deeper waters. In contrast, the first Zn isotope profile for seawater, obtained by Bermin et al. (2006) in the northeast Pacific, showed that surface and deep waters exhibited Zn isotope equivalence, with a slight decrease in δ^{66}Zn just below the euphotic zone. Recent methodological improvements (e.g., Conway et al., 2013; Takano et al., 2017) have permitted investigation of this surprising pattern in detail for a number of ocean basins.

A consistent picture of the distribution of δ^{66}Zn in the ocean has since emerged. The deep ocean is almost homogeneous, with a δ^{66}Zn of about +0.45 ‰ (Fig. 9; Conway & John, 2014b; Zhao et al., 2014; Conway & John, 2015a; Samanta et al., 2017; Takano et al., 2017; John et al., 2018b; Wang et al., 2019a; Vance et al., 2019; Sieber et al., 2020; Liao et al., 2020; Lemaitre et al., 2020). The deep ocean is thus slightly isotopically heavier than the upper continental crust (UCC), which possesses δ^{66}Zn =+0.3 ‰ (Moynier et al., 2017). We note that Zn isotope data are reported relative to JMC-Lyon, though since this standard is now exhausted, most data are measured relative to AA-ETH or IRMM-3702 and reported relative to JMC-Lyon by means of a fixed offset of ≈0.3‰ (see Moeller et al., 2006; Archer et al., 2017).

Though most of the deep ocean is characterized by δ^{66}Zn = +0.45 ‰, there are some deviations to values as light as −0.2 ‰ close to Zn point sources, such as margin sediments or hydrothermal vents (Conway and John; 2014b; Lemaitre et al., 2020). In the surface, while heavy δ^{66}Zn isotope compositions have been observed, this pattern is not seen everywhere; the upper water column for Zn is often isotopically lighter compared with deeper samples or, in the Southern Ocean and North Pacific, only very slightly fractionated towards heavier values (Conway & John, 2014b; 2015a; Zhao et al., 2014; Samanta et al., 2017; Takano et al., 2017; Wang et al., 2019a; Sieber et al., 2020; Vance et al., 2019; Liao et al., 2020; Lemaitre et al., 2020). Thus, despite the nutrient-like distribution of Zn, the lack of consistent covariation between [Zn] and dissolved δ^{66}Zn precludes the use of the isotope reactor framework outlined in Sec. 2.2. Possible reasons for the lack of 'heavy' surface δ^{66}Zn are discussed in the next section, and include: preferential scavenging of isotopically heavy Zn on particle surfaces (e.g., John & Conway, 2014; Weber et al., 2018) and pervasive isotopically light sources of Zn to the surface ocean, possibly from shallow remineralization of organic material (Samanta et al., 2017; Vance et al., 2019) or from anthropogenic aerosols (Liao et al., 2020; Lemaitre et al., 2020). Given these complexities, we believe it will be extremely challenging to use Zn isotopes as a paleoproductivity proxy.

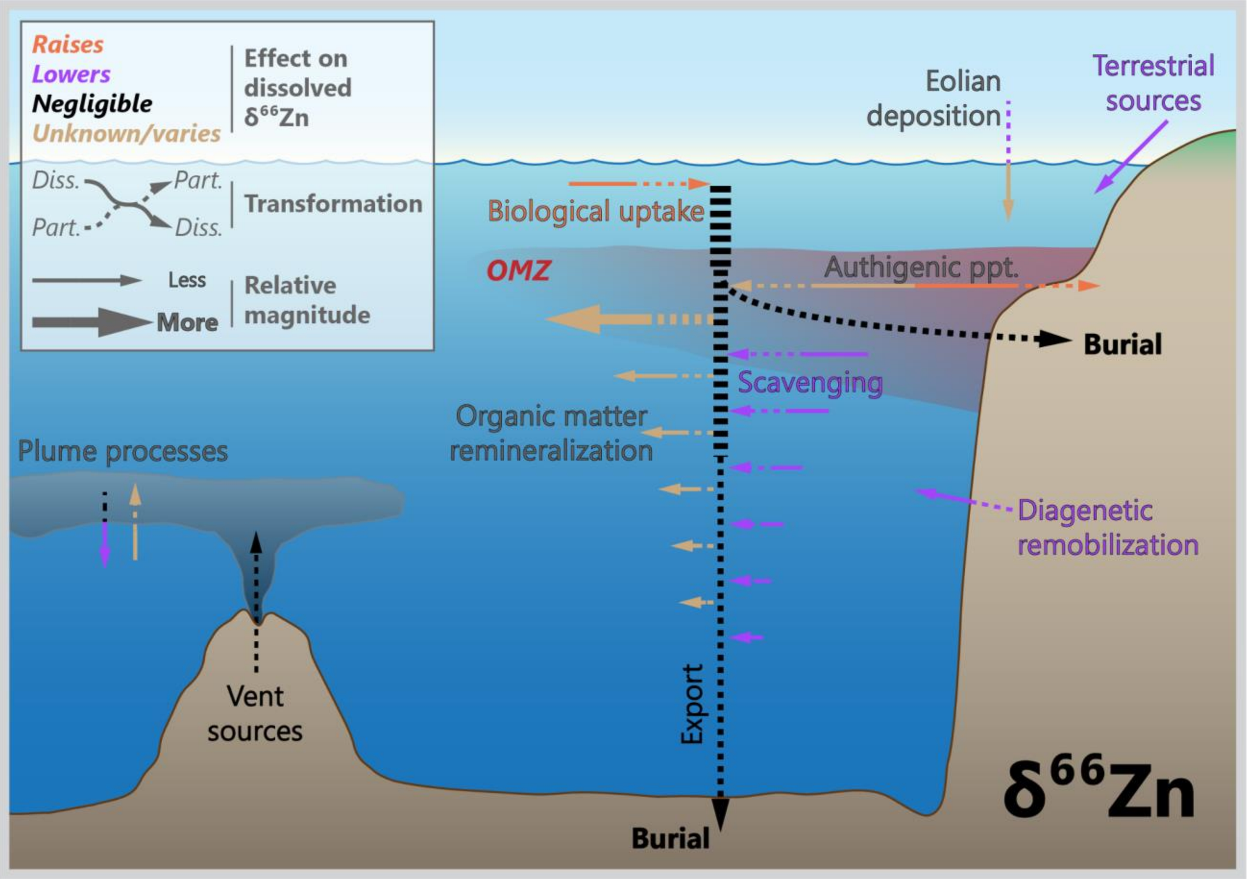

Figure 10 | Processes driving Zn isotope variations in modern seawater. Though biological processes are capable of influencing dissolved δ^{66}Zn, they do not appear to be the dominant driver of Zn isotope variations in the marine realm.

4.2. Driving processes

4.2.1. Biological

Zinc is a metal center in two key enzymes: carbonic anhydrase, necessary for carbon fixation, and alkaline phosphatase, necessary for dissolved organic phosphorus uptake by marine organisms (Morel et al., 1994; Shaked et al., 2006; reviewed by Sinoir et al., 2012). Zinc also has an array of other physiological roles in marine organisms, as exemplified by the observation that Zn contents of phytoplankton cells are of similar magnitude to the micronutrient Fe (Twining & Baines, 2013).

Zinc can be growth-limiting for phytoplankton grown in culture (Anderson et al., 1978; Brand et al., 1983; Morel et al., 1994), but Zn colimitation (with Fe, Co) has only rarely been observed in the open ocean (e.g., Coale, 1991; Coale et al., 2003; Franck et al., 2003; Ellwood, 2004; Lohan et al., 2005; Chappell et al., 2016). This difference between culture and field may reflect the ability of some phytoplankton to substitute

Cd or Co for Zn in some enzyme systems when ambient [Zn] is low (e.g., Morel et al., 1994; Lee & Morel, 1995; Yee & Morel, 1996; Kellogg et al., 2020). Nevertheless, Zn availability has been shown to influence species composition and phytoplankton growth, including rates of calcification and alkaline phosphatase activity (Sunda & Huntsman, 1995; Crawford et al., 2003; Schulz et al., 2004; Shaked et al., 2006; Mahaffey et al., 2014). In culture, phytoplankton biomass is typically enriched in the light isotopes of Zn (John et al., 2007; Köbberich and Vance, 2017; 2019; Samanta et al., 2018). Rather than reflecting a kinetic isotope effect expressed during uptake, it has been suggested that Zn speciation in the media controls cellular δ^{66}Zn; specifically, strong organic ligands present in the growth media, such as ethylenediaminetetraacetic acid, preferentially complex heavy Zn isotopes, rendering the bioavailable Zn pool isotopically light (Fig. 10; John et al., 2007; Köbberich and Vance, 2017; 2019). An analogous process has also been suggested to occur between bioavailable Zn and that bound by natural organic ligands in the surface ocean, though this remains to be proven.

4.2.2. Chemical

Like most bioessential metals, Zn bioavailability is dictated by its chemical speciation (e.g., Anderson et al., 1978), which is dominated in the ocean by complexation to strong (K' ~ 10^9 – 10^{11}) organic ligands (Bruland, 1989; Donat & Bruland, 1990; Ellwood & Van Den Berg, 2000; Jakuba et al., 2012; Kim et al., 2015). Inorganic Zn is considered to make up <5% of the total Zn pool in most ocean regions, with the exception of the Southern Ocean, where strong upwelling of nutrient-rich deep waters leads to [Zn] in excess of complexing ligands (Baars & Croot, 2011). Note that while strongly complexed Zn is unlikely to be bioavailable, the presence of 'weak' ligands (or more labile ligands) can enhance Zn uptake (Aristilde & Xu, 2012). As noted above, the role of the diversity of organic (and inorganic) Zn-binding ligands in determining dissolved and particulate δ^{66}Zn values remains to be fully evaluated.

A role for scavenging in the marine cycling of [Zn] and Zn isotopes has been widely cited but remains under debate (Fig. 10; e.g., John & Conway, 2014; Weber et al., 2018; Roshan et al., 2018; Liao et al., 2020). It is argued that scavenging can explain both the widespread observation of isotopically light Zn in the upper ocean, via preferential removal of heavy Zn isotopes on particles (and release at depth), and also explain the elevated concentration of Zn in the deep Pacific compared to that supplied in southern-sourced deep waters (Fig. 9; Weber et al., 2018; Roshan et al., 2018). Indeed, Weber et al. (2018) propose that the light Zn isotope compositions exhibited by phytoplankton are a result of scavenging removing isotopically heavy Zn from surface seawater, leaving the residual bioavailable Zn pool isotopically light.

Basin-scale elevated [Zn] in the deep Pacific has also been attributed to additional Zn inputs, particularly from hydrothermalism (Roshan et al., 2018), which possesses δ^{66}Zn < +0.45 ‰ (John et al., 2018b). Likewise, local- and regional-scale deviations towards lighter δ^{66}Zn in the deep Atlantic and Pacific are attributed to sedimentary (Conway & John, 2014b; John et al., 2017; Liao et al., 2020; Lemaitre et al., 2020) and hydrothermal inputs (Conway & John, 2014b; John et al., 2018b; Lemaitre et al., 2020). Anthropogenic aerosol deposition is thought to supply significant Zn to regions of the surface ocean (e.g., Liao & Ho, 2018), with possible direct and indirect (via scavenging) regional impacts on upper ocean δ^{66}Zn values (Liao et al., 2020; Lemaitre et al., 2020).

Lastly, Janssen & Cullen (2015) suggest that decoupling of [Zn] and [Si] in the northeast Pacific reflects the formation of Zn sulfides within the North Pacific OMZ, directly equivalent to proposed Cd sulfide precipitation; this hypothesis is discussed in more detail in Sec. 5.2.3. To date, however, there remains scant evidence for water column Zn-sulfide precipitation in OMZs (e.g., Conway & John, 2014b; John et al., 2018b; Vance et al., 2019), with the patterns described by Janssen & Cullen alternatively attributed to shallower remineralisation of Zn (from organic 'soft parts') relative to Si (from opal; Vance et al., 2019). That said, Zn-sulfide precipitation is undoubtedly important in euxinic basins such as the Black Sea and Cariaco Basin (Vance et al., 2016; Isson et al., 2018), and has been postulated to occur within the porewaters of oxygen deficient, organic-rich sediments (Sec. 4.3.4.; Little et al., 2016).

4.2.3. Physical

In common with many of the trace metal isotope systems discussed here, the physical ocean circulation exerts a first order control on the distribution of [Zn] and dissolved δ^{66}Zn compositions (Vance et al., 2017; de Souza et al., 2018; Weber et al., 2018; Sieber et al., 2020). Subantarctic water masses have distinctive and low [Zn]:[PO_4^{3-}] and [Si]:[PO_4^{3-}] ratios, due to the elevated uptake of Zn and Si by diatoms in the surface Southern Ocean (Sarmiento et al., 2004; Vance et al., 2017). Remineralization of these Zn- and Si-rich diatoms at depth imprints a correspondingly high [Zn]:[PO_4^{3-}] and high [S]i:[PO_4^{3-}] fingerprint on Antarctic bottom waters. This coupling of [Zn] and [Si] in the Southern Ocean forms the basis of the global [Zn]:[Si] correlation via the advection of southern sourced water masses towards the low latitudes, where they fill much of the ocean interior (de Souza et al., 2012; Holzer et al., 2014). The homogeneity of deep ocean dissolved Zn isotope compositions reflects the limited degree of Zn isotope fractionation on uptake by Southern Ocean diatoms (Zhao et al., 2014; Wang et al., 2019a), which results in intermediate and deep southern-sourced water masses with limited or no Zn isotope contrast (Sieber et al., 2020). Although exceptions exist (see Section 4.2.2.), generally, the oceanic [Zn]:[Si] correlation persists despite shallower remineralization of Zn relative to Si (Twining et al., 2014), and is especially clear in the South Atlantic, underlining that the mixing of water masses acts as the dominant control on [Zn] (Vance et al., 2017; de Souza et al., 2018; Middag et al., 2019). While Weber et al. (2018) concur with these other studies about the dominant importance of ocean circulation on setting [Zn] and [Zn]:[Si] distributions, they also argue that reversible scavenging is needed to fully explain the observed global patterns. Further, any Zn addition from hydrothermal vents or sediments will also be superimposed on the circulation pattern, adding further complexity to the [Zn]:[Si] relationship (Sec. 4.2.2.).

4.3. Sedimentary archives

4.3.1. Ferromanganese sediments

Manganese oxides are strong sorbents of positively charged, divalent trace metals, due to their negative layer charge at the pH of natural waters (e.g., Koschinsky & Halbach, 1995). The phyllomanganate birnessite is the main Mn- and TE-bearing phase in oxic marine sediments (e.g., Koschinsky and Hein, 2003), as well as for several elements described here, including Zn, Cu, Ni, Cd, and Mo (though Mo exists in seawater as the molybdate anion). Ferromanganese crusts and nodules incorporate TEs during growth, leading to 10^6-fold enrichments compared to seawater concentrations (e.g., Arrhenius, 1963; Aplin and Cronan, 1985). As a result, Fe–Mn sediments are often one of the first marine sediment types to be targeted in the development of a new metal isotope tracer.

In the case of Zn, Fe–Mn crusts and nodules are isotopically heavy compared to seawater (≈ +0.45‰), exhibiting compositions between +0.9 to +1 ‰ (Fig. 11; Maréchal et al., 2000; Little et al., 2014a). The heavy signature is broadly consistent with inorganic sorption experiments of Zn on birnessite, with experiments at high ionic strength yielding $\Delta^{66}\mathrm{Zn}_{\text{sorbed-aqueous}}$ (where $\Delta^{66}\mathrm{Zn}_{\text{sorbed-aqueous}} = \delta^{66}\mathrm{Zn}_{\text{sorbed}} - \delta^{66}\mathrm{Zn}_{\text{aqueous}}$) of +0.16 to +2.7‰ (Bryan et al., 2015). The magnitude of fractionation observed in experiments is typically considerably larger than in natural Fe–Mn crusts and nodules, which Bryan et al. (2015) suggest may reflect sorption of Zn on birnessite via two different molecular mechanisms, each associated with different isotopic fractionation factors, as is the case for thallium (e.g., Nielsen et al., 2013). In addition, the influence of organic and inorganic speciation of Zn in seawater may play a role, though this remains to be fully evaluated (e.g., Little et al., 2014b).

Little et al. (2014a) observed no marked temporal changes in δ^{66}Zn values for three Fe–Mn crusts from each of the major ocean basins over the last ~20 Ma. Zinc is somewhat immobile in Fe–Mn crusts, with a calculated effective diffusivity $<10^{-8}$ cm^2 yr^{-1}, similar to Hf (Henderson & Burton, 1999) and Ba (Sec. 8.3.).

Assuming that Fe–Mn crusts preserve primary δ^{66}Zn, the various records suggest that on a global basis, the marine Zn cycle has been in isotopic steady state for at least 20 Myr (Fig. 11).

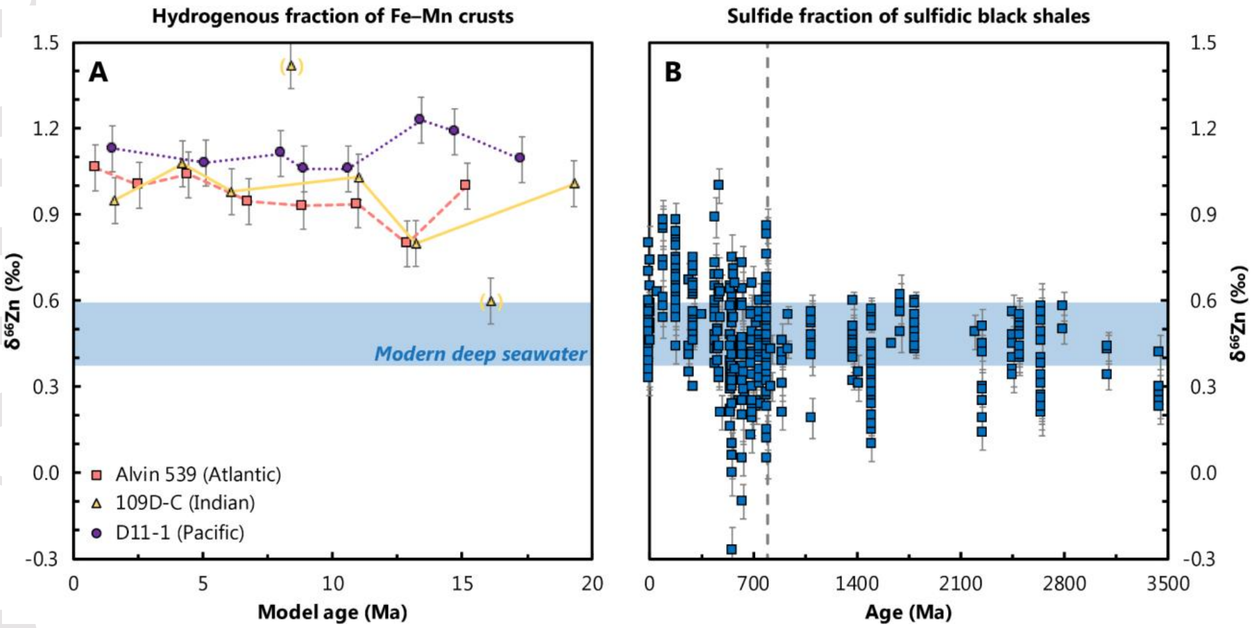

Figure 11 | Records of deep ocean δ^{66}Zn through time. A Three records from Fe–Mn crusts recovered from the Atlantic (square, dashed line), Indian (triangle, solid line), and Pacific Oceans (circle, dotted line; Little et al., 2014b). Assuming the isotopic offset between dissolved Zn in seawater and Fe–Mn crusts has remained unchanged at ≈0.55 ‰ over this interval, these records imply only minimal Zn isotope variations in the deep ocean over the past ~20 Myr. Two anomalous measurements from 109D-C (in parentheses) possess low levels of authigenic Zn enrichment, indicative of detrital contamination. **B** Records recovered from the sulfide fraction of sulfidic black shales over the last 3,500 Myr (Isson et al., 2018). Assuming that sulfidic black shales record ambient seawater with no Zn isotope offset, this record can be interpreted as reflecting deep-ocean δ^{66}Zn over much of Earth's history. The dashed line indicates an apparent reorganization of the marine Zn isotope cycle around 800 Ma, interpreted by Isson et al. (2018) to reflect the rise of eukaryotes to ecological prominence.

4.3.2. Biogenic silica

The correlation of Zn with Si in the modern ocean led to the suggestion that Zn:Si measured in diatom opal may be a proxy for Zn:Si (and thus [Zn]) of past seawater. However, culturing and μ-XRF analyses revealed that only a small fraction (1–3%) of the diatom Zn quota is incorporated into the opal frustules, with the remainder present in the organic 'soft parts' of the diatom cells (Ellwood & Hunter, 2000; Twining et al., 2004). The Zn concentration in opal (Zn_{opal}) also more closely reflects the bioavailable Zn in seawater than ambient Zn:Si (Ellwood & Hunter, 2000). Nevertheless, if the mechanisms of Zn incorporation into biogenic opal can be understood, and calibrated, a Zn:Si proxy of Zn bioavailability could help shed light on micronutrient limitation of the biological pump.

Andersen et al. (2011) analyzed Zn isotopes ($\delta^{66}Zn_{opal}$) and $Zn:Si_{opal}$ in diatom opal isolated from core top sediments from the Southern Ocean. They observed isotopically heavy Zn in opal (at +0.7 to +1.5‰), and an inverse relationship of $\delta^{66}Zn_{opal}$ with $Zn:Si_{opal}$. Consistent with culturing studies, core top $Zn:Si_{opal}$ appears to be linked to bioavailable Zn concentrations in ambient surface seawater. The authors suggested that $\delta^{66}Zn_{opal}$ should also reflect the isotope composition of bioavailable Zn in surface seawater, which, they predicted, should be isotopically heavy due to the predicted preferential incorporation of light isotopes into phytoplankton organic material. In this view, the extent of uptake—nutrient utilization—would be recorded by the systematics of $Zn:Si_{opal}$ and $\delta^{66}Zn_{opal}$. However, this study predated the recent surge in seawater δ^{66}Zn measurements. As discussed above, surface water δ^{66}Zn analyses in the Southern Ocean have not borne out the prediction of isotopically heavy residual surface waters (Fig. 9), with little to no fractionation observed (Zhao et al., 2014; Wang et al., 2019a; Sieber et al., 2020).

Hendry & Andersen (2013) showed that sponge spicules can faithfully record seawater δ^{66}Zn. Sponges are primarily deep-sea organisms. Hence, if we can deconvolve the controls on diatom Zn:Si and $\delta^{66}Zn_{opal}$, a combination of Zn:Si and δ^{66}Zn measurements in diatoms and sponges (as used for Si isotopes, Farmer et al., *this issue*) could provide a strong basis for unravelling the past ocean global Zn cycle, including the role of Southern Ocean processes in the biological carbon pump.

4.3.3. Carbonates

Carbonates may provide an alternative archive for [Zn] (as Zn:Ca) and δ^{66}Zn. For example, Marchitto et al. (2000) showed that Zn:Ca ratios in benthic foraminifera are sensitive to bottom water dissolved [Zn]. However, the Zn content in individual microfossil shells is extremely low (typically <0.1 ng); at this level, with current analytical capabilities and blank contributions, many tens to hundreds of benthic foraminifera would be required for a single Zn isotope measurement.

To circumvent the issue of low Zn contents of individual shells, Pichat et al. (2003) utilized a selective carbonate dissolution procedure on bulk sediment from the equatorial Pacific, mostly consisting of coccoliths. These authors argued that isotopically heavy δ^{66}Zn in carbonates reflected surface seawater, with values modulated by changes in biological productivity due to varying seasonal insolation. Similarly isotopically heavy Zn in ancient carbonates has also been argued to reflect strong biological utilization in surface waters (Kunzmann et al., 2013; cf. John et al., 2017; Liu et al., 2017). More recently, Zhao et al. (2021) surveyed carbonates from the Great Bahama Bank, observing carbonate-bound δ^{66}Zn ranging from ≈−0.5 to +1.1 ‰. Given the local seawater value of ≈+0.1 ‰, this large range is surprising, and implies a number of additional factors that fractionate Zn isotopes during incorporation into and recovery from carbonates. These factors include: stable isotope fractionation during Zn incorporation into $CaCO_3$, contamination from non-$CaCO_3$ phases (e.g., lithogenic or authigenic phases), and methodological issues (e.g., non-quantitative selective leaching leading to stable isotope fractionation; Revels et al., 2015). Regardless, the relationship between bulk carbonate and seawater δ^{66}Zn is not straightforward.

Despite the difficulty in interpreting bulk carbonate δ^{66}Zn, phase-specific (particularly, aragonitic) $CaCO_3$ archives appear more promising. For example, Zhao et al. (2021) identify carbonate ooids as a promising archive of past seawater δ^{66}Zn. Likewise, Little et al. (2017a) showed that deep-sea coral skeletons record intermediate and deep water δ^{66}Zn (e.g., Little et al., 2017a). Given the large size of specimens and their global distribution, combined with the ability to assign precise ages to individual specimens, deep-sea corals may provide an archive of seawater compositions that are amenable to Zn isotope analysis. However, recent Zn isotope studies of shallow-water zooxanthellate corals suggests that the relationship with seawater δ^{66}Zn is complicated by temperature and photosynthetic effects (Ferrier-Pagès et al., 2018; Xiao et al., 2020).

4.3.4. Organic-rich sediments

The isotope composition of Zn in organic-rich sediments deposited along productive continental margins is typically ≈+0.1 ‰, which is lighter than ambient seawater by ≈0.4 ‰ (Little et al., 2016). This light δ^{66}Zn signature likely arises from one of two processes. In the first process, isotopically light Zn is preferentially removed from seawater during precipitation of sulfides (Fujii et al., 2011a; Vance et al., 2016). This precipitation may occur directly from seawater and into sediments, or possibly within reducing microenvironments that develop within particles sinking through low-[O_2] water columns (Janssen & Cullen, 2015; Little et al., 2016; Vance et al., 2016; Bianchi et al., 2018). Regardless, so long as Zn removal is non-quantitative, these processes act to bury isotopically light Zn from the ocean. In the euxinic Black Sea, where Zn drawdown with sulfides is quantitative, sedimentary δ^{66}Zn is expected to reflect the deep seawater composition from above the chemocline (analogous to Mo; Sec. 7; Vance et al., 2016), and euxinic black shales represent a promising archive of past deep seawater δ^{66}Zn. This prediction was confirmed by Isson et al. (2018), who reported that sulfide-bound Zn in black shales from the euxinic Cariaco Basin exhibited the expected deep seawater-like δ^{66}Zn of +0.5±0.1 ‰. Using this calibration, Isson et al. (2018) analyzed δ^{66}Zn in hundreds of euxinic black shales generating a 3,500 Myr record of deep-ocean Zn isotope evolution (Fig. 11B). Though a full discussion of this dataset is beyond the scope of our review, this record reveals a shift in deep ocean δ^{66}Zn around 800 Ma, which Isson et al. (2018) interpret as reflecting a reorganization of the marine Zn cycle driven by the rising ecological prominence of eukaryotes.

A second process that can deliver isotopically light Zn to sediments is organic matter. That is, presuming that phytoplankton assimilate isotopically light Zn from seawater, the export of this organic matter to sediments can bury light Zn in margin settings (Little et al., 2016; John et al., 2017). If dominant, this biologically driven process might suggest some utility for δ^{66}Zn in organic-rich sediments to reconstruct paleoproductivity, especially in low-oxygen settings. Alternatively, if the scavenging-centered view proposed by Weber et al. (2018) is correct, the δ^{66}Zn of exported Zn—while still light relative to deep seawater—would not represent a simple measure of either Zn uptake or primary productivity. This view implies that there would be considerable spatial complexity in the δ^{66}Zn delivered to sediments that depends on factors such as scavenging intensity relative to upwelling, which is not directly linked to biological productivity. Moreover, Weber et al. (2018) even suggest that some regions of the ocean might bury isotopically heavy organic matter-associated Zn, either due to variability in surface water δ^{66}Zn resulting from scavenging, or via burial of isotopically heavy Zn adsorbed to organic matter.

Overall, the uncertainties in Zn delivery mechanisms and the connection between δ^{66}Zn and primary productivity means that there are considerable obstacles to interpreting organic-rich sedimentary δ^{66}Zn as a direct tracer of productivity.

4.4. Prospects

Despite the complexities and remaining unknowns in oceanic δ^{66}Zn cycling reviewed above, we note that there are systematic variations in sedimentary Zn isotope compositions recorded in geologic archives on Myr and Gyr timescales. In addition to the organic sediment record of Isson et al. (2018), described above, Yan et al. (2019) compiled three δ^{66}Zn datasets from contemporaneous Ediacaran (635 Ma, Marinoan) postglacial cap carbonates (Kunzmann et al., 2013; John et al., 2017; Lv et al., 2018), which show systematic changes in Zn isotope compositions over this period of marked global change. Secondly, Sweere et al. (2018) presented data showing marked shifts in carbonate-bound Zn isotope compositions in several geological sections spanning a Cretaceous ocean anoxic event (OAE 2). While there is no consensus on the causes of these intriguing isotopic shifts within carbonates (e.g., the role of redox vs. source/sinks vs. productivity), the coherency of the records is encouraging and their full interpretation awaits identification of the driving processes.

On longer timescales, the importance of Earth's overall redox state on marine Zn isotope systematics requires elucidation. There are several other explanations for the shift in deep-ocean δ^{66}Zn at ≈800 Ma besides a switch to more eukaryotic-dominated oceans, such as changes in Zn speciation, variations in other

Zn sinks, or diagenesis (see Isson et al., 2018); indeed, we are not aware of any studies exploring how primary sedimentary δ^{66}Zn may be modified by diagenetic processes. Moreover, the assumption that the high affinity for Zn exhibited by eukaryotes translates into higher eukaryotic Zn:C (compared to prokaryotes) is not supported by culture data, which showed that cyanobacterial Zn:C is comparable to—or can even exceed that of—eukaryotes grown under the same conditions (Köbberich & Vance, 2019). Thus, developing a more complete interpretation of δ^{66}Zn in the sedimentary record requires building a more complete understanding of the biological and biologically mediated processes cycling δ^{66}Zn in the upper water column.

Lastly, we recommend that future studies target coupled dissolved and particulate phase δ^{66}Zn data, in concert with detailed biological and chemical speciation data. To date, particulate phase δ^{66}Zn data has proven challenging to obtain due to pervasive Zn contamination. Zinc isotope characterization of sediments and sediment porewater is needed to constrain the role of early diagenetic reactions, as well as their importance to the mass balance of Zn isotopes in the ocean. Sediment studies would also benefit from further investigation of whether specific phases offer more robust archives of past seawater δ^{66}Zn, potentially exploiting selective extraction methods. We also recommend revisiting published records in light of recent seawater δ^{66}Zn data.

5. Copper

As with Fe and Zn, Cu is used in a number of cellular processes, most notably electron transport (e.g., Twining & Baines, 2013). Unlike Fe and Zn however, Cu is toxic to phytoplankton, even at extremely low free [Cu^{2+}] (pM; Brand et al., 1996). Dissolved Cu—in seawater and within marine organisms—is thus strongly regulated by organic complexes that maintain low free [Cu^{2+}] (e.g., Moffett & Dupont, 2007; Waldron & Robinson, 2009). Some archives have shown promise for recording aspects of surface and deep ocean δ^{65}Cu, such as organic-rich sediments and authigenic Fe–Mn oxides, respectively. Despite the strong biological control over marine [Cu] distributions, our present understanding of the biogeochemical cycle of Cu suggests there is no clear route to developing [Cu] or δ^{65}Cu as paleoproductivity proxies, and Cu cannot be modeled within the simple reactor framework (Sec. 2.2.). However, there are a number of sensitivities in the marine Cu isotope cycle that are indirectly related to paleoproductivity that may render δ^{65}Cu as a proxy of processes related to metal complexation by organic ligands and/or marine redox evolution.

5.1. Marine distribution

The distribution of Cu in the ocean has been described as 'hybrid-type', because it is intermediate between nutrient- and scavenged-type elements (Bruland & Lohan, 2003). Depth profiles of [Cu] typically show approximately linear increases with depth (e.g., Boyle et al., 1977; Fig. 12A). Surface [Cu] are typically about 0.5 to 1 nmol kg^{-1}, compared to deep Atlantic [Cu] of ~2.5 nmol kg^{-1} and deep Pacific [Cu] of ~4 nmol kg^{-1} (Fig. 12). Unlike the other metals discussed here (with the possible exception of Cr), and despite the existence of a large seawater [Cu] dataset, some discrepancy still exists in the [Cu] measured by different techniques, with methodological details such as storage time, acidification strength, UV oxidation (or not) prior to analysis all thought to be potentially important, and requiring further intercomparison efforts (Posacka et al., 2017). Nevertheless, the [Cu] distribution pattern has been attributed to a combination of biological uptake and remineralization, benthic flux from sediments (e.g., Boyle et al., 1977; Roshan & Wu, 2015a; Little et al., 2018), and/or reversible scavenging (Little et al., 2013; Richon et al., 2019). These processes are superimposed on the first-order distribution established via the physical ocean circulation (Roshan & Wu, 2015a).

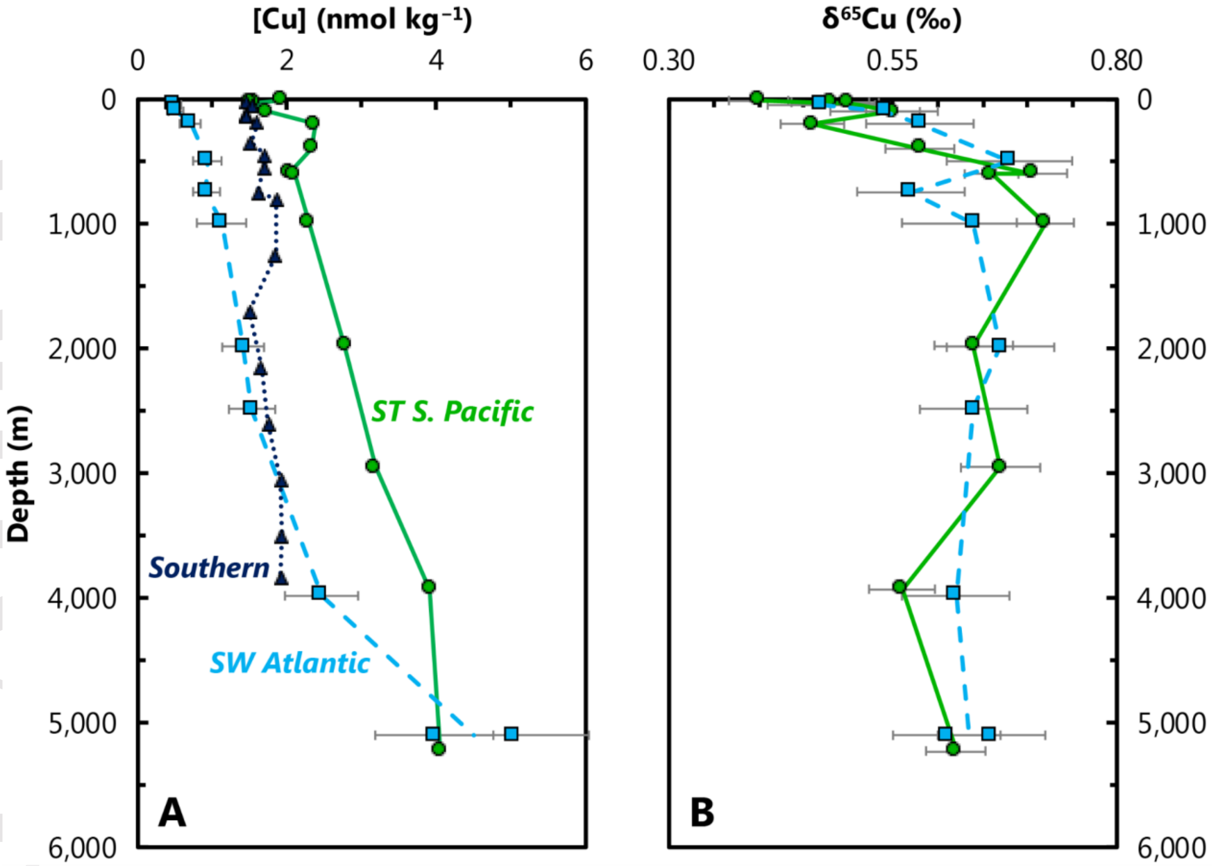

Figure 12 | Representative profiles of dissolved Cu concentrations ([Cu]; A) and Cu isotope compositions (δ^{65}Cu; B). Data from the Southwest Atlantic (squares, dashed line; Little et al., 2018), Subtropical South Pacific (circles, solid line; Takano et al., 2017) and Southern Oceans (triangles, dotted line; Boye et al., 2012). Station locations as per Fig. 1. This comparison illustrates that the isotopic behavior of Cu is similar between basins, reflecting the importance of complexation by strong organic ligands. Note that there are no Cu isotope data available for the Southern Ocean at this time.

Copper isotopes are reported as relative to the NIST SRM 976 standard, though due to a shortage of this material, two other certified reference standards are now available: ERM-AE633 ($\delta^{65}Cu_{SRM976} = -0.01\pm0.05$ ‰) and ERM-AE647 ($\delta^{65}Cu_{SRM976}$ = +0.21±0.05 ‰; Moeller et al., 2012; Moynier et al., 2017). For consistency and ease of comparison, Moynier et al. (2017) recommend that future data be reported relative to NIST SRM 976. We adopt this convention. The analysis of Cu isotopes in seawater is challenging, due to both Cu's strong organic complexation, and only two isotopes precluding the use of a double spike technique (reviewed in Little et al., 2018). The data presented to date indicate that deep seawater δ^{65}Cu values are isotopically heavy (at about +0.7 ‰; Fig. 12B) compared to the upper continental crust (UCC; at about +0.1 ‰; Table 1; Moynier et al., 2017). Lighter Cu isotope compositions in the upper water column and along margins are thought to reflect local sources of isotopically light Cu (e.g., aerosols, riverine particulates, sediments; Takano et al., 2014; Little et al., 2018). While sample treatment may be a concern for quantitative [Cu] measurements (Posacka et al, 2017), it remains unclear to what extent this might also be an issue for measurements of δ^{65}Cu made using different techniques, depending on storage time, acidification and oxidation with UV or H_2O_2 prior to analysis (see discussion in Little et al 2018). Reassuringly, however, Little *et al*. did note that despite potential underestimation of [Cu] by some methods, a general homogeneity of seawater δ^{65}Cu persists between labs and geographic location and depth of samples (Little et al., 2018; Yang et al., 2020; Fig. 12). As such, the expected methodological effects of incomplete Cu recovery on δ^{65}Cu may be slight, though it remains unclear how the size of this effect might vary with sample location and oceanographic conditions (e.g., surface or low [O_2]). As the seawater δ^{65}Cu dataset continues to grow, we echo the calls of previous authors that further urgent intercalibration of methods is needed (e.g., Posacka et al.. 2017; Little et al., 2018; Bacconais et al., 2019).

Figure

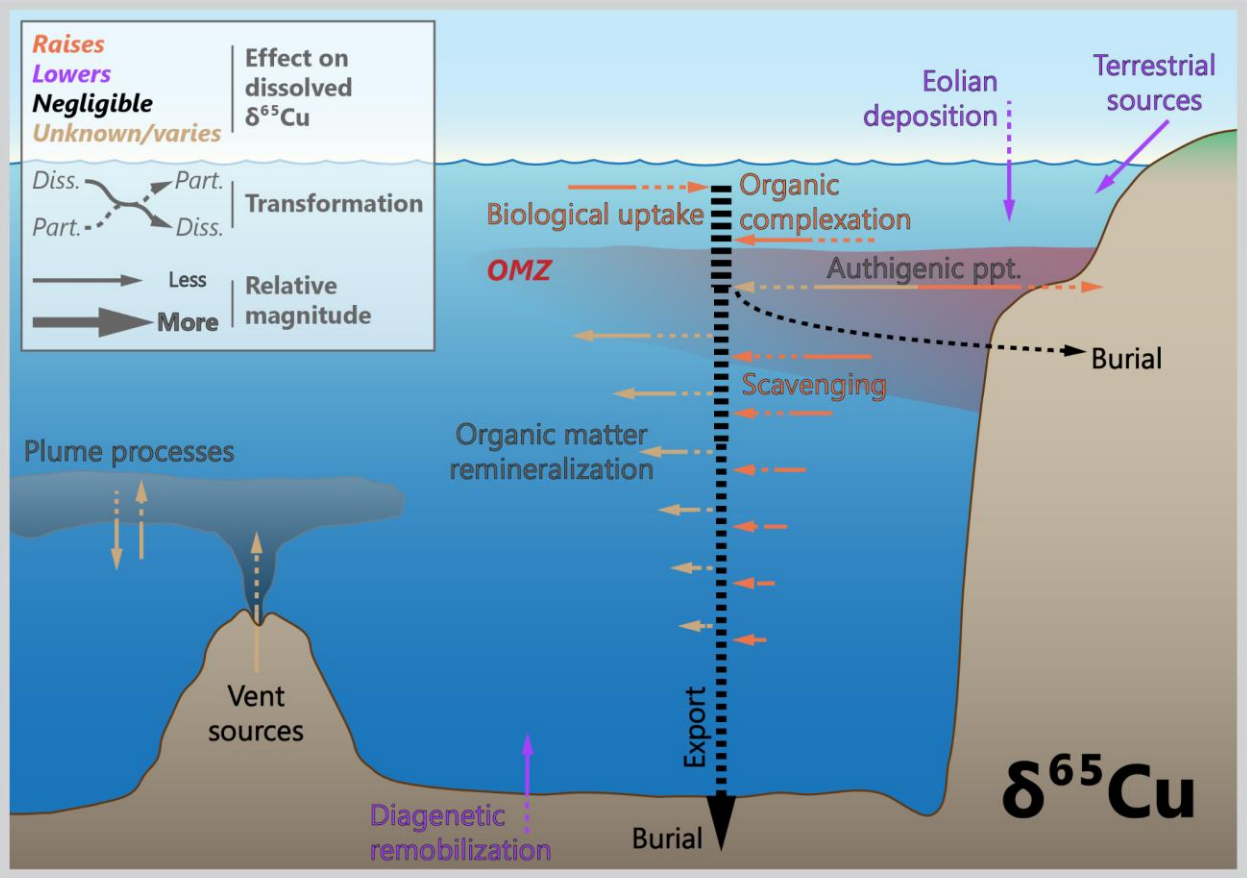

Figure 13 | Processes driving Cu isotope variations in modern seawater. Biological productivity exerts only a modest impact on the marine Cu isotope cycle and thus there is no obvious route to developing Cu isotopes (or Cu concentrations) as a paleoproductivity proxy.

5.2. Driving processes

5.2.1. Biological

Copper is bioessential, but cellular Cu contents are approximately 2–10 fold lower than the micronutrients Fe and Zn (Twining & Baines, 2013). The redox-active behaviour of Cu (existing as Cu^{2+} or Cu^{+} in biological systems) enables its role in electron transport, for example in the Cu-containing proteins plastocyanin and cytochrome c oxidase (Ridge et al., 2008). Copper uptake by some Fe-limited phytoplankton may increase, either due to the replacement of Fe-containing with Cu-containing enzymes (e.g., Peers and Price, 2006), or the involvement of Cu in the high affinity Fe uptake systems (Annett et al., 2008; Maldonado et al., 2006; Guo et al., 2012). Despite its biological function, Cu is also extremely toxic due to the formation of reactive oxygen species, which pose a threat to DNA, lipids, and proteins (Ridge et al., 2008). Copper toxicity thresholds vary by phytoplankton group, with smaller organisms generally more sensitive than larger ones (e.g., cyanobacteria cf. diatoms; Brand et al., 1986), and coastal strains more resistant than open ocean strains (e.g., Peers et al., 2005).

A small number of studies have investigated Cu isotope fractionation during cellular uptake or cell surface adsorption by microorganisms (Pokrovsky et al., 2008; Navarrete et al., 2011; Cadiou et al., 2017; Coutaud et al., 2018; 2019). The results of these experiments are somewhat variable, with enrichment of either light or heavy Cu isotopes observed during assimilation and adsorption. However, assimilation in culture generally favours light Cu isotopes (Navarrete et al., 2011; Cadiou et al., 2017; Fig. 13). The complexity in Cu isotopic behaviour has been attributed to small changes in Cu speciation or redox during uptake and/or release of Cu (Coutaud et al., 2018; 2019).

5.2.2. Chemical

In seawater, the vast majority of Cu is complexed to strong organic ligands (more than 99.8% complexed in surface northeast Pacific), which lower free [Cu^{2+}] to below toxic levels (e.g., Coale & Bruland, 1988; 1990; Moffett & Dupont, 2007). It is thought that ligands are primarily produced by biota for the purpose of detoxification (e.g., Moffett et al., 1990; Moffett & Brand, 1996), although recent work suggests that strongly complexed Cu is bioavailable to some eukaryotes, which appear to have a higher cellular Cu requirement (and higher thresholds of Cu toxicity) than prokaryotes (Semeniuk et al., 2009; 2015).

Both theory and experiments predict preferential complexation of heavy isotopes by strong organic ligands (Sherman, 2013; Fujii et al., 2013; Ryan et al., 2014; Sherman et al., 2015), and organic complexation is thought to play a key role in the modern oceanic budget and distribution of Cu isotopes (Vance et al., 2008; Little et al., 2014a; Thompson & Ellwood, 2014; Takano et al., 2014; Little et al., 2018). The small pool of non-complexed Cu^{2+} in seawater is thus expected to be isotopically light (e.g., Little et al., 2014b, 2018).

Based on a surface complexation model with the phyllomanganate birnessite, the principal scavenging phase of divalent trace metals in oxic sediments, Sherman & Peacock (2010) calculated that [Cu] in deep waters should be orders of magnitude lower than is actually observed. They attribute this difference to the chelation of "*essentially all dissolved Cu*" by organic ligands (Sherman & Peacock, 2010), consistent with observations (e.g., Moffett & Dupont, 2007; Heller & Croot, 2015; Jacquot & Moffett, 2015). Nevertheless, some form or forms of scavenging are also thought to play a role in the oceanic Cu distribution.

Reversible scavenging, a term used to describe the equilibrium between a scavenged and dissolved metal pool, has been proposed as the driving process behind the generally monotonic, linear increases in [Cu] with depth (Little et al., 2013; Richon et al., 2019; Fig. 12). In some regions with high particulate loads (e.g., some hydrothermal plumes, benthic nepheloid layers), scavenging removal of Cu has been observed (Jacquot and Moffett, 2015; Roshan & Wu, 2015a). Preferential scavenging of light Cu isotopes by particulate (e.g., oxyhydroxide) phases has also been proposed as an explanation for isotopically heavy seawater Cu isotope compositions (e.g., Takano et al., 2014), though the driving mechanisms leading to isotopically light particulate Cu remain to be fully established (see Sec. 5.3; Fig. 13).

The shorter residence time of Cu (2-3.3 kyr; Little et al., 2017b), compared to trace metals with longer residence times (e.g., Cd, Zn, Ni), mean that, as for Fe, regional and local sources of Cu to the ocean play a relatively larger role in determining [Cu] distributions than for some other metals. Sources of Cu include aerosols (both natural and anthropogenic; e.g., Takano et al., 2014; Yang et al., 2019), benthic fluxes from sediments (e.g., Boyle et al., 1977; Heller & Croot, 2015; Roshan & Wu, 2015a; Little et al., 2018), and dissolved or particulate riverine sources (e.g., Vance et al., 2008; Little et al., 2018; Richon et al., 2019; Fig. 13). A possible small hydrothermal source has been identified in the South Pacific from the East Pacific Rise (Roshan & Wu, 2018), which is in contrast to the scavenging removal of Cu observed around hydrothermal vents elsewhere (e.g., Jacquot and Moffett, 2015).

5.2.3. Physical

Copper's shorter residence time relative to Cd, Zn and Ni also means that the Southern Ocean and wider physical ocean circulation play a somewhat smaller role in oceanic [Cu] and δ^{65}Cu distributions compared to many of the other bioactive trace metals discussed herein. Nonetheless, the imprint of circulation is evident in certain circumstances, such as in the Atlantic and the upper 2 km of the South Pacific where [Cu] is correlated with [Si] (Roshan & Wu, 2015a; 2018; Little et al., 2018).

5.3. Marine archives

5.3.1. Ferromanganese sediments

Ferromanganese sediments (crusts and nodules) exhibit Cu isotope compositions of +0.3 to +0.5 ‰ (Albarède, 2004; Little et al., 2014). This means that, on average, Fe–Mn sediments are approximately 0.35 ‰ lighter than deep seawater, which averages +0.7 ‰ (Fig. 14). The explanation for this offset is uncertain, but may reflect either strong organic complexation of Cu in seawater (Little et al., 2014b), or the enrichment of light Cu isotopes on the birnessite mineral surface. The latter has been observed in inorganic experiments, whereby sorbed Cu exhibited δ^{65}Cu that was 0.45±0.18 ‰ lower than δ^{65}Cu in solution (Ijichi et al., 2018). Consistent with these experiments, light isotope fractionation on sorption of Cu to birnessite has also been predicted from first-principles *ab initio* calculations (Sherman and Little, 2020). At equilibrium in seawater, however, the strong complexation and mineral sorption effects should be additive, leading to a much larger isotopic offset than the ~0.35 ‰ observed, suggesting that one of the two effects is not expressed in nature for reasons as yet unclear (Sherman and Little, 2020).

Little et al. (2014a) observed no marked changes in deep ocean δ^{65}Cu recovered from three Fe–Mn crusts from each of the major ocean basins over the last ~20 Ma. Copper is relatively immobile in Fe–Mn crusts, with a calculated effective diffusivity $\leq 10^{-9}$ cm^2 yr^{-1} (Henderson & Burton, 1999), similar to Ni (Sec. 9.3.1.). Assuming that Fe–Mn crusts preserve primary δ^{65}Cu, the various records suggest that on a global basis, the marine Cu cycle has been in isotopic steady state for at least 20 Myr (Fig. 14).

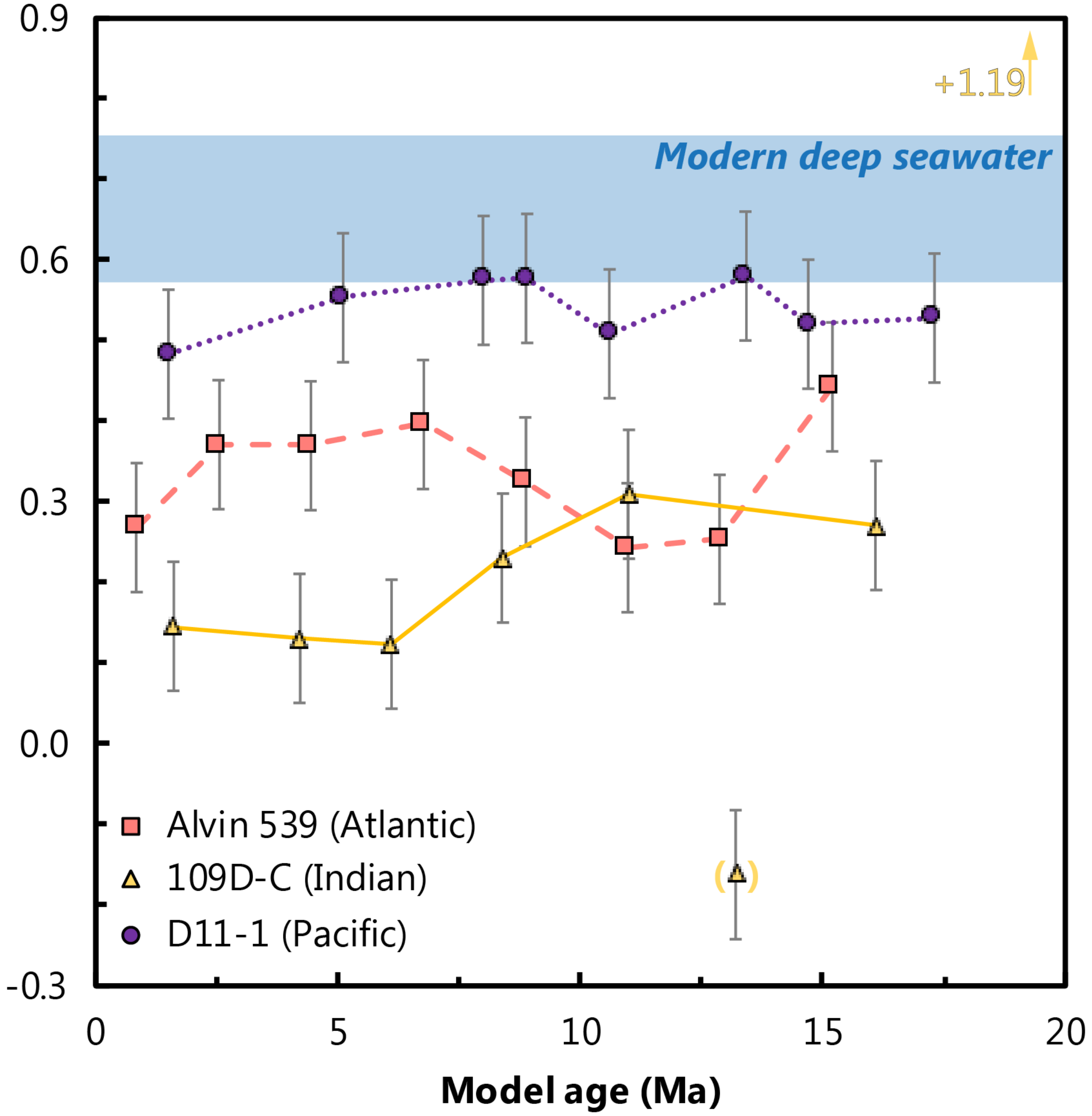

Figure 14 | Deep ocean δ^{65}Cu constancy over the past 20 Myr. These records are derived from Fe–Mn crusts recovered from the Atlantic (square, dashed line), Indian (triangle, solid line), and Pacific Oceans (circle, dotted line; data from Little et al., 2014b). Assuming the isotopic offset between dissolved Cu in seawater and Fe–Mn crusts has remained unchanged at ≈0.35 ‰ over this time, these records imply that the inter-basin Cu isotope variations observed in modern crusts and the Cu isotope cycle itself have remained relatively stable for at least 20 Myr. Two samples from 109D-C possess low levels of authigenic Cu enrichment indicating detrital contamination (parentheses, arrow; see Little et al., 2014b).

5.3.2. Organic-rich sediments

Qualitative arguments for high organic matter fluxes (i.e., higher paleoproductivity) have been made based on elevated Cu (and Ni) contents of ancient organic-rich sediments (e.g., Tribovillard et al., 2006). This approach is supported by positive correlations between Cu (and Ni, Sec. 9.3.2.) with TOC content in modern continental margin sediments (e.g., Böning et al., 2012). For this approach to offer mechanistic insights into past export productivity, organic matter (or a biologically associated mineral phase, such as $CaCO_3$ or $BaSO_4$), must be the primary vector for that metal to sediments. This condition is not met for Cu, nor for other chalcophile elements (e.g., Mo), thus presenting a significant challenge to the use of sediment Cu content to trace past export productivity. Copper exhibits a strong reactivity toward sulfide, as illustrated by the quantitative removal of Cu from the euxinic Black Sea water column and resultant enrichment in underlying sediments (Tankéré et al., 2001; Little et al., 2015).

Despite the strong reactivity of Cu towards sulfide, and unlike Zn (Sec. 4.3.4.) and Mo (Sec 7.2.3.), Cu in euxinic sediments from the Black Sea and Cariaco Basin do not record open marine $\delta^{65}Cu$ (Little et al., 2017b). In fact, authigenic Cu in modern organic-rich sediments (from both euxinic basins and continental margin settings) is generally similar in isotopic composition to Fe–Mn sediments and to suspended particulate material collected from the South Atlantic, all at about +0.3‰ (Little et al., 2017b; 2018; Ciscato et al., 2019). The homogeneity in authigenic sedimentary Cu isotope compositions has been suggested to reflect an equilibrium isotope fractionation in the aqueous phase between organically complexed Cu and inorganic Cu^{2+}, with the latter approximately 0.4 ‰ lighter than ligand-bound Cu, followed by near quantitative scavenging of inorganic Cu^{2+} by particulate material of any type (Little et al., 2017b; 2018). For example, in the Black Sea, transfer of Cu to the deep euxinic basin may be mediated by cycling with nanoparticulate Fe and Mn oxides at the redoxcline, linked to the benthic Fe–Mn redox shuttle (Lyons & Severmann, 2006; Little et al., 2017b). If correct, this hypothesis suggests that authigenic Cu isotope compositions in marine sediments may reflect the evolution of organic complexation on geological timescales.

Ciscato et al. (2018; 2019) developed a new approach to isolate trace elements associated with two different fractions in organic-rich sediments, the 'organic-pyrite fraction' (OPF) and 'HF digestible fraction' (HFD). They find that the OPF of modern Peru margin sediments typically contains >50 % of total Cu and is variably isotopically light compared to bulk authigenic Cu. They suggest this signature reflects incomplete sulfidation under variable water column and sedimentary redox conditions (e.g., Bianchi et al., 2018). Unlike in modern sediments, in ancient shales (ranging in age from 0.4 to 3.4 Ga) bulk Cu content does not correlate with TOC and >80 % of Cu is hosted in the HFD fraction. In addition, the OPF fraction in ancient shales is markedly isotopically heavier than it is in modern sediments (Ciscato et al., 2019). This difference between modern and ancient Cu partitioning may reflect diagenetic or metamorphic processing, or it may be a primary feature relating to differences in the Cu isotope composition of seawater, or differences in the mechanism(s) of Cu sequestration into sediments.

5.4. Prospects

Despite the biological importance of Cu, the modern biogeochemical cycle of Cu suggests there is no clear route to developing Cu isotopes (or [Cu]) as a paleoproductivity proxy. Work is also urgently needed to better understand the role of processing and storage effects on the accuracy of the oceanic [Cu] database, perhaps providing the opportunity to better understand the speciation of the dissolved Cu pool. Similarly, work is needed to firmly establish the fidelity of δ^{65}Cu measurements and ensure that different datasets can be synthesized. Despite these challenges, however, it is known that organic ligands play a key role in the cycling of Cu and Cu isotopes, suggesting a potential for the use of Cu isotopes in tracing the evolution of organic complexation on geological timescales. Additionally, careful sequential extraction procedures, such as those described by Ciscato et al. (2019), may allow for the direct probing of past seawater properties, such as redox state.

At present, there are few applications of Cu isotopes to study ancient biogeochemical cycles. Interestingly however, there are two black shale records that indicate a shift from UCC-like to heavy Cu isotope values across the Great Oxidation Event (GOE, ~2.4 Ga; Chi Fru et al., 2016; Ciscato et al., 2019). Chi Fru et al. (2016) interpreted this shift as reflecting the onset of oxidative weathering and waning of iron formation deposition, with the latter process driving pre-GOE seawater isotopically light due to the preferential scavenging of heavy Cu isotopes to Fe oxides. However, a recent analysis of two classic pre-GOE sequences containing iron formations do not support this earlier hypothesis, with δ^{65}Cu remaining close to 0 ‰ (Thibon et al., 2019). Thus, while the limited available data preclude confident interpretations, there are tantalizing tastes of future research directions in Cu isotope geochemistry.

6. Cadmium

The distribution of [Cd] closely correlates with macronutrient [PO_4^{3-}] in the oceans (; e.g., Boyle et al., 1976; Bruland, 1980). The nutrient-like properties of [Cd] and attendant correlations with [PO_4^{3-}] have been documented in multiple ocean basins, in multiple dimensions (i.e., vertically, spatially, and temporally), and are faithfully captured by certain sediments (e.g., Boyle, 1981). Moreover, many marine microbes assimilate isotopically light Cd from their environment (e.g., Lacan et al., 2006), consistent with the direction and magnitude of Cd isotope fractionation in seawater (e.g., Ripperger et al., 2007). Though the overall geochemical distribution of Cd is promising from the perspective of tracing paleoproductivity, there remain three broadly three issues that require addressing. Briefly, these relate to uncertainties surrounding: how, why, and which organisms contribute to Cd cycling in seawater; the significance of the decoupling between Cd and major nutrients in sinking particles, particularly in low [O_2] settings; and, identification of sedimentary archives that capture surface water δ^{114}Cd. Despite these uncertainties, the first-order features of marine Cd geochemistry are characteristic of a nutrient-type element, meaning that Cd can be modelled in a simple reactor scheme (see Sec. 2.2. and Fig. 4), and that the distributions of [Cd] and δ^{114}Cd appear broadly connected to underlying patterns of productivity.

6.1. Marine distribution

Away from major upwelling regions, surface water [Cd] are typically between 1–100 pmol kg^{-1}, but can reach as low as 30 fmol kg^{-1} (Schlitzer et al., 2018; Fig. 15). The majority of this small surface inventory is thought to be complexed by strong organic ligands (e.g., Bruland, 1992; Ellwood, 2004). In intermediate and deep waters, [Cd] are significantly elevated relative to surface waters, ranging from 0.5 nmol kg^{-1} in intermediate and deep waters in the north Atlantic to ≈1.2 nmol kg^{-1} in the oldest deep waters of the north Pacific (Schlitzer et al., 2018). As with Zn (Sec. 3.), the overall distribution of [Cd] throughout the oceans is driven principally by biological and physical processes in the Southern Ocean, and the lateral circulation of Southern Ocean water masses (e.g., Baars et al., 2014; Xie et al., 2017; Middag et al., 2018; Sieber et al., 2019a). Thus, the shape of vertical [Cd] profiles at lower latitudes arises largely from horizontal transport and mixing of high-Cd Southern Ocean-sourced water masses, with a modest contribution from regeneration of sinking particles (i.e., 5–40 %; Middag et al., 2018). These processes result in Cd having ‘nutrient-type’ one-dimensional water column profiles, with a progressive increase in intermediate and deep water [Cd] along the pathways of meridional overturning circulation (e.g., de Baar et al., 1994; Middag et al., 2018).

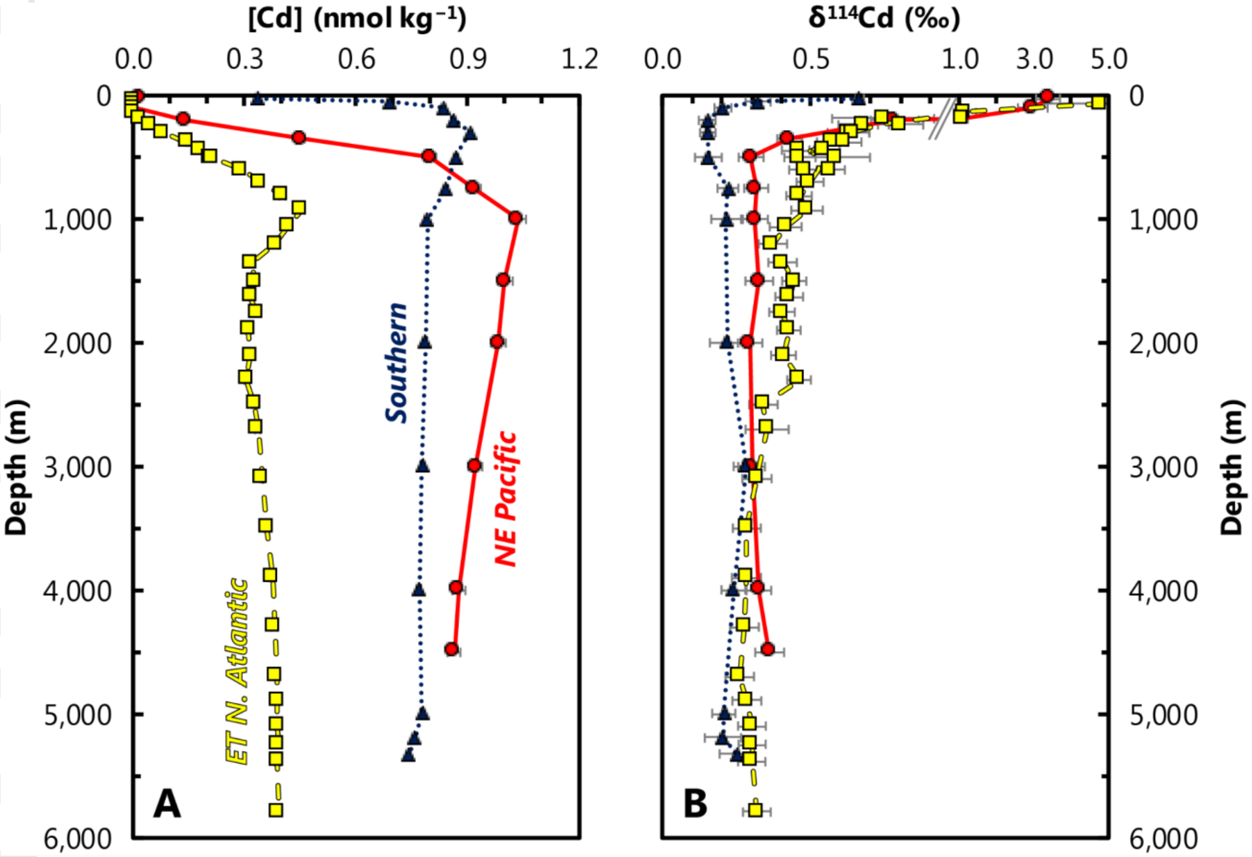

Figure 15 | Representative profiles of dissolved Cd concentrations ([Cd]; A) and Cd isotope compositions (δ^{114}Cd; B). Data from the Eastern Tropical North Atlantic (squares, dashed line; Conway & John, 2015b), Northeast Pacific (circles, solid line; Conway & John, 2015a), and Southern Oceans (triangles, dotted line; Abouchami et al., 2014). Station locations as per Fig. 1.Note the break in scale in δ^{114}Cd above 1 ‰, illustrating the extreme isotopic compositions observed in the most Cd-depleted surface samples. Notably, such extreme compositions are generally not observed in the similarly Cd-depleted surface waters of the Southern Hemisphere gyres (e.g., Gault-Ringold et al., 2011; Xie et al., 2017; George et al., 2019), nor in the surface of the high latitude Southern Ocean, where dissolved [Cd] is elevated (e.g., Abouchami et al., 2011; 2014). This comparison illustrates that the processes leading to distinct dissolved concentration profiles effect only modest changes in dissolved δ^{114}Cd between basins.

The past decade has seen an explosion in the number of studies employing Cd stable isotopes to investigate marine Cd cycling. The majority of extant Cd isotope data are reported relative to the NIST SRM 3108 standard, though several earlier studies, reviewed by Rehkämper et al. (2012), were reported relative to other in-house materials. Cross-calibration of these materials is described in detail by Abouchami et al. (2013). While the earliest study of Cd isotope variations in seawater was unable to unambiguously identify systematic patterns in the water column, the authors noted that cultures of phytoplankton preferentially incorporated isotopically light Cd relative to the media (Lacan et al., 2006). Assuming biological processes were responsible for Cd uptake, this observation led to two key predictions for marine Cd isotope systematics: that Cd-depleted surface waters should exhibit isotopically 'heavier' compositions than Cd-replete deep waters; and, that the degree of isotopic fractionation should be proportional to the extent of Cd removal into particles. Indeed, this is precisely the pattern that was first reported by Ripperger et al. (2007).

Subsequent studies have corroborated this general one-dimensional pattern in the Southern (e.g., Abouchami et al., 2011; 2014; Xue et al., 2013; Sieber et al. 2019a), Atlantic (e.g., Xue et al., 2012; Conway & John, 2015a; Xie et al., 2017; Xie et al., 2019a; Bryan et al., 2021), Arctic (Zhang et al., 2019), and Pacific Oceans (Yang et al., 2012; Yang et al., 2014; Conway & John, 2015b; Janssen et al., 2017; John et al., 2018; Yang et al., 2018; Xie et al., 2019b; Sieber et al., 2019b). These studies have shown that the deep ocean (>500–1,000 m) is largely homogenous in Cd isotope composition (δ^{114}Cd of +0.2 to +0.3 ‰; Fig. 15). This deep water δ^{114}Cd value is heavier than the upper continental crust δ^{114}Cd signature of ~0‰ (Schmitt et al., 2009a), similar to that observed for other metals such as Zn, Ba, and Ni (Secs. 3, 7, and 8.). Intermediate-depth waters relating to water masses such as Antarctic Intermediate Water (AAIW) exhibit slightly heavier δ^{114}Cd values (+0.4 to +0.5 ‰), with waters above these typically exhibiting heavier isotopic compositions (up to ~+1‰; Fig. 15). As for [Cd], these one-dimensional δ^{114}Cd profile shapes arise largely from the combination of Southern Ocean biological processes and lateral circulation of water masses, as well as some contribution from local surface uptake and regeneration (Abouchami et al., 2014; Sieber et al., 2019b).

Although the first-order distributions of [Cd] and δ^{114}Cd in surface waters are consistent with intense cycling by biological processes, when considering the global database of surface δ^{114}Cd data, this simple 'nutrient-like' reactor scheme with a single fractionation factor breaks down. For example, while studies have reported δ^{114}Cd values of up to +5 ‰ in Cd-depleted surface waters of the Northern Hemisphere gyres (Ripperger et al., 2007; Xue et al., 2012; Conway & John, 2015a; 2015b), others have reported more muted fractionation or even a switch to lighter than deep ocean compositions in surface waters (Gault-Ringold et al., 2012; Xie et al., 2017; Janssen et al., 2017; Xie et al., 2019a; George et al., 2019; Sieber et al., 2019b; Xie et al., 2019). This range of observations suggests that the processes influencing surface Cd isotope compositions may be more complex than simple biological uptake (Fig. 16). For example, interactions with ligands, effects arising from recycling of organic matter, differences in fractionation factor between different organisms, and supply of Cd from external Cd sources may all influence surface water dissolved δ^{114}Cd. This raises three related questions to be addressed in the remainder of this section: What are the candidate biological processes that drive these patterns? How do other physical or chemical processes play a role in setting marine Cd distributions? Can Cd-based reconstructions of these processes be used to inform on past productivity? Further to these questions, are the extreme heavy δ^{114}Cd observed in Northern Hemisphere gyres, and so far only twice in the Southern hemisphere (Sieber et al., 2019b; Bryan et al., 2021), real, or analytical artifacts?

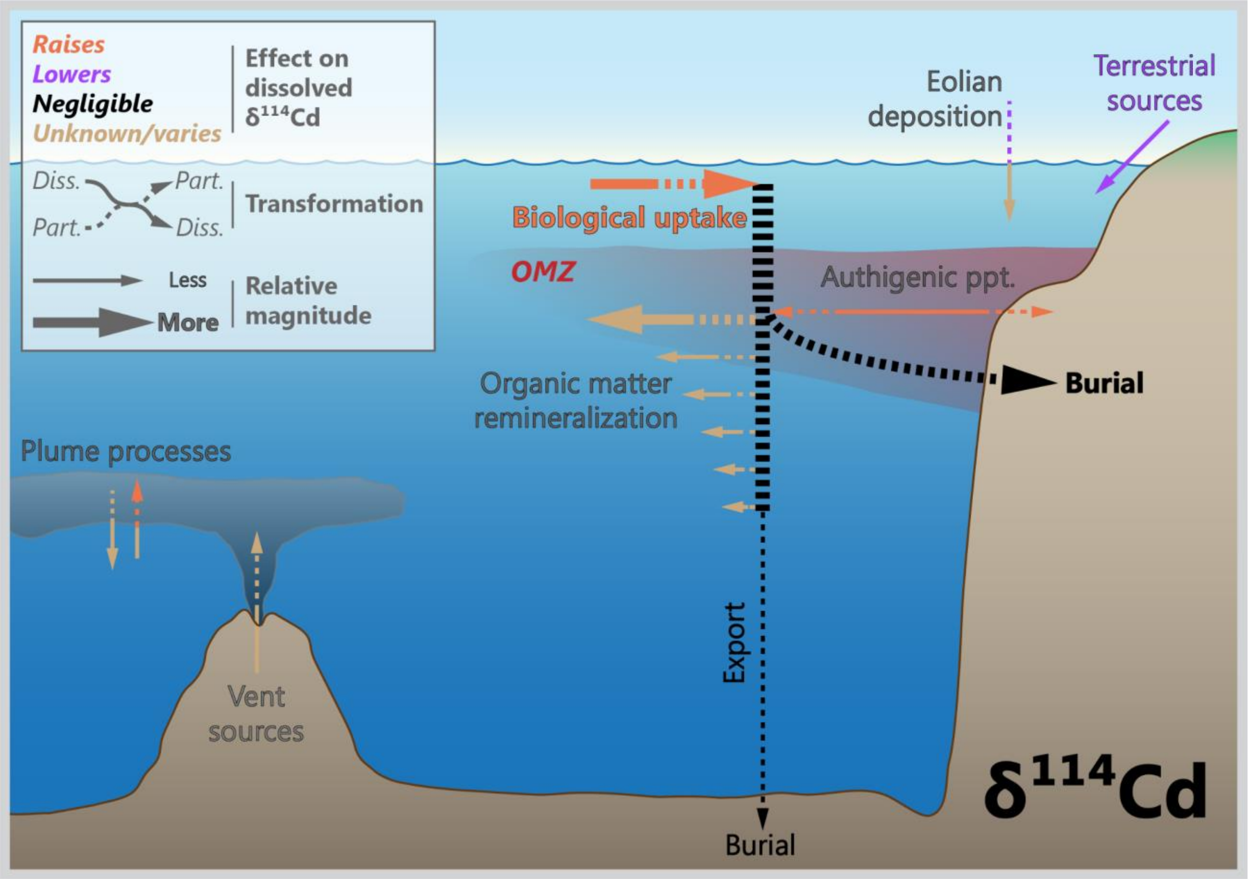

Figure 16 | Processes driving Cd isotope variations in modern seawater. Biological processes exert a significant control on surface water Cd cycling, implying that δ^{114}Cd is broadly responsive to productivity. However, important redox-dependent processes remain to be fully elucidated, particularly those occurring around OMZs.

6.2. Driving processes

6.2.1. Biological

As noted above, the nutrient-like distribution of [Cd] implies intense biological cycling in seawater, even though Cd is considered toxic (e.g., Waldron & Robinson, 2009). This dichotomy has inspired a significant body of research investigating the role that Cd plays in microbial physiology. These studies showed that Cd uptake by marine microbes exhibits three noteworthy dependencies. First, cellular Cd quotas are strongly positively correlated with the Cd content of their environment, both in culture (see compilation by Twining & Baines, 2013) and from oceanographic data (Middag et al., 2018). Second, microbial Cd uptake is diminished when the concentration of other divalent cations increases, particularly so for Fe, Mn, and Zn. Likewise, lower concentrations of these divalent cations cause increases in Cd uptake (e.g., Sunda & Huntsman, 2000; Cullen et al., 2003). Some diatoms have even shown capacity to substitute much of their metabolic Zn requirements with Cd (Price & Morel, 1990). Third, Cd uptake is also influenced by speciation of inorganic carbon, with low $p\mathrm{CO}_2$ promoting higher cellular Cd quotas (e.g., Cullen et al., 1999; Cullen & Sherrell, 2005; de Baar et al., 2017). The connection between Cd and carbon speciation is particularly intriguing given the discovery of the ζ-class of carbonic anhydrase that can utilize Cd (or Zn) as the catalytic metal (e.g., Lane et al., 2005; Xu et al., 2008). Despite these dependencies, however, the extent to which active physiological utilization of Cd controls global patterns of Cd uptake is unclear. For example, genes encoding the ζ-class of carbonic anhydrase were not found in green algae nor coccolithophores, and were similarly absent from many diatom species (Park et al., 2007). Thus, it is similarly plausible that some part of the biological Cd cycle is driven by organisms inadvertently removing Cd from seawater while attempting to source other metals (e.g., Boyle, 1988b; Horner et al., 2013), or that microbes require Cd to populate other Cd-centered metalloenzymes that await discovery.

The role of microbial physiology in mediating Cd isotope fractionation is also comparatively understudied. However, it does appear that biological fractionation of Cd isotopes is ubiquitous; fresh- (Lacan et al., 2006) and saltwater (John & Conway, 2014) green algae, incubations of unfiltered seawater (Xue et al., 2012), heterotrophic bacteria (Horner et al., 2013), and shallow marine particles (e.g., Yang et al., 2015; Janssen et al., 2019) all indicate that biological particles accumulate isotopically light Cd from their environment with a fractionation between −0.3 to −0.8 ‰ (Fig. 16). The limited depth profile data of suspended particulates that exist suggests subsequent partial respiration of already-light particulate organic matter also induces a second fractionation, further enriching light isotopes in the remnant particulate phase (Janssen et al., 2019). Additionally, as discussed in Sec. 6.1. and 6.2.2., variability in surface dissolved δ^{114}Cd data even at similarly low [Cd], ranging from extremely heavy δ^{114}Cd values to no apparent fractionation suggests that surface Cd isotope cycling cannot be simply driven by removal of isotopically light Cd from surface waters, and a mechanistic understanding of this remains limited.

6.2.2. Chemical

The role of chemical processes in mediating global Cd distributions is the most underconstrained of the three processes discussed in this review. Recent studies suggested that pelagic partitioning of Cd into sulfides in OMZs may be a significant loss term (Janssen et al., 2014; Bianchi et al., 2018; Plass et al., 2020). Moreover, the Cd isotope effect associated with sulfide precipitation identified by Guinoiseau et al.

(2018) is consistent with field data, and particulate Cd is known to accumulate more rapidly in sediments that are bathed by bottom waters containing low [O_2] (Fig. 16; Sec. 5.3.; e.g., van Geen et al., 1995). Collectively, these observations suggest a potential redox sensitivity in sedimentary Cd isotope distributions that deserves additional scrutiny. Indeed, the influence of sediments as the most important marine Cd sink can be seen in some water column profiles of δ^{114}Cd (Xie et al., 2019b). Similarly, data from the hydrothermal TAG site in the North Atlantic suggests that hydrothermal plumes may scavenge Cd from seawater, constituting a small sink of isotopically light Cd, though this does not have an observable effect on deep ocean δ^{114}Cd values outside of the plume itself (Fig. 16; Conway & John, 2015b).

Other potential sources and sinks include rivers, atmospheric deposition, and sediments; however, none of these interfaces exhibit significant anomalies in [Cd] or δ^{114}Cd in GEOTRACES-era datasets. This finding is in accord with earlier research by Martin & Thomas (1994), though there exist two possible exceptions. The first concerns the role of atmospheric aerosols, which have been invoked to explain the Cd isotope composition of surface waters in the Southwest Pacific (e.g., George et al., 2019) and South China Sea (e.g., Yang et al., 2012). Modern aerosol inputs may be largely anthropogenic in origin. Anthropogenic forms of Cd exhibit a relatively narrow range of isotopic compositions that are typically—though not always (e.g., Shiel et al., 2010)—lighter than dust-derived Cd (e.g., Bridgestock et al., 2017). Second, interactions with organic ligands have also been invoked to explain the relatively muted pattern of Cd isotope fractionation in the surface of the south Atlantic Ocean (e.g., Xie et al., 2017; Guinoiseau et al., 2018), but there are as yet no corroborating field or experimental data examining the role of organic ligands in mediating Cd isotope fractionation in seawater.

6.2.3. Physical

Physical processes are similarly influential in mediating the global distribution of [Cd] and δ^{114}Cd throughout the global oceans, particularly those processes occurring in the Southern Ocean. Antarctic Intermediate and Bottom Waters possess higher [Cd]:[PO_4^{3-}] than North Atlantic Deep Water (e.g., de Baar et al., 1994; Middag et al., 2018). Mixing between these southern- and northern-sourced water masses likely contributes to the well-known ‘kink’ in the [Cd]:[PO_4^{3-}] relationship (e.g., Frew & Hunter, 1992; Elderfield & Rickaby, 2000; Quay & Wu, 2015). Why northern- and southern-sourced intermediate and deep waters possess different [Cd]:[PO_4^{3-}] is debated, and likely reflects regionally distinct fractionation of Cd and P during biological uptake (e.g., Sunda & Huntsman, 2000; Cullen et al., 2003) and during remineralization (e.g., Baars et al., 2014; Roshan & Wu, 2015). In the Atlantic, however, the importance of remineralization to deep water Cd budgets is of secondary significance: the ratio of regenerated-to-preformed [Cd] is ~30 %

in the mesopelagic, and generally <10 % in the deep ocean (Roshan & Wu, 2015b; Middag et al., 2018). Given the low proportion of regenerated Cd in the deep Atlantic, the ratio of [Cd]:[PO_4^{3-}] and the overall distribution of [Cd] are essentially governed by the [Cd]:[PO_4^{3-}] of the source waters (Middag et al., 2018) and the prevailing geometry of ocean circulation, respectively (Boyle, 1988b).

Recent Cd isotope data from the South Atlantic (Xie et al., 2017), South Pacific (George et al., 2019; Sieber et al., 2019a), and Arctic (Zhang et al., 2019) also support the importance of mixing in mediating deep ocean [Cd] and δ^{114}Cd distributions, though it should be noted that the isotopic contrast between mixing endmembers is small, relative to measurement precision (Fig. 15; e.g., Janssen et al., 2017). For example, biological uptake of light Cd in the source regions of intermediate waters in the surface Southern Ocean results in isotopically heavy preformed δ^{114}Cd signatures being imparted to Cd-depleted intermediate water masses (e.g., +0.45 ‰ in AAIW; +0.65 ‰ in Subantarctic Mode Water, SAMW; Xue et al., 2013; Abouchami et al., 2014; Sieber et al., 2019b). Lateral circulation of these southern-sourced water masses then transfers this signature northward to intermediate depths in the Atlantic and Pacific Oceans (e.g., Xue et al., 2012; Abouchami et al., 2014; Conway & John, 2015a; Sieber et al., 2019b). This effect is more pronounced in the North Atlantic than in the Pacific, where southward flowing NADW also carries isotopically heavy Cd southward at depths of 1000–3000 m (Fig. 15; Xue et al., 2012; Conway & John, 2015a).

6.3. Marine archives

6.3.1. Carbonates

There is a long history of the measurement of Cd contents of marine carbonates, particularly corals and foraminifera, most commonly reported as Cd:Ca molar ratios. In principle, carbonates are an appealing archive of ambient Cd chemistry since inorganic partition coefficients are ≫1 (e.g., Tesoriero & Pankow, 1996) and the Cd:Ca of many types of carbonate exhibit a strong proportionality with ambient [Cd]. In practice, however, most biogenic carbonates exhibit partition coefficients closer to unity (Boyle, 1988b), and resultant Cd:Ca is also sensitive to the species (Boyle, 1992) and temperature of calcification (e.g., Rickaby & Elderfield, 1999). As such, Cd:Ca in carbonates has found the most utility where ambient [Cd]—and attendant carbonate Cd:Ca—exceeds several 100 pmol kg^{-1}, such as in tracing industrial fallout (e.g., Shen et al., 1987) or in studies of Quaternary deep ocean circulation (e.g., Boyle & Keigwin, 1985; van Geen et al., 1992; Adkins et al., 1998; Farmer et al., 2019).

There are far fewer studies examining the Cd isotope composition of marine carbonates as tracers of historical Cd isotope chemistry. Inorganic partitioning experiments indicate that Cd isotopes are fractionated during incorporation into calcite by ≈−0.5 ‰ (Horner et al., 2011). The isotopic effect is temperature- and Mg-independent, but vanishes at low salinity. This inorganic calibration has been used to interpret patterns of Cd isotope fractionation preserved in bulk carbonates from the Neoproterozoic Eon (1,000–541 Ma). The variations in these sediments are interpreted as evidencing changes in biological productivity (e.g., Hohl et al., 2017) and Cd sinks through time (e.g., John et al., 2017). Applications of Cd isotopes to foraminifera to study problems in Quaternary paleoceanography are precluded by the large sample requirements; obtaining ~1 ng of Cd—typically the minimum quantity needed for a reasonably precise Cd isotope measurement (Ripperger & Rehkämper, 2007; Schmitt et al., 2009b)—requires picking and cleaning of 10's of mg of foraminiferal tests. Alleviation of such limitations awaits development of automated picking and screening systems (e.g., Mitra et al., 2019), or vast improvements in ion transmission efficiency for isotope ratio mass spectrometry.

6.3.2. Ferromanganese sediments

Ferromanganese sediments have shown the most promise for recording deep ocean Cd isotope chemistry. Both ferromanganese nodules (Schmitt et al., 2009a) and crusts (Horner et al., 2010) reflect ambient seawater Cd isotope compositions with negligible fractionation (Fig. 17A), consistent with Cd–Mn-oxyhydroxide partitioning experiments conducted at high ionic strength that show only minor Cd isotope fractionation (Wasylenki et al., 2014). Horner et al. (2010) estimated that Cd is somewhat mobile in Fe–Mn crusts, with a predicted diffusivity $\leq 10^{-7}$ cm^2 yr^{-1}, similar to Hf (Henderson & Burton), Mo (Sec. 7.3.), Cr (Sec. 10.3.2.), and Ag (Sec. 11.3.). This rate implies that long-term records of δ^{114}Cd derived from Fe–Mn are likely to exhibit some diffusive smoothing while preserving larger perturbations. As with Zn and Cu isotopes however, time-resolved records of δ^{114}Cd recovered from Fe–Mn crusts indicate minimal variation over the last 20–60 Myr (Fig. 17B). The lack of variation may indicate that the sources and sinks of Cd have been in isotopic steady state throughout the Cenozoic. Alternatively, the lack of variation in

δ^{114}Cd over the Cenozoic may simply reflect a 'resetting' of all crust layers toward modern deep ocean Cd isotope compositions, as recently suggested by Murphy (2016).

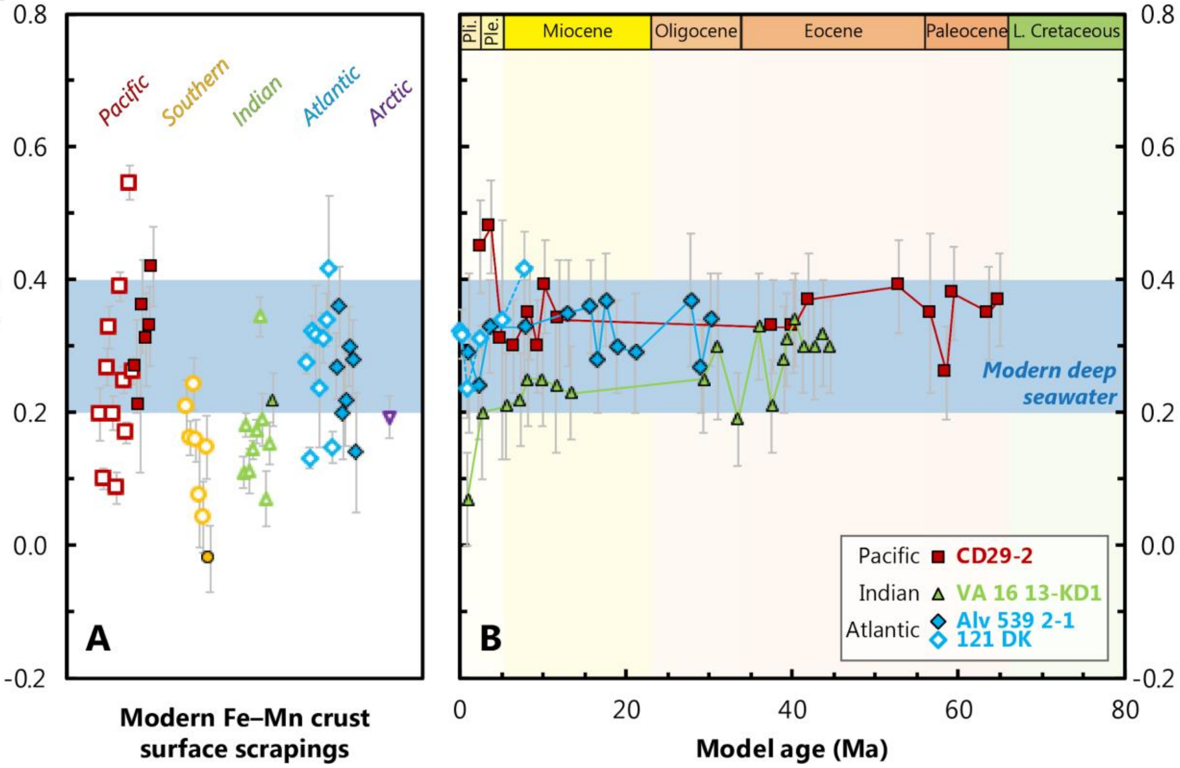

Figure 17 | Ferromanganese crusts records of deep-water δ^{114}Cd. A: Compilation of 'coretop' Fe–Mn crust δ^{114}Cd; data from Schmitt et al. (2009a; open symbols) and Horner et al. (2010; closed symbols). In general, Southern Ocean samples exhibit lighter δ^{114}Cd than other basins, consistent with profiles of δ^{114}Cd (e.g., Fig. 15). **B:** Cenozoic records of deep-water δ^{114}Cd recovered from four Fe–Mn crusts; data from Murphy, 2016 (closed symbols) and Schmitt et al. (2009a; open symbols). These records have been plotted using the authors' preferred age models, meaning that there are some differences between the chronology of CD29-2 shown here compared to Fig. 8. Such differences may be immaterial however, given that Cd isotopes in Fe–Mn crusts are potentially subject to diffusive 'resetting' over time (Murphy, 2016).

6.3.3. Organic-rich sediments

Organic-rich sediments are the principal sink of dissolved Cd from the modern oceans (e.g., Rosenthal et al., 1995; van Geen et al., 1995; Little et al., 2015). A significant fraction of the total Cd in organic-rich sediments is derived from sinking organic matter. Accordingly, the Cd content of organic-rich sediments or of multiple paired sedimentary phases has been applied as a proxy for past productivity (e.g., Brumsack, 2006; Hohl *et al.*, 2019). However, there is also a redox sensitivity: Cd contents are generally elevated in organic-rich sediments that are bathed by low [O_2] waters (Fig. 18). This enrichment likely derives from three processes. First, low [O_2] environments may limit oxidation—and thus favor preservation—of settling Cd sulfide particles formed in the water column. Second, the chalcophile nature of Cd means that even trace levels of hydrogen sulfide may cause Cd to precipitate into sulfides. Thus, as organic matter is remineralized within the sediment column, any Cd liberated to porewaters is proportionally more likely to reprecipitate into sulfide minerals, relative to harder metals (and carbon), effectively ‘trapping’ remineralized Cd in sediments (e.g., Rosenthal et al., 1995). Third, recent evidence suggests that Cd may also directly precipitate from seawater and into sediments when plumes of hydrogen sulfide interact with bottom waters (e.g., Xie et al., 2019b; Plass et al., 2020). The relative importance of these three processes to the O_2-dependent pattern of Cd accumulation remains to be fully elucidated.

While the contribution of organic-rich sediments to the isotopic mass balance of Cd is presently limited, their significance to the marine Cd budget suggests that, globally, the Cd isotope composition of these sediments should balance the riverine flux δ^{114}Cd ≈+0.1±0.1‰ (Lambelet et al., 2013). Recent data from organic-rich sediments (Chen et al., 2021), suboxic sediments (Bryan et al., 2021), and intermediate-depth biogenic particles (Janssen et al., 2019) generally support this view, and that low [O_2] settings may help to close the isotope mass balance of Cd. Alternatively, the other minor sinks of Cd—carbonates, ferromanganese oxides, clays—must possess large isotopic offsets relative to seawater, which seems unlikely given existing field and experimental data. Obtaining further modern calibrations of Cd isotope partitioning into organic-rich sediments should be considered a priority.

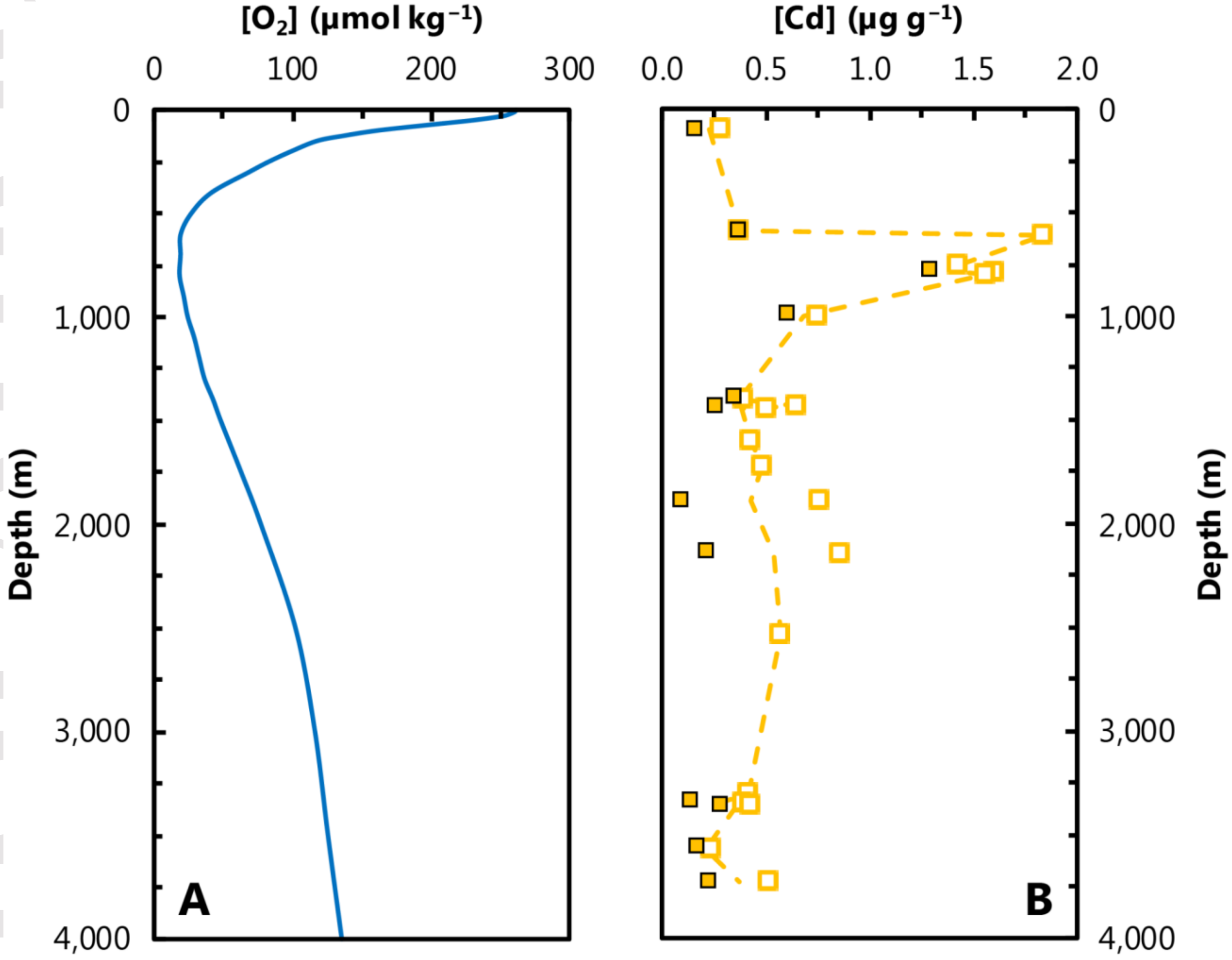

Figure 18 | Cadmium concentrations in California Margin sediments. A: Regionally representative [O_2] profile from the northeast Pacific showing broad minimum between 600–800 m. Profile from 35.5°N, 122.5°W (from World Ocean Atlas; Garcia et al., 2013). **B:** Solid phase Cd concentration data from van Geen et al. (1995) for northeast Pacific coretop (closed symbols) and "*slightly deeper*" (8–10 cm; open symbols) sediment samples; dashed line indicates arithmetic mean. These samples evidence a maximum in authigenic Cd deposition at the top of the OMZ, which may originate from processes occurring in the water or sediment column.

6.4 Prospects

The overview provided above indicates that Cd participates in marine biological processes and that its distribution is sensitive to the biological productivity of the oceans. How this sensitivity is transcribed into marine sediments remains uncertain, however. Additionally, there are several other processes that have the potential to render isotope effects that require further exploration before Cd isotopes can be solely interpreted as a productivity proxy, such as: biological fractionation effects, authigenic transformations, and redox sensitivities. Relatedly, the fidelity of many types of marine sediment to record ambient Cd isotope chemistry remain inadequately constrained. With these two themes in mind, we suggest several areas for additional research that may help to address the overarching question as to whether Cd isotope-based reconstructions can be used to inform on past ocean productivity.

6.4.1. Modern

Several questions persist regarding the modern Cd isotope cycle. We list five of the most pressing below and offer possible remedies to each. First, are the 'extreme' (i.e., δ^{114}Cd of + 5 ‰; Fig. 15) values seen in surface waters of the Northern Hemisphere gyres (and only measured by MC-ICPMS techniques) real? That is, are these heavy compositions true oceanographic features that are generally absent from the Southern Hemisphere, or do they represent analytical artifacts unique to MC-ICPMS? This question remains to be answered, and will require measurement of the same low [Cd] surface samples by multiple MC-ICPMS and MC-TIMS groups. To date, this exercise has proven difficult because of the difficulty of collecting surface low [Cd] seawater (where heavy δ^{114}Cd has been reported by MC-ICPMS) in sufficient quantities to permit analyses by multiple groups.

Second, to what extent do local Cd isotope compositions in surface waters reflect larger-scale processes versus local features? While available data consistently show biological Cd uptake removes isotopically light Cd, not all surface waters generally show the expected progressive increase in δ^{114}Cd with decreasing [Cd]. Addressing this issue will require elucidating the role of external sources (e.g., dust, margin sediments), organismal uptake, ligands, and mixing, which would benefit from conducting additional experimentation with plankton, coupling of isotope methods with electrochemistry, and numerical modeling, respectively.

Third, is there a 'Redfield' stoichiometry for Cd in organic matter? If so, what controls it? Existing culture (Ho et al., 2003) and field (Ohnemus et al., 2017) data suggest a wide range of cellular Cd:P, which have been suggested as reflecting species and local supply ratios, respectively (in addition to the aforementioned feedback interactions). Further experimentation with model organisms is needed.

Fourth, it is unclear if cells must possess a true physiological use for Cd in order to contribute to Cd isotope fractionation in seawater. The uptake of Cd into cells is widespread, whereas the genes encoding the ζ-class of carbonic anhydrases are not. The importance of this enzyme to Cd geochemistry could be tested by characterizing the Cd isotope composition of organisms that are known to produce Cd-containing carbonic anhydrases and comparing against those that cannot. Such experiments may also benefit from use of mutant cell lines with targeted ‘knockouts’ or by culturing phytoplankton in the presence of carbonic anhydrase inhibitors.

Last, how are the ‘light’ Cd isotope compositions seen in suspended biogenic particles above OMZs related to those within OMZ layers and to those putatively accumulating in sediments? Does biogenic particulate Cd reach sediments? Do particulate Cd isotope signatures within OMZ particles relate to sulfide precipitation and what is their influence on the global mass balance? What controls the Cd isotope composition of these particles? Addressing these questions will require examining the Cd isotope composition of particles from oxygenated oceanographic regions, identifying whether processes associated with particle regeneration affect Cd isotope compositions, and surveying coretop sediments.

6.4.2. Paleo

As with the modern cycle, several ambiguities persist, though the most pressing relates to archives. Indeed, it appears that a major obstacle preventing the widespread application of Cd isotope-based proxies in paleoceanography has been the lack of suitable archives. Concerning carbonates, the main question is still whether it is possible to isolate sufficient quantities of foraminiferal-bound Cd to reconstruct past seawater δ^{114}Cd. Does species matter, or can mixed assemblages be used? For organic-rich sediments, the role of biology itself must be considered. That is, how important might it be that different organisms exhibit different magnitudes of Cd isotope fractionation (and Cd:C stoichiometry)? If important, how best to interpret Cd isotope records—species, evolutionary innovations, productivity?

7. Molybdenum

Molybdenum is a cofactor in several key enzymes in the nitrogen cycle, and Mo availability in the ancient oceans may have helped shape the Precambrian biosphere (e.g., Anbar & Knoll, 2002). Today, Mo is the scarcest of the essential trace metals in phytoplankton (Eq. 3), but is one of the most abundant transition metals in the ocean (Morris, 1975; Bruland 1983; Collier 1985). Indeed, Mo possesses a long residence time (~440,000 yr; Miller et al., 2011; Table 1), is conservative with respect to salinity, and exhibits a uniform isotopic composition in oxygenated seawater (e.g., Barling et al., 2001; Siebert et al., 2003; Fig. 19). Given the lack of [Mo] and δ^{98}Mo variability in the modern ocean, the isotope reactor framework outlined in Sec. 2.2. cannot be applied to Mo and thus there is no simple way to link δ^{98}Mo with paleoproductivity. Despite this, Mo is a widely used tracer of paleoredox conditions, and emerging fossil-specific measurements of δ^{98}Mo provide a promising future means to reconstruct high-resolution records of ocean oxygenation.

7.1. Marine distribution

Based on 168 seawater samples from the Atlantic, Pacific, and Southern Oceans analyzed by Nakagawa et al. (2012), the average salinity-normalized [Mo] and δ^{98}Mo of the ocean are 107±6 nmol kg^{-1} and +2.36±0.10 ‰, respectively (both values ±2 SD; Fig. 19).

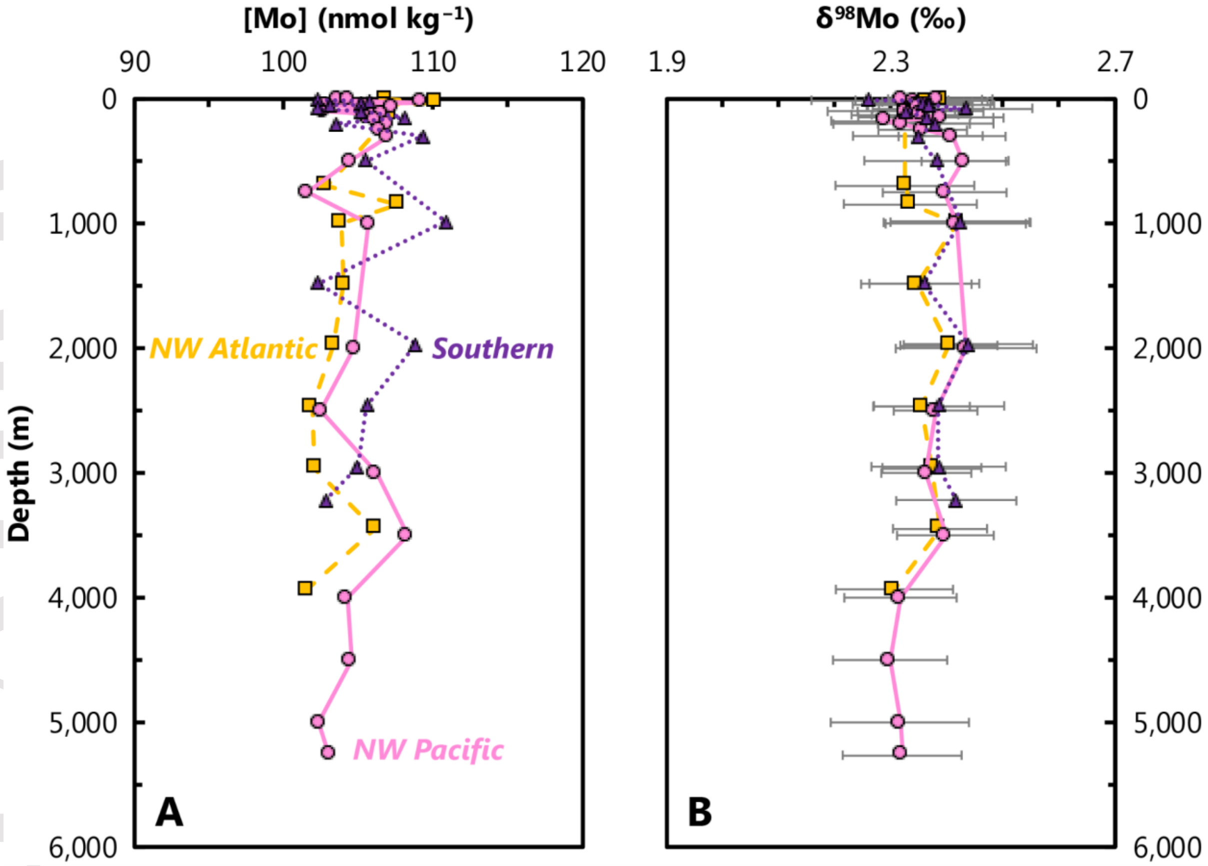

Figure 19 | Representative profiles of dissolved Mo concentrations ([Mo]; A) and Mo isotope compositions (δ^{98}Mo; B). Data from the Northwest Atlantic (squares, dashed line), Southern (triangles, dotted line), and Northwest Pacific Oceans (circles, solid line; all data from Nakagawa et al., 2012). Station locations as per Fig. 1. This comparison illustrates that the dissolved behavior of Mo is essentially invariant throughout the global oceans.

Given that no significant gradients in [Mo] are expected, there are few new open ocean δ^{98}Mo data measured as part of GEOTRACES. However, [Mo] has been measured on two GEOTRACES transects (GP16 and GA02), demonstrating four intriguing instances where [Mo] deviated from an otherwise conservative distribution. These instances are briefly described below and covered in detail by Ho et al. (2018). First, the most significant [Mo] anomalies (~5 % drawdown) are associated with intense scavenging by particulate Fe hydroxides and oxyhydroxides close to the Peruvian OMZ. Second, Mo is slightly drawn down (<5 %) in some samples directly above the East Pacific Rise hydrothermal ridge crest, again mostly likely driven by scavenging onto hydrothermally derived Fe–Mn oxides. Some Mo drawdown is also observed in some far-field hydrothermal samples, though the mechanism is unclear. Third, following normalization to a salinity of 35, surface seawater shows a minor Mo drawdown, implying either biological uptake or adsorption to biotic particles. Though not a true oceanographic feature, a fourth type of [Mo] anomaly is also noteworthy: bottle storage artefacts. Ho et al. (2018) found that many samples with initially low values showed an increase in [Mo] with increasing storage time, implying a change in Mo speciation to a form that is detectable by ICP-MS. In contrast to the relative constancy of [Mo] in open ocean settings, a number of studies show striking [Mo] variations in coastal and estuarine systems (e.g., Dalai et al., 2005; Dellwig et al., 2007; Joung and Shiller, 2016; Wang et al., 2016) as well as in modern restricted settings, such as the Black and Baltic Seas (Nägler et al., 2011).

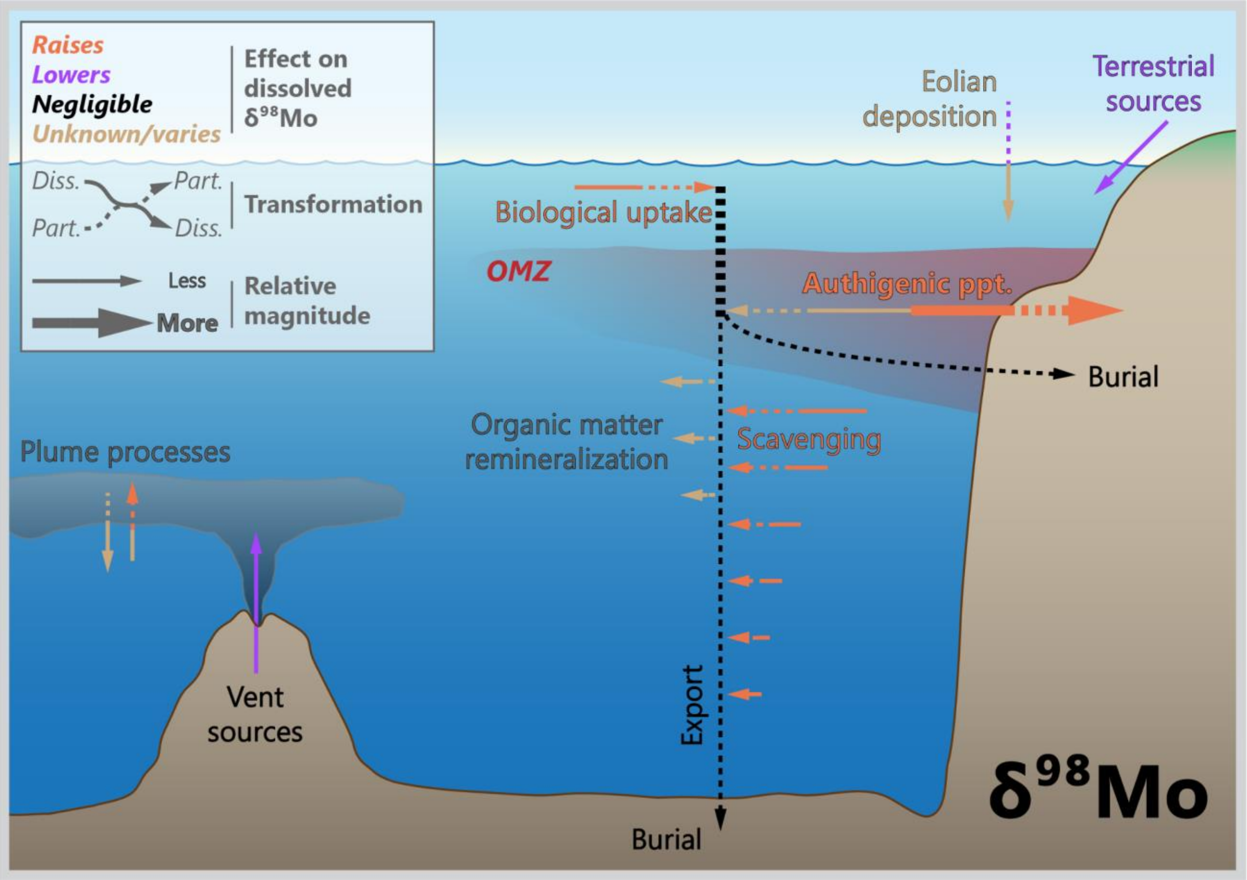

Figure 20 | Processes driving Mo isotope variations in modern seawater. While biological processes may exert a slight influence on surface water Mo distributions, the main drivers of marine Mo cycling are related to the balance between scavenging pathways, which are redox dependent.

7.2. Driving processes

7.2.1. Biological

Molybdenum is an essential micronutrient required by enzymes that catalyze key reactions in the global C, N, and S cycles (Mendel & Bittner, 2006). Importantly, Mo is a co-factor of the primary nitrogenase enzyme complex, meaning that Mo is required for energy-efficient nitrogen fixation. Additionally, Mo is required for over 30 other enzymes that control biologically essential redox processes (Kendall et al., 2017). Despite its biological importance, biological activity does not appear to be a dominant process in setting the distribution of Mo in seawater (Fig. 20), likely due to the high abundance of Mo in the modern ocean. Results from the GEOTRACES GP16 East Pacific Zonal Transect do, however, suggest some Mo removal by biological uptake and/or adsorption onto biogenic particles within regions of elevated chlorophyll (Ho et al., 2018). Experimental data indicate that biological uptake of Mo imparts a small negative isotope fractionation on the order of −0.3 ‰ (Wasylenki et al., 2007; Fig. 20).

Enhanced removal of Mo from seawater in regions with high export of organic carbon likely explains some of the nonconservative behavior observed in modern coastal regions. A significant relationship between Mo and total organic carbon content is observed in marine euxinic sediments (e.g., Helz et al., 1996; Algeo & Lyons, 2006; McManus et al., 2006; Lyons et al., 2009), though this appears to be more a function of euxinia rather than organic C burial. Furthermore, it has been shown that Mo interactions with organic matter can control Mo cycling in both soils (Wichard et al., 2009; King et al., 2014, 2016; Marks et al., 2015; Siebert et al., 2015) and marine sediments (Wagner et al., 2017; Tessin et al., 2019). The formation of Mo complexes containing organic ligands has been proposed as an explanation for the correlation between sedimentary Mo and organic carbon, suggesting that organic matter may play an important role in both the delivery and burial of Mo in sediments (Wagner et al., 2017).

7.2.2. Chemical

Due to the long residence time and abundance of Mo, nonconservative Mo behavior is typically localized to areas with high particle concentrations, such as close to the continental margin, in the euphotic ocean, or around hydrothermal vents (e.g., Goto et al., 2020). In the present oxic water column, Mo is present primarily as the oxyanion molybdate (MoO_4^{2-}) and Mo sorption onto Mn oxyhydroxides represents the most significant modern Mo sink (Fig. 20; Bertine & Turekian, 1973; Scott & Lyons, 2012). Since the Fe–Mn oxide sink preferentially removes Mo from seawater with an isotopic effect of ≈−3.0 ‰ (Barling et al., 2001; Siebert et al., 2003; Fig. 21), the fraction of Mo that is buried in Fe–Mn oxides exerts a major control over the Mo isotope composition of seawater.

In the presence of sulfide, the oxygen atoms in molybdate are progressively substituted for sulfur, producing particle reactive thiomolybdate species ($MoO_{4-x}S_x^{2-}$; Erickson & Helz, 2000; Vorlicek et al., 2015). Dissolved Mo can thus be strongly drawn down in sulfidic environments, such as the Black Sea. Importantly, this drawdown occurs with a small, but non-zero isotope effect of ≈−0.5±0.3 ‰, whereby isotopically light Mo is preferentially scavenged (e.g., Nägler et al., 2011). Thiomolybdate may also be scavenged from sulfidic sedimentary porewaters leading to significant Mo accumulations within sediments deposited in anoxic and euxinic environments (e.g., Emerson & Huested, 1991; Crusius et al., 1996; Scott & Lyons, 2012). Long term Mo burial is associated with Fe–S minerals (Chappaz et al., 2014; Vorlicek et al., 2018) and/or organic matter (Dahl et al., 2017; Tessin et al., 2019), depending on the biogeochemical conditions prevailing at a given basin.

7.2.3. Physical

The residence time of dissolved Mo is significantly longer than the mixing time of the ocean (Table 1). Thus, variations in [Mo] and dissolved δ^{98}Mo are not influenced by the geometry of modern overturning circulation. Whole ocean changes in [Mo] and dissolved δ^{98}Mo are, however, possible, and much of what we know about such changes is gleaned from studies of the geological past, particularly during periods of ocean anoxia. Based on this research, it has been suggested that during intervals of lower ocean oxygenation, the ocean Mo inventory may have been low enough to limit marine primary productivity (Anbar & Knoll, 2002; Algeo, 2004; Glass et al., 2009; Reinhard et al., 2013). This limitation has been demonstrated in certain lake ecosystems (Goldman, 1960; Glass et al., 2012). Under strongly euxinic conditions ($[H_2S]_{aq} > 11$ μM), thermodynamic calculations predict that tetrathiomolybdate (MoS_4^{2-}) becomes the predominant Mo species (Erickson and Helz, 2000). The transformation can result in quantitative drawdown of Mo from seawater and into sediments with negligible net isotope fractionation, a mechanism that has been evidenced in Lake Cadagno (Dahl et al., 2010), the Black Sea (e.g., Neubert et al., 2008; Nägler et al., 2011), and Kyllaren fjord (a seasonally anoxic basin off of the west coast of Norway; Noordmann et al., 2015). Indeed, the quantitative drawdown mechanism is the foundation of several paleoceanographic studies that assume that the sedimentary Mo isotopic signatures, deposited in euxinic settings, faithfully capture the δ^{98}Mo of oxygenated (surface) seawater and can be further interpreted in terms of the fraction of the seafloor that is oxygenated (e.g., Kendall et al., 2015; Dickson, 2017).

7.3. Sedimentary archives

The majority of Mo paleoceanographic studies focus on the measurement of the Mo content and isotopic composition of bulk sediments, spanning early Earth (e.g., Arnold et al., 2004) to the Holocene (e.g., Hardisty et al., 2016; van Helmond et al., 2018). However, the vast majority of these studies applied Mo and its isotopes to trace ocean redox conditions rather than productivity (e.g., Anbar, 2004; Kendall et al., 2017). Similar to the other elements reviewed here, there are measurements of δ^{98}Mo in Fe–Mn sediments (e.g., Barling et al., 2001). Siebert et al. (2003) reported a time series from two Fe–Mn crusts implying no variations in the δ^{98}Mo of seawater, relative to modern values, over the Cenozoic. Molybdenum is somewhat mobile in Fe–Mn crusts, with a calculated effective diffusivity $\leq 10^{-7}$ cm^2 yr^{-1} (see Henderson & Burton, 1999 for calculation details), similar to Cd (Sec. 6.3.2.), Cr (Sec. 10.3.2.), and Ag (Sec. 11.3.). Thus, the invariance of the Fe–Mn crust δ^{98}Mo record may imply that the relative balance of Mo sinks has not shifted by more than 10 % over the Cenozoic (e.g., Siebert et al., 2003; Anbar, 2004), or could reflect some degree of post-depositional resetting.

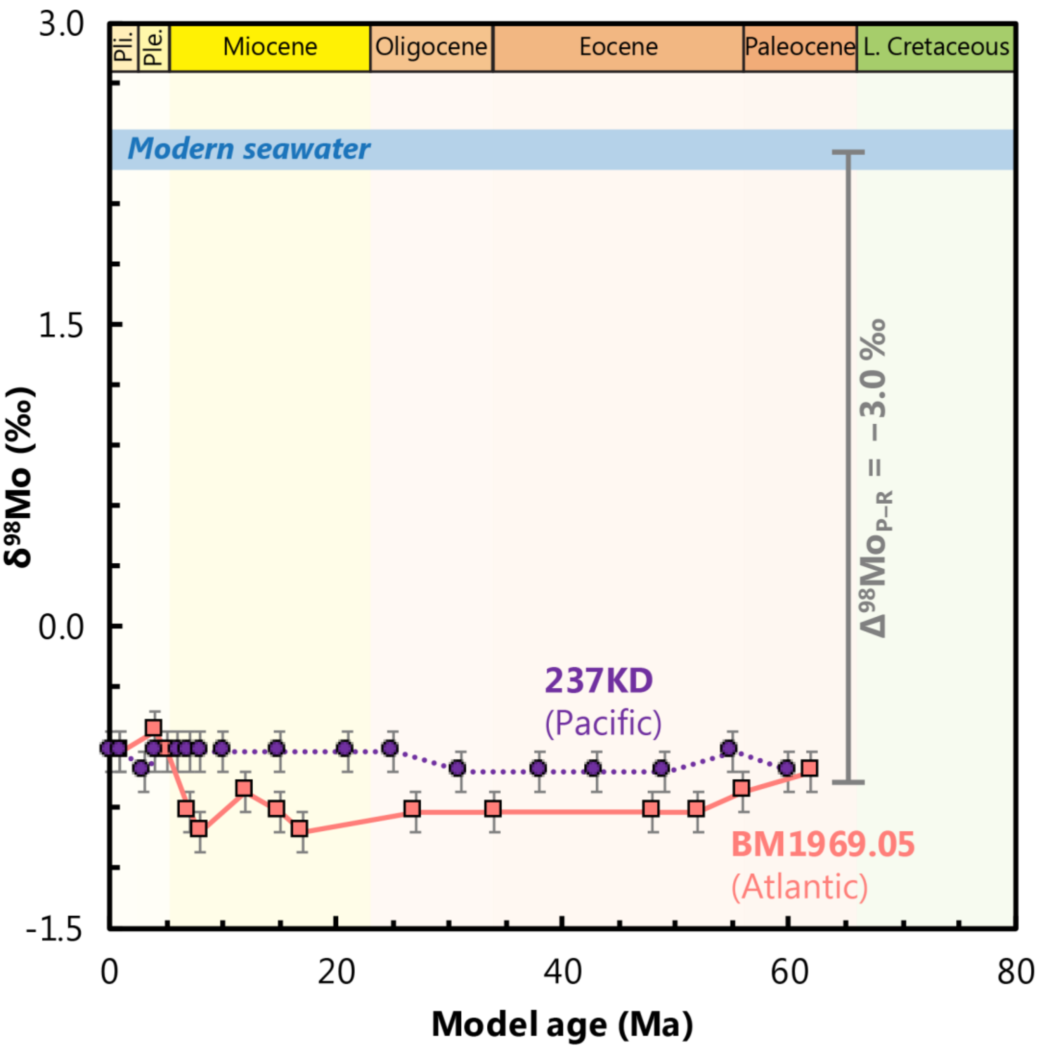

Figure 21 | Two Fe–Mn records of δ^{98}Mo spanning the Cenozoic. Data from the Atlantic (squares, solid line) and Pacific Oceans (circles, dotted line; Siebert et al., 2003). Assuming that these Fe–Mn crusts have always formed with an offset ≈−3.0 ‰ with respect to dissolved Mo in seawater, these records indicate that the δ^{98}Mo of seawater has minimally varied over the Cenozoic (Siebert et al., 2003; Anbar, 2004). However, given the effective diffusivity of Mo in Fe–Mn crusts, it is possible that the lack of variation may also reflect post-depositional resetting to modern-like values.

Despite the ambiguity surrounding Fe–Mn sediments, research on biological archives of [Mo] and δ^{98}Mo has found with mixed results. Research examining δ^{98}Mo in corals indicates that corals may accurately record ambient seawater Mo isotopic composition (Voegelin et al., 2009). However, later studies suggested a temperature-dependent fractionation between seawater and corals that is related to the activity of symbiotic zooxanthellae (Wang et al., 2019b). Moreover, bivalve shell Mo:Ca ratios have been determined to have no relationship to oceanographic conditions (Vihtakari et al., 2017), whereas Tabouret et al. (2012) suggest a mechanism related to trophic uptake, but not to ambient [Mo]. A third study proposed that Mo:Ca peaks in bivalve carbonate are controlled by ingestion of phytoplankton grown on NO_3^- (due to high Mo associated with NO_3^- reductase), indicating that bivalves may provide an archive for surface water NO_3^- uptake and a potential proxy for the balance between new and regenerated productivity (Thébault et al., 2009).

7.4. Prospects

At present, it does not appear that bulk sediment δ^{98}Mo will be useful for reconstructing biological productivity, even though Mo is cycled by organic matter, both actively (e.g., Liermann et al., 2005; Wasylenki et al., 2007) and passively (e.g., Kowalski et al., 2013; King et al., 2018). That we see no pathway to using Mo as a productivity tracer reflects, in part, the difficulty in disentangling biological processes that exert relatively modest Mo isotope fractionations from those associated with thiomolybdate transformations (Tossell, 2005), or scavenging processes that possess large fractionation effects (Fig. 20; e.g., Mn- or Fe-oxide scavenging; Siebert et al., 2003; Barling & Anbar, 2004; Wasylenki et al., 2008; Brucker et al., 2009; Goldberg et al, 2009; 2012). Additionally, within the modern ocean and likely within the recent geologic past, the global ocean reservoir of Mo is too large and well mixed for biological associated fractionations to significantly impact the global Mo isotopic composition.

The use of bulk sedimentary Mo concentrations as a proxy for export of organic carbon to the seafloor is more promising, but numerous caveats exist. Specifically, other mechanisms for enhanced delivery, sequestration, and burial complicate any efforts to quantitatively relate Mo enrichments to increased export productivity (e.g., Scholz et al., 2017). Redox conditions and, in particular, the presence of sulfide in the water column and sediment porewaters will be a primary control on Mo accumulation (e.g., Hardisty et al., 2018). Sedimentary Mo enrichments can also be produced through shuttling of Mo adsorbed to the surface of Fe and Mn oxides to the seafloor (Algeo & Lyons, 2006; Algeo & Tribovillard, 2009; Dellwig et al., 2010; Scholz et al., 2013). At a minimum, independent constraints on water column and porewater redox conditions using Fe speciation, other trace metals and/or fossil redox proxies are required before an argument can be made relating Mo contents to export productivity. Additionally, the quantitative relationship between Mo and organic carbon may be impacted by aqueous [Mo], which may have varied over Earth's history, or if depositional environments become restricted (i.e., Mo drawdown leads to a lower Mo:TOC ratio; Algeo & Lyons, 2006). Conversely, the utility of bulk sediment Mo content and isotopic composition may lie in constraining redox conditions to improve the interpretation of other trace metal proxies that are more strongly controlled by primary and/or export productivity.

The most promising future avenue for Mo-based productivity proxies may emerge from fossil-specific measurements of Mo content, and perhaps δ^{98}Mo. Currently, research has focused on large fossils (corals and bivalves; e.g., Thébault et al., 2009) and has led to mixed results on the utility of Mo in reconstructing productivity-related parameters. However, analytical progress may allow for measurement of smaller sample sizes, which may provide opportunities to explore new archives of past marine Mo geochemistry.

8. Barium

Like Zn, [Ba] exhibits a strong correlation with [Si] (e.g., Chan et al., 1977). Unlike Zn and Si however, Ba is not an essential nutrient and has no known enzymatic functions. The mechanisms underpinning the nutrient-like behavior of Ba instead relate to its cycling by the mineral $BaSO_4$ (barite), which is thought to precipitate during the microbial oxidation of sinking organic matter (e.g., Chow & Goldberg, 1960). Barite precipitation also drives a sizeable, negative isotope fractionation of Ba stable isotopes (e.g., Von Allmen et al., 2010), consistent with the direction and magnitude of Ba isotope variations in seawater (e.g., Horner et al., 2015a). Though the connections between [Ba] and productivity are thus not direct, patterns of Ba sedimentation are strongly correlated with those of export production (e.g., Eagle et al., 2003), and Ba stable isotope distributions are consistent with underlying variations in $BaSO_4$ cycling and ocean circulation (e.g., Horner & Crockford, 2021). As such, [Ba] and dissolved δ^{138}Ba can be described using the reactor framework outlined in Sec. 2.2., and—despite some uncertainties outlined later in this section—represents a promising tool for tracing aspects of paleoproductivity.

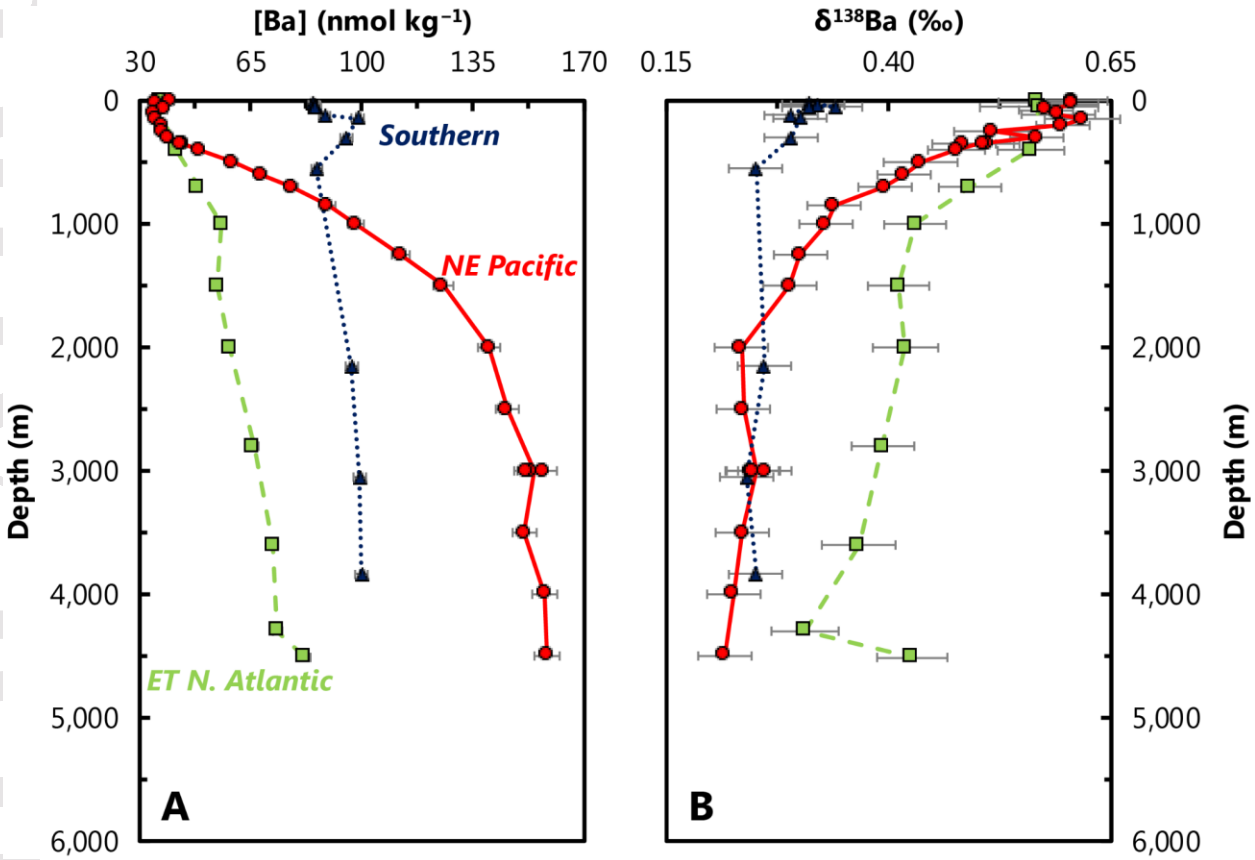

Figure 22 | Representative profiles of dissolved Ba concentrations ([Ba]; A) and Ba isotope compositions (δ^{138}Ba; B). Data from the Eastern Tropical North Atlantic (squares, dashed line; Bates et al., 2017), northeast Pacific (circles, solid line line; Geyman et al., 2019), and Southern Oceans (triangles, dotted lines; Hsieh & Henderson, 2017). Station locations as per Fig. 1. This comparison illustrates that the oceanographic processes leading to distinct dissolved concentration profiles render significant changes in dissolved δ^{138}Ba between basins.

8.1. Marine distribution

The nutrient-like distribution of [Ba] has been documented in the literature since the 1970s (e.g., Wolgemuth & Broecker, 1970; Fig. 22). However, it was not until later in the decade that the GEOSECS Program fully revealed the three-dimensional marine distribution of [Ba] (e.g., Chan et al., 1976; 1977). These geochemical ocean sections highlighted vertical, zonal, and meridional variations in [Ba] related to the major biogeochemical and hydrographic features of the ocean. In nutrient-depleted surface waters, [Ba] is low, between 35–45 nmol kg^{-1}. Nutrient-replete deep waters are enriched in Ba, though typically by no more than a factor of four above surface values. The spatial resolution of GEOSECS illustrated the importance of hydrography; [Ba] increases along the meridional overturning circulation from ≈50 nmol $\mathrm{kg^{-1}}$ in deep waters of the North Atlantic, to ≈90 nmol $\mathrm{kg^{-1}}$ in the Southern Ocean, up to ≈180 nmol $\mathrm{kg^{-1}}$ in the deep northeast Pacific (Fig. 22; Chan et al., 1976; 1977).

Though it was long suspected that the major dissolved–particulate transformation of Ba was related to the mineral barite ($BaSO_4$; e.g., Chow & Goldberg, 1960; Turekian, 1968), this was not confirmed until the 1980s (e.g., Dehairs et al., 1980; Bishop, 1988). Barite crystals are now recognized as an ubiquitous component of marine particulate matter, with up to 10^4 discrete, micron-sized crystals present per L of seawater (Dehairs et al., 1980). The distribution of particulate $BaSO_4$ is distinct from primary biogenic phases that exhibit Martin-like distributions with maxima in the euphotic zone that subsequently decay along power-law trajectories (Martin et al., 1987). Particulate Ba typically exhibits a minimum in the euphotic zone and the maximum slightly below, usually near the top of the mesopelagic (e.g., Ohnemus & Lam, 2015; Ohnemus et al., 2019). This distribution likely reflects the fact that neither Ba nor $BaSO_4$ are utilized for physiological processes by any of the major marine primary producers. Particulate Ba fluxes are nevertheless strongly correlated with export productivity in well-oxygenated environments (e.g., Bishop, 1988; Dymond et al., 1992; Francois et al., 1995; Dymond & Collier, 1996; McManus et al., 2002) and therefore sedimentary Ba content has been widely used as a proxy to reconstruct past changes in ocean export production (e.g., Francois et al., 1995; Paytan et al., 1996; Paytan & Griffith, 2007 and references therein; Costa et al., 2016, Winckler et al., 2016).

Recent studies of Ba stable isotope geochemistry have added a new dimension with which to study marine Ba cycling. Von Allmen et al. (2010) first reported that isotopically light Ba is preferentially incorporated into $BaSO_4$, with a particulate–dissolved Ba isotopic offset of ≈−0.3 ‰. The direction of this offset implies that residual solutions, such as seawater, should exhibit Ba isotopic compositions heavier than those of sedimented $BaSO_4$. This was corroborated for Atlantic seawater by Horner et al. (2015a), showing that dissolved δ^{138}Ba displays a mirror image of [Ba]: Ba-depleted surface water masses exhibited 'heavy' Ba isotopic compositions (≈+0.6 ‰), whereas Ba-replete deep waters possessed 'lighter' values ≈+0.3 ‰. (Notably, all values are considerably heavier than the upper continental crust, which possesses δ^{138}Ba ≈0.0±0.1 ‰; Nan et al., 2018.) Similar patterns have since been corroborated in other ocean basins (Bates et al., 2017; Hsieh & Henderson, 2017; Bridgestock et al., 2018; Geyman et al., 2019; Cao et al., 2020a; Fig. 22). The first order pattern is thus consistent with the removal of isotopically light Ba from surface waters and its regeneration at depth. Further, the longer a water mass remains isolated from the surface, the more isotopically light Ba is able to accumulate, hence why Ba-replete northeast Pacific seawater ~2,000 m depth exhibits the lightest dissolved δ^{138}Ba yet observed in the global ocean (≈+0.2 ‰; Geyman et al., 2019; Fig. 22).

The isotopic studies have yielded a number of novel insights into the marine Ba cycle. First, the data underscore the importance of physical mixing (i.e., ocean circulation) in mediating patterns of dissolved δ^{138}Ba and, by extension, [Ba]. Second, both the regression of dissolved Ba isotopic data (Bates et al., 2017; Hsieh & Henderson, 2017) and comparison of colocated seawater and particulates (Horner et al., 2017; Cao et al., 2020b) imply an average particulate–dissolved Ba isotopic offset ≈−0.5 ‰, which is somewhat larger than the experimental results reported by Von Allmen et al. (2010). Third, marine sediments—both bulk (Bridgestock et al., 2018) and $BaSO_4$ isolates (Crockford et al., 2019)—faithfully reflect the ≈−0.5 ‰ Ba isotopic offset from surface seawater. Consequently, the mean δ^{138}Ba of globally sedimented $BaSO_4$ is ≈+0.1±0.1 ‰ (Crockford et al., 2019). Since $BaSO_4$ is the dominant oceanic output (e.g., Paytan & Kastner, 1996), these data imply that mean isotopic composition of Ba delivered to the ocean should possess an average composition ≈+0.1±0.1 ‰ (Horner & Crockford, 2021). At present however, the main Ba inputs are unable to close the marine Ba isotopic budget: rivers, the principal Ba source to seawater, rivers, are too heavy, exhibiting compositions generally ≥+0.2 ‰ (e.g., Cao et al., 2020a; Gou et al., 2020); and, groundwater discharge, while possessing the necessary 'light' composition of ≈+0.1 ± 0.1 ‰, is too small a Ba flux to balance the budget (Mayfield et al., 2021). Thus, either the marine Ba isotopic budget is currently out of steady state, or an additional Ba source possessing a light isotopic composition remains to be identified.

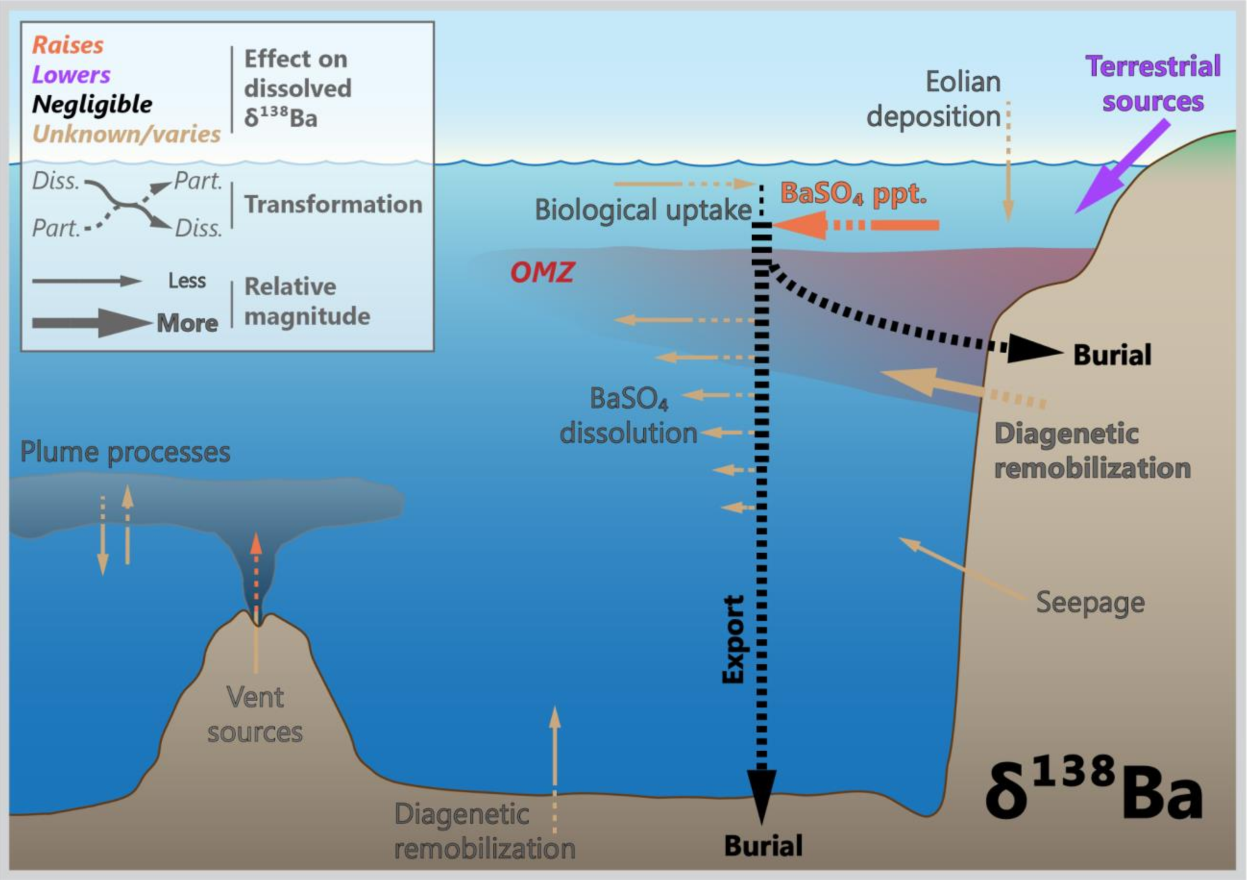

Figure 23 | Processes driving Ba isotope variations in modern seawater. Though biological processes exert only a minor direct influence on δ^{138}Ba, the biologically mediated cycling of $BaSO_4$ drives large variations in marine Ba isotope cycling, thereby connecting δ^{138}Ba to paleoproductivity.

8.2. Driving processes

Seawater is undersaturated with respect to $BaSO_4$ almost everywhere (Monnin et al., 1999; Rushdi et al., 2000). However, micro-crystalline $BaSO_4$ is ubiquitous in the ocean. This ‘barite paradox’ remains an area of active research. Proposed driving mechanisms broadly fall into two categories: ‘active’ biological and ‘passive’ chemical precipitation.

8.2.1. Biological

Several organisms are known to precipitate $BaSO_4$ intracellularly, possibly for the purposes of gravitropism (e.g., Gooday & Nott, 1982; Finlay et al., 1983). However, the organisms known to actively precipitate $BaSO_4$ are neither abundant in seawater, nor do they constitute a significant fraction of marine primary productivity. Likewise, acantharea—organisms that precipitate $SrSO_4$ (celestite) tests that can contain considerable quantities of Ba (e.g., Bernstein & Byrne, 2004)—are not necessary for driving significant Ba drawdown from the ocean (Esser & Volpe, 2002) nor for barite precipitation (Ganeshram et al., 2003). Thus, existing evidence does not support a significant role for active biological processes in driving the open marine Ba cycle (Fig. 23).

8.2.2. Chemical

Passive chemical precipitation is likely the major contributor to particulate $BaSO_4$ stocks and sedimentation. We focus our discussion on those $BaSO_4$ formed through association with the biological pump, though we note that other types of $BaSO_4$ exist in the ocean and their occurrence and geochemistry are reviewed in detail elsewhere (e.g., Hanor, 2000; Griffith & Paytan, 2012). Given that seawater is largely undersaturated with respect to $BaSO_4$, passive precipitation is thought to occur within particle-associated microenvironments that are supersaturated with respect to $BaSO_4$ (e.g., Chow & Goldberg, 1960; Dehairs et al., 1987). The development of $BaSO_4$-supersaturated microenvironments is hypothesized to relate to the heterotrophic oxidation of organic matter (Chow & Goldberg, 1960), whereby Ba and sulfate ions are concentrated in chemically isolated microzones during bacterially mediated mineralization of organic matter. Once sufficient quantities of Ba and sulfate ions have accumulated and the microenvironment becomes supersaturated, $BaSO_4$ precipitation occurs. Thus, passive precipitation of $BaSO_4$ is possible even in strongly undersaturated environments with low ambient sulfate (e.g., Horner et al., 2017). Continued mineralization destroys the microenvironment, ceasing precipitation and exposing $BaSO_4$ precipitates to undersaturated seawater where they begin to dissolve.

The widespread association between pelagic $BaSO_4$ and aggregates of decaying organic matter provides indirect support for this process (Dehairs et al., 1980; Bishop, 1988). Indeed, the peak in particulate Ba—

and presumably $BaSO_4$—abundance is found in the upper mesopelagic zone where most organic matter mineralization occurs (e.g., Sternberg et al., 2008). Though many of the microscale mechanisms remain unresolved, recent studies indicate that biofilms likely play an important role in accumulating Ba from seawater (e.g., Martinez-Ruiz et al., 2019; 2020), and can promote precipitation of $BaSO_4$ nanoparticles from undersaturated solutions (Deng et al., 2019).

Regardless of the precise microscale mechanism, precipitation of particulate $BaSO_4$ is ubiquitous in the marine realm. Given that $BaSO_4$ precipitation renders an apparent negative isotope fractionation of ≈−0.5 ‰, it is highly likely that $BaSO_4$ cycling drives much of the Ba isotope variability in the ocean (Fig. 23). From a paleoproxy perspective, this is ideal; $BaSO_4$ formation is related to the decay of organic matter and not by the presence of any specific organism (e.g., Jacquet et al., 2007; Dehairs et al., 2008). Downward transport of particulate $BaSO_4$ is driven by aggregation with larger particles (Lam & Marchal, 2014) and the efficiency of this downward transport depends on the same biophysical processes that export organic matter, thus connecting the export flux of $BaSO_4$ to that of organic carbon (Eagle et al., 2003).

Barites formed in the ocean through this passive chemical pathway are commonly termed marine, pelagic, authigenic, or biogenic. Though none of these terms are perfect descriptors of the chemical processes involved, 'marine' and 'biogenic' are the most ambiguous and their use is discouraged; the former encompasses all $BaSO_4$ formed in the marine realm—including diagenetic, cold seep, and hydrothermal—whereas the latter could be taken to imply only those precipitates brought about by active biological processes. While 'authigenic' is an informative descriptor, it has also been used to describe sedimentary $BaSO_4$ that formed via diagenetic redistribution on or below the seafloor (e.g., Torres et al., 1996). Thus, we recommend use of the term 'pelagic' when describing chemically precipitated microcrystalline $BaSO_4$, and encourage authors to include this definition in their works.

8.2.3. Physical

Similar to that of Si (silicic acid) and alkalinity, [Ba] exhibits a nutrient like profile in the oceans (Fig. 22). However, the extent to which this pattern arises from nonconservative biogeochemical processes versus physical mixing remains unresolved. Results from the GEOTRACES program are facilitating renewed interest into this topic, which is being investigated using two complementary approaches. In the first, biogeochemical contributions to basin-scale [Ba] distributions are isolated using statistical methods, such as OMPA (Optimum Multiparameter water mass Analysis). These statistical methods showed that mixing is dominant in the Mediterranean (Jullion et al., 2017) and North Atlantic (Le Roy et al., 2018), but that sea ice-related processes may be important in the high latitudes (Hendry et al., 2018). Second, the influence of mixing is evidenced from emerging Ba stable isotope data. Indeed, the importance of mixing has been documented vertically (Horner et al., 2015a), zonally (Bates et al., 2017; Bridgestock et al., 2018), and meridionally (Bates et al., 2017; Hsieh & Henderson, 2017). Together, these new approaches imply that *in situ* biogeochemical processes exert a relatively minor influence on basin-scale [Ba] distributions.

8.3. Marine archives

Given the connections between export production and $BaSO_4$ fluxes, the major archive of historical changes in Ba cycling is $BaSO_4$ itself (e.g., Griffith & Paytan, 2012). Indeed, the sedimentary accumulation of $BaSO_4$—often determined as the fraction of Ba in excess of the detrital Ba background or the deposition rate of $BaSO_4$ itself—has been extensively used to reconstruct past changes in export production (e.g., Schmitz, 1987; Francois et al., 1995; Paytan et al., 1996; Frank et al., 2000; Jaccard et al., 2005; Jaccard et al., 2013; Ma et al., 2014; 2015, Costa et al. 2016, Winckler et al., 2016). An estimated 30 % of the $BaSO_4$ microcrystals formed in seawater are buried in oxygenated sediments (e.g., Dymond et al., 1992), a considerably higher fraction than for organic carbon (Paytan & Kastner, 1996). However, in oligotrophic regimes where both $BaSO_4$ fluxes and sedimentation rates are low, prolonged exposure to undersaturated seawater results in poor preservation (Eagle et al., 2003; Serno et al., 2014). Similarly, in high productivity coastal upwelling settings, mineralization of organic matter in sediments consumes porewater O_2, driving conditions down the redox tower and toward sulfate reduction, hampering $BaSO_4$ preservation (McManus et al., 1998; Paytan & Griffith, 2007; Carter et al., 2020).

The isotopic composition of Ba in sediments has been investigated as a proxy for the Ba isotope composition of the Ba source (i.e., dissolved Ba in epipelagic and upper mesopelagic seawater). Applications to date have explored the recovery of the biological carbon pump following the Paleocene–Eocene Thermal Maximum (~56 Ma; Bridgestock et al., 2019) and the origin of enigmatic sedimentary $BaSO_4$ deposited in the aftermath of the Marinoan glaciation (~635 Ma; Crockford et al., 2019) and Great Oxidation Event (~2,000 Ma; Hodgskiss et al., 2019). These three applications are reviewed in detail in Horner & Crockford (2021).

Unlike many of the other TEIs reviewed here, we are not aware of any studies exploring δ^{138}Ba in Fe–Mn crusts. Barium is somewhat immobile in Fe–Mn crusts, with a calculated effective diffusivity $\leq 10^{-8}$ cm^2 yr^{-1} (see Henderson & Burton, 1999, for calculation details), similar to Zn (Sec. 9.3.1.). While this implies that Fe–Mn crusts have the potential to record variations in deep ocean δ^{138}Ba, a significant fraction of the total Ba in Fe–Mn crusts is associated with CFA (carbonate fluorapatite; Koschinsky & Hein, 2003). Since the CFA is secondary—filling voids around the layered Fe- and Mn-oxide minerals—it is unclear if Fe–Mn crusts can be developed into a useful archive of δ^{138}Ba.

Lastly, the amount of Ba in marine carbonates, typically reported as Ba:Ca has been extensively used to reconstruct the Ba content of past environments, specifically for constraining historical patterns of upwelling and/or terrestrial runoff (e.g., Lea et al., 1989; Gebregiorgis et al., 2016). More recently, a number of studies have investigated the fidelity of surface- (Liu et al., 2019) and deep-sea corals (Hemsing et al., 2018; Geyman et al., 2019), finding that a number of species are faithful archives of ambient [Ba] and δ^{138}Ba. These findings are highly promising from a proxy standpoint, as they indicate that a number of archives may be suitable for paleo Ba reconstructions.

8.4. Prospects

Barium exhibits several nutrient-like properties: first, [Ba] distributions resemble those of other nutrients and second, particulate abundances are intimately associated with the processes of organic carbon remineralization and export. Despite these connections, several aspects of Ba cycling—both in the modern and past oceans—remain unresolved. We thus suggest several areas for additional research that will help widen the applicability of Ba-based proxies in paleoceanography.

8.4.1. Modern

Several issues remain regarding the modern Ba cycle. Many of these are reviewed in detail by Horner & Crockford (2021), though we outline the four most pressing (and possible remedies) here. First, to what extent do the similar distributions in [Ba], [Si], alkalinity, and [^{226}Ra] reflect true biogeochemical coupling versus passive physical mixing? These correlations have been the subject of scrutiny for over 40 years (e.g., Chan et al., 1976; Chung, 1980), and recent GEOTRACES sections are facilitating a reevaluation of these relationships. As noted above, statistical analysis of Ba (and Si, Ra) distributions in regions will offer valuable insights, particularly if conducted in regions with weaker overturning circulation. Likewise, additional profiles of δ^{138}Ba from regions with strong *in situ* influences—Ba point sources (e.g., seeps, Torres et al., 1996; margin sediments, McManus et al., 1998), or point sinks (e.g., plankton blooms, Esser & Volpe, 2002)—should enable testing the importance of local processes to regional Ba isotope distributions.

Second, the Ba isotopic mass balance of the ocean must be closed. This will require detailed evaluation of other putative Ba sources, such as diagenetic remobilization (e.g., Hoppema et al., 2010), atmospheric deposition, and the importance of estuarine enhancement of riverine Ba fluxes (e.g., Hanor & Chan, 1977; Edmond et al., 1978). Large intra-marine Ba point sources, such as such as hydrothermal vents, can drive $BaSO_4$ supersaturation, leading to precipitation; indeed, a recent study suggests that the net effect of such point sources may be to increase deep δ^{138}Ba through $BaSO_4$ precipitation, further imbalancing the Ba isotope budget (e.g., Hsieh et al., 2021; Fig. 23). Barium isotope fractionation associated with other minera sinks, such as adsorption onto Fe–Mn oxyhydroxides, also remains uncharacterized.

Third, what is the mechanism of $BaSO_4$ precipitation? While the microenvironment mediated model appears most likely, many microscale mechanisms of precipitation remain ambiguous: How and from what are Ba and sulfate ions liberated during mineralization? How and why are they accumulated onto biofilms? Do different substrate organisms and/or heterotrophic communities influence the amount of $BaSO_4$ precipitated? Addressing these questions will require additional field and laboratory studies, which can then be compared against distributions of particulate $BaSO_4$ in the ocean interior. Depending on their importance, these nuances may require ecological parameterizations in numerical models of Ba cycling.

Finally, additional experiments are needed to narrow estimates of the fractionation factor between $BaSO_4$ and seawater. Existing laboratory studies place this estimate ≈ −0.3 ‰, whereas a wide range of field data suggest that it is considerably larger at ≈−0.5 ‰. Accounting for this ≈0.2 ‰ difference is both important and justifies additional experimentation, as it indicates incomplete understanding of the processes that fractionate Ba isotopes in the marine realm.

8.4.2. Paleo

As with the modern cycle, several ambiguities persist. Assuming that $BaSO_4$ remains the preferred archive of past Ba cycle variations, it is imperative to constrain the effect of early diagenesis on the Ba isotope composition of sedimentary $BaSO_4$. Likewise, it is unknown if diagenetic $BaSO_4$ retains any primary Ba isotope information. Assessing these issues will require studies of co-located $BaSO_4$ and porewaters from environments at various stages of early diagenesis. Answering these questions is critical in establishing the validity of Ba isotopes in barite as a paleoceanographic proxy.

Additionally, there are uncertainties relating to whether $BaSO_4$ cycling is impacted by ambient [Ba] during $BaSO_4$ precipitation and burial. For example, does more $BaSO_4$ precipitation occur at higher ambient [Ba]?

While there is evidence indicating that this is not a major influence in the modern ocean (e.g., Fagel et al., 2004; Serno et al., 2014), a relationship between ambient [Ba] and $BaSO_4$ precipitation is likely necessary to maintain steady state in the Ba cycle over geological timescales (e.g., Horner & Crockford, 2021). Likewise, to what extent does $BaSO_4$ preservation depend on ambient [Ba]? These considerations are significant when considering longer-term records, particularly when marine sulfate levels were lower-than-modern (and [Ba] presumably higher; e.g., Walker, 1983; Wei & Algeo, 2020). Finally, does the seawater temperature at the depth of POC mineralization impact the relationship between POC and $BaSO_4$ formation? These questions are best addressed through a combination of experimentation (e.g., cultures, precipitation), field studies in basins with large gradients in [Ba], and numerical experiments incorporating saturation state modeling.

9. Nickel

Nickel is biologically utilized, for example by diazotrophs during nitrogen fixation and by microorganisms catalysing the breakdown of reactive oxygen species (Twining & Baines, 2013). Particularly relevant to early Earth reconstructions is the fact that methanotrophs have an obligate requirement for Ni. Several promising archives have been identified for marine Ni isotope chemistry, however, determination of the composition of Ni isotope ratios in seawater has lagged behind other nutrient-like metals such as Zn and Cd. Recent datasets do indicate that Ni is cycled by phytoplankton, with a resultant isotope fractionation in the euphotic zone dependent on the dominant ecology of the region. As such, Ni isotope variations are likely to be broadly responsive to biological productivity, but the assumption of a constant fractionation factor (i.e., $\Delta_{\mathrm{P-R}}$) may be violated, which may complicate use of Ni isotopes as a quantitative paleoproductivity proxy, and the applicability of a simple reactor scheme. Additionally, the secondary sinks of Ni, such as those associated with Mn oxides, are associated with large Ni isotope fractionations, opening up the possibility of using Ni isotopes to track aspects of marine paleoredox.

9.1. Marine distribution

Nickel has a classic nutrient-type distribution in the oceans with one unusual feature; surface [Ni] never drops below ~1.8–2 nmol kg^{-1} (e.g., Sclater et al., 1976; Bruland, 1980; Fig. 24). There is evidence, however, that this residual pool in surface waters is not bioavailable, as summarized recently by Archer et al. (2020). Deep water [Ni] are 4–5 nmol kg^{-1} in the Atlantic, and ~9 nmol kg^{-1} in the north Pacific (Fig. 24).

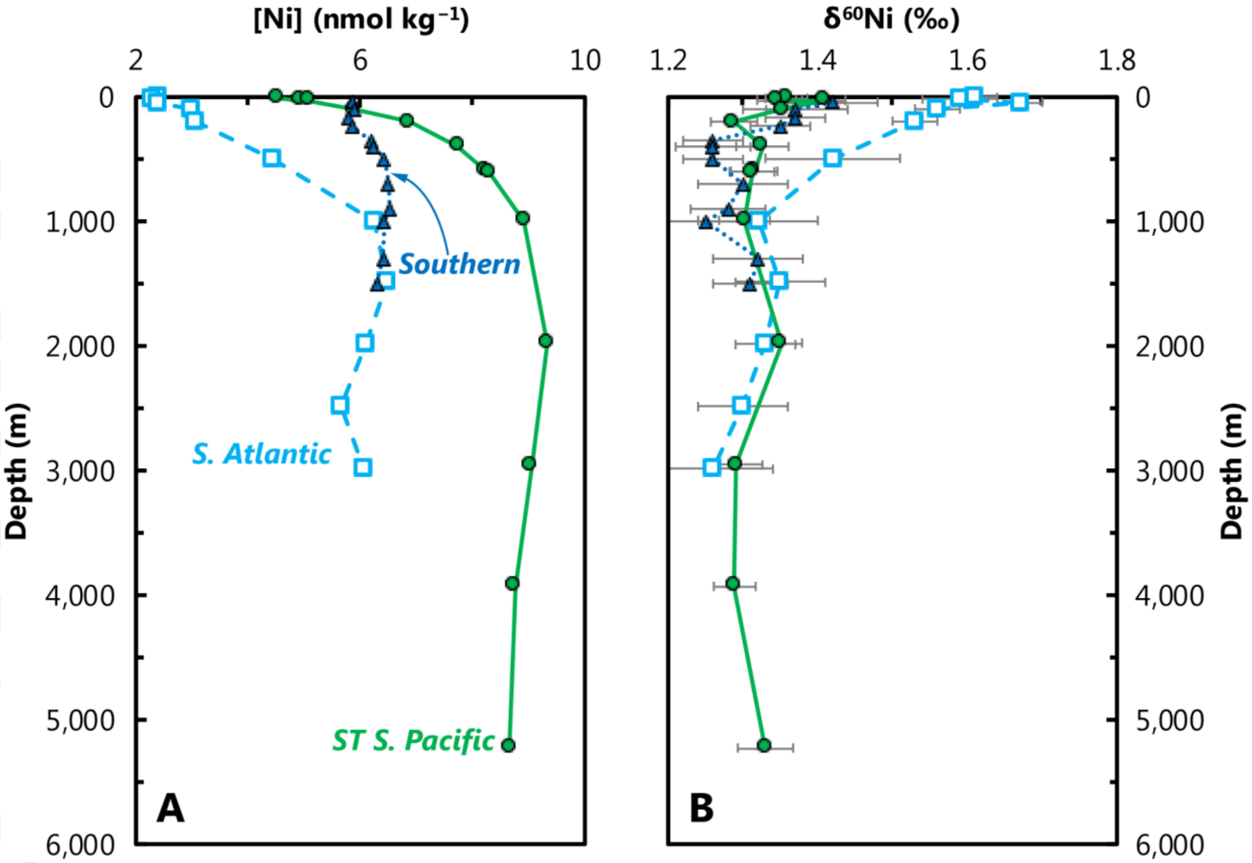

Figure 24 | Representative profiles of dissolved Ni concentrations ([Ni]; A) and Ni isotopic compositions (δ^{60}Ni; B). Data from the South Atlantic (squares, dashed line; Archer et al., 2020), Southern (triangles, dotted line; Wang et al., 2019a), and Subtropical South Pacific Oceans (circles, solid line; Takano et al., 2017). Station locations as per Fig. 1. This comparison illustrates that the oceanographic processes leading to distinct dissolved concentration profiles render only small changes in dissolved δ^{60}Ni between basins.

Developing robust analytical protocols for analyzing Ni isotopes for a range of sample matrices has proven somewhat more challenging than for some of the other trace metals discussed here due to the difficulty in separating Ni from interfering elements (e.g., Fe, a major isobaric interference on ^{58}Ni). Chemical purification protocols now use a sequence of resins including anion exchange (e.g., AG MP-1M or AG1-X8, Bio-Rad) and either a Ni-specific resin (containing dimethylglyoxime) or Nobias PA-1 (Hitachi High Technologies; e.g., Cameron et al., 2009; Gueguen et al., 2013; Wang et al., 2019a; Yang et al., 2020). The limited data since reported for the oceanic dissolved pool of Ni indicates relatively little variability in δ^{60}Ni at depth (+1.2 to +1.4 ‰), with a small shift towards heavier values up to +1.7 ‰ in the upper water column (Fig. 24; Takano et al., 2017; Wang et al., 2019a; Yang et al., 2020; Archer et al., 2020). The upper water column shift is proposed to reflect a small kinetic isotope fractionation during biological uptake. Similar to Zn, Cu, Cd, Mo, Ba and Cr, the isotopic composition of Ni in seawater is isotopically heavy compared to the UCC (Table 1).

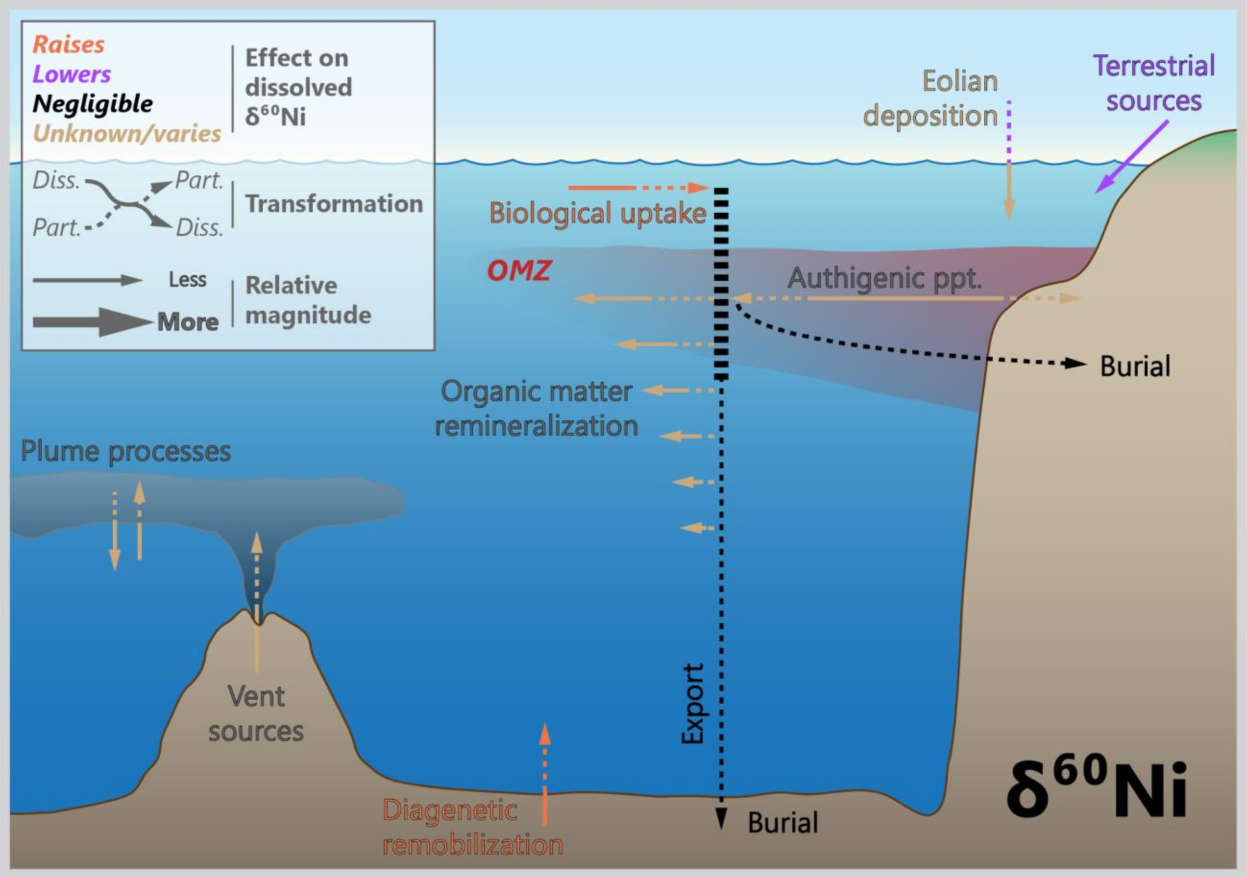

Figure 25 | Processes driving Ni isotope variations in modern seawater. Biological processes are recognized to drive a small, but systematic increase in dissolved δ^{60}Ni and marine Ni isotope values are preserved in certain sediments. Other abiotic Ni cycling processes may be important however, such as sorption to Mn-oxide minerals, and the significance of these fractionations to global Ni cycling remains to be fully elucidated.

9.2. Driving processes

9.2.1 Biological

To date, eight Ni-based enzyme systems have been identified (Ragsdale, 2009), including urease, which is key to the global nitrogen cycle, and methyl-CoM reductase, which catalyses the production of all biologically generated methane on Earth. The obligate requirement of methanogens for Ni has led to interest in developing Ni and Ni isotopes as a tracer of methane production on the early Earth (e.g., Cameron et al., 2009; Konhauser et al., 2009; Wang et al., 2019c). In the modern ocean the highest Ni quotas are found in diazotrophs (N-fixers), thought to reflect the presence of Ni-Fe hydrogenases (which catalyse H_2 produced during N fixation), Ni-superoxide dismutase (Ni-SOD) and urease (Tamagnini et al., 2002; Dupont et al., 2008a; 2008b; Nuester et al., 2012). Nickel limitation of phytoplankton grown on urea has been shown in culture and in natural assemblages, suggesting the Ni-N colimitation of phytoplankton growth may be relevant in the ocean (Price & Morel, 1991; Dupont et al. 2008a; 2010). Significant Ni is also found in diatom frustules (about 50 % of diatom cellular quotas; Twining et al., 2012). The latter observation is thought to play a role in the similarity of Ni and Si oceanic distributions (Twining et al., 2012).

No culture data are available to determine the degree of Ni isotope fractionation during biological uptake. Upper ocean data suggest no fractionation or a small preference for the light isotope, equivalent to ≈−0.3 ‰ (Takano et al., 2017; Archer et al., 2020; Yang et al., 2020; Fig. 25), consistent with the Ni isotope systematics observed in organic-rich sediments (Ciscato et al., 2018) and water column particulates (Takano et al., 2020). Interestingly, new water column data from the South Atlantic suggest distinct ecological differences in Ni drawdown and Ni isotope fractionation compared to other bioactive trace metals (e.g., Zn, Cd). Limited drawdown and Ni isotope fractionation is observed in the diatom-dominated regime south of the Polar Front in the Southern Ocean. In contrast, more marked drawdown and significant Ni isotope fractionation is observed north of the Polar Front, which has been attributed to the predominance of nitrate-limited, Ni-requiring cyanobacteria (Archer et al., 2020).

9.2.2 Chemical

Nickel is partially complexed by strong organic ligands in coastal and open ocean environments (5–70 %; e.g., Donat et al., 1994; Saito et al., 2004; Boiteau et al., 2016), though slow water exchange kinetics of Ni make these complexation measurements particularly challenging (Hudson & Morel, 1993). Slow exchange kinetics may also explain the residual pool of non-bioavailable Ni in the surface ocean (e.g., Mackay et al., 2002; Dupont et al., 2010). Speciation models suggest that the remainder of the Ni is present as free Ni^{2+} and $NiCl^{+}$, with a small fraction present as $NiCO_3^0$ (Zirino and Yamamoto, 1972; Turner et al., 1981).

Nickel cycling is tightly coupled to that of Mn—in sediments (Koschinsky & Hein, 2003), during removal from hydrothermal fluids (e.g., Gueguen et al. 2021), within porewaters (Klinkhammer, 1980), and across the redoxcline of the Black Sea (Vance et al., 2016). In the Black Sea, for example, Mn redox cycling is associated with preferential sorption of light Ni isotopes, with a large negative fractionation of ≈–4‰ (Vance et al., 2016). This large fractionation is consistent with experimental sorption of Ni on birnessite (Wasylenki et al., 2014; Sorensen et al., 2020).

Unlike more strongly chalcophile elements like Cd, Cu, and Zn, Ni is not strongly drawn down in the euxinic portion of the Black Sea water column (Tankéré et al., 2001; Vance et al., 2016) and in other euxinic basins (e.g., Jacobs & Emerson, 1982; Jacobs et al., 1985). However, Ni is enriched in Black Sea sediments

(Little et al., 2015), with δ^{60}Ni compositions notably lighter (at +0.3 to +0.6‰) than Ni sources to the basin (at about +1.3‰; Vance et al., 2016). Vance et al. (2016) attributed these light isotope compositions to the scavenging of sulfidized Ni species, which are predicted to be isotopically light (Fujii et al., 2011b).

Dissolved Ni is added to the ocean from rivers, hydrothermal vents, and dust (Fig. 25). All three sources possess δ^{60}Ni between +0.1 to +0.8 ‰, which is lighter than deep ocean seawater (see recent summaries by Little et al., 2020; Gueguen and Rouxel, 2021). In general, these Ni sources are not of a sufficient magnitude to generate deviations in deep ocean dissolved δ^{60}Ni, and are therefore unlikely to compromise use of δ^{60}Ni as a paleoproductivity tracer (similar to δ^{114}Cd; Sec. 6.). The main output flux of Ni from seawater is believed to be burial with Mn oxides, which have a wide range of reported Ni isotope compositions. While hydrogenetic ferromanganese crusts are generally isotopically heavy, from about +0.9 to +2.5‰ (Gall et al., 2013; Gueguen et al., 2016; Gueguen et al., 2021), Mn-rich pelagic clays possess δ^{60}Ni between −0.8 and +1.0‰ (Little et al., 2020; Gueguen & Rouxel, 2021). The Ni isotope difference between sources and sinks implies the existence of a missing 'heavy' Ni source. Recently, Little et al. (2020) and Gueguen & Rouxel (2021) hypothesised that this source is related to benthic release from sediments and predicted that it possesses an extremely fractionated Ni isotope composition of $\approx$ +3 ‰.

9.2.3 Physical

The most recent estimate for the residence time of Ni in the ocean is approximately ~20 kyr (Little et al., 2020), considerably longer than the mixing time of the ocean. As a result, in parallel with the other bioactive trace metals discussed herein, Ni and Ni isotope distributions are modulated at first order by the geometry of physical ocean circulation. The importance of diatom uptake in the Southern Ocean in partially coupling oceanic Ni and Si (Twining et al., 2012) was introduced above, and the relative homogeneity of deep ocean Ni isotope compositions supports an important role for southern-sourced water masses in the Ni distribution (Fig. 24; Takano et al., 2017; Wang et al., 2019a; Archer et al., 2020).

9.3. Marine archives

9.3.1. Ferromanganese sediments

Ferromanganese crusts exhibit variable Ni isotope compositions (Fig. 26; Gall et al., 2013; Gueguen et al., 2016a), which are, on average, slightly isotopically heavier (at δ^{60}Ni of +1.6‰) than seawater (δ^{60}Ni at about +1.3‰). Nickel is relatively immobile in Fe–Mn crusts, with a calculated effective diffusivity $\leq 10^{-9}$

$cm^2\ yr^{-1}$ (see Henderson & Burton, 1999, for calculation details), similar to Cu (Sec. 5.3.1.), implying that Fe–Mn crusts preserve primary information about dissolved δ^{60}Ni. However, experiments suggest that sorption of Ni to birnessite (the primary Ni-hosting phase in Fe–Mn sediments) should be associated with a large negative isotope effect (of about 3 to 4 ‰; Wasylenki et al., 2014; Sorensen et al., 2020). It remains unclear why the full isotope effect is not expressed in Fe–Mn crusts. Intense Mn cycling occurs across the redoxcline of the Black Sea; this cycling is associated with large variations in Ni and Ni isotopes, consistent with the experimentally observed light isotope effect on sorption to birnessite (Vance et al., 2016). Recent data from Mn-rich sediments that have undergone diagenesis also point to the preservation of a large negative Ni isotope effect, and predict a concomitant isotopically heavy benthic Ni source (Little et al., 2020; Gueguen & Rouxel, 2021).

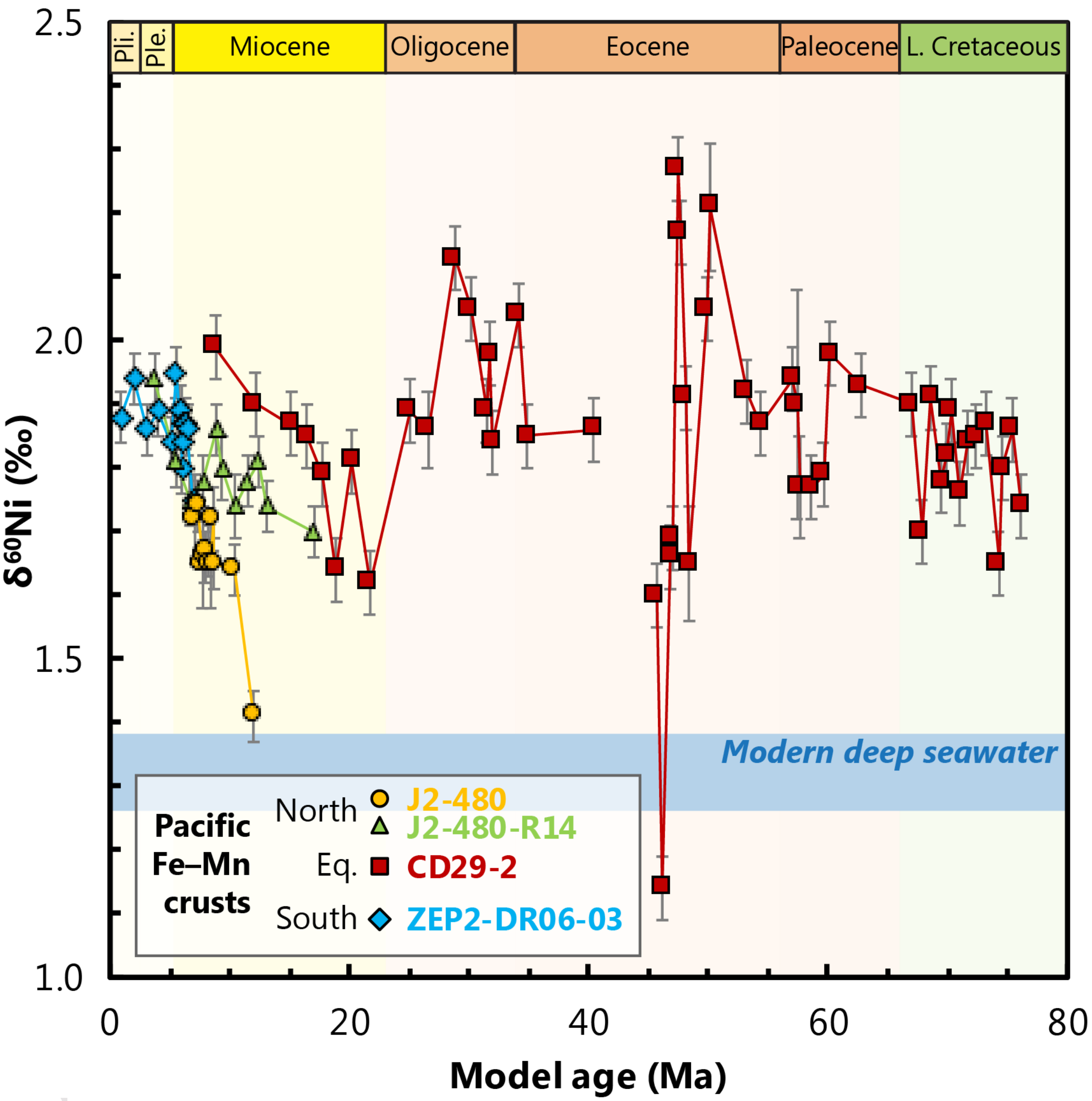

Figure 26 | Four Fe–Mn records of δ^{60}Ni from the Pacific Ocean. Assuming that Fe–Mn crusts have always formed with an offset ≈+0.5 ‰ with respect to ambient dissolved Ni in seawater, these records illustrate that the Ni isotope composition of seawater has varied by only ±0.2 ‰ over the Cenozoic. Data for J2-480, J2-480-R14, and ZEP2-DR06-03 are from Gueguen et al. (2016). Data from CD29-2 are from Gall et al. (2013). All four records have been plotted using the authors' preferred age model, meaning that there are some differences between the chronology of CD29-2 shown here compared to Figs. 8, 17.

Though promising, the development of Fe–Mn crusts as a tracer of past oceanic Ni cycling awaits a mechanistic understanding of the processes driving their variably isotopically heavy signature, as well as an awareness of the likely complicating role of diagenetic remobilisation of Ni (e.g., Atkins et al., 2016; Little et al., 2020).

9.3.2. Organic-rich sediments

As introduced in Sec. 4.3.2. (Cu), qualitative arguments for high organic matter fluxes (i.e., increased paleoproductivity) have been made based on enriched Ni (and Cu) content in ancient organic-rich sediments (e.g., Tribovillard et al., 2006). For Ni, this approach is supported by positive correlations with TOC in modern continental margin sediments (Fig. 27).

Nickel does not precipitate in the presence of water column dissolved sulfide and is therefore less susceptible to decoupling from TOC fluxes compared to chalcophile elements such as Cu, Zn and Cd. Nevertheless, Ni cycling is strongly linked to the redox cycling of Mn, potentially complicating Ni–TOC coupling in settings with active diagenetic cycling of Mn. Sedimentary and water column data from the Black Sea indicate that cycling associated with the benthic Fe–Mn redox shuttle (e.g., Lyons & Severmann, 2006) provides an alternative supply route for Ni to the deep euxinic basin in this setting (Little et al., 2015; Vance et al., 2016). Therefore, open marine settings would be the most promising from which to make estimates of the relative productivity of two different sites based on their absolute measured Ni:TOC ratios. Otherwise the degree of basin restriction will exert the primary control on nutrient supply, and therefore the degree of trace metal enrichment (Algeo & Maynard, 2008; Little et al., 2015).

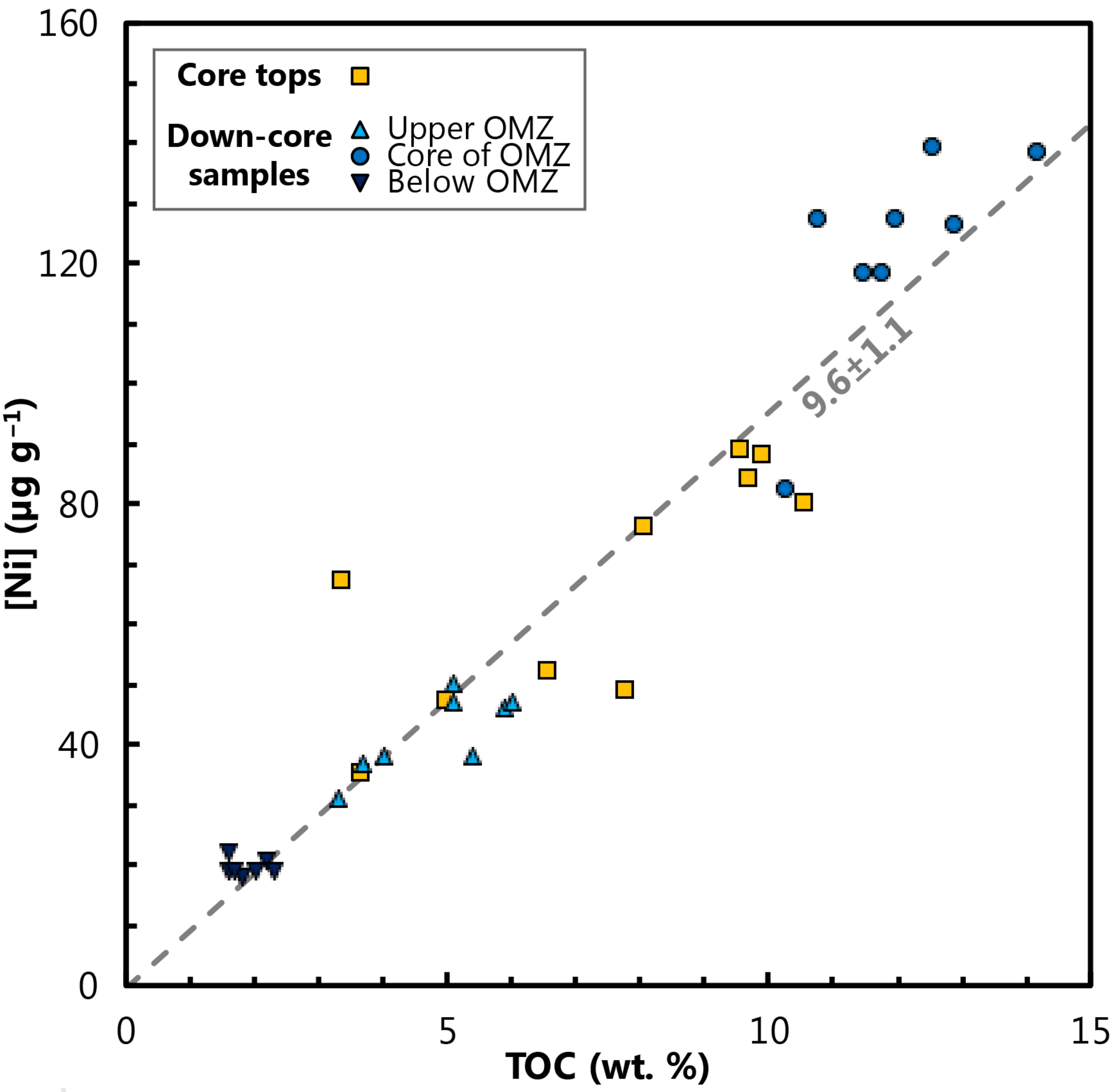

Figure 27 | Correlation of Ni and TOC content in organic-rich sediments from the Peru Margin. Data from Ciscato et al. (2018). The best-fit regression of these data yields a Ni–TOC slope of 9.6±1.1 (mean ± 2 SD), similar to the "≈9" reported by Böning et al. (2015).

Ciscato et al. (2018) investigated the distribution of Ni and its isotopes in two fractions isolated from Peru margin organic-rich sediments. The HF-HCl digestible fraction (usually containing >80% of total Ni) exhibited δ^{60}Ni values similar to modern deep seawater (at about +1.2‰). Meanwhile, these authors found variable Ni isotope compositions in the organic pyrite fraction (OPF), which they suggested record the fractionation imparted by biological uptake in the euphotic zone. Systematic relationships between Ni–TOC, $\delta^{60}\mathrm{Ni}_{\mathrm{OPF}}$, and δ^{13}C indicate that there is merit in continuing to investigate Ni and Ni isotopes as a paleoproductivity tracer (Ciscato et al., 2018).

9.4. Prospects

To date, Ni and its isotopes have been under developed as a potential paleoproductivity proxy. Recent data, both from the dissolved phase in seawater and in two different fractions isolated from anoxic organic-rich sediments, suggest promise in the coupling of Ni and C and their isotopes. However, in oxic-to-suboxic settings, Ni contents and isotopic composition of sediments are strongly influenced by the diagenetic redox cycling of Mn (e.g., Gueguen & Rouxel, 2021). We recommend additional study of Ni content and isotopic compositions in sediments, focusing specifically on carbonate and siliceous biominerals, which is increasingly tractable with new and improved chemical separation and analytical techniques.

Finally, in a completely different approach, Wang et al. (2019c) presented δ^{60}Ni values of Precambrian glacial diamictites, which are suggested to represent the chemical weathering residues of the UCC. They find a small shift towards heavier Ni isotope compositions across the Great Oxidation Event, which they relate to the onset of oxidative weathering of crustal sulfides (Wang et al., 2019c). Combined with the proposed importance of Ni to the maintenance of methanogenesis during this time period (e.g., Konhauser et al., 2009), it is hoped that future Ni stable isotope analyses will shed further light on the paleoenvironmental conditions on the early Earth.

10. Chromium

Chromium (Cr) stable isotope composition (δ^{53}Cr) has received significant attention over the past decade as a proxy of paleoredox conditions. These applications have generally used a framework where isotope fractionation is driven by subaerial weathering, with the partial pressure of atmospheric O_2 controlling δ^{53}Cr signatures in resultant paleorecords (e.g., Frei et al., 2009; 2014). However, subsequent studies have identified numerous challenges to this framework, including questions about the fidelity of sediment records (e.g., Remmelzwaal et al., 2019; Frank et al., 2020; Wang et al., 2021) as well as the very processes driving Cr cycling in seawater. Indeed, recent studies suggest that the most spatially expansive Cr isotope variations in the ocean are not related to oxygen availability but rather uptake by phytoplankton (e.g., Janssen et al., 2020). This means that Cr isotopes may serve as a novel productivity tracer that is reasonably well described by the isotope reactor framework (Sec. 2.2.). However, until recently, marine Cr data have not seen the significant improvements in quality control as other metals in the GEOTRACES repertoire, and there are currently no consensus values for [Cr] and δ^{53}Cr in GEOTRACES reference materials. Consequently, there is a degree of discrepancy among literature data that likely does not wholly represent natural variability (see discussions in Goring-Harford et al., 2018; Rickli et al., 2019; Moos et al., 2020; Nasemann et al., 2020; Huang et al., 2021), limiting our understanding of modern Cr cycling and thus paleoproxy validation. Given the issues surrounding the measurement of—and mechanisms driving—Cr isotope variation in seawater, we focus our assessment of Cr on open ocean GEOTRACES-era data that are not considered equivocal by subsequent studies. We suggest that these new insights offer an opportunity to re-assess the fidelity of different sediments as archives of past seawater δ^{53}Cr.

10.1. Marine distribution

In the ocean, [Cr] follows a nutrient-type vertical distribution (e.g., Campbell & Yeats, 1981), suggesting involvement in biological processes; however, concentration gradients with depth are minor relative to other algal macro- and micronutrients (Fig. 28). Open ocean surface [Cr] are 2–4 nmol kg^{-1}, with lower concentrations in the oligotrophic gyres than at higher latitudes (Scheiderich et al., 2015; Goring-Harford et al., 2018; Moos & Boyle, 2019; Rickli et al., 2019; Janssen et al., 2020). Chromium is elevated in Pacific and Southern Ocean deep waters, with [Cr] of 3.5–6.0 nmol kg^{-1} (Fig. 28; Moos & Boyle., 2019; Rickli et al., 2019; Nasemann et al., 2020; Huang et al., 2021). Although inter-basin deep water [Cr] gradients are small relative to other trace metals (e.g., [Cd], [Zn]) and macronutrients ([PO_4^{3-}], [NO_3^-], [Si]), clear increases in [Cr] are seen in deep waters advected northward from the Southern Ocean. These observations reflect, in part, a deep regeneration cycle for Cr, with maxima in the abyssal ocean (e.g., Jeandel & Minster, 1987).

The two primary redox forms of Cr in the ocean are Cr(VI), an oxyanion with limited particle reactivity, and Cr(III), a poorly soluble cation that readily adsorbs to mineral and organic phases (e.g., Wang et al., 1997; Semeniuk et al., 2016). In oxic seawater, thermodynamic calculations predict that Cr(VI) should be the only species present (Elderfield, 1970); however, Cr(III) is regularly reported as representing 5–15 % of [Cr] (e.g., Cranston & Murray, 1978; Jeandel & Minster, 1987; Davidson et al., 2020; Janssen et al., 2020), and Cr(III) abundance is elevated in OMZs and anoxic waters (Murray et al., 1983; Rue et al., 1997; Davidson et al., 2020; Huang et al., 2021). Due to the differences in solubility and reactivity of these species, redox cycling plays an important role in setting [Cr] distributions. The primary oceanic Cr reductants are ferrous Fe (Pettine et al., 1998) and H_2S (Kim et al., 2001). Chromium(III) maxima in surface waters suggests that biological or photochemical processes, possibly involving dissolved organic matter, are also important (e.g., Kieber & Helz, 1992; Achterberg & van den Berg, 1997; Janssen et al., 2020); however, these processes may occur indirectly through the generation of Cr reductants such as ferrous Fe (Hug et al., 1997). The primary marine Cr oxidants are Mn oxides (van der Weijden & Reith, 1982; Milletto et al., 2021) and H_2O_2 (Pettine et al., 1991); Cr oxidation by O_2 is insignificant due to kinetic limitations. Chromium redox cycling is accompanied by isotope fractionation, with reduction consistently resulting in an enrichment of light isotopes in the reduced phase (e.g., Ellis et al., 2002; Wanner & Sonnenthal, 2013), and therefore redox cycling—biologically mediated or otherwise—is likely important for dissolved Cr stable isotope distributions as well as [Cr]. Fractionation during Cr oxidation is more poorly constrained, with variable fractionation patterns reported (Zink et al., 2010; Milletto et al., 2021).

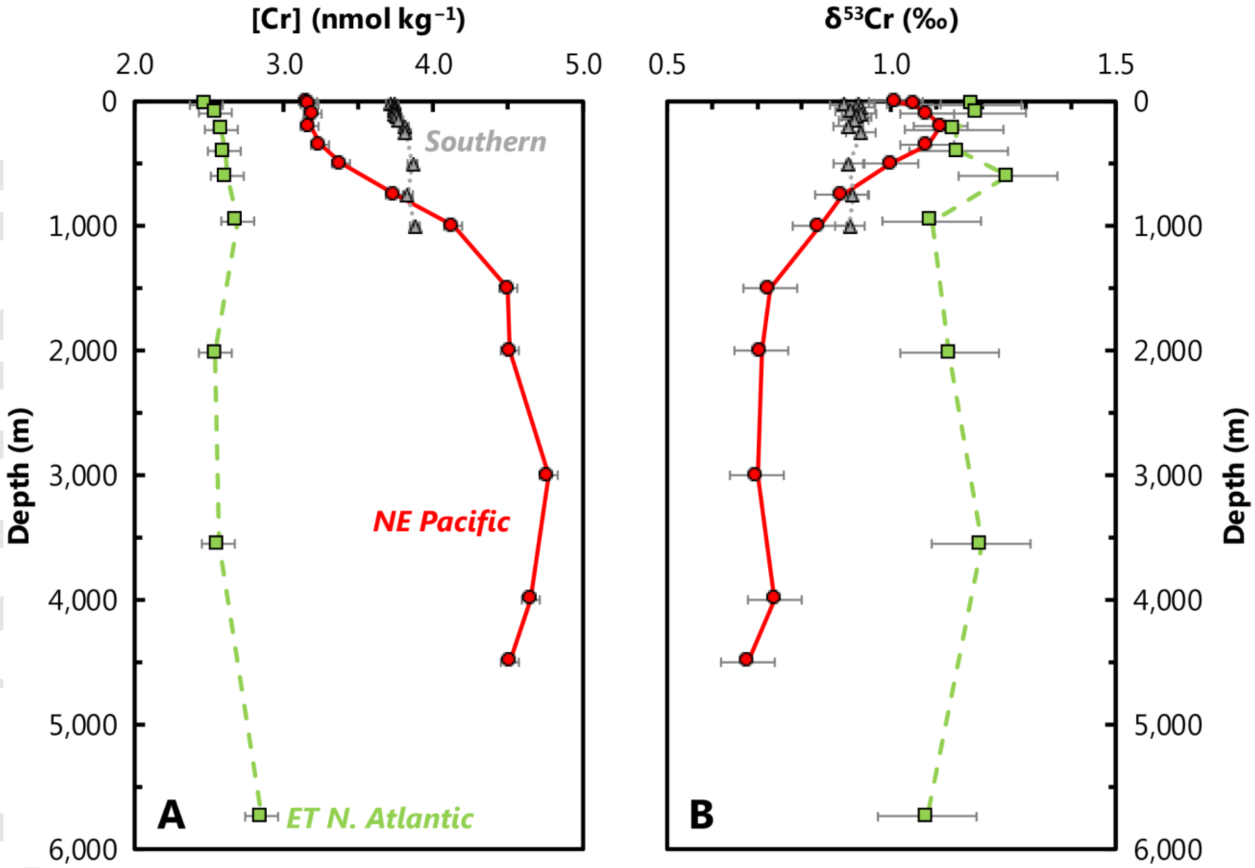

Figure 28 | Representative profiles of dissolved Cr concentrations ([Cr]; A) and Cr isotopic compositions (δ^{53}Cr; B). Data from the Eastern Tropical North Atlantic (squares, dashed line; Goring-Harford et al., 2018), Southern (triangles, dotted line; Rickli et al., 2019), and northeast Pacific Oceans (circles, solid line; Moos & Boyle, 2019). Station locations as per Fig. 1. These profiles illustrate that the decrease in surface ocean [Cr] from the Southern to low-latitude oceans is accompanied by a modest, but significant increase in δ^{53}Cr. Likewise, deep waters with elevated [Cr] exhibit lighter δ^{53}Cr, consistent with regeneration of an isotopically light Cr-bearing phase.

Chromium stable isotope compositions are reported relative to NIST SRM 979. The pioneering study of Scheiderich et al. (2015) reported much of the first oceanographically consistent δ^{53}Cr data. These and subsequent data show enrichments of heavy isotopes in open ocean surface waters (+0.9 to +1.4 ‰) relative to most deep waters (+0.7 to +0.9 ‰; Scheiderich et al., 2015; Goring-Harford et al., 2018; Moos et al., 2019; Rickli et al., 2019; Janssen et al., 2020; Moos et al., 2020; Nasemann et al., 2020; Fig. 28). Importantly, the first global δ^{53}Cr compilation also identified a tight linear correlation between δ^{53}Cr and ln[Cr], suggesting that the controls on [Cr] also regulate δ^{53}Cr—reduction and removal in OMZs and biological export from the surface ocean—and that these processes are accompanied by an isotope fractionation of approximately −0.7 to −0.8 ‰ (Scheiderich et al., 2015; Goring-Harford et al., 2018; Rickli et al., 2019; Janssen et al., 2020; Moos et al., 2020; Nasemann et al., 2020; Fig. 29; see also reactor model, Secs. 2.2., 12.2.). Subsequent studies have focused on understanding and constraining the sensitivities of these processes. Isotopic fractionation during Cr removal in OMZs has been reported both in the water column (Moos et al., 2020; Huang et al., 2021) and at the sediment–water interface (Moos et al., 2020; Nasemann et al., 2020). Similarly, fractionation is observed during Cr export coupled to the biological pump based on data from the open ocean (Janssen et al., 2020) and coastal waters (Goring-Harford et al., 2018).

While the understanding of [Cr] and dissolved δ^{53}Cr in the modern ocean has seen substantial improvements in the GEOTRACES-era, key uncertainties in Cr biogeochemical cycling remain. In turn, these uncertainties limit the potential of δ^{53}Cr paleoproxy applications and the identification of faithful δ^{53}Cr paleoarchives. The following sections present a more detailed summary of the marine Cr cycle and Cr archives, with a focus on the δ^{53}Cr paleoproxy outlook related to marine Cr cycling and the key remaining uncertainties.

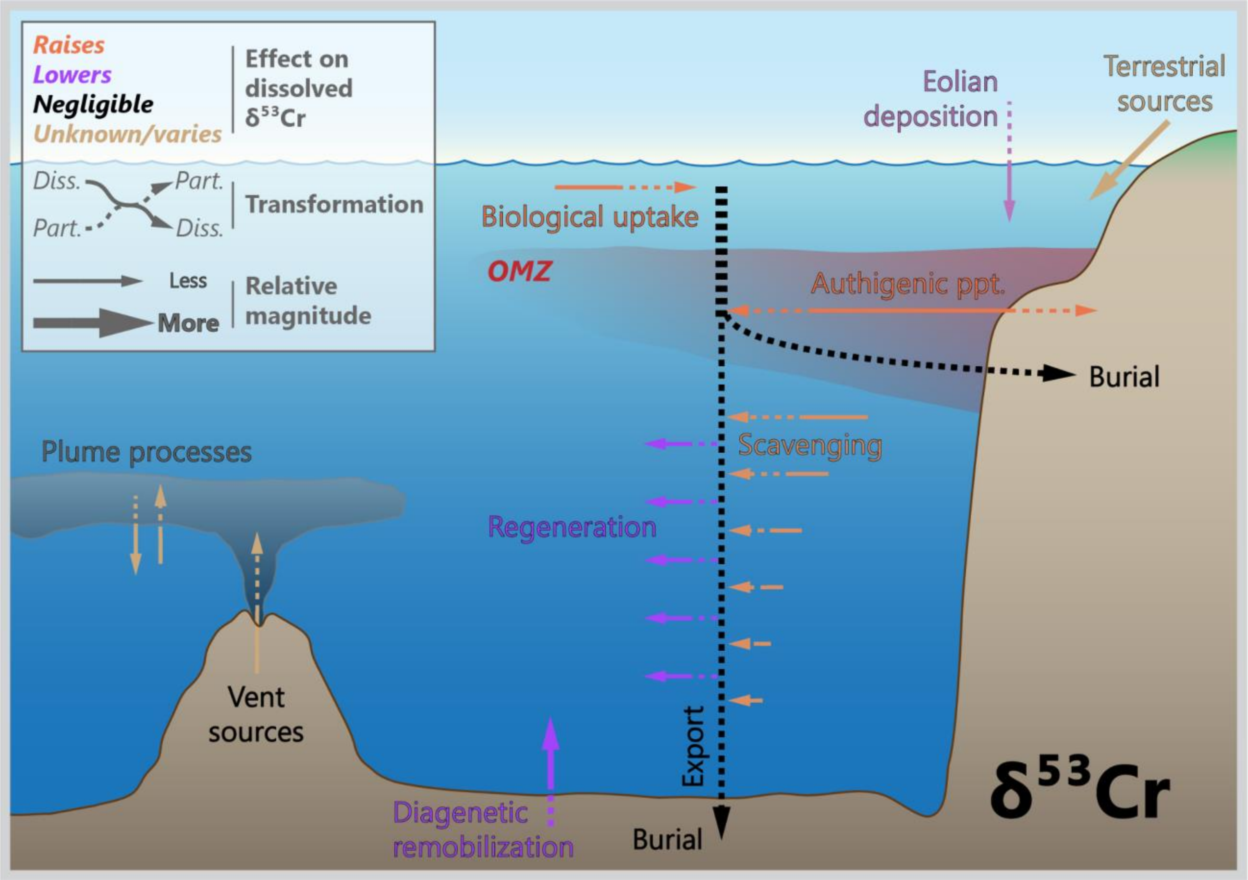

Figure 29 | Processes driving Cr isotope variations in modern seawater. Though muted, biological processes exert a control on Cr and δ^{53}Cr, and therefore δ^{53}Cr shows some response to productivity. The degree to which δ^{53}Cr may ultimately be useful as a productivity proxy will depend on how globally important productivity is relative to other controls on Cr distributions, such as Cr reduction and removal in OMZs and the fidelity of sediment records, which currently remain unresolved.

10.2. Driving processes

10.2.1. Biological

Although Cr(VI) can be toxic (e.g., Wong & Trevors, 1988) and there is no known biological function for Cr in marine phytoplankton, [Cr] distributions reflect biogenic controls (e.g., Campbell & Yeats, 1981). This appears to be driven not by internalization but by adsorption of Cr(III) onto phytoplankton (Wang et al., 1997; Semeniuk et al., 2016). This scavenging removes isotopically light Cr from the surface ocean (Scheiderich et al., 2015; Goring-Harford et al., 2018; Janssen et al., 2020;), and has been shown to quantitatively explain patterns of oceanic [Cr] and dissolved δ^{53}Cr (Janssen et al., 2020). The magnitude of Cr export associated with the biological pump has been estimated at approximately 0.1–1 Gmol Cr yr^{-1} (Jeandel & Minster, 1987; Janssen et al., 2020), of comparable magnitude to known Cr sources (Wei et al., 2018).

10.2.2. Chemical

Chromium is reduced and removed in OMZs and anoxic waters (Murray et al., 1983; Rue et al., 1997; Davidson et al., 2020; Moos et al., 2020; Nasemann et al., 2020; Huang et al., 2021). This removal may occur in the water column (Rue et al., 1997; Davidson et al. 2020; Moos et al., 2020; Huang et al., 2021) or at the sediment–water interface, though it is presently unclear which is of greater importance (cf. Moos et al., 2020; Nasemann et al., 2020). Approximate isotope fractionation factors for OMZ Cr reduction and removal are estimated as being ≈−0.7 ‰, similar to those implied by the global dissolved δ^{53}Cr – [Cr] array. However, these fractionation factors are considerably smaller than the expectations based on laboratory constrained fractionation factors (e.g., Wanner & Sonnenthal, 2013), likely reflecting an incomplete removal of Cr(III) resulting in a lower effective fractionation (Moos et al., 2020; Nasemann et al., 2020; Huang et al., 2021) and the fact that isotope reactor models will underestimate true isotope separation factors in the presence of mixing. Water column-based estimates of the OMZ Cr sink are not available, and deep water data suggest that some of the Cr removed in OMZs is released in underlying oxic waters and/or sediments (e.g., Murray et al., 1983).

10.2.3. Physical

Riverine fluxes are believed to represent the main source of Cr to the oceans, accounting for approximately 1 Gmol Cr yr^{-1} (Wei et al., 2018). High variability has been reported for riverine dissolved δ^{53}Cr, though available data suggest that rivers are isotopically heavy relative to the continental crust (e.g., Frei et al., 2014; D'Arcy et al., 2016; Goring-Harford et al., 2020). The role of estuarine processes is unclear at present. Earlier studies suggested scavenging of Cr at low salinity (Cranston & Murray, 1980; Campbell & Yeats, 1984), therefore lowering of riverine Cr fluxes; however, recent data have found conservative mixing of Cr(III), Cr(VI) and δ^{53}Cr (Goring-Harford et al., 2020) or release of particulate Cr to the dissolved phase (Sun et al., 2019).

As with other trace metals (e.g., Zn, Cd, Ba; Secs. 4., 6., 8.), deep water circulation plays an important role in shaping [Cr] and dissolved δ^{53}Cr distributions. The advection of Cr-rich intermediate and deep waters formed in the Southern Ocean helps to explain [Cr] enrichments seen at depth in the Pacific (Fig. 28A; cf. Rickli et al., 2019; Moos et al., 2019). Data from NADW, while more limited, suggest it is more Cr-depleted than waters formed in the Southern Ocean (Fig. 28A; cf. Goring-Harford et al., 2018; Rickli et al., 2019).

10.3. Marine archives

10.3.1. Carbonates

Chromium(VI) is incorporated into the $CaCO_3$ matrix during carbonate formation (e.g., Tang et al., 2007). Because Cr(VI) dominates the [Cr] pool in the oxic ocean, this suggests that carbonates may serve as a suitable proxy for ambient dissolved δ^{53}Cr, motivating numerous δ^{53}Cr-based reconstructions as well as a significant body of research to ground-truth the theory-based motivations. A recent review of δ^{53}Cr-based paleo reconstructions in carbonates can be found in Wei et al. (2020) and below we highlight relevant assessments of the utility of carbonate archives from the modern ocean.

Inorganic calcite precipitation at oceanographically relevant pH results in an enrichment of light isotopes in $CaCO_3$ up to 0.7 ‰ lighter than the solution (Füger et al., 2019), though data at an oceanographically relevant ionic strength are not available. The Cr content of carbonates is low (from <1 to ~10 µg g^{-1}; Holmden et al., 2016; Pereira et al., 2016; Remmelzwaal et al., 2019), and therefore $CaCO_3$ is not a major Cr sink (Bonnand et al., 2013). Studies of Cr incorporated into a diverse range of biogenic carbonates show an enrichment in isotopically light Cr relative to ambient seawater, but with a wide range of fractionation factors. This fractionation is believed to reflect redox processes during Cr uptake into calcifying organisms or preceding Cr incorporation into $CaCO_3$ (Holmden et al., 2016; Pereira et al., 2016; Farkas et al., 2018). Marine carbonate-hosted δ^{53}Cr archives are, however, susceptible to meteoric (Wang et al., 2021) and marine diagenetic overprinting (e.g., Remmelzwaal et al., 2019).

10.3.2. Ferromanganese crusts

Ferromanganese (Fe–Mn) crusts from the Pacific are isotopically light (δ^{53}Cr = −0.85 to −0.15 ‰, average = −0.42 ‰, Wei et al., 2018) relative to North Pacific deep water (≈ +0.7 to +0.8 ‰, Moos & Boyle, 2019; Fig. 28B), equivalent to an isotope separation factor of approximately −0.9 to −1.6 ‰. The low abundance of Cr in Fe–Mn crusts (~7 µg g^{-1}) indicates that, globally, Cr removal to Fe–Mn oxides is not important in controlling [Cr] and δ^{53}Cr budgets (Wei et al., 2018). Additionally, Cr is likely somewhat mobile in Fe–Mn crusts, with a predicted diffusivity $\leq 10^{-7}$ cm^2 yr^{-1} (see Henderson & Burton, 1999, for calculation details), similar to Cd (Sec. 6.3.2.), Mo (Sec. 7.3.), and Ag (Sec. 11.3.). This rate implies that long-term records of δ^{53}Cr derived from Fe–Mn are likely to exhibit some diffusive smoothing while preserving larger perturbations. The large range of δ^{53}Cr in modern Fe–Mn crusts, relative to the modest variations in δ^{53}Cr of surrounding intermediate and deep waters, suggests that Fe–Mn crusts are unlikely to be developed into a reliable archive for past marine δ^{53}Cr.

The Cr content of other types of oxygenated sediments are generally low (≈60 µg g^{-1}; Gueguen et al., 2016b), with Cr:Ti ratios comparable to the continental crust. Some samples, however, do show apparent authigenic Cr enrichments of a similar magnitude to anoxic and suboxic sediments.

10.3.3. Suboxic and anoxic sediments

Chromium is generally enriched in suboxic and anoxic surface sediments relative to upper continental crust and oxic sediments (Reinhard et al., 2014; Gueguen et al., 2016b), with an average Cr content of surface sediments of 108 ± 28 µg g^{-1} (1SD, *n* = 12, Gueguen et al., 2016b; Bruggmann et al., 2019), suggesting authigenic Cr enrichments in these environments may present a major Cr sink (Reinhard et al., 2013; Wei et al., 2018). Suboxic and anoxic sediment leaches targeting authigenic Cr are isotopically light relative to regional and basin-scale deepwater (Gueguen et al., 2016b; Bruggmann et al., 2019), in agreement with predictions for Cr removal in OMZs and biological export (Janssen et al., 2020; Moos et al., 2020; Nasemann et al., 2020; Huang et al., 2021). Down-core records of δ^{53}Cr in suboxic sediments demonstrate glacial–interglacial variability, which has been interpreted to reflect changes in ocean oxygenation

(Gueguen et al., 2016b). However, given the relationships between biological export and ocean deoxygenation for sediment metal accumulation (e.g., Nameroff et al., 2004) and similar fractionations reported for biogenic export and OMZ removal, it may be difficult to disambiguate these two controls on sedimentary δ^{53}Cr.

Initial interpretations inferred quantitative removal of Cr to anoxic sediments, suggesting they may serve as an archive of oceanic δ^{53}Cr (Reinhard et al., 2014), in a manner analogous to Zn (Sec. 4.3.4.) However, reinterpretations of Cariaco Basin surface sediments (δ^{53}Cr ≈ +0.4±0.1; Gueguen et al., 2016b) alongside nearby and oceanographically consistent water column data (dissolved δ^{53}Cr ≈ +1.2±0.1; Goring-Harford et al., 2018; Fig. 28), suggest that δ^{53}Cr in anoxic sediments may in fact be lighter than ambient seawater by ≈0.8±0.2 ‰, which is similar to the isotope separation implied by the global [Cr] - dissolved δ^{53}Cr–array ($\Delta_{P\text{–}R} \approx -0.7$ to -0.8). While a full assessment of this offset requires truly colocated water and sediment samples, existing data do not support the hypothesis that anoxic sedimentary δ^{53}Cr reflects ambient dissolved δ^{53}Cr with no isotope offset.

10.4. Prospects

The sensitivity of both [Cr] and dissolved δ^{53}Cr to biotic and abiotic redox cycling makes Cr a potentially promising redox proxy. Historically, δ^{53}Cr has received most attention as a paleoredox proxy, with most interpretations based on the framework that terrestrial processes result in isotopically heavy Cr reaching the oceans via rivers, without further alteration of δ^{53}Cr through oceanic cycling (e.g., Frei et al., 2009; Frei et al., 2014). Although this model may remain generally valid under atmospheric oxygen levels relevant to the early Earth, internal processes in the ocean, including biological productivity, dominate modern δ^{53}Cr records and may still be influential under strongly reducing conditions (e.g. Bauer et al., 2018).

As the body of high quality [Cr] and dissolved δ^{53}Cr data continue to grow through GEOTRACES, two primary areas of uncertainty have emerged that are currently limiting δ^{53}Cr paleoproxy applications: a quantitative apportionment of the balance between productivity- and O_2-related Cr cycling, and identification of archives that reliably record dissolved δ^{53}Cr.

10.4.1. Modern

The most pressing issue for the Cr isotope community is to ensure that future water column data are reported according to high standards of intercalibration and quality control. In addition to this issue, several targets are needed to address specific mechanistic controls on the modern ocean Cr and δ^{53}Cr cycles. First, improved constraints on biological and OMZ-mediated Cr removal and the relative importance of these two processes would help to better understand the modern Cr biogeochemical cycle. Direct and robust determinations of fractionation factors associated with biologically mediated Cr export should be prioritized, along with a better understanding of differences in Cr removal among taxa, as well as interrogation of the mechanisms by which phytoplankton reduce and scavenge Cr. More studies have assessed fractionation factors for OMZs, but quantitative constraints are still limited and it is unclear as to what extent OMZ-related processes influence open marine [Cr] and dissolved δ^{53}Cr.

Second, central to OMZ and biogenic Cr removal are understandings of how much Cr is exported with particles, how much of this reaches the seafloor, and how much is eventually buried in marine sediments. Data from marine particulates, currently limited by high filter blanks and low particulate Cr concentrations, are sorely needed to address these points. Additionally, data for marine particles may help to assess to what extent mid-depth scavenging outside of OMZs, known to be important for other scavenging-prone metals (e.g., Ohnemus et al., 2019, Secs. 3.–5.), shapes Cr distributions. More data are needed from porewaters and surface sediments to better understand benthic Cr fluxes and Cr burial. Finally, some aspects of the modern global biogeochemical cycle, such as fluxes from hydrothermal vents, remain completely unconstrained.

10.4.2. Paleo

Ideal archives for δ^{53}Cr paleoproxy applications should faithfully reflect a known oceanic condition (e.g., dissolved δ^{53}Cr) or processes (e.g., Cr removal in OMZs) and should have a sufficient Cr content so that sample availability is not a limiting factor. It is also clear from the δ^{53}Cr paleoproxy research to date that careful record selection is necessary to avoid samples with minimal overprinting or alteration of primary δ^{53}Cr records (e.g., Albut et al., 2018; Remmelzwaal et al., 2019; Wang et al., 2021). Given these constraints, the following points summarize the most promising archives, which may also offer an opportunity to reevaluate literature data—mostly interpreted in terms of paleoredox—in the context of paleoproductivity.

At present, carbonate-hosted δ^{53}Cr remains a challenging archive for several reasons, including: low Cr:Ca, taxon-dependent Cr isotope fractionations, fractionation during inorganic calcite precipitation, and potential diagenetic overprinting in marine sediments (e.g. Holmden et al., 2016; Pereira et al., 2016; Remmelzwaal et al., 2019). Additional research is needed to assess to what extent variable taxon-dependent fractionations and diagenetic overprinting can be recognized and corrected before applying δ^{53}Cr in marine carbonates. Existing data indicate that Fe–Mn crusts are not suitable δ^{53}Cr archives (Wei et al., 2018). Other oxic sedimentary archives, such as authigenic clays, may be suitable, but little is known about the degree to which sedimentary and oceanic Cr and δ^{53}Cr exchange, the role of oxic sedimentary phases in the Cr cycle (and the relevant isotope separation factors), and the depths recorded by these phases.

Black shale records of δ^{53}Cr have been used to investigate oceanic oxygenation levels over time. However, the uncertainty regarding how faithfully anoxic and suboxic sediments record conditions in the modern ocean combined with potential δ^{53}Cr homogenization among sediment phases (Frank et al., 2020) suggests more research is needed to validate shales as reliable records before further applications. Furthermore, early interpretations of quantitative removal of Cr to anoxic sediments are not supported by the current body of water column data. Consequently, more research is needed to validate the use of anoxic sediments to reconstruct water column δ^{53}Cr, such as identification of suitable correction factors based on colocated water column and sediment data. Similarly, oceanographically consistent water column data are sparse relative to suboxic sedimentary measurements, complicating assessments of the impact of Cr loss to sediments. Disentangling local reduction-based accumulation from Cr delivery to suboxic and anoxic sediments via biogenic particles may be challenging, given the importance of both these processes on Cr cycling and the linkages between biological export and oxygen depletion.

11. Silver

Silver is the scarcest of the bioactive trace metals described here—within Earth's crust, in the modern ocean (Table 1), and from an observational point of view. Like Ba, Ag is an unusual candidate for a paleoproductivity proxy given that it possesses no known biological function and is most widely known for its antimicrobial properties. Despite this, [Ag] exhibits a characteristic nutrient-like profile in seawater, most similar to that of [Si] (or [Zn], [Ba]; Figs. 1, 30), and Ag content in certain sediments is positively correlated with organic C. These intriguing features warrant further investigation into whether and how marine Ag cycling might reflect ocean productivity.

11.1. Marine distribution

Dissolved Ag occurs primarily as chloride complexes in seawater (Cowan et al., 1985, Miller & Bruland, 1995) and exhibits a nutrient-type depth profile; [Ag] in surface waters are typically <5 pmol kg^{-1}, and range from 5–30 pmol kg^{-1} in deep waters of the Atlantic Ocean to 50–114 pmol kg^{-1} in the Pacific Ocean (Fig. 30; Flegal et al., 1995; Rivera-Duarte et al., 1999; Ndung'u et al., 2001; Zhang et al., 2001; 2004; Ranville and Flegal, 2005; Kramer et al, 2011; Boye et al., 2012). The total observed range in seawater is 0.2–115 pmol kg^{-1} (Gallon and Flegal, 2014). Despite its potential as a biogeochemical proxy, no Ag isotope data currently exist for dissolved or particulate phases in the water column, nor in marine sedimentary archives. Accordingly, we cannot directly assess the utility of δ^{109}Ag to infer paleoproductivity, though we can deduce a number of processes that are likely to influence dissolved δ^{109}Ag based on the processes known to cycle Ag (Fig. 31).

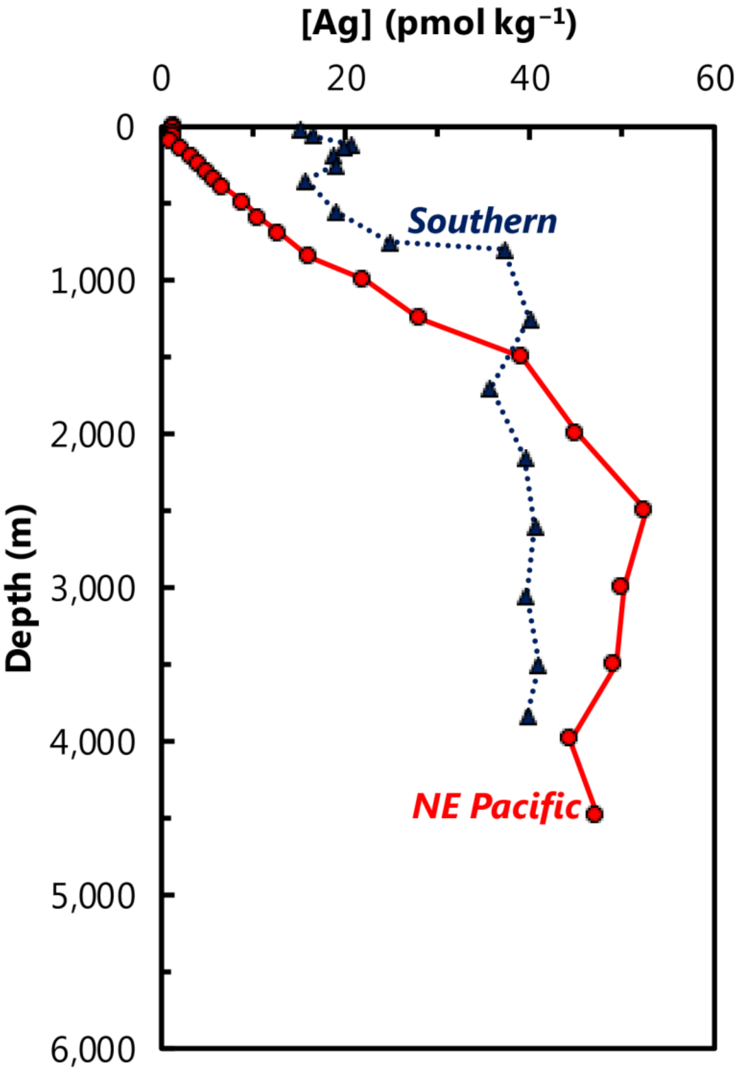

Figure 30 | Representative profiles of dissolved Ag concentrations ([Ag]). Data from the Northeast Pacific (circles, solid line; Fisher et al., 2018) and Southern Oceans (triangles, dotted line; Boye et al., 2012). Station locations as per Fig. 1. Data from the Northeast Pacific were extracted graphically using WebPlotDigitizer (Rohatgi, 2019). The authors are not aware of the existence of any Ag isotope data for seawater at this time.

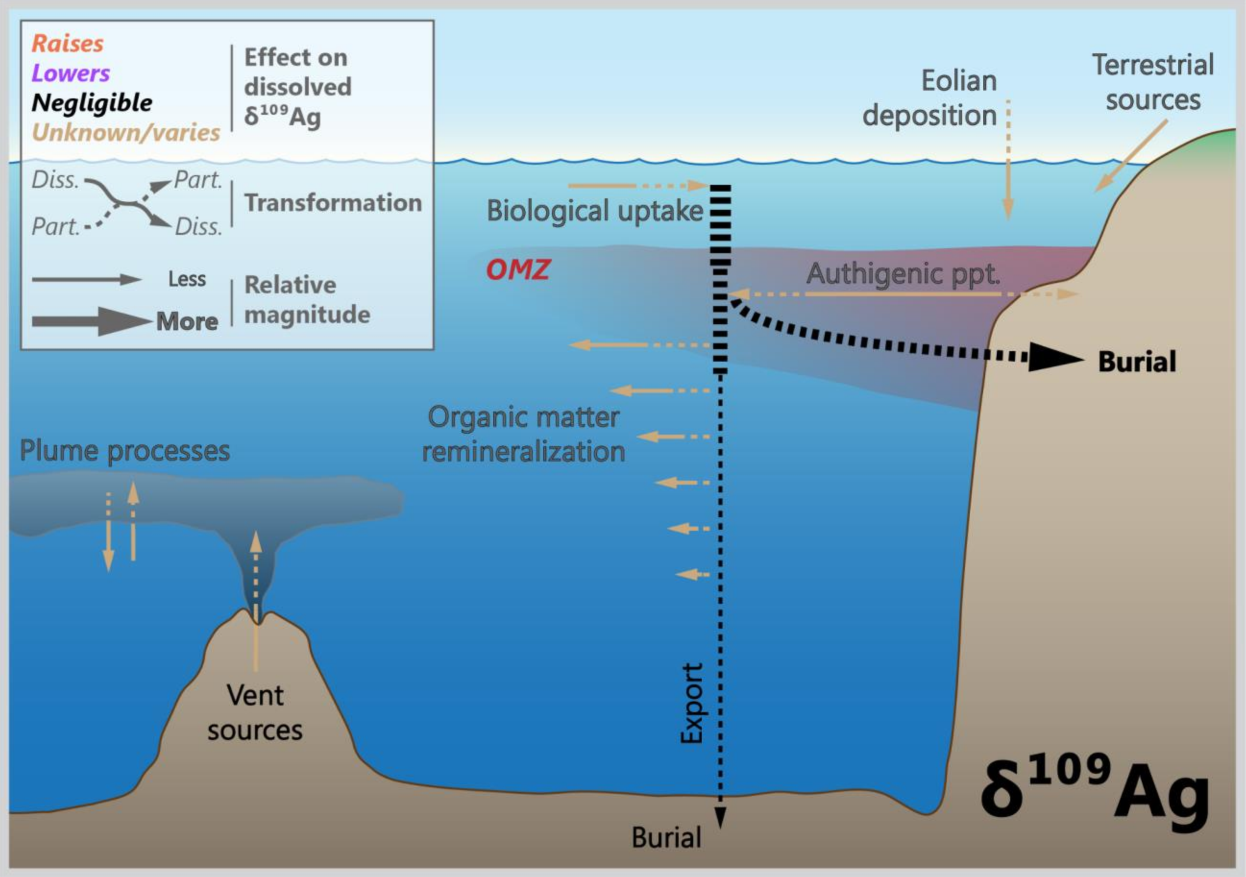

Figure 31 | Processes likely to drive Ag isotope variations in modern seawater. Despite there being no Ag isotope data for seawater at this time, we can infer a number of processes that are most likely to influence dissolved δ^{109}Ag from measurements of [Ag] in seawater and sediments.

11.2. Driving processes

The typical [Ag] depth profile (Fig. 30) is similar to that of [Si], resulting in a strong positive correlation between these elements in existing datasets. This has led researchers to suggest that Ag is taken up by diatoms, incorporated into their frustules, and then released as the frustules dissolve (e.g., Flegal et al., 1995). Silver might then be delivered to the seafloor with opal, potentially making it useful as a paleoproductivity proxy (Friedl & Pedersen, 2002). However, the correlation between [Ag] and [Si] is non linear, indicating that other factors are at play (Zhang et al., 2001; 2004). Furthermore, while Ag is taken up by various types of phytoplankton, including diatoms (Fisher & Wente, 1993), experiments conducted using the marine diatom *Thalassiosira pseudonana* show that most of the Ag is associated with the organic fraction rather than the opal (Wagner, 2013). Martin et al. (1983) also hypothesized that high particulate Ag concentration within the euphotic zone (40–70 m) off the west coast of Mexico were due to the formation of Ag-organic complexes. Interestingly, particulate Ag concentrations are even higher well below the euphotic zone, at a depth corresponding to the upper portion of the local OMZ (Martin et al., 1983). It could also be that a global [Ag]:[Si] correlation arises at least in part from biological processes occurring in the surface of the Southern Ocean, whereby intermediate and mode waters with low preformed [Ag] are advected to lower latitudes, analogous to the mechanism proposed for [Zn]:[Si] (Vance et al., 2017) and [Ba]:[Si] coupling (Horner et al., 2015a). If correct, Ag is unlikely to be coupled directly to opal via a simple relationship that can be used to reconstruct past diatom productivity.

Even if driven by productivity, [Ag] distributions may become decoupled from productivity by possessing different source and sink terms relative to carbon and the macronutrients (Gallon & Flegal, 2014 and references therein). For example, Ranville & Flegal (2005) and Ranville et al. (2010) invoked an anthropogenic aerosol source of Ag to surface and intermediate waters to explain north Pacific water column data. Other complications may arise under low [O_2] environments—waters from the northeast Pacific (Kramer et al., 2011) and southeastern Atlantic (Boye et al., 2012) exhibit a deficit in [Ag] relative to [Si] within their respective OMZs. These deficits imply preferential removal of Ag over Si, which may occur locally or ‘upstream’. If occurring locally, a putative mechanism is co-precipitation with other chalcophile elements, analogous to the sulfide-mediated mechanism proposed for Cd in OMZs (Janssen et al., 2014; Sec. 5). Alternatively, the deficit may reflect low preformed [Ag]:[Si] in intermediate waters, which is inherited from preferential drawdown of Ag over Si in regions upstream where these intermediate waters were last ventilated. Both interpretations have implications for the use of Ag or δ^{109}Ag as a paleoproxy: the former implies a redox sensitivity that depends on the changing location, spatial extent, and intensity of low [O_2] regions in the oceans over time; the latter implies a sensitivity to ecology and the geometry of ocean circulation. Both warrant additional scrutiny.

11.3. Marine archives

Bulk sediments are the main archive that has been investigated for their potential to record information about the marine Ag cycle. The Ag content of bulk sediments from open marine environments range from ≤100 ng g^{-1} (i.e., typical lithogenic values) up to 100s of ng g^{-1} (Koide et al., 1986). In general, low Ag content is typical of well-oxygenated sediments, while higher Ag contents are typical of sediments formed in oxygen-poor and euxinic environments. The general consensus has been that Ag enrichment in anoxic sediments is the result of post-depositional precipitation of Ag_2S (Koide et al., 1986) or possibly Ag selenide (Crusius & Thomson, 2003; Böning et al., 2005). However, high Ag content is also documented in marine sediments that are only weakly reducing (Böning et al., 2004, 2005; McKay & Pedersen, 2008; Morford et al., 2008). Furthermore, even in anoxic sediments, the degree of Ag enrichment exceeds what would be expected from post-depositional Ag precipitation alone (Borchers et al., 2005; McKay and Pedersen, 2008; Böning et al., 2009). Thus, redox-controlled, post-depositional precipitation is not the primary control on Ag accumulation in marine sediments, impling that there must also be a flux of non-lithogenic, particulate Ag to the seafloor (McKay & Pedersen, 2008).

McKay & Pedersen (2008) hypothesized that Ag, like Ba, accumulates in organic-rich settling particles. However, in contrast to Ba, Ag precipitation requires a reduced microenvironment within the particle, which is generally only possible in waters that possess relatively low [O_2] (e.g., Bianchi et al., 2018). The analysis of sediment trap samples from the northeast Pacific show that the fluxes of particulate Ag and particulate organic carbon flux positively correlate (Martin et al., 1983). This correlation is also seen in surface sediments (McKay & Pedersen, 2008) and sediment cores from the northeastern Pacific (Fig. 32). These data broadly support the use of particulate Ag flux as a paleoproductivity proxy, with an important caveat: the post-depositional preservation of particulate Ag requires that sediments remain reducing, as settling particulate Ag formed below the euphotic zone is not preserved if sediments are oxidizing (McKay and Pedersen, 2008; Morford et al., 2008). Thus, while the delivery of particulate Ag to sediments appears related to productivity (Wagner et al., 2013), Ag delivery to—and preservation within—sediments is sensitive to [O_2]; low water column [O_2] favors higher Ag:C of sinking particles and greater Ag preservation at the seafloor. By analogy to other metals (e.g., Twining & Baines, 2013), variations in surface water [Ag] may also modulate Ag:C, though remains to be tested. These three sensitivities likely explain why different regions exhibit distinct arrays in Ag–TOC space (Fig. 32). Despite these regional variations, the relationships between Ag and organic matter are promising from the point of view of tracing past productivity.

Though yet to be investigated for δ^{109}Ag, Ag is predicted to be somewhat mobile in Fe–Mn crusts, with a predicted diffusivity $\leq 10^{-7}$ cm^2 yr^{-1} (see Henderson & Burton, 1999, for calculation details), similar to Cd (Sec. 6.3.2.), Mo (Sec. 7.3.), and Cr (Sec. 10.3.2.). This rate implies that, should any long-term records be forthcoming, Fe–Mn crust based reconstructions of δ^{109}Ag are likely to exhibit some diffusive smoothing while preserving larger perturbations.

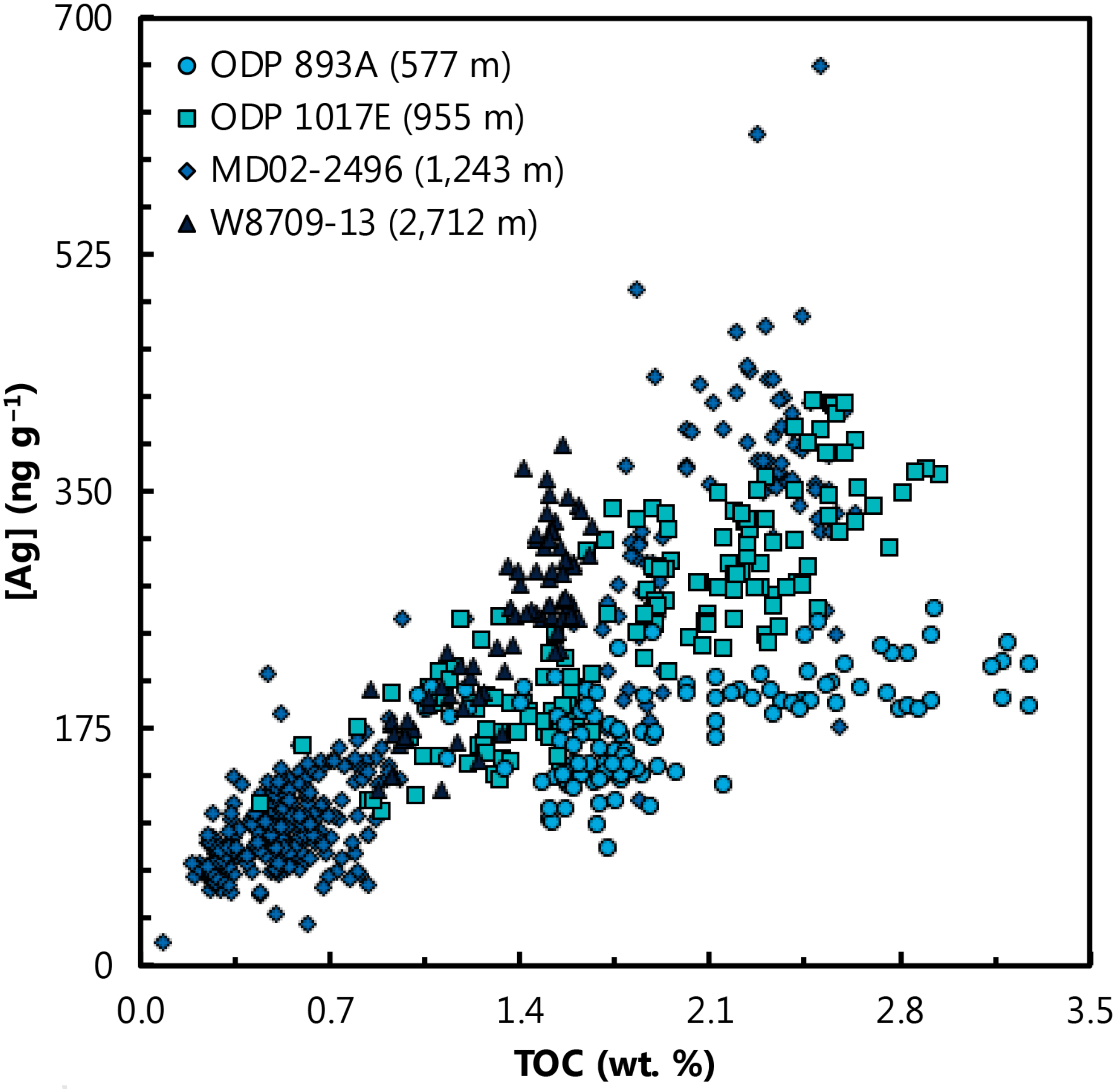

Figure 32 | Concentrations of Ag and total organic carbon in sediment cores from the northeast Pacific Ocean. These data illustrate that Ag is broadly correlated with organic matter in bulk sediments, which is highly promising from the perspective of developing Ag as a paleoproductivity proxy. Core MD02-2496 (Vancouver Island Margin; 48.97°N, 127.04°W, 1,243 m water depth) from Chang et al., 2014; Core W8709-13PC (Oregon Margin; 42.116°N, 125.75°W; 2,712 m water depth) from Kienast, 2003; ODP 1017E (Southern California; 34.53°N, 121.1°W; 955 m water depth) from Hendy & Pedersen, 2005; ODP 893A (Santa Barbara Basin; 34.287°N, 120.036°W; 576.5 m water depth) from Ivanochko, 2001.

11.4. Prospects

The apparent linkages between [Ag] and particulate Ag, macronutrients, and organic matter provides tantalizing evidence that Ag cycling may be related to surface productivity (Fig. 30). Moreover, coretop studies indicate that the geochemical signature of this coupling is preserved under certain environmental conditions (Fig. 32). Despite this progress, the study of Ag in marine biogeochemical cycles remains in its infancy, particularly compared to many of the other elements described here. Additional constraints are needed in several areas, including: the role of biogeochemical processes in mediating Ag distributions in the water column, the dominant controls on the downward transport of Ag through the oceans, and on the controls on Ag preservation in sediments. Given what has been learned from the application of the other trace metal isotope systems described here, new analytical developments in Ag isotope geochemistry could help place valuable constraints on these areas.

12. Synthesis

In this final section, we synthesize and describe the overall suitability to trace productivity (Sec. 12.1.), explore inter-element similarities (Sec. 12.2.), define proxy readiness (Sec. 12.3.), and outline a number of research priorities (Sec. 12.4.) for using Fe, Zn, Cu, Cd, Mo, Ba, Ni, Cr, and Ag and their isotopes as paleoproductivity proxies.

12.1. Overall state of the proxies

Taking a general view, the review of each element highlights that our knowledge of bioactive trace metal isotope systematics lags behind those of trace element abundances and far behind those of macronutrient isotopes (e.g., Farmer et al., *this volume*). The bioactive metal isotope field is nascent; excepting Mo, the very first isotope data for seawater for all of the elements reviewed here were published within the last 15 years, or—in the case of Ag—are yet to be reported. The field is thus decades behind the trace metal concentration community. Despite the lack of detail, we can begin to classify the metals reviewed here into three broad categories: those where there are clear and promising signs that a metal can serve as a proxy of paleoproductivity, such as for δ^{114}Cd, δ^{138}Ba, δ^{60}Ni, and δ^{53}Cr; those where a metal is unlikely to directly inform on paleoproductivity, as for δ^{56}Fe, δ^{66}Zn, δ^{65}Cu, and δ^{98}Mo; and those where simply too little is known to confidently assign utility at this time, as for δ^{109}Ag.

More specifically, this review highlights the importance of ocean circulation in mediating the distribution of several bioactive trace metals and their isotopes. Key features of the isotope distributions reviewed here reflect a mixture of local (i.e., *in situ)* and regional (or *ex situ*) processes, with the latter often set far 'upstream' of any given locality. Indeed, researchers are recognizing that, much like the macronutrients (see Farmer et al., *this issue*), the first-order features of many metals are not controlled locally by a given dissolved–particulate transformations, but reflect a regionally integrated history of vertical cycling and mixing that is imparted over the scale of an ocean basin, which we discuss next.

12.2. The reactor model applied to select trace metal isotope systems

Today, the Southern Ocean represents the common starting point and ultimate source of many TEIs for low latitude thermoclines (e.g., Sarmiento et al., 2004; Talley, 2013). If we assume that the reaction progress term in the reactor model is analogous to the fraction of initially supplied nutrient left unconsumed by phytoplankton, the concentration and isotope composition of a Me in the Southern Ocean can be assumed to represent the starting composition of a metal in the isotope reactor (i.e., [Me] and $\delta^i\mathrm{Me}_{\mathrm{R},0}$ when $f = 0$). Our study suggests that four of the nine bioactive trace metals reviewed here (Cd, Ba, Ni, Cr) are suitable candidates for the isotope reactor model, which we now use to constrain $\Delta_{\mathrm{P-R}}$ for both Steady State (SS) and Rayleigh Distillation (RD). We assume that samples from the upper 1,000 m of the Southern Ocean represent the initial reactor conditions (Fig. 33); downstream of the Southern Ocean, we consider only those samples shallower than 200 m to ensure that the models only regress productivity-associated Me drawdown. Our example calculations are intended to be illustrative, rather than the definitive estimate of $\Delta_{\mathrm{P-R}}$ for each metal; comprehensive, global compilations are described elsewhere for Cd (Xie et al., 2017; Sieber et al., 2019), Ba (Hsieh & Henderson, 2017; Horner & Crockford, 2021), Ni (Yang et al., 2020), and Cr (Rickli et al., 2019; Wei et al., 2020). Accordingly, we limit our example to the stations shown in Fig. 1.

Excepting the RD model for Cd, the reactor models generate a reasonable fit to the data, with best-fit $\Delta_{\mathrm{P-R}}$ of −0.75±0.02 ‰ (SS) and −0.23±0.16 ‰ (RD) for Cd (n=6), −0.54±0.03 ‰ (SS) and −0.35±0.03 ‰ (RD) for Ba (n=16), −0.54±0.04 ‰ (SS) and −0.36±0.04 ‰ (RD) for Ni (n=20), and −0.84±0.04 ‰ (SS) and −0.71±0.04 ‰ (RD) for Cr (n=18; all ± represent the root-mean-square deviation). These values are generally within the accepted ranges reported for each metal, either for oceanographic data or specific experiments (e.g., culture studies, mineral precipitation). The reactor models illustrate that best-fit $\Delta_{\mathrm{P-R}}$ for SS are larger in magnitude than for RD. This difference derives from mixing. Open-system models account for continuous uptake and removal of Me from the reactor, thus requiring a larger $\Delta_{\mathrm{P-R}}$ to render an equivalent change in $\delta^i\mathrm{Me}_{\mathrm{R}}$ compared to RD. In general therefore, calculations assuming SS will be closer to the underlying value of $\Delta_{\mathrm{P-R}}$, since the surface ocean is poorly represented by a closed-system reactor.

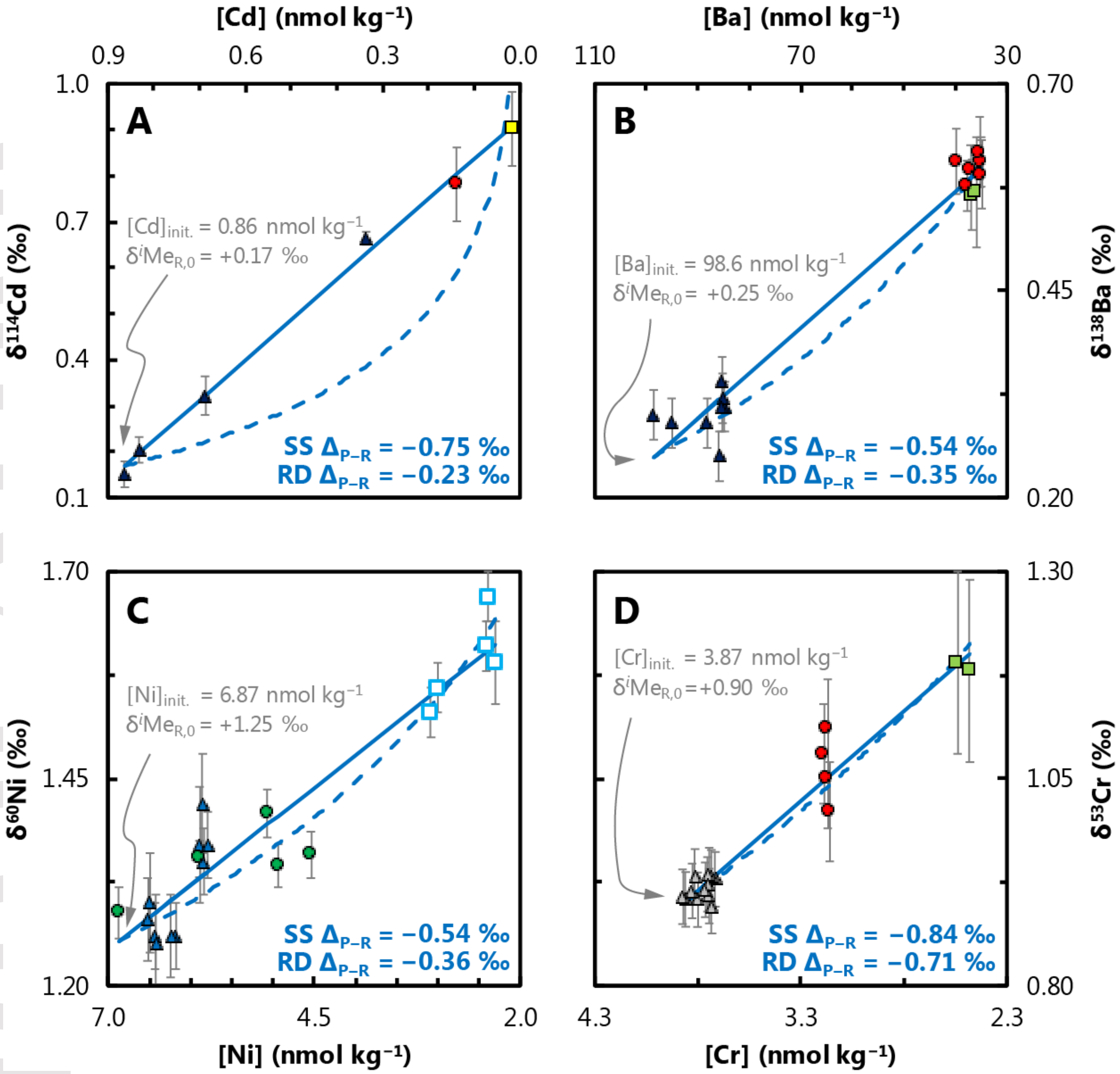

Figure 33 | Reactor framework applied to select bioactive trace metal isotope systems. Station locations and symbols as per Fig. 1. **A–D** Isotope reactor models for Cd (A), Ba (B), Ni (D), and Cr (D) showing evolution of the residual reactant during Me consumption. Best-fit Δ_{P-R} are shown for SS (solid) and RD fractionation (dashed lines). Data from the upper 1,000 m of the Southern Ocean are assumed as the common starting point for each Me (arrow). To limit the models to productivity-associated processes, only data shallower than 200 m are included in the model for samples collected outside of the Southern Ocean. Samples with extreme Cd isotope compositions (δ^{114}Cd >+1‰) are excluded from the model given that it is unclear if these are true oceanographic features (see Sec. 6.4.1.).

In practical terms, knowledge of Δ_{P-R}, derived using the reactor framework, allows for the isotope compositions of Cd, Ba, Ni, and Cr to be interpreted in terms of reflecting the balance between supply and demand for that metal within the reactor (i.e., *f*). Though this does not confer direct information about the total quantity of nutrients consumed in the reactor, it offers a means to assess the spatial pattern of nutrient utilization in Earth's past. The spatial dependency is particularly important to consider, since the geometry of ocean circulation cannot be assumed constant over time. Moreover, if assuming that the flux of a Me to the seafloor is proportional to export productivity, the combination of metal fluxes with metal isotopes *can* offer insights into patterns of paleoproductivity by constraining export and fractional nutrient use within that system.

Combined C export–*f* approaches are largely unexplored in paleoceanographic studies, and we believe they offer the best opportunity for using bioactive trace metal isotope systems to constrain paleoproductivity. These approaches will prove most powerful when the constraints on C export and *f* are derived from the same Me system, since this minimizes the importance of other metal-cycling processes. However, multi-proxy approaches may also prove useful in differentiating between productivity- and non productivity-driven variations in metal cycling. For example, Cd, Ba, Ni, and Cr isotopes are all expected to exhibit coherent variations in their distributions if productivity or ocean circulation varied. In contrast, changes in mean ocean redox state, benthic fluxes, or terrestrial sources would render distinct changes in the distribution of each Me consistent with its sensitivity to that process. The cycling of other metals that are not directly sensitive to productivity—Fe, Zn, Cu, and Mo—could also be used to provide oceanographic context for paleoproductivity records, thus helping to build a more robust picture of marine biogeochemistry at key points in Earth's history.

12.3. Proxy readiness

We now assess the overall readiness of each bioactive trace metal isotope system to reconstruct productivity, summarized in Table 2. This exercise is analogous to the assessment of analytical techniques used in chemical oceanography described by Fassbender et al. (2017). Our assessment is similarly conducted in two dimensions. First, we identify five objectives toward the development of a reliable productivity proxy, ranging from development of the analytical capabilities necessary to measure that species, to constraining diagenetic effects, and ending with the goal of using that species to reliably reconstruct paleoproductivity itself. Second, we assess the level of development within each objective. Our reasoning behind the assignments is described above in Sec. 3–11.

Reliable application of a TEI as a proxy requires that five objectives be serially met (e.g., Hillaire-Marcel & Vernal, 2007; Table 2). In practical terms, however, the final stage (proxy application) is often realized before many of the supporting objectives; variations in elemental or isotopic ratios in the sedimentary record commonly provide the motivation for developing a more holistic understanding of that isotope system in the modern environment. *A common critique of this approach is that subsequent studies often invalidate earlier interpretations.* The five objectives that follow are common to the development of almost any proxy. First, it is essential to develop the analytical capability to measure the species of interest commensurate with the quantities typically encountered in the environment. In the case of trace element abundance proxies, the development and widespread adoption of ICP-MS instrumentation coupled to automated sample preparation systems has enabled low-blank, high-throughput, high-sensitivity analyses of multiple trace elements in both seawater (e.g., Wuttig et al., 2019) and sediments alike (e.g., Wefing et al., 2017). In contrast, the techniques required to measure many trace metal isotope systems have only been developed within the past decade—or are still in development—and generally remain labor intensive and time consuming. Second, it is important to map the broad vertical and spatial patterns of a TEI system in the modern ocean. The GEOTRACES program has provided a coordinated opportunity to study the basin-scale distributions of multiple TEIs. Third, the utility of a proxy is significantly increased if the driving processes are understood. These processes may be isolated through a number of approaches, including: lab-based analogue experimentation, numerical modeling, and high-resolution spatiotemporal environmental studies. Fourth, paleoceanographic proxies require sedimentary archives—a substrate from which to reconstruct the variable of interest. The latter necessitates knowledge of how a trace metal partitions between seawater and sediment, such as through a coretop study, ideally conducted across large environmental gradients. Since many marine sedimentary archives are biogenic in origin, additional experimentation isolating 'vital effects' may be necessary. Fifth, proxies are only as reliable as their archives are hardy. Diagenetic processes may alter primary environmental signatures, and recognizing these effects is imperative for reliably reconstructing past environmental conditions.

Here, we assess the level of development for each marine bioactive trace metal isotope system within each objective on a four point scale: unknown, developing, applied, and unlikely. The levels define a continuum from least to most understood, and are a useful shorthand for illustrating where additional work is most needed. Assignment of 'unknown,' implies that too little is presently known to reliably assess progress towards that objective; we cannot judge if these isotope systems may or may not ultimately be useful in reconstructing ocean productivity. 'Developing' objectives are those where there are pilot studies on that topic, but overall there are an insufficient number to define general rules for that system. If a trace metal isotope system is widely recognized to be useful towards some objective, it is given a score of 'applied.' If the evidence indicates that a trace metal isotope system is not suitable for reconstruction of paleoproductivity, a score of 'unlikely' is given. This does not rule out future developments, such as identification of environmental control variables or new sedimentary archives, only that current data (and archives) do not support use of the isotope system towards this goal. Lastly, we recognize that there are continual refinements to analytical protocols, environmental distributions, etc. and thus, at some level, all five objectives could reasonably be described as ‘developing.’ Rather, our assignments are intended to give a relative sense of understanding between different metal isotope systems toward the overarching goal of reconstructing past ocean productivity.

Table 2 | Proxy development assessment. The progress toward five objectives is assessed for each bioactive metal proxy system and assigned a development level ranging unknown to unlikely, corresponding to the least and most certain assignments, respectively. Some trace metal isotope systems possess split designations (stripes). Definitions of each development level are described in Sec. 12.3 and discussed in detail for each metal system in the corresponding section.

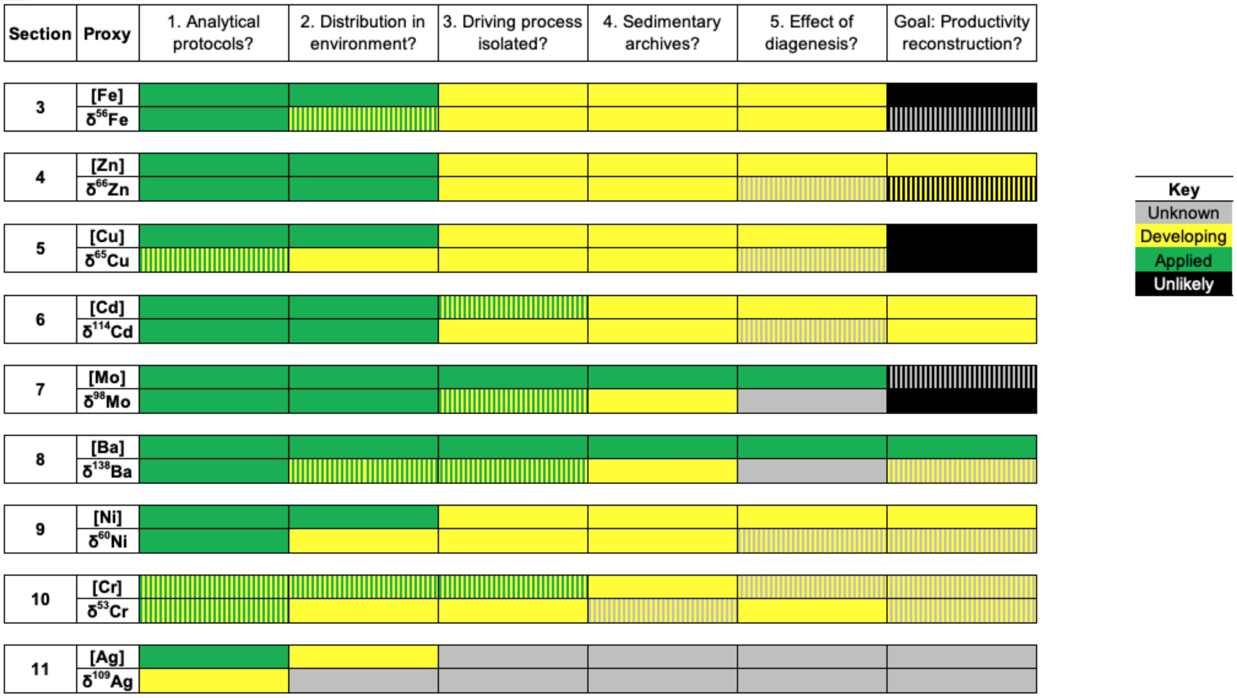

Section	Proxy	1. Analytical protocols?	2. Distribution in environment?	3. Driving process isolated?	4. Sedimentary archives?	5. Effect of diagenesis?	Goal: Productivity reconstruction?
3	[Fe]	🟩	🟩	🟨	🟨	🟨	⬛
	δ^{56}Fe	🟩	🟩🟨	🟨	🟨	🟨	⬛⬜
4	[Zn]	🟩	🟩	🟨	🟨	🟨	🟨
	δ^{66}Zn	🟩	🟩	🟨	🟨	🟨⬜	🟨⬛
5	[Cu]	🟩	🟩	🟨	🟨	🟨	⬛
	δ^{65}Cu	🟩🟨	🟨	🟨	🟨	🟨⬜	⬛
6	[Cd]	🟩	🟩	🟩🟨	🟨	🟨	🟨
	δ^{114}Cd	🟩	🟩	🟨	🟨	🟨⬜	🟨
7	[Mo]	🟩	🟩	🟩	🟩	🟩	⬛⬜
	δ^{98}Mo	🟩	🟩	🟩🟨	🟨	⬜	⬛
8	[Ba]	🟩	🟩	🟩	🟩	🟩	🟩
	δ^{138}Ba	🟩	🟩🟨	🟩🟨	🟨	⬜	🟨⬜
9	[Ni]	🟩	🟩	🟨	🟨	🟨	🟨
	δ^{60}Ni	🟩	🟨	🟨	🟨	🟨⬜	🟨⬜
10	[Cr]	🟩🟨	🟩🟨	🟩🟨	🟨	🟨⬜	🟨⬜
	δ^{53}Cr	🟩🟨	🟨	🟨	🟨⬜	🟨	🟨⬜
11	[Ag]	🟩	🟨	⬜	⬜	⬜	⬜
	δ^{109}Ag	🟨	⬜	⬜	⬜	⬜	⬜

Key
⬜ Unknown
🟨 Developing
🟩 Applied
⬛ Unlikely

12.4. Outlook

Finally, we outline three general priorities for further study. First, a number of modern ambiguities require addressing. Most notable is the apparent ‘missing’ source and/or sink terms for the whole ocean isotopic budgets of several bioactive metals, including Cu, Cd, Ba, and Ni. Though it is possible that these missing source and sink terms represent true non-steady state imbalances in the flux of these elements to and from the ocean, we view it more likely that there are major fluxes that remain uncharacterized. The origin of these imbalances is most pressing for those elements where the output flux associated with organic matter constitutes a minor sink (e.g., Zn, Ni), as the isotopic budget of these elements is most susceptible to decoupling from productivity. Second, the significance of ocean circulation in mediating basin-scale trace metal distributions implies that paleoceanographic interpretations made from a single site cannot be uniquely interpreted in terms of either changes in productivity or ocean circulation without additional constraints. Such constraints could take the form of independent circulation estimates—from numerical models or canonical circulation proxies measured in the same samples—or by measuring trace metal isotope distributions in spatially distributed sediment samples. Third, the lack of suitable archives with which to reconstruct surface water trace metal isotopic compositions afflicts almost every element reviewed here. Overcoming this limitation will require the most creativity; we suggest more studies testing the fidelity of non-traditional substrates (e.g., mixed foraminiferal assemblages, coccolith calcite, diatom opal), periodic reassessment of the feasibility of traditional substrates following analytical advancements (e.g., improvements in ion transmission efficiency, large-scale [automated and/or crowd-sourced] picking of monospecific foraminiferal assemblages), and development and validation of selective extraction protocols that can be used to isolate phases of interest from complex matrices. Though attempting to overcome these limitations may be considered high risk, we believe that this risk is more than justified by the reward of developing a more complete understanding of Earth's biogeochemical history.

Postscripts

Acknowledgments

This contribution grew (and grew) out of a joint workshop between GEOTRACES and Past Global Changes (PAGES) held in Aix-en-Provence in December 2018. The workshop was funded by the U.S. National Science Foundation (NSF) through the GEOTRACES program, the international PAGES project, which in turn received support from the Swiss Academy of Sciences and NSF, and the French program Les Enveloppes Fluides et l'Environnement. The authors extend tremendous thanks to the GEOTRACES–PAGES workshop organizers, particularly Bob Anderson, Catherine Jeandel, Laurence Vidal, and Kazuyo Tachikawa. This synthesis benefited from the insights of the Associate Editor (Noah Planavsky) and from two detailed and constructive reviews by Seth John and an anonymous reviewer. T.J.H. acknowledges support from NSF; S.H.L. from the U.K. Natural Environment Research Council (NE/P018181/1); T.M.C. from the University of South Florida; and, J.R.F. from the Max Planck Society, the Tuttle Fund of the Department of Geosciences of Princeton University, the Grand Challenges Program of the Princeton Environmental Institute, and the Andlinger Center for Energy and the Environment of Princeton University. Most importantly, we acknowledge the hundreds of scientists who have generated GEOTRACES-compliant TEI data that made this synthesis possible.

Data sources

The majority of the dissolved data were sourced from the GEOTRACES Intermediate Data Products in 2014 (Mawji et al., 2015) and 2017 (Schlitzer et al., 2018). Regardless, citations to the primary data sources are given in the caption to each figure. Data sources for Fig. 1 and and Table 1 are given below.

Figure 1

Iron: Conway & John, 2014a (Atlantic); Conway & John, 2015a (Pacific); Abadie et al., 2017 (Southern). Zinc: Conway & John, 2014b (Atlantic); Conway & John, 2015a (Pacific); Wang et al., 2019a (Southern). Copper: Little et al., 2018 (Atlantic); Takano et al., 2017 (Pacific); Boye et al., 2012 (Southern). Cadmium: Conway and John, 2015b (Atlantic); Conway & John, 2015a (Pacific); Abouchami et al., 2014 (Southern). Molybdenum: Nakagawa et al., 2012 (all basins). Barium: Bates et al., 2017 (Atlantic); Geyman et al., 2019 (Pacific); Hsieh & Henderson, 2017 (Southern). Nickel: Archer et al., 2020 (Atlantic); Takano et al., 2017 (Pacific); Wang et al., 2019a (Southern). Chromium: Goring-Harford et al., 2018 (Atlantic); Moos & Boyle, 2019 (Pacific); Rickli et al., 2019 (Southern). Silver: Fischer et al., 2018 (Pacific); Boye et al., 2012 (Southern).

Table 1

[a]Schlitzer (2017); [b]Morris et al. (1975); [c]Section 10 and references therein; [d]Gallon and Flegal, 2014; [e]Dauphas et al. (2017); [f]Moynier et al. (2017) and references therein; [g]Abouchami et al. (2013); [h]Nägler et al. (2014); [i]Horner et al. (2015a); [j]Elliott & Steele (2017); [k]Ellis et al. (2002); [l]Woodland et al. (2005); [m]Gong et al. (2017); [n]Schmitt et al. (2009a); [o]Willbold & Elliott (2017); [p]Nan et al., 2018; [q]Cameron et al. (2009); [r]Shoenberg et al. (2018); [s]USGS reference material SCO-1 (Cody Shale) is used given paucity of representative data; Schönbächler et al. (2007); [t]Section 3 and references therein; [u]Section 4 and references therein; [v]Section 5 and references therein; [w]Section 6 and references therein; [x]Data from Nakagawa et al. (2012) renormalized to NIST SRM 3134 + 0.25 ‰ based on Goldberg et al. (2013); [y]Section 8 and references therein; [z]Yang et al. (2020); [aa]Hayes et al. (2018) and references therein; [ab]Miller et al. (2011); [ac]Dickens et al. (2003); [ad]Cameron & Vance (2014) and references therein; [ae]Wei et al. (2018); [af]Broecker & Peng (1982).

Competing interests

The authors declare that they are not aware of any financial conflicts of interest, real or perceived.

GEOTRACES–PAGES Biological Productivity Working Group Members

C. Bolton (CEREGE, Univ. Aix-Marseille, CNRS, IRD, Collège de France, INRAE, Aix-en-Provence, France); E. Calvo (Institut de Ciències del Mar, CSIC, Barcelona, Spain); D. Cardinal (LOCEAN (UMR7159), Sorbonne Université, IRD, CNRS, MNHN, Paris, France); T. de Garidel-Thoron (CEREGE, Univ. Aix-Marseille, CNRS, IRD, Collège de France, INRAE Aix-en-Provence, France); S. Fietz (Department of Earth Sciences, Stellenbosch University, Stellenbosch South Africa); K. R. Hendry (School of Earth Sciences, University of Bristol, Bristol, UK); F. Marcantonio (Department of Geology and Geophysics, Texas A&M University), P. A. Rafter (Department of Earth System Science, University of California, Irvine, CA, USA); H. Ren (Department of Geosciences, National Taiwan University, Taipei, Taiwan); C. J. Somes (GEOMAR Helmholtz Centre for Ocean Research Kiel, 24105 Kiel, Germany); J. N. Sutton (Univ Brest, CNRS, IRD, Ifremer, Institut Universitaire Européen de la Mer, LEMAR, Plouzané, France); A. Torfstein (Institute of Earth Sciences, Hebrew University, Jerusalem, & InterUniversity Institute for Marine Sciences, Eilat, Israel); G. Winckler (Lamont-Doherty Earth Observatory of Columbia University, Palisades, NY, USA).

References

Abadie, C., Lacan, F., Radic, A., Pradoux, C., & Poitrasson, F. (2017). Iron isotopes reveal distinct dissolved iron sources and pathways in the intermediate versus deep Southern Ocean. *Proc. Natl. Acad. Sci.*, **114**, 858-863.

Abouchami, W., Galer, S. J. G., de Baar, H. J. W., Alderkamp, A. C., Middag, R., Laan, P., Feldmann, H., & Andreae, M. O. (2011). Modulation of the Southern Ocean cadmium isotope signature by ocean circulation and primary productivity. *Earth Planet. Sci. Lett.*, **305**(1-2), 83-91.

Abouchami, W., Galer, S. J. G., Horner, T. J., Rehkämper, M., Wombacher, F., Xue, Z., Lambelet, M., Gault-Ringold, M., Stirling, C. H., Schönbächler, M., Shiel, A. E., Weis, D., & Holdship, P. F. (2013). A common reference material for cadmium isotope studies–NIST SRM 3108. *Geostandards and Geoanalytical Research*, **37**(1), 5-17.

Abouchami, W., Galer, S. J. G., de Baar, H. J. W., Middag, R., Vance, D., Zhao, Y., Klunder, M., Mezger, K., Feldmann, H., & Andreae, M. O. (2014). Biogeochemical cycling of cadmium isotopes in the Southern Ocean along the Zero Meridian. *Geochim. Cosmochim. Acta*, **127**, 348-367.

Achterberg, E. P. & van den Berg, C. M. G. (1997). Chemical speciation of chromium and nickel in the western Mediterranean. *Deep-Sea Res. II*. **44**, 693–720, doi: 10.1016/S0967-0645(96)00086-0.

Adkins, J. F., Cheng, H., Boyle, E. A., Druffel, E. R., & Edwards, R. L. (1998). Deep-sea coral evidence for rapid change in ventilation of the deep North Atlantic 15,400 years ago. *Science*, **280**(5364), 725-728.

Akerman, A., Poitrasson, F., Oliva, P., Audry, S., Prunier, J., & Braun, J. J. (2014). The isotopic fingerprint of Fe cycling in an equatorial soil-plant-water system: The Nsimi watershed, South Cameroon. *Chem. Geol*., **385**, 104–116.

Albarède, F. (2004). The stable isotope geochemistry of copper and zinc. *Reviews in Mineralogy and Geochemistry*, *55*(1), 409-427.

Albut, G., Babechuk, M. G., Kleinhanns, I. C., Benger, M., Beukes, N. J., Steinhilber, B., Smith, A. J. B., Kruger, S. J., & Schoenberg, R. (2018). Modern rather than Mesoarchaen oxidative weathering responsible for the heavy stable Cr isotopic signatures of the 2.95 Ga old Ijzermijn iron formation (South Africa). *Geochem. Cosmochim. Acta*, **228**, 157-189, doi:10.1016/j.gca.2018.02.034.

Algeo, T. J. (2004). Can marine anoxic events draw down the trace element inventory of seawater? *Geology*, **32** (12), 1057-1060, doi:10.1130/G20896.1.

Algeo, T. J., & Lyons, T. W. (2006). Mo-total organic carbon covariation in modern anoxic marine environments: Implications for analysis of paleoredox and paleohydrographic conditions: *Paleoceanography*, **21**, doi:10.1029/2004PA001112.

Algeo T. J., & Maynard J. B. (2008). Trace-metal covariation as a guide to water-mass conditions in ancient anoxic marine environments. *Geosphere* **4**, 872.

Algeo, T. J., & Tribovillard, N. (2009). Environmental analysis of paleoceanographic systems based on molybdenum-uranium covariation: *Chem. Geol.*, **268**, 211–225, doi:10.1016/j.chemgeo.2009.09.001.

Alldredge, A. L., & Silver, M. W. (1988). Characteristics, dynamics and significance of marine snow. *Prog. Oceanogr.*, **20**(1), 41-82.

Anbar, A. D., & Knoll, A. H. (2002). Proterozoic Ocean Chemistry and Evolution: A Bioinorganic Bridge? *Science*, **297**, 1137–1142, doi:10.1126/science.1069651.

Anbar, A. D. (2004). Molybdenum stable isotopes: observations, interpretations and directions. *Rev. Min. Geochem.*, **55**(1), 429-454.

Anbar, A. D., Jarzecki, A. A., & Spiro, T. G. (2005) Theoretical investigation of iron isotope fractionation between $Fe(H_2O)_6^{3+}$ and $Fe(H_2O)_6^{2+}$: Implications for iron stable isotope geochemistry. *Geochim. Cosmochim. Acta.* **69**, 825–837. https://doi.org/10.1016/j.gca.2004.06.012.

Andersen, M. B., Vance, D., Archer, C., Anderson, R. F., Ellwood, M. J., & Allen, C. S. (2011). The Zn abundance and isotopic composition of diatom frustules, a proxy for Zn availability in ocean surface seawater. *Earth Planet. Sci. Lett.*, **301**, 137–145. http://dx.doi.org/10.1016/j.epsl.2010.10.032.

Anderson, M. A., Morel, F. M. M., & Guillard, R. R. L. (1978). Growth limitation of a coastal diatom by low zinc ion activity. *Nature*, **276**, 70-71.

Annett, A. L., Lapi, S., Ruth, T. J., & Maldonado, M. T. (2008). The effects of Cu and Fe availability on the growth and Cu:C ratios of marine diatoms. *Limnol. Oceanogr.* **53**, 2451–2461.

Aplin, A. C., & Cronan, D. S. (1985). Ferromanganese oxide deposits from the central Pacific Ocean, I. Encrustations from the Line Islands Archipelago. *Geochim. Cosmochim. Acta*, **49**(2), 427-436.

Archer, C., Andersen, M. B., Cloquet, C., Conway, T. M., Dong, S., Ellwood, M., Moore, R, Nelson, J., Rehkämper, M., Rouxel, O., Samanta, M., Shin, K.-C., Sohrin, Y., Takano, S., & Wasylenki, L. (2017). Inter-calibration of a proposed new primary reference standard AA-ETH Zn for zinc isotopic analysis. *Journal of Analytical Atomic Spectrometry*, **32**(2), 415-419.

Archer, C., Vance, D., Milne, A., & Lohan, M. C. (2020). The oceanic biogeochemistry of nickel and its isotopes: New data from the South Atlantic and the Southern Ocean biogeochemical divide. *Earth Planet. Sci. Lett.*, **535**, 116118.

Arnold, G. L., Anbar, A. D., Barling, J., & Lyons, T. W. (2004). Molybdenum isotope evidence for widespread anoxia in mid-Proterozoic oceans. *Science*, **304**(5667), 87-90.

Aristilde, L., & Xu, Y. (2012). Weak organic ligands enhance Zinc uptake in Marine phytoplankton. *Environ. Sci. Technol.*, **46**, 5438-5445.

Arrhenius, G. (1963). *Pelagic sediments*. Scripps Institution of Oceanography, University of California.

Atkins, A. L., Shaw, S., & Peacock, C. L. (2016). Release of Ni from birnessite during transformation of birnessite to todorokite: Implications for Ni cycling in marine sediments. *Geochim. Cosmochim. Acta*, **189**, 158-183.

Baars, O., & Croot, P. L. (2011). The speciation of dissolved zinc in the Atlantic sector of the Southern Ocean. *Deep. Res. Part II Top. Stud. Oceanogr.*, **58**, 2707–2719. http://dx.doi.org/10.1016/j.dsr2.2010.10.041.

Baars, O., Abouchami, W., Galer, S. J., Boye, M., & Croot, P. L. (2014). Dissolved cadmium in the Southern Ocean: distribution, speciation, and relation to phosphate. *Limnol. Oceanogr.*, **59**(2), 385-399.

Bacon, M.P. and Anderson, R.F. (1982). Distribution of thorium isotopes between dissolved and particulate forms in the deep sea. *J. Geophys. Res. Oceans*, **87**(C3), 2045-2056.

Badaut, D., & Risacher, F. (1983). Authigenic smectite on diatom frustules in Bolivian saline lakes. *Geochim. Cosmochim. Acta*, **47**(3), 363-375.

Barling, J., Arnold, G., & Anbar, A. D., (2001). Natural mass-dependent variations in the isotopic composition of molybdenum. *Earth Planet. Sci. Lett.*, **193**, 447–457, doi:10.1016/S0012-821X(01)00514-3.

Barling, J., & Anbar, A. D. (2004). Molybdenum isotope fractionation during adsorption by manganese oxides. *Earth Planet. Sci. Lett.*, **217**, 315-329, doi:10.1016/S0012-821X(03)00608-3.

Bates, S. L., Hendry, K. R., Pryer, H. V., Kinsley, C. W., Pyle, K. M., Woodward, E. M. S., & Horner, T. J. (2017). Barium isotopes reveal role of ocean circulation on barium cycling in the Atlantic. *Geochim. Cosmochim. Acta,* **204**, 286-299.

Bauer, K. W., Gueguen, B., Cole, D. B., Francois, R., Kallmeyer, J., Planavsky, N., & Crowe, S. A. (2018). Chromium isotope fractionation in ferruginous sediments. *Geochim. Cosmochim. Acta,* **223**, 198-215, doi: 10.1016/j.gca.2017.10.034.

Bauer, K. W., Cole, D. B., Asael, D., Francois, R., Calvert, S. E., Poulton, S. W., Planavsky, N., & Crowe, S. A. Chromium isotopes in marine hydrothermal sediments. *Chem. Geol.,* **529**, 119286, doi: 10.1016/j.chemgeo.2019.119286.

Beard, B.L., Johnson, C.M., Cox, L., Sun, H., Nealson, K.H., & Aguilar, C. (1999). Iron Isotope Biosignatures. *Science* **285**, 1889-1892.

Beard, B. L., Johnson, C. M., Skulan, J. L., Nealson, K. H., Cox, L., & Sun, H. (2003). Application of Fe isotopes to tracing the geochemical and biological cycling of Fe. *Chem. Geol.*, **195**(1-4), 87-117.

Bennett, S. A., Rouxel, O., Schmidt, K., Garbe-Schönberg, D., Statham, P. J., & German, C. R. (2009). Iron isotope fractionation in a buoyant hydrothermal plume, 5 S Mid-Atlantic Ridge. *Geochim. Cosmochim. Acta*, **73**(19), 5619-5634.

Bergquist, B. A., & Boyle, E. A. (2006). Iron isotopes in the Amazon River system: Weathering and transport signatures. *Earth Planet, Sci. Lett*., **248**(1–2), 54–68. https://doi.org/10.1016/j.epsl.2006.05.004.

Berger, W. H., Smetacek, V., & Wefer, G. (1989). Ocean productivity and paleoproductivity - an overview. In W. H. Berger, V. S. Smetacek, G. Wefer (Eds) *Productivity of the Oceans present and past: Report of the Dahlem Workshop on Productivity of the Ocean, Berlin, 1988,* Life Sciences Research Reports 44, Wiley & Sons, Chichester, pp. 1-34.

Bermin, J., Vance, D., Archer, C., & Statham, P. J. (2006). The determination of the isotopic composition of Cu and Zn in seawater. *Chem. Geol.,* **226**, 280–297.

Berner, R. A., Petsch, S. T., Lake, J. A., Beerling, D. J., Popp, B. N., Lane, R. S., Laws, E. A., Westley, M. B., Cassar, N., Woodward, F. I. & Quick, W. P. (2000). Isotope fractionation and atmospheric oxygen: implications for Phanerozoic O_2 evolution. *Science*, **287**(5458), 1630-1633.

Bernstein, R. E., & Byrne, R. H. (2004). Acantharians and marine barite. *Mar. Chem.,* **86** (1-2), 45-50.

Bertine, K. K., & Turekian, K. K. (1973). Molybdenum in marine deposits. *Geochim. Cosmochim. Acta*, **37** (6), 1415-1434.

Bianchi, D., Weber, T. S., Kiko, R., & Deutsch, C. (2018). Global niche of marine anaerobic metabolisms expanded by particle microenvironments. *Nat. Geosci.,* **11**, 1–6.

Bishop, J. K. (1988). The barite-opal-organic carbon association in oceanic particulate matter. *Nature*, **332** (6162), 341.

Böning, P., Brumsack, H.-J., Böttcher, M.E., Schnetger, B., Kriete, C., Kallmeyer, J., & Borchers, S.L. (2004). Geochemistry of Peruvian near-surface sediments. *Geochim. Cosmochim. Acta*, **68**, 4429-4451.

Böning, P., Cuypers, S., Grunwald, M., Schnetger, B., & Brumsack, H.-J. (2005). Geochemical characteristics of Chilean upwelling sediments at ~36°S. *Mar. Geol.,* **220**, 1-21.

Böning, P., Brumsack, H.-J., Schnetger, B., & Grunwald, M. (2009). Trace element signatures of Chilean upwelling sediments at ~36°S. *Mar. Geol.*, **259**, 112-121.

Böning, P., Shaw, T., Pahnke, K., & Brumsack, H.-J. (2015). Nickel as an indicator of fresh organic matter in upwelling sediments. *Geochim. Cosmochim. Acta*, **162**, 99-108, doi:10.1016/j.gca.2015.04.027.

Bonnard, P., James, R. H., Parkinson, I. J., Connelly, D. P., & Fairchild, I. J. (2013). The chromium isotopic composition of seawater and marine sediments. *Earth Planet. Sci. Lett.*, **382**, 10-20. doi: 10.1016/j.epsl.2013.09.001.

Borchers, S.L., Schnetger, B., Boning, P., & Brumsack, H.-J. (2005). Geochemical signatures of the Namibian diatom belt: Perennial upwelling and intermittent anoxia. *Geochemistry, Geophysics, Geosystems*, **6**(4), Q06006, doi:10.1029/2004GC000886.

Boyd, P. W., Claustre, H., Levy, M., Siegel, D. A., & Weber, T. (2019). Multi-faceted particle pumps drive carbon sequestration in the ocean. *Nature*, **568**(7752), 327-335.

Boyd, P. W., Jickells, T., Law, C. S., Blain, S., Boyle, E. A., Buesseler, K. O., Coale, K. H., Cullen, J. J., de Baar, H. J. W., Follows, M., Harvey, M., Lancelot, C., Levasseur, M., Owens, N. P. J., Pollard, R., Rivkin, R. B., Sarimento, J., Schoemann, V., Smetacek, V., Takeda, S., Tsuda, A., Turner, S., & Watson, A. J.. (2007). Mesoscale iron enrichment experiments 1993-2005: synthesis and future directions. *Science*, **315**(5812), 612-617.

Boyd, P. W., & Ellwood, M. J. (2010). The biogeochemical cycle of iron in the ocean. *Nat. Geosci.* **3**(10), 675-682.

Boyd, P. W., Ellwood, M. J., Tagliabue, A., & Twining, B. S. (2017). Biotic and abiotic retention, recycling and remineralization of metals in the ocean. *Nat. Geosci.*, **10**(3), 167-173.

Boye, M., Wake, D. B., Lopez Gracia, P., Bown, J., Baker, A. R., & Achterberg, E. P. (2012). Distributions of dissolved trace metals (Cd, Cu, Mn, Pb, Ag) in the southeastern Atlantic and the Southern Ocean. *Biogeosciences*, **9**, 3231-3246, doi:10.5194/bg-9-3231-2012.

Boyle, E. A. (1981). Cadmium, zinc, copper, and barium in foraminifera tests. *Earth Planet. Sci. Lett.*, **53**(1), 11-35.

Boyle, E. A. (1988a). Vertical oceanic nutrient fractionation and glacial/interglacial CO_2 cycles. *Nature*, **331**(6151), 55-56.

Boyle, E. A. (1988b). Cadmium: Chemical tracer of deepwater paleoceanography. *Paleoceanography*, **3**(4), 471-489.

Boyle, E. A. (1992). Cadmium and δ^{13}C paleochemical ocean distributions during the stage 2 glacial maximum. *Annual Review of Earth and Planetary Sciences*, **20**(1), 245-287.

Boyle, E. A., & Keigwin, L. D. (1985). Comparison of Atlantic and Pacific paleochemical records for the last 215,000 years: Changes in deep ocean circulation and chemical inventories. *Earth Planet. Sci. Lett.*, **76**(1-2), 135-150.

Boyle, E. A., Sclater, F., & Edmond, J. M. (1976). On the marine geochemistry of cadmium. *Nature*, **263**(5572), 42.

Boyle, E. A., Sclater, F. R., & Edmond, J. M. (1977). The distribution of dissolved copper in the Pacific. *Earth Planet. Sci. Lett.*, **37**, 38-54.

Brand, L. E., Sunda, W. G., & Guillard, R. R. L. (1983). Limitation of marine phytoplankton by zinc, manganese, and iron. *Limnol. Oceanogr.*, **28**, 1182–1198.

Brand L. E., Sunda, W. G., & Guillard, R. R. L. (1986). Reduction of marine phytoplankton reproduction rates by copper and cadmium. *J. Exp. Mar. Bio. Ecol.* **96**, 225–250.

Bridgestock, L., Rehkämper, M., van de Flierdt, T., Murphy, K., Khondoker, R., Baker, A. R., Chance, R., Strekopytov, S., Humphreys-Williams, E., Achterberg, E. P. (2017). The Cd isotope composition of atmospheric aerosols from the Tropical Atlantic Ocean. *Geophys. Res. Lett.* **44**(6), 2932-2940. https://doi.org/10.1002/2017GL072748.

Bridgestock, L., Hsieh, Y. T., Porcelli, D., Homoky, W. B., Bryan, A., & Henderson, G. M. (2018). Controls on the barium isotope compositions of marine sediments. *Earth Planet. Sci. Lett.*, **481**, 101-110.

Bridgestock, L., Hsieh, Y. T., Porcelli, D., & Henderson, G. M. (2019). Increased export production during recovery from the Paleocene–Eocene thermal maximum constrained by sedimentary Ba isotopes. *Earth Planet. Sci. Lett.*, **510**, 53-63.

Broecker, W.S. (1982). Glacial to interglacial changes in ocean chemistry. *Prog. Oceanogr*. **11**, 151-197.

Broecker, W.S., & Peng, T. H. (1982). Tracers in the Sea. Eldigo Press, Palisades, NY.

Brucker, R. L. P., McManus, J., Severmann, S., & Berelson, W. M. (2009). Molybdenum behavior during early diagenesis: Insights from Mo isotopes. *Geochemistry, Geophysics, Geosystems*, **10**, doi:10.1029/2008GC002180.

Bruggmann, S., Scholz, F., Klaebe, R. M., Canfield, D. E., & Frei, R. (2019). Chromium isotope cycling in the water column and sediments of the Peruvian continental margin. *Geochim. Cosmochim. Acta*, **257**, 224–242, doi: 10.1016/j.gca.2019.05.001.

Bruland, K. W. (1980). Oceanographic distributions of cadmium, zinc, nickel, and copper in the North Pacific. *Earth Planet. Sci. Lett.*, **47**(2), 176-198.

Bruland, K. W. (1989). Complexation of zinc by natural organic ligands in the central North Pacific. *Limnol. Oceanogr.*, **34**, 269–285.

Bruland, K. W. (1992). Complexation of cadmium by natural organic ligands in the central North Pacific. *Limnol. Oceanogr.*, **37**(5), 1008-1017.

Bruland, K. W., & Lohan, M. C. (2003). Controls of Trace Metals in Seawater. In *Treatise on Geochemistry*, Elsevier, 23-47.

Bruland, K. W., Knauer, G. A., & Martin, J. H. (1978). Zinc in north-east Pacific water. *Nature*, **271**(5647), 741-743.

Brumsack, H. J. (2006). The trace metal content of recent organic carbon-rich sediments: implications for Cretaceous black shale formation. *Palaeogeography, Palaeoclimatology, Palaeoecology*, **232**(2-4), 344-361.

Bryan, A. L., Dong, S., Wilkes, E. B., & Wasylenki, L. E. (2015). Zinc isotope fractionation during adsorption onto Mn oxyhydroxide at low and high ionic strength. *Geochim. Cosmochim. Acta*, **157**, 182-197.

Bryan, A. L., Dickson, A. J., Dowdall, F., Homoky, W. B., Porcelli, D., & Henderson, G. M. (2021). Controls on the cadmium isotope composition of modern marine sediments. *Earth Planet. Sci. Lett.*, **565**, 116946, doi:10.1016/j.epsl.2021.116946.

Cadiou, J. L., Pichat, S., Bondanese, V. P., Soulard, A., Fujii, T., Albarède, F., & Oger, P. (2017). Copper transporters are responsible for copper isotopic fractionation in eukaryotic cells. *Sci. Rep.*, **7**(1), 1-10.

Cameron, V., Vance, D., Archer, C., & House, C. H. (2009). A biomarker based on the stable isotopes of nickel. *Proceedings of the National Academy of Sciences*, *106*(27), 10944-10948.

Campbell, J. A., & Yeats, P. A. (1981). Dissolved chromium in the northwest Atlantic Ocean. *Earth. Planet. Sci. Lett.*, **53**, 427-433.

Campbell, J. A., & Yeats, P. A. (1984). Dissolved chromium in the St. Lawrence estuary. *Estuar. Coast. Shelf Sci.*, **19**, 513-522.

Carlson, C. A., Hansell, D. A., Nelson, N. B., Siegel, D. A., Smethie, W. M., Khatiwala, S., Meyers, M. M., & Halewood, E. (2010). Dissolved organic carbon export and subsequent remineralization in the mesopelagic and bathypelagic realms of the North Atlantic basin. *Deep Sea Res. Pt. II*, **57**(16), 1433-1445.

Cao, Z., Siebert, C., Hathorne, E. C., Dai, M., & Frank, M. (2020a). Corrigendum to "Constraining the oceanic barium cycle with stable barium isotopes" [*Earth Planet. Sci. Lett.*, **434** (2016) 1-9], doi: 10.1016/j.epsl.2019.116003.

Cao, Z., Li, Y., Rao, X., Yu, Y., Hathorne, E. C., Siebert, C., Dai, M., & Frank, M. (2020b). Constraining barium isotope fractionation in the upper water column of the South China Sea. *Geochim. Cosmochim. Acta*, **288**, 120-137.

Cartapanis, O., Bianchi, D., Jaccard, S. L., & Galbraith, E. D. (2016). Global pulses of organic carbon burial in deep-sea sediments during glacial maxima. *Nat. Commun.*, **7**, 10796, doi:10.1038/ncomms10796.

Carter, S. C., Paytan, A., & Griffith, E. M. (2020). Toward an Improved Understanding of the Marine Barium Cycle and the Application of Marine Barite as a Paleoproductivity Proxy. *Minerals*, **10**(5), 421.

Chan, L. H., Edmond, J. M., Stallard, R. F., Broecker, W. S., Chung, Y. C., Weiss, R. F., & Ku, T. L. (1976). Radium and barium at GEOSECS stations in the Atlantic and Pacific. *Earth Planet. Sci. Lett.*, **32**(2), 258-267.

Chan, L. H., Drummond, D., Edmond, J. M., & Grant, B. (1977). On the barium data from the Atlantic GEOSECS expedition. *Deep Sea Res.*, **24**(7), 613-649.

Chang, A. S., Pedersen, T. F., & Hendy, I. L. (2014). Effects of productivity, glaciation, and ventilation on late Quaternary sedimentary redox and trace element accumulation on the Vancouver Island margin, western Canada. *Paleoceanogr.*, **29**(7), 730-746.

Chappaz, A., Lyons, T. W., Gregory, D. D., Reinhard, C. T., Gill, B. C., Li, C., & Large, R. R. (2014). Does pyrite act as an important host for molybdenum in modern and ancient euxinic sediments? *Geochim. Cosmochim. Acta*, **126**, 112–122, doi:10.1016/j.gca.2013.10.028.

Chappell, P. D., Vedmati, J., Selph, K. E., Cyr, H. A., Jenkins, B. D., Landry, M. R., & Moffett, J. W. (2016). Preferential depletion of zinc within Costra Rica upwelling dome creates conditions for zinc co-limitation of primary production. *J. Plankton Res.*, **38**, 244-255, doi:10.1093/plankt/fbw018.

Charette, M. A., et al. (2020). The Transpolar Drift as a Source of Riverine and Shelf-Derived Trace Elements to the Central Arctic Ocean. *J. Geophys. Res. Oceans*, **125**(5), e2019JC015920. https://doi.org/10.1029/2019JC015920.

Chen, J.-B., Busigny, V., Gaillardet, J., Louvat, P., & Wang, Y.-N. (2014). Iron isotopes in the Seine River (France): Natural vs anthropogenic sources. *Geochim. Cosmochim. Acta*, **128**, 128-143.

Chen, L., Little, S. H., Kreissig, K., Severmann, S., & McManus, J. (2021). Isotopically Light Cd in Sediments Underlying Oxygen Deficient Zones. *Front. Earth Sci.*, **9**, 97.

Chen., T., Wenqiang, L., Gao, B., Liu, R., Li, G., Zhao, L., and Ji, J. (2020). Reactive iron isotope signatures of the East Asian dust particles: Implications for iron cycling the deep North Pacific. *Chem. Geol.* **531**, 119342. https://doi.org/10.1016/j.chemgeo.2019.119342.

Cheng, H., Adkins, J., Edwards, R. L., & Boyle, E. A. (2000). U-Th dating of deep-sea corals. *Geochim. Cosmochim. Acta*, **64**(14), 2401-2416.

Chever, F., Bucciarelli, E., Sarthou, G., Speich, S., Arhan, M., Penven, P., & Tagliabue, A. (2010). Physical speciation of iron in the Atlantic sector of the Southern Ocean along a transect from the subtropical domain to the Weddell Sea Gyre. *J. Geophys. Res. Oceans*, **115**, C10059, doi:10.1029/2009JC005880.

Chever. F., Rouxel, O. J., Croot, P. L., Ponzevera, E., Wuttig, K., & Auro, M. (2015). Total dissolvable and dissolved iron isotopes in the water column of the Peru upwelling regime. *Geochim. Cosmochim. Acta*, **162**, 66-82. https://doi.org/10.1016/j.gca.2015.04.031.

Chow, T. J., & Goldberg, E. D. (1960). On the marine geochemistry of barium. *Geochim. Cosmochim. Acta*, **20**(3-4), 192-198.

Chung, Y. (1980). Radium-barium-silica correlations and a two-dimensional radium model for the world ocean. *Earth Planet. Sci. Lett.*, **49**(2), 309-318.

Chu, N., Johnson, C., Beard, B., German, C., Nesbitt, R., Frank, M., Bohn, M., Kubik, P., Usui, A., & Graham, I. (2006). Evidence for hydrothermal venting in Fe isotope compositions of the deep Pacific Ocean through time. *Earth Planet. Sci. Lett.*, **245**, 202-217.

Ciscato E. R., Bontognali T. R. R., & Vance, D. (2018). Nickel and its isotopes in organic-rich sediments: implications for oceanic budgets and a potential record of ancient seawater. *Earth Planet. Sci. Lett.* **494**, 239–250. https://doi.org/10.1016/j.epsl.2018.04.061.

Ciscato, E. R., Bontognali, T. R., Poulton, S. W., & Vance, D. (2019). Copper and its Isotopes in Organic-Rich Sediments: From the Modern Peru Margin to Archean Shales. *Geosciences*, **9**(8), 325.

Clarkson, M., Müsing, K., Andersen, M. B., & Vance, D. (2018). Reducing the role of contaminant phases for metal isotopes in carbonates. In *Goldschmidt Abstracts* p. 441.

Coale, K. H. (1991). Effects of iron, manganese, copper and zinc enrichments on productivity and biomass in the subarctic Pacific. *Limnol. Oceanogr.*, **36**, 1851–1864.

Coale K. H., & Bruland K. W. (1988). Copper complexation in the Northeast Pacific. *Limnol. Oceanogr.* **33**, 1084–1101.

Coale K. H., & Bruland K. W. (1990). Spatial and temporal variability in copper complexation in the North Pacific. *Deep Sea Res. Part A, Oceanogr. Res. Pap.* **37**, 317–336.

Coale, K. H., Wang, X., Tanner, S. J., & Johnson, K. S. (2003). Phytoplankton growth and biological response to iron and zinc addition in the Ross Sea and Antarctic Circumpolar Current along 170°W. *Deep. Res. Part II Top. Stud. Oceanogr.*, **50**, 635–653.

Collier, R. W. (1985). Molybdenum in the Northeast Pacific Ocean. *Limnol. Oceanogr.*, **30**, 1351–1354, doi:10.4319/lo.1985.30.6.1351

Conway, T. M., & John, S. G. (2014a). Quantification of dissolved iron sources to the North Atlantic Ocean. *Nature*, 511, 212-215.

Conway, T. M., & John, S. G. (2014b). The biogeochemical cycling of zinc and zinc isotopes in the North Atlantic Ocean. *Global Biogeochem. Cycles*, 1111–1128.

Conway, T. M., & John, S. G. (2015a). The cycling of iron, zinc and cadmium in the North East Pacific Ocean–Insights from stable isotopes. *Geochim. Cosmochim. Acta*, **164**, 262-283.

Conway, T. M., & John, S. G. (2015b). Biogeochemical cycling of cadmium isotopes along a high-resolution section through the North Atlantic Ocean. *Geochim. Cosmochim. Acta*, **148**, 269-283.

Conway, T. M., Rosenberg, A. D., Adkins, J. F., & John, S. G. (2013). A new method for precise determination of iron, zinc and cadmium stable isotope ratios in seawater by double-spike mass spectrometry. *Anal. Chim. Acta,* **793**, 44–52.

Conway, T. M., Hamilton, D. S., Shelley, R. U., Aguilar-Islas, A. M., Landing, W. M., Mahowald, N. M., & John, S. G. (2019). Tracing and constraining anthropogenic aerosol iron fluxes to the North Atlantic Ocean using iron isotopes. *Nat. Commun.*, **10**, 2628, doi:10.1038/s41467-019-10457-w.

Coplen, T. B. (2011). Guidelines and recommended terms for expression of stable-isotope-ratio and gas-ratio measurement results. *Rapid communications in mass spectrometry*, **25**(17), 2538-2560.

Costa, K. M., McManus, J. F., Anderson, R. F., Ren, H., Sigman, D. M., Winckler, G., Fleisher, M. Q., Marcantonio, F., & Ravelo, A. C. (2016). No iron fertilization in the equatorial Pacific Ocean during the last ice age. *Nature,* **529**(7587), 519-522.

Costa, K. M., McManus, J. F., Middleton, J. L., Langmuir, C. H., Huybers, P. J., Winckler, G., & Mukhopadhyay, S. (2017). Hydrothermal deposition on the Juan de Fuca Ridge over multiple glacial–interglacial cycles. *Earth Planet. Sci. Lett.*, **479**, 120-132.

Coutaud, M., Méheut, M., Glatzel, P., Pokrovski, G. S., Viers, J., Rols, J. L., & Pokrovsky, O. S. (2018). Small changes in Cu redox state and speciation generate large isotope fractionation during adsorption and incorporation of Cu by a phototrophic biofilm. *Geochim. Cosmochim. Acta,* **220**, 1-18.

Coutaud, M., Méheut, M., Viers, J., Rols, J. L., & Pokrovsky, O. S. (2019). Copper isotope fractionation during excretion from a phototrophic biofilm. *Chem. Geol.*, **513**, 88-100.

Cowan, C .E., Jenne, E. A., & Crecelius, E. A. (1985). Silver speciation in seawater: The importance of sulfide and organic complexes. In: A.C. Sigleo and A. Hattori (Eds.), *Marine and Estuarine Geochemisty,* Lewis Publishers Inc., Chelsea, MI, USA.

Cranston, R. E., & Murray, J. W. (1978). Determination of chromium species in natural waters. *Anal. Chim. Acta*, **99**, 275-282.

Cranston, R. E., & Murray, J. W. (1980). Chromium species in the Columbia River and estuary. Limnol. Oceanogr. 25, 1104–1112.

Crawford, D. W. W., Lipsen, M. S. S., Purdie, D. A. A., Lohan, M. C. C., Statham, P. J. J., Whitney, F. A. A., Putland, J. N. N., Johnson, W. K. K., Sutherland N., Peterson, T. D. D., Harrison, P. J. J., & Wong C. S. S. (2003). Influence of zinc and iron enrichments on phytoplankton growth in the northeasten subarctic Pacific. *Limnol. Oceanogr.*, **48**, 1583–1600.

Crockford, P. W., Wing, B. A., Paytan, A., Hodgskiss, M. S., Mayfield, K. K., Hayles, J. A., Middleton, J. E., Ahm, A.-S. C., Johnston, D. T., Caxito, F., Uhlein, G., Halverson, G. P., Eickmann, B., Torres, M., & Horner, T. J. (2019). Barium-isotopic constraints on the origin of post-Marinoan barites. *Earth Planet. Sci. Lett.*, **519**, 234-244.

Crusius, J., & Thomson, J. (2003). Mobility of authigenic rhenium, silver, and selenium during postdepositional oxidation in marine sediments. *Geochim. Cosmochim. Acta,* **67**(2), 265-273.

Crusius, J., Calvert, S., Pedersen, T., & Sage, D. (1996). Rhenium and molybdenum enrichments in sediments as indicators of oxic, suboxic and sulfidic conditions of deposition. *Earth Planet. Sci. Lett.*, **145**, 65–78, doi:10.1016/S0012-821X(96)00204-X.

Cullen, J. T. (2006). On the nonlinear relationship between dissolved cadmium and phosphate in the modern global ocean: could chronic iron limitation of phytoplankton growth cause the kink? *Limnol. Oceanogr.*, **51**(3), 1369-1380.

Cullen, J. T., & Sherrell, R. M. (2005). Effects of dissolved carbon dioxide, zinc, and manganese on the cadmium to phosphorus ratio in natural phytoplankton assemblages. *Limnol. Oceanogr.*, **50**(4), 1193-1204.

Cullen, J. T., Chase, Z., Coale, K. H., Fitzwater, S. E., & Sherrell, R. M. (2003). Effect of iron limitation on the cadmium to phosphorus ratio of natural phytoplankton assemblages from the Southern Ocean. *Limnology and Oceanography*, **48**(3), 1079-1087.

Cullen, J. T., Lane, T. W., Morel, F. M., & Sherrell, R. M. (1999). Modulation of cadmium uptake in phytoplankton by seawater CO_2 concentration. *Nature*, **402**(6758), 165.

Cullen, J. T., Chase, Z., Coale, K. H., Fitzwater, S. E., & Sherrell, R. M. (2003). Effect of iron limitation on the cadmium to phosphorus ratio of natural phytoplankton assemblages from the Southern Ocean. *Limnol. Oceanogr.*, **48**(3), 1079-1087.

Cullen, J. T., & Coogan, L. A. (2017). Changes in Fe Oxidation Rate in Hydrothermal Plumes as a Potential Driver of Enhanced Hydrothermal Input to Near-Ridge Sediments During Glacial Terminations. *Geophys. Res. Lett.*, **44**(23), 11-951.

Cutter, G., Casciotti, K., Croot, P., Geibert, W., Heimbürger, L.-E., Lohan, M., & van de Flierdt, T. (2017). *Sampling and Sample-handling Protocols for GEOTRACES Cruises*, Version 3. http://www.geotraces.org/images/stories/documents/intercalibration/Cookbook.pdf [accessed 2020-06-23].

D'Arcy, J., Babechuk, M. G., Døssing, L. N., Gaucher, C., & Frei, R. (2016). Processes controlling the chromium isotopic composition of river water: constraints from basaltic river catchments. *Geochim. Cosmochim. Acta*, **186**, 296–315, doi:10.1016/j.gca.2016.04.027.

da Silva, J. F., & Williams, R. J. P. (1991). *The biological chemistry of the elements: the inorganic chemistry of life*. Oxford University Press.

Dahl, T. W., Anbar, A. D., Gordon, G. W., Rosing, M. T., Frei, R., & Canfield, D. E. (2010). The behavior of molybdenum and its isotopes across the chemocline and in the sediments of sulfidic Lake Cadagno, Switzerland. *Geochim. Cosmochim. Acta*, **74**, 144–163, doi:10.1016/j.gca.2009.09.018.

Dahl, T. W., Chappaz, A., Hoek, J., McKenzie, C. J., Svane, S., and Canfield, D. E. (2017). Evidence of molybdenum association with particulate organic matter under sulfidic conditions. *Geobiology*, **15**, 311–323, doi:10.1111/gbi.12220.

Dalai, T.K., Nishimura, K., & Nozaki, Y. (2005). Geochemistry of molybdenum in the Chao Phraya River estuary, Thailand: Role of suboxic diagenesis and porewater transport. *Chem. Geol.*, **218**, 189–202, doi:10.1016/j.chemgeo.2005.01.002.

Davidson, A. B., Semeniuk, D. M., Koh, J., Holmden, C., Jaccard, S. L., Francois, R. & Crowe, S. A. (2020) A $Mg(OH)_2$ coprecipitation method for determining chromium speciation and isotopic composition in seawater. *Limnol. Oceanogr. Meth.*, **18**, 8–19, doi:10.1002/lom3.10342.

de Baar, H. J. W., Saager, P. M., Nolting, R. F., & van der Meer, J. (1994). Cadmium versus phosphate in the world ocean. *Mar. Chem.*, **46**(3), 261-281.

de Baar, H. J., Boyd, P. W., Coale, K. H., Landry, M. R., Tsuda, A., Assmy, P., ... & Buesseler, K. O. (2005). Synthesis of iron fertilization experiments: from the iron age in the age of enlightenment. *Journal of Geophysical Research: Oceans*, **110**(C9).

de Baar, H. J. W., van Heuven, S. M., Abouchami, W., Xue, Z., Galer, S. J. G., Rehkämper, M., Middag, R. & van Ooijen, J. (2017). Interactions of dissolved CO_2 with cadmium isotopes in the Southern Ocean. *Mar. Chem.* **195**, 105-121.

de Souza, G. F., Reynolds, B. C., Rickli, J., Frank, M., Saito, M. A., Gerringa, L. J., & Bourdon, B. (2012). Southern Ocean control of silicon stable isotope distribution in the deep Atlantic Ocean. *Global Biogeochem. Cycles*, **26**(2).

de Souza, G. F., Khatiwala, S. P., Hain, M. P., Little, S. H., & Vance, D. (2018). On the origin of the marine zinc–silicon correlation. *Earth Planet. Sci. Lett.*, **492**, 22-34.

Défarge, C. (2011). Organomineralization. Reitner, J., & Thiel, V. (eds.). *Encyclopedia of Geobiology*, Springer Verlag, pp.697-701, 2011, doi:10.1007/978-1-4020-9212-1_159.

Dehairs, F., Chesselet, R., & Jedwab, J. (1980). Discrete suspended particles of barite and the barium cycle in the open ocean. *Earth Planet. Sci. Lett.*, **49**(2), 528-550.

Dehairs, F., Lambert, C. E., Chesselet, R., & Risler, N. (1987). The biological production of marine suspended barite and the barium cycle in the Western Mediterranean Sea. *Biogeochemistry*, **4**(2), 119-140.

Dehairs, F., Jacquet, S., Savoye, N., Van Mooy, B. A., Buesseler, K. O., Bishop, J. K., Lamborg, C. H., Elskens, M., Baeyens, W., Boyd, P. W., Casciotti, K. L., & Monnin, C. (2008). Barium in twilight zone suspended matter as a potential proxy for particulate organic carbon remineralization: Results for the North Pacific. *Deep Sea Res. Pt. II*, **55**(14-15), 1673-1683.

Dellwig, O., Beck, M., Lemke, A., Lunau, M., Kolditz, K., Schnetger, B., & Brumsack, H.-J. (2007). Non-conservative behaviour of molybdenum in coastal waters: Coupling geochemical, biological, and sedimentological processes. *Geochim. Cosmochim. Acta*, **71**, 2745–2761, doi:10.1016/j.gca.2007.03.014.

Dellwig, O., Leipe, T., März, C., Glockzin, M., Pollehne, F., Schnetger, B., Yakushev, E. V., Böttcher, M. E., & Brumsack, H. J. (2010). A new particulate Mn-Fe-P-shuttle at the redoxcline of anoxic basins. *Geochim. Cosmochim. Acta*, **74**, 7100–7115, doi:10.1016/j.gca.2010.09.017.

Deng, N., Stack, A. G., Weber, J., Cao, B., De Yoreo, J. J., & Hu, Y. (2019). Organic–mineral interfacial chemistry drives heterogeneous nucleation of Sr-rich $(Ba_x, Sr_{1-x})SO_4$ from undersaturated solution. *Proc. Natl. Acad. Sci.*, 201821065.

Dickens, G.R., Fewless, T., Thomas, E. & Bralower, T.J. (2003). Excess barite accumulation during the Paleocene–Eocene Thermal Maximum: Massive input of dissolved barium from seafloor gas hydrate reservoirs. In Wing, S. L, Gingerich, P. D., Schmitz, B., & Thomas, E. (Eds.) *Causes and consequences of globally warm climates in the early Paleogene*, **369**, 11-23, Geological Society of America Special Papers; doi:10.1130/0-8137-2369-8.11.

Dickson, A. J. (2017). A molybdenum-isotope perspective on Phanerozoic deoxygenation events. *Nat. Geosci.*, **10**, 721–726, doi:10.1038/NGEO3028.

Dideriksen, K., Baker, J. A., & Stipp, S. L. S. (2008). Equilibrium Fe isotope fractionation between inorganic aqueous Fe (III) and the siderophore complex, Fe (III)-desferrioxamine B. *Earth Planet. Sci. Lett.*, **269**(1-2), 280-290.

Donat, J. R., & Bruland, K. W. (1990). A comparison of two voltammetric techniques for determining zinc speciation in Northeast Pacific Ocean waters. *Mar. Chem.*, **28**, 301–323.

Donat J. R., Lao, K. A., & Bruland, K. W. (1994) Speciation of dissolved copper and nickel in South San Francisco Bay: a multi-method approach. *Anal. Chim. Acta* **284**, 547–571.

Dunlea, A. G., Murray, R. W., Sauvage, J., Spivack, A. J., Harris, R. N., & D'Hondt, S. (2015). Dust, volcanic ash, and the evolution of the South Pacific Gyre through the Cenozoic. *Paleoceanogr.*, **30**(8), 1078-1099.

Dunlea, A. G., Tegler, L. A., Peucker-Ehrenbrink, B., Anbar, A. D., Romaniello, S. J., & Horner, T. J. (2021). Pelagic clays as archives of marine iron isotope chemistry. *Chem. Geol.*, 120201.

Dupont, C. L., Moffett, J. W., Bidigare, R. R., & Ahner, B. A. (2006). Distributions of dissolved and particulate biogenic thiols in the subarctic Pacific Ocean. *Deep. Res. Part I Oceanogr. Res. Pap.*, **53**, 1961–1974.

Dupont, C. L., Butcher, A., Valas, R. E., Bourne, P. E., & Caetano-Anolles, G. (2010). History of biological metal utilization inferred through phylogenomic analysis of protein structures. *Proc. Natl. Acad. Sci.*, **107**, 10567–10572.

Dutkiewicz, A., Müller, R. D., O'Callaghan, S., & Jónasson, H. (2015). Census of seafloor sediments in the world's ocean. *Geology*, **43**(9), 795-798, doi:10.1130/G36883.1.

Dymond, J., Suess, E., & Lyle, M. (1992). Barium in deep‐sea sediment: A geochemical proxy for paleoproductivity. *Paleoceanography*, **7**(2), 163-181.

Dymond, J., & Collier, R. (1996). Particulate barium fluxes and their relationships to biological productivity. *Deep Sea Research Part II: Topical Studies in Oceanography*, **43**(4-6), 1283-1308.

Eagle, M., Paytan, A., Arrigo, K. R., van Dijken, G., & Murray, R. W. (2003). A comparison between excess barium and barite as indicators of carbon export. *Paleoceanography*, **18**(1), 1021, https://doi.org/10.1029/2002PA000793.

Edmond, J. M., Boyle, E. D., Drummond, D., Grant, B., & Mislick, T. (1978). Desorption of barium in the plume of the Zaire (Congo) River. *Netherlands Journal of Sea Research*, **12**(3-4), 324-328.

Elderfield, H. (1970). Chromium speciation in sea water. *Earth Planet. Sci. Lett.*, **9**, 10–16.

Elderfield, H., & Rickaby, R. E. M. (2000). Oceanic Cd/P ratio and nutrient utilization in the glacial Southern Ocean. *Nature*, **405**(6784), 305-310.

Elliott, T., & Steele, R. C. (2017). The isotope geochemistry of Ni. *Reviews in Mineralogy and Geochemistry*, **82**(1), 511-542.

Ellis, A. S., Johnson, T. M., & Bullen, T. D. (2002) Chromium isotopes and the fate of hexavalent chromium in the environment. *Science*, **295**, 2060–2062, doi:10.1126/science.1068368.

Ellwood, M. J. (2004). Zinc and cadmium speciation in subantarctic waters east of New Zealand. *Mar. Chem.*, **87**(1-2), 37-58.

Ellwood, M. J., & Hunter, K. A. (2000). The Incorporation of Zinc and Iron into the Frustule of the Marine Diatom *Thalassiosira pseudonana*. *Limnol. Oceanogr.*, **45**, 1517–1524.

Ellwood, M. J., & Van Den Berg, C. M. G. (2000). Zinc speciation in the Northeastern Atlantic Ocean. *Mar. Chem,*. **68**, 295–306.

Ellwood, M.J., Hutchins, D.A., Lohan, M.C., Milne, A., Nasemann, P., Nodder, S.D., Sander, S.G., Strzepek, R., Wilhelm, S.W., & Boyd, P.W. (2015). Iron stable isotopes track pelagic iron cycling during a subtropical phytoplankton bloom. *Proc. Natl. Acad. Sci. U. S. A.* **112**, E15-E20.

Ellwood, M. J., Strzepek, R. F., Strutton, P. G., Trull, T. W., Fourquez, M., & Boyd, P. W. (2020). Distinct iron cycling in a Southern Ocean eddy. *Nature Communications*, **11**(1), 1-8.

Emerson, S. R., & Huested, S. S. (1991). Ocean anoxia and the concentrations of molybdenum and vanadium in seawater. *Mar. Chem.* **34**, 177–196, doi:10.1016/0304-4203(91)90002-E.

Erickson, B. E., & Helz, G. R. (2000). Molybdenum(VI) speciation in sulfidic waters: Stability and lability of thiomolybdates. *Geochim. Cosmochim. Acta*, **64**, 1149–1158, doi:10.1016/S0016-7037(99)00423-8.

Escoube, R., Rouxel, O. J., Pokrovsky, O. S., Schroth, A., Max Holmes, R., & Donard, O. F. X. (2015). Iron isotope systematics in Arctic rivers. *Comptes Rendus Geosci*,, **347**(7–8), 377–385.

Escoube, R., Rouxel, O. J., Sholkovitz, E., & Donard, O. F. X. (2009). Iron isotope systematics in estuaries: The case of North River, Massachusetts (USA). *Geochim. Cosmochim. Acta*, **73**(14), 4045–4059.

Esser, B. K., & Volpe, A. M. (2002). At-sea high-resolution chemical mapping: extreme barium depletion in North Pacific surface water. *Mar. Chem.*, **79**(2), 67-79.

Fagel, N., Dehairs, F., Peinert, R., Antia, A., & André, L. (2004). Reconstructing export production at the NE Atlantic margin: potential and limits of the Ba proxy. *Mar. Geol.*, **204**(1-2), 11-25.

Fantle, M. S., & DePaolo, D. J., (2004). Iron isotopic fractionation during continental weathering. *Earth Planet. Sci. Lett.*, **228**(3-4), 547-562.

Farmer, J. R., Hönisch, B., Haynes, L. L., Kroon, D., Jung, S., Ford, H. L., Raymo, M. E., Jaume-Seguí, M., Bell, D. B., Goldstein, S. L., Pena, L. D., Yehudai, M., & Kim, J. (2019). Deep Atlantic Ocean carbon storage and the rise of 100,000-year glacial cycles. *Nat. Geosci.* **12**, 355-360, https://doi.org/10.1038/s41561-019-0334-6.

Farkaš, J., Frýda, J., Paulukat, C., Hathorne, E. C., Matoušková, Š., Rohovec, J., Frýdová, B., Francová, M., & Frei, R. (2018). Chromium isotope fractionation between modern seawater and biogenic carbonates from the Great Barrier Reef, Australia: implications for the paleo-seawater δ^{53}Cr reconstruction. *Earth Planet. Sci. Lett.*, **498**, 140–151, doi:10.1016/j.epsl.2018.06.032.

Fassbender, A. J., Palevsky, H. I., Martz, T. R., Ingalls, A. E., Gledhill, M., Fawcett, S. E., Brandes, J. A., Aluwihare, L. I., & the participants of COME ABOARD and DISCO XXV (2017). Perspectives on Chemical Oceanography in the 21st century: Participants of the COME ABOARD Meeting examine aspects of the field in the context of 40 years of DISCO. *Mar. Chem.*, **196**, 181-190.

Ferrier-Pagès, C., Sauzéat, L., & Balter, V. (2018). Coral bleaching is linked to the capacity of the animal host to supply essential metals to the symbionts. *Glob. Change Biol.*, **24**(7), 3145-3157.

Finlay, B. J., Hetherington, N. B., & Da Vison, W. (1983). Active biological participation in lacustrine barium chemistry. *Geochim. Cosmochim. Acta*, **47**(7), 1325-1329.

Fischer, L., Smith, G., Hann, S., & Bruland, K. W. (2018). Ultra-trace analysis of silver and platinum in seawater by ICP-SFMS after off-line matrix separation and pre-concentration. *Mar. Chem.*, **199**, 44-52.

Fisher, N.S., & Wente, M. (1993). The release of trace elements by dying marine phytoplankton. *Deep-Sea Research I*, 40(4), 671-694.

Fishwick, M. P., Sedwick, P. N., Lohan, M. C., Worsfeld, P. J., Buck, K. N., Church, T. M., Ussher, S. J. (2014). The impact of changing surface ocean conditions on the dissolution of aerosol iron. *Global Biogeochem. Cycles*, **28**(11), 1235-1250. https://doi.org/10.1002/2014GB004921.

Fitzsimmons, J. N., & Boyle, E. A. (2014). Both soluble and colloidal iron phases control dissolved iron variability in the tropical North Atlantic Ocean. *Geochim. Cosmochim. Acta*, **125**, 539-550.

Fitzsimmons, J. N., Carrasco, G. G., Wu, J., Roshan, S., Hatta, M., Measures, C. I., Conway, T. M., John, S.G., & Boyle, E. A. (2015). Partitioning of dissolved iron and iron isotopes into soluble and colloidal phases along the GA03 GEOTRACES North Atlantic Transect. *Deep Sea Res. Pt. II*, **116**, 130-151.

Fitzsimmons, J. N., Conway, T. M., Lee, J.-M., Kayser, R., Thyng, K. M., John, S. G. and Boyle, E. A. (2016). Dissolved iron and iron isotopes in the Southeastern Pacific Ocean. *Global Biogeochem. Cycles*, **30**(10), 1372-1395. https://doi.org/10.1002/2015GB005357.

Fitzsimmons, J. N., John, S. G., Marsay, C. M., Hoffman, C. L., Nicholas, S. L., Toner, B. M., German, C. R., & Sherrell, R. M. (2017). Iron persistence in a distal hydrothermal plume supported by dissolved–particulate exchange. *Nature Geoscience*, **10**(3), 195-201.

Flegal, A.R., Sanudo-Wilhelmy, S.A., & Scelfo, G.M. (1995). Silver in the eastern Atlantic Ocean. *Mar. Chem.*, **49**, 315-320.

Franck, V. M., Bruland, K. W., Hutchins, D. A., & Brzezinski, M. A. (2003). Iron and zinc effects on silicic acid and nitrate uptake kinetics in three high-nutrient, low-chlorophyll (HNLC) regions. *Mar. Ecol. Prog. Ser.*, **252**, 15–33.

Frank, A. B., Klaebe, R. M., Löhr, S., Xu, L., & Frei, R. (2020). Chromium isotope composition of organic-rich marine sediments and their mineral phases and implications for using black shales as a paleoredox archive. *Geochim. Cosmichim. Acta*, **270**, 338-359, doi:10.1016/j.gca.2019.11.035.

François, R., Honjo, S., Manganini, S. J., & Ravizza, G. E. (1995). Biogenic barium fluxes to the deep sea: Implications for paleoproductivity reconstruction. *Global Biogeochem. Cycles*, **9**(2), 289-303.

François, R., Altabet, M. A., Yu, E. F., Sigman, D. M., Bacon, M. P., Frank, M., Bohrmann, G. Bareille, G., & Labeyrie, L. D. (1997). Contribution of Southern Ocean surface-water stratification to low atmospheric CO_2 concentrations during the last glacial period. *Nature*, **389**(6654), 929-935.

Frei, R., Gaucher, C., Poulton, S. W., & Canfield, D. E. (2009). Fluctuations in Precambrian atmospheric oxygenation recorded by chromium isotopes. *Nature*, **461**, 250–254, doi:10.1038/nature08266

Frei, R., Poiré, D., & Frei, K. M. (2014). Weathering on land and transport of chromium to the ocean in a subtropical region (Misiones, NW Argentina): a chromium stable isotope perspective. *Chem. Geol.*, **381**, 110–124. doi:10.1016/j.chemgeo.2014.05.015.

Frei, R., Lehmann, B., Xu, L., & Frederiksen, J. A. (2020). Surface water oxygenation and bioproductivity–A link provided by combined chromium and cadmium isotopes in Early Cambrian metalliferous black shales (Nanhua Basin, South China). *Chem. Geol*, **552**, 119785.

Frew, R. D., & Hunter, K. A. (1992). Influence of Southern Ocean waters on the cadmium–phosphate properties of the global ocean. *Nature*, **360**(6400), 144.

Friedl, G., & Pedersen, T. (2002). Silver as a new tracer for diatom production. *Eawag News*, 52, 14-15.

Froelich, P., Klinkhammer, G. P., Bender, M. L., Luedtke, N. A., Heath, G. R., Cullen, D., Dauphin, P., Hammond D., Hartman, B., & Maynard, V. (1979). Early oxidation of organic matter in pelagic sediments of the eastern equatorial Atlantic: suboxic diagenesis. *Geochimica et Cosmochimica Acta*, **43**(7), 1075-1090.

Fru, E. C., Rodríguez, N. P., Partin, C. A., Lalonde, S. V., Andersson, P., Weiss, D. J., El Albani, A., Rodushkin, I., & Konhauser, K. O. (2016). Cu isotopes in marine black shales record the Great Oxidation Event. *Proceedings of the National Academy of Sciences*, **113**(18), 4941-4946.

Fujii, T., Moynier, F., Pons, M. L., & Albarède, F. (2011a). The origin of Zn isotope fractionation in sulfides. *Geochim. Cosmochim. Acta*, **75**(23), 7632-7643.

Fujii, T., Moynier, F., Dauphas, N., & Abe, M. (2011b). Theoretical and experimental investigation of nickel isotopic fractionation in species relevant to modern and ancient oceans. *Geochim. Cosmochim. Acta*, **75**(2), 469-482.

Fujii, T., Moynier, F., Abe, M., Nemoto, K., & Albarède, F. (2013). Copper isotope fractionation between aqueous compounds relevant to low temperature geochemistry and biology. *Geochim. Cosmochim. Acta*, **110**, 29-44.

Gall, L., Williams, H. M., Siebert, C., Halliday, A. N., Herrington, R. J., & Hein, J. R. (2013). Nickel isotopic compositions of ferromanganese crusts and the constancy of deep ocean inputs and continental weathering effects over the Cenozoic. *Earth Planet. Sci. Lett.*, **375**, 148-155.

Gallon, C., & Flegal, A. R. (2015). Sources, Fluxes, and Biogeochemical Cycling of Silver in the Oceans. In: Whitacre, D. (eds) *Rev. Environ. Contamin. Toxicol.* **235**. Springer, Cham. https://doi.org/10.1007/978-3-319-10861-2_2.

Ganeshram, R. S., François, R., Commeau, J., & Brown-Leger, S. L. (2003). An experimental investigation of barite formation in seawater. *Geochim. Cosmochim. Acta*, **67**(14), 2599-2605.

Garcia, H. E., R. A. Locarnini, T. P. Boyer, J. I. Antonov, O.K. Baranova, M.M. Zweng, J.R. Reagan, D.R. Johnson, 2014. World Ocean Atlas 2013, Volume 3: Dissolved Oxygen, Apparent Oxygen Utilization, and Oxygen Saturation. S. Levitus, Ed., A. Mishonov Technical Ed.; *NOAA Atlas NESDIS 75*, 27 pp.

Gault-Ringold, M., Adu, T., Stirling, C. H., Frew, R. D., & Hunter, K. A. (2012). Anomalous biogeochemical behavior of cadmium in Subantarctic surface waters: mechanistic constraints from cadmium isotopes. *Earth Planet. Sci. Lett.*, **341**, 94-103.

Gebregiorgis, D., Hathorne, E. C., Sijinkumar, A. V., Nath, B. N., Nürnberg, D., & Frank, M. (2016). South Asian summer monsoon variability during the last∼ 54 kyrs inferred from surface water salinity and river runoff proxies. *Quaternary Science Reviews*, 138, 6-15.

George, E., Stirling, C. H., Gault-Ringold, M., Ellwood, M. J., & Middag, R. (2019). Marine biogeochemical cycling of cadmium and cadmium isotopes in the extreme nutrient-depleted subtropical gyre of the South West Pacific Ocean. *Earth Planet. Sci. Lett.*, **514**, 84-95.

Georgiev, S. V., Horner, T. J., Stein, H. J., Hannah, J. L., Bingen, B., & Rehkämper, M. (2015). Cadmium-isotopic evidence for increasing primary productivity during the Late Permian anoxic event. *Earth Planet. Sci. Lett.*, **410**, 84-96.

Geyman, B. M., Ptacek, J. L., LaVigne, M., & Horner, T. J. (2019). Barium in deep-sea bamboo corals: Phase associations, barium stable isotopes, & prospects for paleoceanography. *Earth Planet. Sci. Lett.*, **525**, 115751.

Giering, S. L., Sanders, R., Lampitt, R. S., Anderson, T. R., Tamburini, C., Boutrif, M., Zubkov, M. V., Marsay, C. M., Henson, S. A., Saw, K., Cook, K., & Mayor, D. J.(2014). Reconciliation of the carbon budget in the ocean's twilight zone. *Nature*, **507**(7493), 480-483.

Glass, J. B., Axler, R. P., Chandra, S., & Goldman, C. R. (2012). Molybdenum limitation of microbial nitrogen assimilation in aquatic ecosystems and pure cultures. *Frontiers in Microbiology*, **3**, 1–11, doi:10.3389/fmicb.2012.00331.

Glass, J. B., Wolfe-Simon, F., & Anbar, A. D. (2009). Coevolution of metal availability and nitrogen assimilation in cyanobacteria and algae. *Geobiology*, **7**, 100–123, doi:10.1111/j.1472-4669.2009.00190.x.

Goldberg, T., Archer, C., Vance, D., & Poulton, S. W. (2009). Mo isotope fractionation during adsorption to Fe (oxyhydr)oxides. *Geochim. Cosmochim. Acta*, **73**, 6502–6516, doi:10.1016/j.gca.2009.08.004.

Goldberg, T., Archer, C., Vance, D., Thamdrup, B., McAnena, A., & Poulton, S. W. (2012). Controls on Mo isotope fractionations in a Mn-rich anoxic marine sediment, Gullmar Fjord, Sweden. *Chem. Geol.*, **296-297**, 73-82, doi:10.1016/j.chemgeo.2011.12.020.

Goldberg, T., Gordon, G., Izon, G., Archer, C., Pearce, C. R., McManus, J., Anbar, A. D., & Rehkämper, M. (2013). Resolution of inter-laboratory discrepancies in Mo isotope data: an intercalibration. *Journal of Analytical Atomic Spectrometry*, **28**(5), 724-735.

Goldman, C. R. (1960). Molybdenum as a Factor Limiting Primary Productivity in Castle Lake, California. *Science*, **132**, 1016–1017, doi:10.1126/science.132.3433.1016.

Gong, Y., Xia, Y., Huang, F., & Yu, H. (2017). Average iron isotopic compositions of the upper continental crust: constrained by loess from the Chinese Loess Plateau. *Acta Geochim.*, **36**, 125-131, doi:10.1007/s11631-016-0131-5.

Gooday, A. J., & Nott, J. A. (1982). Intracellular barite crystals in two xenophyophores, Aschemonella ramuliformis and *Galatheammina sp.* (Protozoa: Rhizopoda) with comments on the taxonomy of *A. ramuliformis*. *Journal of the Marine Biological Association of the United Kingdom*, **62**(3), 595-605.

Goring-Harford, H. J., Klar, J. K., Pearce, C. R., Connelly, D. P., Achterberg, E. P., & James, R. H. (2018). Behaviour of chromium isotopes in the eastern sub-tropical Atlantic Oxygen Minimum Zone. *Geochim. Cosmochim. Acta*, **236**, 41-59, doi:10.1016/j.gca.2018.03.004.

Goto, K. T., Sekine, Y., Shimoda, G., Hein, J. R., Aoki, S., Ishikawa, A., Suzuki, K., Gordon, G. W., & Anbar, A. D. (2020). A framework for understanding Mo isotope records of Archean and Paleoproterozoic Fe-and Mn-rich sedimentary rocks: Insights from modern marine hydrothermal Fe-Mn oxides. *Geochim. Cosmochim. Acta*, **280**, 221-236.

Gou, L. F., Jin, Z., Galy, A., Gong, Y. Z., Nan, X. Y., Jin, C., Wang, X.-D., Bouchez, J., Cai, H.-M., Chen, J.-B., Yu, H.-M., & Huang, F. (2020). Seasonal riverine barium isotopic variation in the middle Yellow River: Sources and fractionation. *Earth and Planetary Science Letters*, **531**, 115990.

Griffith, E. M., & Paytan, A. (2012). Barite in the ocean–occurrence, geochemistry and palaeoceanographic applications. *Sedimentology*, **59**(6), 1817-1835.

Gueguen, B., Rouxel, O., Ponzevera, E., Bekker, A., & Fouquet, Y. (2013). Nickel isotope variations in terrestrial silicate rocks and geological reference materials measured by MC-ICP-MS. *Geostandards and Geoanalytical Research*, **37**(3), 297-317.

Gueguen, B., Rouxel, O., Rouget, M. L., Bollinger, C., Ponzevera, E., Germain, Y., & Fouquet, Y. (2016a). Comparative geochemistry of four ferromanganese crusts from the Pacific Ocean and significance for the use of Ni isotopes as paleoceanographic tracers. *Geochim. Cosmochim. Acta*, **189**, 214-235.

Gueguen, B., Reinhard, C. T., Algeo, T. J., Peterson, L. C., Nielsen, S. G., Wang, X., Rowe, H., & Planavsky, N. J. (2016b). The chromium isotope composition of reducing and oxic marine sediments. *Geochim. Cosmochim. Acta*, **184**, 1–19. doi: 10.1016/j.gca.2016.04.004.

Gueguen, B., Rouxel, O., & Fouquet, Y. (2021). Nickel isotopes and rare earth elements systematics in marine hydrogenetic and hydrothermal ferromanaganese deposits. *Chem. Geol.*, **560**, 119999, doi:10.1016/j.chemgeo.2020.119999.

Gueguen, B., & Rouxel, O. (2021). The Nickel isotope composition of the authigenic sink and the diagenetic flux in modern oceans. *Chem. Geol*, **563**, 120050. doi.org/10.1016/j.chemgeo.2020.120050.

Guinoiseau, D., Galer, S. J., & Abouchami, W. (2018). Effect of cadmium sulphide precipitation on the partitioning of Cd isotopes: Implications for the oceanic Cd cycle. *Earth Planet. Sci. Lett.*, **498**, 300-308.

Guo, J., Lapi, S., Ruth, T. J., & Maldonado, M. T. (2012). The effects of iron and copper availability on the copper stoichiometry of marine phytoplankton. *J. Phycol.* **48**, 312–325.

Hanor, J. S., & Chan, L. H. (1977). Non-conservative behavior of barium during mixing of Mississippi River and Gulf of Mexico waters. *Earth and Planetary Science Letters*, **37**(2), 242-250.

Hanor, J. S. (2000). Barite–celestine geochemistry and environments of formation. *Rev. Mineral. Geochem.*, **40**(1), 193-275.

Hardisty, D. S., Riedinger, N., Planavsky, N. J., Asael, D., Andrén, T., et al. (2016). A Holocene history of dynamic water column redox conditions in the Landsort Deep, Baltic Sea. *Am. J. Sci.*, **316**, 713-745, doi:10.2475/08.2016.01.

Hardisty, D. S., Lyons, T. W., Riedinger, N., Isson, T. T., Owens, J. D., Aller, R. C., Rye, D. M., Planavsky, N. J., Reinhard, C. T., Gill, B. C., Masterson, A. L., Asael, D., & Johnston, D. T. (2018). An evaluation of sedimentary molybdenum and iron as proxies for pore fluid paleoredox conditions. *Am. J. Sci.*, **318**(5), 527-556.

Hartnett, H. E., Keil, R. G., Hedges, J. I., & Devol, A. H. (1998). Influence of oxygen exposure time on organic carbon preservation in continental margin sediments. *Nature*, **391**(6667), 572-575.

Hawco, N. J., Lam, P. J., Lee, J. M., Ohnemus, D. C., Noble, A. E., Wyatt, N. J., Lohan, M. C., & Saito, M. A. (2018). Cobalt scavenging in the mesopelagic ocean and its influence on global mass balance: Synthesizing water column and sedimentary fluxes. *Marine Chemistry*, **201**, 151-166.

Hayes, C. T., Anderson, R. F., Cheng, H., Conway, T. M., Edwards, R. L., Fleisher, M. Q., Ho, P., Huang, K.-F., John, S. G., Landing, W. M., Little, S. H., Lu, Y., Morton, P. L., Moran, S. B., Robinson, L. F., Shelley, R. U., Shiller, A. M., & Zheng, X.-Y. (2018). Replacement times of a spectrum of elements in the North Atlantic based on thorium supply. *Global Biogeochem. Cycles*, **32**(9), 1294-1311.

Hayes, J. M. (2004). *An introduction to isotopic calculations*. Woods Hole Oceanographic Institution, Woods Hole, MA, available from: https://www.whoi.edu/cms/files/jhayes/2005/9/IsoCalcs30Sept04_5183.pdf

Heller, M. I., & Croot, P. L. (2015). Copper speciation and distribution in the Atlantic sector of the Southern Ocean. *Mar. Chem.*, **173**, 253-268.

Helz, G. R., Miller, C. V., Charnock, J. M., Mosselmans, J. F. W., Pattrick, R. A. D., Garner, C. D., & Vaughan, D. J. (1996). Mechanism of molybdenum removal from the sea and its concentration in black shales: EXAFS evidence. *Geochim. Cosmochim. Acta*, **60**, 3631–3642, doi:10.1016/0016-7037(96)00195-0.

Hemsing, F., Hsieh, Y. T., Bridgestock, L., Spooner, P. T., Robinson, L. F., Frank, N., & Henderson, G. M. (2018). Barium isotopes in cold-water corals. *Earth and Planetary Science Letters*, **491**, 183-192.

Henderson, G. M., & Burton, K. W. (1999). Using (234U/238U) to assess diffusion rates of isotope tracers in ferromanganese crusts. *Earth Planet. Sci. Lett.*, **170**(3), 169-179.

Hendry, K. R., & Andersen, M. B. (2013). The zinc isotopic composition of siliceous marine sponges: Investigating nature's sediment traps. *Chem. Geol.*, **354**, 33–41. Available at: http://dx.doi.org/10.1016/j.chemgeo.2013.06.025.

Hendry, K. R., Pyle, K. M., Barney Butler, G., Cooper, A., Fransson, A., Chierici, M., Leng, M. J., Meyer, A., & Dodd, P.A. (2018). Spatiotemporal Variability of Barium in Arctic Sea-Ice and Seawater. *J. Geophys. Res. Oceans*, **123**(5), 3507-3522.

Hendy, I. L., & Pedersen, T. F. (2005). Is pore water oxygen content decoupled from productivity on the California Margin? Trace element results from Ocean Drilling Program Hole 1017E, San Lucia slope, California. *Paleoceanography*, **20**(4).

Henkel, S., Kasten, S., Hartmann, J. F., Silva-Busso, A., & Staubwasser, M. (2018). Iron cycling and stable Fe isotope fractionation in Antarctic shelf sediments, King George Island. *Geochim. Cosmochim. Acta*, **237**, 320-338. https://doi.org/10.1016/j.gca.2018.06.042.

Hillaire-Marcel, C., & De Vernal, A. (Eds.). (2007). *Proxies in Late Cenozoic Paleoceanography*. Elsevier.

Ho, P., Lee, J. M., Heller, M. I., Lam, P. J., and Shiller, A. M. (2018). The distribution of dissolved and particulate Mo and V along the U.S. GEOTRACES East Pacific Zonal Transect (GP16): The roles of oxides and biogenic particles in their distributions in the oxygen deficient zone and the hydrothermal plume. *Mar. Chem.*, **201**, 242–255, doi:10.1016/j.marchem.2017.12.003.

Ho, T. Y., Quigg, A., Finkel, Z. V., Milligan, A. J., Wyman, K., Falkowski, P. G., & Morel, F. M. (2003). The elemental composition of some marine phytoplankton 1. *Journal of Phycology*, **39**(6), 1145-1159.

Hodgskiss, M. S., Crockford, P. W., Peng, Y., Wing, B. A., & Horner, T. J. (2019). A productivity collapse to end Earth's Great Oxidation. *Proc. Natl. Acad. Sci.*, **116**(35), 17207-17212.

Hohl, S. V., Galer, S. J. G., Gamper, A., & Becker, H. (2017). Cadmium isotope variations in Neoproterozoic carbonates–A tracer of biologic production? *Geochemical Perspective Letters*, **3**, 32-44.

Hohl, S. V., Jiang, S. Y., Wei, H. Z., Pi, D. H., Liu, Q., Viehmann, S., & Galer, S. J. (2019). Cd Isotopes trace periodic (bio)geochemical metal cycling at the verge of the Cambrian animal evolution. *Geochim. Cosmochim. Acta*, **263**, 195-214, doi:10.1016/j.gca.2019.07.036.

Holmden, C., Jacobson, A. D., Sageman, B. B., & Hurtgen, M. T. (2016). Response of the Cr isotope proxy to Cretaceous Ocean Anoxic Event 2 in a pelagic carbonate succession from the Western Interior Seaway. *Geochim. Cosmochim. Acta*, **186**, 277-295, doi:10.1016/j.gca.2016.04.039.

Holzer, M., Primeau, F. W., DeVries, T., & Matear, R. (2014). The Southern Ocean silicon trap: Data-constrained estimates of regenerated silicic acid, trapping efficiencies, and global transport paths. *J. Geophys. Res. Oceans*, **119**(1), 313-331.

Homoky, W. B.., Severmann, S., Mills, R. A., & Fones, G. R. (2009). Pore-fluid Fe isotopes reflect the extent of benthic Fe redox recycling: evidence from continental shelf and deep-sea sediments. *Geology*, **37**, 751–754. https://doi.org/10.1130/G25731A.1.

Homoky, W. B., John, S. G., Conway T. M., & Mills, R. A. (2013). Distinct iron isotopic signatures and supply from marine sediment dissolution. *Nat. Comms*, **4**, 2143. https://doi.org/10.1038/ncomms3143.

Homoky, W. B., Conway, T. M., John, S. G., Koenig, D., Deng, F., Tagliabue, A. & Mills, R. (2021). Iron colloids dominate sedimentary supply to the ocean interior. *Proc. Natl. Acad. Sci. USA*, **118** (13), e2016078118. doi:10.1073/pnas.2016078118.

Hoppema, M., Dehairs, F., Navez, J., Monnin, C., Jeandel, C., Fahrbach, E., & De Baar, H. J. W. (2010). Distribution of barium in the Weddell Gyre: Impact of circulation and biogeochemical processes. *Marine Chemistry*, **122**(1-4), 118-129.

Horner, T.J, & Crockford, P. (2021). *Barium Isotopes: Drivers, Dependencies, and Distributions through Space and Time* (Elements in Geochemical Tracers in Earth System Science). Cambridge University Press. doi:10.1017/9781108865845

Horner, T. J., Schönbächler, M., Rehkämper, M., Nielsen, S. G., Williams, H., Halliday, A. N., Xue, Z., & Hein, J. R. (2010). Ferromanganese crusts as archives of deep water Cd isotope compositions. *Geochemistry, Geophysics, Geosystems*, **11**(4), Q04001, https://doi.org/10.1029/2009GC002987.

Horner, T. J., Rickaby, R. E., & Henderson, G. M. (2011). Isotopic fractionation of cadmium into calcite. *Earth Planet. Sci. Lett.*, **312**(1-2), 243-253.

Horner, T. J., Lee, R. B., Henderson, G. M., & Rickaby, R. E. (2013). Nonspecific uptake and homeostasis drive the oceanic cadmium cycle. *Proc. Natl. Acad. Sci.*, **110**(7), 2500-2505.

Horner, T. J., Kinsley, C. W., & Nielsen, S. G. (2015a). Barium-isotopic fractionation in seawater mediated by barite cycling and oceanic circulation. *Earth Planet. Sci. Lett.*, **430**, 511-522.

Horner, T. J., Williams, H. M., Hein, J. R., Saito, M. A., Burton, K. W., Halliday, A. N., & Nielsen, S. G. (2015b). Persistence of deeply sourced iron in the Pacific Ocean. *Proc. Natl. Acad. Sci*., **112**, 1292-1297.

Horner, T. J., Pryer, H. V., Nielsen, S. G., Crockford, P. W., Gauglitz, J. M., Wing, B. A., & Ricketts, R. D. (2017). Pelagic barite precipitation at micromolar ambient sulfate. *Nat. Commun.*, **8**(1), 1342.

Hsieh, Y. T., & Henderson, G. M. (2017). Barium stable isotopes in the global ocean: tracer of Ba inputs and utilization. *Earth Planet. Sci. Lett.*, **473**, 269-278.

Hsieh, Y. T., Bridgestock, L., Scheuermann, P. P., Seyfried Jr., W. E., & Henderson, G. M. (2021). Barium isotopes in mid-ocean ridge hydrothermal vent fluids: A source of isotopically heavy Ba to the ocean. *Geochim. Cosmochim. Acta*, **292**, 348-363, doi:10.1016/j.gca.2020.09.037.

Huang, T., Moos, S. B., & Boyle, E. A. (2021). Trivalent chromium isotopes in the eastern tropical North Pacific oxygen-deficient zone. *Proc. Nat. Acad. Sci. USA*, **118**(8), e1918605118, doi:10.1073/pnas.1918605118.

Hudson, R. J. M., & Morel, F. M. M. (1993). Trace metal transport by marine microorganisms: Implications of metal coordination kinetics. *Deep Sea Res.* **40**, 129–150.

Hug, S. J., & Laubscher, H.-U. (1997). Iron(III) catalyzed photochemical reduction of chromium(VI) by oxalate and citrate in aqueous solutions. *Environ. Sci. Technol.*, **31**, 160–170, doi:10.1021/es960253l.

Ijichi, Y., Ohno, T., & Sakata, S. (2018). Copper isotopic fractionation during adsorption on manganese oxide: Effects of pH and desorption. *Geochemical Journal*, *52*(2), e1-e6.

Ilina, S. M., Poitrasson, F., Lapitskiy, S. A., Alekhin, Y. V., Viers, J., & Pokrovsky, O. S. (2013). Extreme iron isotope fractionation between colloids and particles of boreal and temperate organic-rich waters. *Geochim. et Cosmochim. Acta*, **101**, 96–111.

Ingri, J., Malinovsky, D., Rodushkin, I., Baxter, D.C., Widerlund, A., Andersson, P., Gustafsson, Ö., Forsling, W. & Öhlander, B. (2006). Iron isotope fractionation in river colloidal matter. *Earth Planet. Sci. Lett*., **245**(3–4), 792–798.

Isson, T. T., Love, G. D., Dupont, C. L., Reinhard, C. T., Zumberge, A. J., Asael, D., Gueguen, B., McCrow, J., Gill, B. C., Owens, J., Rainbird, R. H., Rooney, A. D., Zhao, M. Y., Stueeken, E. E., Konhauser, K. O., John, S. G., Lyons, T. W,. & Planavsky, N. J. (2018). Tracking the rise of eukaryotes to ecological dominance with zinc isotopes. *Geobiology*, **16**, 341–352.

Ivanochko, T. S. (2001). Productivity influences on oxygenation of the Santa Barbara Basin, California, during the Late Quaternary (Doctoral dissertation, University of British Columbia).

Jaccard, S. L., Haug, G. H., Sigman, D. M., Pedersen, T. F., Thierstein, H. R., & Röhl, U. (2005). Glacial/interglacial changes in subarctic North Pacific stratification. Science, **308**(5724), 1003-1006.

Jaccard, S. L., Hayes, C. T., Martínez-García, A., Hodell, D. A., Anderson, R. F., Sigman, D. M., & Haug, G. H. (2013). Two modes of change in Southern Ocean productivity over the past million years. *Science*, **339**(6126), 1419-1423.

Jacobs, L., & Emerson, S. (1982). Trace metal solubility in an anoxic fjord. *Earth Planet. Sci. Lett.*, **60**, 237-252, doi:10.1016/0012-821X(82)90006-1.

Jacobs, L., Emerson, S., & Skei, J. (1985). Partitioning and transport of metals across the O_2H_2S interface in a permanently anoxic basin: Framvaren Fjord, Norway. *Geochim. Cosmochim. Acta*, **49**, 1433-1444, doi:10.1016/0016-7037(85)90293-5.

Jacquet, S. H., Dehairs, F., Elskens, M., Savoye, N., & Cardinal, D. (2007). Barium cycling along WOCE SR3 line in the Southern Ocean. *Mar. Chem.*, **106**(1-2), 33-45.

Jacquot, J. E., & Moffett, J. W. (2015). Copper distribution and speciation across the International GEOTRACES Section GA03. *Deep Sea Res. Pt. II*, **116**, 187-207, doi:10.1016/j.dsr2.2014.11.013.

Jakuba, R. W., Saito, M. A., Moffett, J. W., & Xu, Y. (2012). Dissolved zinc in the subarctic North Pacific and Bering Sea: Its distribution, speciation, and importance to primary producers. *Global Biogeochem. Cycles*, **26**, 1–15.

Janssen, D. J., & Cullen, J. T. (2015). Decoupling of zinc and silicic acid in the subarctic northeast Pacific interior. *Mar. Chem.*, **177**, 124–133. http://dx.doi.org/10.1016/j.marchem.2015.03.014.

Janssen, D. J., Conway, T. M., John, S. G., Christian, J. R., Kramer, D. I., Pedersen, T. F., & Cullen, J. T. (2014). Undocumented water column sink for cadmium in open ocean oxygen-deficient zones. *Proc. Natl. Acad. Sci.*, **111**(19), 6888-6893.

Janssen, D. J., Abouchami, W., Galer, S. J. G., & Cullen, J. T. (2017). Fine-scale spatial and interannual cadmium isotope variability in the subarctic northeast Pacific. *Earth Planet. Sci. Lett.*, **472**, 241-252.

Janssen, D. J., Abouchami, W., Galer, S. J., Purdon, K. B., & Cullen, J. T. (2019). Particulate cadmium stable isotopes in the subarctic northeast Pacific reveal dynamic Cd cycling and a new isotopically light Cd sink. *Earth Planet. Sci. Lett.*, **515**, 67-78.

Janssen, D. J., Rickli, J., Quay, P. D., White, A. E., Nasemann, P., & Jaccard, S. L. (2020). Biological control of chromium redox and stable isotope composition in the surface ocean. *Glob. Biogeochem. Cycles*, **34**, doi:10.1029/2019GB006397.

Jeandel, C. & Minster, J. F. (1987). Chromium behavior in the ocean: global versus regional processes. *Global Biogeochem. Cycles*, **1**, 131–154, doi:10.1029/GB001i002p0013.

John, S. G., & Conway, T. M. (2014). A role for scavenging in the marine biogeochemical cycling of zinc and zinc isotopes. *Earth Planet. Sci. Lett.*, **394**, 159-167.

John, S. G., Geis R. W., Saito M. A., & Boyle E. A. (2007). Zinc isotope fractionation during high affinity and low-affinity zinc transport by the marine diatom *Thalassiosire oceanica*. *Limnol. Oceanogr.*, **52**, 2710–2714.

John, S. G., Mendez, J., Moffett, J., & Adkins, J. (2012). The flux of iron and iron isotopes from San Pedro Basin sediments. *Geochim. Cosmochim. Acta*, **93**, 14-29.

John, S. G., Kunzmann, M., Townsend, E. J., & Rosenberg, A. D. (2017). Zinc and cadmium stable isotopes in the geological record: A case study from the post-snowball Earth Nuccaleena cap dolostone. *Palaeogeography, Palaeoclimatology, Palaeoecology*, **466**, 202-208.

John, S. G., Helgoe, J., Townsend, E., Weber, T., DeVries, T., Tagliabue, A., Moore, K., Lam, P., Marsay, C.M., & Till, C. (2018a). Biogeochemical cycling of Fe and Fe stable isotopes in the Eastern Tropical South Pacific. *Mar. Chem.* **201**, 66-76.

John, S. G., Helgoe, J., & Townsend, E. (2018b). Biogeochemical cycling of Zn and Cd and their stable isotopes in the Eastern Tropical South Pacific. *Mar. Chem.*, **201**, 256-262.

Johnson, C.M., Skulan, J.L., Beard, B. L., Sun, H., Nealson, K. H., & Braterman, P. S. (2002). Isotopic fractionation between Fe(III) and Fe(II) in aqueous solutions. *Earth. Planet. Sci. Lett.*, **195**, 141–153. https://doi.org/10.1016/S0012-821X(01)00581-7.

Johnson, C. M., Beard, B. L., & Roden, E. E. (2008). The iron isotope fingerprints of redox and biogeochemical cycling in modern and ancient Earth. *Annu. Rev. Earth Planet. Sci.*, **36**, 457-493.

Johnson, C. M., Beard, B. L., & Weyer, S. (2020). *Iron Geochemistry: An Isotopic Perspective*. Springer. doi:10.1007/978-3-030-33828-2.

Joung, D. J., and Shiller, A. M. (2016). Temporal and spatial variations of dissolved and colloidal trace elements in Louisiana Shelf waters. *Mar. Chem.* **181**, 25–43, doi:10.1016/j.marchem.2016.03.003.

Jullion, L., Jacquet, S. H. M., & Tanhua, T. (2017). Untangling biogeochemical processes from the impact of ocean circulation: First insight on the Mediterranean dissolved barium dynamics. *Global Biogeochem. Cycles*, **31**(8), 1256-1270.

Kellogg, M. M., McIlvin, M. R., Vedamati, J., Twining, B. S., Moffett, J. W., Marchetti, A., Moran, D. M., & Saito, M. A. (2020). Efficient zinc/cobalt inter-replacement in northeast Pacific diatoms and relationship to high surface dissolved Co: Zn ratios. *Limnol. Oceanogr*. doi:10.1002/lno.11471.

Kendall, B., Komiya, T., Lyons, T. W., Bates, S. M., Gordon, G. W., Romaniello, S. J., Jiang, G., Creaser, R. A., Xiao, S., McFadden, K., Sawaki, Y., Tahata, M., Shu, D., Han, J., Li, Y., Chu, X., & Anbar, A. D. (2015). Uranium and molybdenum isotope evidence for an episode of widespread ocean oxygenation during the late ediacaran period. *Geochim. Cosmochim. Acta*, **156**, 173–193, doi:10.1016/j.gca.2015.02.025.

Kendall, B., Dahl, T. W., & Anbar, A. D. (2017). The Stable Isotope Geochemistry of Molybdenum. *Rev. Min. Geochem.*, **82**, 683–732, doi:10.2138/rmg.2017.82.16.

Khatiwala, S., Schmittner, A., & Muglia, J. (2019). Air-sea disequilibrium enhances ocean carbon storage during glacial periods. *Science Advances*, **5**(6), eaaw4981.

Kieber, R. J., & Helz, G. R. (1992). Indirect photoreduction of aqueous chromium (VI). *Environ. Sci. Technol.*, **26**, 307–312, doi:10.1021/es00026a010.

Kienast, S. (2003). Palaeoceanography of the mid-latitude North East Pacific: during the late Pleistocene (Doctoral dissertation, University of British Columbia).

Kim, C., Zhou, Q., Deng, B., Thornton, E. C., & Xu, H. (2001). Chromium(VI) Reduction by Hydrogen Sulfide in Aqueous Media: Stoichiometry and Kinetics. *Environ. Sci. Technol.*, **35**(11), 2219-2225, doi:10.1021/es0017007.

Kim, T., Obata, H., Kondo, Y., Ogawa, H., & Gamo, T. (2015). Distribution and speciation of dissolved zinc in the western North Pacific and its adjacent seas. *Mar. Chem.*, **173**, 330–341. http://dx.doi.org/10.1016/j.marchem.2014.10.016.

King, E. K., Thompson, A., Hodges, C., & Pett-Ridge, J. C. (2014). Towards Understanding Temporal and Spatial Patterns of Molybdenum in the Critical Zone. *Procedia Earth and Planetary Science*, **10**, 56–62, doi:10.1016/j.proeps.2014.08.011.

King, E. K., Thompson, A., Chadwick, O. A., & Pett-Ridge, J. C. (2016). Molybdenum sources and isotopic composition during early stages of pedogenesis along a basaltic climate transect. *Chem. Geol.*, **445**, 54–67, doi:10.1016/j.chemgeo.2016.01.024.

King, E. K., Perakis, S. S., & Pett-Ridge, J. C. (2018). Molybdenum isotope fractionation during adsorption to organic matter. *Geochim. Cosmochim. Acta*, **222**, 584–598, doi:10.1016/j.gca.2017.11.014.

Klar, J. K., James, R. H., Gibbs, D., Lough, A., Parkinson, I., Milton, J. A., Hawkes, J. A., & Connelly, D. P. (2017a). Isotopic signature of dissolved iron delivered to the Southern Ocean from hydrothermal vents in the East Scotia Sea. *Geology*, 4**5**(4), 351-354. https://doi.org/10.1130/G38432.1.

Klar, J. K., Homoky, W. B., Statham, P. J., Birchill, A. J., Harris, E. L., Woodward, E. M. S., Silburn, B., Cooper, M. J., James, R. H., Connelly, D. P., Chever, F., Lichtschlag, A., & Graves, C. (2017b). Stability of dissolved and soluble Fe(II) in shelf sediment pore waters and release to an oxic water column. *Biogeochem*., **135,** 1-19. https://doi.org/10.1007/s10533-017-0309-x.

Klar, J. K., Schlosser, C., Milton, J. A., Woodward, E. M. S., Lacan, F., Parkinson, I. J., Achterberg, E., & James, R. H. (2018). Sources of dissolved iron to oxygen minimum zone waters on the Senegalese continental margin in the tropical North Atlantic Ocean: Insights from iron isotopes. *Geochim. Cosmochim. Acta*, **236**, 60-78. https://doi.org/10.1016/j.gca.2018.02.031.

Klinkhammer, G. P. (1980). Early diagenesis in sediments from the eastern equatorial Pacific, II. Pore water metal results. *Earth Planet. Sci. Lett.*, **49**(1), 81-101.

Klunder, M. B., Laan, P., Middag, R., De Baar, H. J. W., & van Ooijen, J. C. (2011). Dissolved iron in the Southern Ocean (Atlantic sector). *Deep Sea Res. Pt. II*, **58**, 2678-2694, doi:10.1016/j.dsr2.2010.10.042.

Köbberich, M., & Vance, D. (2017). Kinetic control on Zn isotope signatures recorded in marine diatoms. *Geochim. Cosmochim. Acta*, **210**, 97–113. http://dx.doi.org/10.1016/j.gca.2017.04.014.

Köbberich, M., & Vance, D. (2019). Zn isotope fractionation during uptake into marine phytoplankton: Implications for oceanic zinc isotopes. *Chem. Geol.*, **523**, 154-161, doi:10.1016/j.chemgeo.2019.04.004.

Koide, M., Hodge, V.F., Yang, J.S., Stallard, M., & Goldberg, E.G. (1986). Some comparative marine chemistries of rhenium, gold, silver and molybdenum. *Appl. Geochem.*, **1**, 705-714.

Konhauser, K. O., Pecoits, E., Lalonde, S. V., Papineau, D., Nisbet, E. G., Barley, M. E., Arndt, N. T., Zahnle, K., & Kamber, B. S. (2009). Oceanic nickel depletion and a methanogen famine before the Great Oxidation Event. *Nature*, **458**(7239), 750-753.

Koschinsky, A., & Halbach, P. (1995). Sequential leaching of marine ferromanganese precipitates: Genetic implications. *Geochim. Cosmochim. Acta*, **59**(24), 5113-5132.

Koschinsky, A., & Hein, J. R. (2003). Uptake of elements from seawater by ferromanganese crusts: solid-phase associations and seawater speciation. *Mar. Geol.*, **198**(3-4), 331-351.

Kowalski, N., Dellwig, O., Beck, M., Gräwe, U., Neubert, N., Nägler, T. F., Badewien, T. H., Brumsack, H. J., van Beusekom, J. E. E., & Böttcher, M. E. (2013). Pelagic molybdenum concentration anomalies and the impact of sediment resuspension on the molybdenum budget in two tidal systems of the North Sea. *Geochim. Cosmochim. Acta*, **119**, 198–211, doi:10.1016/j.gca.2013.05.046.

Kramer, D., Cullen, J. T., Christian, J. R., Johnson, W. K., & Pedersen, T. F. (2011). Silver in the subarctic northeast Pacific Ocean: Explaining the basin scale distribution of silver. *Mar. Chem.*, **123**, 133-142.

Kurisu, M., Takahashi, Y., Iizuka, T. & Uematsu, M. (2016a). Very low isotope ratio of iron in fine aerosols related to its contribution to the surface ocean. *J. Geophys. Res. Atmos*. **121**, 11,119–11,136. https://doi.org/10.1002/2016JD024957.

Kurisu, M., Sakata, K., Miyamoto, C., Takaku, Y., Iizuka, T., & Takahashi, Y. (2016b). Variation of iron isotope ratios in anthropogenic materials emitted through combustion processes. *Chem. Lett.* 45, 970–972 (2016). https://doi.org/10.1246/cl.160451.

Kunzmann, M., Halverson, G. P., Sossi, P. A., Raub, T. D., Payne, J. L., & Kirby, J. (2013). Zn isotope evidence for immediate resumption of primary productivity after snowball Earth. *Geology*, **41**, 27–30.

Labatut, M., Lacan, F., Pradoux, C., Chmeleff, J., Radic, A., Murray, J. W., Poitrasson, F., Johansen, A. M., & Thil, F. (2014). Iron sources and dissolved-particulate interactions in the seawater of the Western Equatorial Pacific, iron isotope perspectives. *Global Biogeochem. Cycles* **28**, 1044-1065.

Lacan, F., Francois, R., Ji, Y., & Sherrell, R. M. (2006). Cadmium isotopic composition in the ocean. *Geochim. Cosmochim. Acta*, **70**(20), 5104-5118.

Lacan, F., Radic, A., Jeandel, C., Poitrasson, F., Sarthou, G., Pradoux, C., & Freydier, R. (2008). Measurement of the isotopic composition of dissolved iron in the open ocean. *Geophys. Res. Lett.*, **35**, L24610, doi:10.1029/2008GL035841.

Lal, D., Charles, C., Vacher, L., Goswami, J. N., Jull, A. J. T., McHargue, L., & Finkel, R. C. (2006). Paleo-ocean chemistry records in marine opal: Implications for fluxes of trace elements, cosmogenic nuclides (Be-10 and Al-26), and biological productivity. *Geochim. Cosmochim. Acta* **70**, 3275-3289.

Lam, P. J., & Marchal, O. (2015). Insights into particle cycling from thorium and particle data. *Annual Review of Marine Science*, **7**, 159-184.

Lambelet, M., Rehkämper, M., van de Flierdt, T., Xue, Z., Kreissig, K., Coles, B., Porcelli, D., & Andersson, P. (2013). Isotopic analysis of Cd in the mixing zone of Siberian rivers with the Arctic Ocean—New constraints on marine Cd cycling and the isotope composition of riverine Cd. *Earth Planet. Sci. Lett.*, **361**, 64-73.

Lane, T. W., Saito, M. A., George, G. N., Pickering, I. J., Prince, R. C., & Morel, F. M. (2005). Biochemistry: a cadmium enzyme from a marine diatom. *Nature*, **435**(7038), 42.

Lauderdale, J. M., Braakman, R., Forget, G., Dutkiewicz, S., & Follows, M. J. (2020). Microbial feedbacks optimize ocean iron availability. *Proc. Natl. Acad. Sci.*, **117**(9), 4842-4849.

Lea, D. W., Shen, G. T., & Boyle, E. A. (1989). Coralline barium records temporal variability in equatorial Pacific upwelling. *Nature*, 340(6232), 373-376.

Lee, J. G., & Morel, F. M. M. (1995). Replacement of zinc by cadmium in marine phytoplankton. *Mar. Ecol. Prog. Ser.*, **127**, 305–309.

Lemaitre, N., de Souza, G. F., Archer, C., Wang, R. M., Planquette, H., Sarthou, G., & Vance, D. (2020). Pervasive sources of isotopically light zinc in the North Atlantic Ocean. *Earth Planet. Sci. Lett.*, **539**, doi:10.1016/j.epsl.2020.116216.

Lerner, P., Marchal, O., Lam, P. J., & Solow, A. (2018). Effects of particle composition on thorium scavenging in the North Atlantic. *Geochimica et Cosmochimica Acta*, **233**, 115-134.

Le Roy, E. L., Sanial, V., Charette, M. A., van Beek, P., Lacan, F., Jacquet, S. H., Henderson, P. B., Souhaut, M., García-Ibáñez, M. I., Jeandel, C., Pérez, F. F., & Sarthou, G. (2018). The ^{226}Ra–Ba relationship in the North Atlantic during GEOTRACES-GA01. *Biogeosciences*, **15**(9), 3027-3048.

Levasseur, S., Frank, M., Hein, J. R., & Halliday, A. N. (2004). The global variation in the iron isotope composition of marine hydrogenetic ferromanganese deposits: implications for seawater chemistry? *Earth Planet. Sci. Lett.*, **224**(1-2), 91-105.

Liao, W. H., & Ho, T. Y. (2018). Particulate trace metal composition and sources in the Kuroshio adjacent to the East China Sea: The importance of aerosol deposition. *Journal of Geophysical Research: Oceans*, **123**(9), 6207-6223.

Liao, W. H., Takano, S., Yang, S. C., Huang, K. F., Sohrin, Y., & Ho, T. Y. (2020). Zn isotope composition in the water column of the Northwestern Pacific Ocean: the importance of external sources. *Global Biogeochem. Cycles*, **34**(1), e2019GB006379.

Liermann, L. J., Guynn, R. L., Anbar, A., & Brantley, S. L. (2005). Production of a molybdophore during metal-targeted dissolution of silicates by soil bacteria. *Chem. Geol.*, **220**, 285–302, doi:10.1016/j.chemgeo.2005.04.013.

Little, S.H., Vance, D., Siddall, M. and Gasson, E. (2013). A modeling assessment of the role of reversible scavenging in controlling oceanic dissolved Cu and Zn distributions. *Global Biogeochem. Cycles* **27**(3), 780-791.

Little, S.H., Sherman, D.M., Vance, D. and Hein, J.R. (2014a). Molecular controls on Cu and Zn isotopic fractionation in Fe–Mn crusts. *Earth Planet. Sci. Lett.* **396**, 213-222.

Little, S. H., Vance, D., Walker-Brown, C., & Landing, W. M. (2014b). The oceanic mass balance of copper and zinc isotopes, investigated by analysis of their inputs, and outputs to ferromanganese oxide sediments. *Geochim. Cosmochim. Acta* **125**, 673–693.

Little, S. H., Vance, D., Lyons, T. W., & McManus, J. (2015). Controls on trace metal authigenic enrichment in reducing sediments: insights from modern oxygen-deficient settings. *Am. J. Sci.*, **315**(2), 77-119.

Little, S. H., Vance, D., McManus, J., & Severmann, S. (2016). Key role of continental margin sediments in the oceanic mass balance of Zn and Zn isotopes. *Geology*, **44**, 207–210.

Little, S. H., van de Flierdt, T., Rehkämper, M., Wilson, D. J., Adkins, J. F., & Robinson, L. F. (2017a). Deep sea corals as archives of seawater Zn isotopes. In *Goldschmidt Abstracts*, p. 2387.

Little, S.H., Vance, D., McManus, J., Severmann, S. and Lyons, T.W. (2017b). Copper isotope signatures in modern marine sediments. *Geochim. Cosmochim. Acta*, *212*, 253-273.

Little, S. H., Archer, C., Milne, A., Schlosser, C., Achterberg, E. P., Lohan, M. C., & Vance, D. (2018). Paired dissolved and particulate phase Cu isotope distributions in the South Atlantic. *Chem. Geol.*. **502**, 29-43.

Little, S.H., Archer, C., McManus, J., Najorka, J., Wegorzewski, A.V. and Vance, D. (2020). Towards balancing the oceanic Ni budget. *Earth Planet. Sci. Lett.* **547**, p.116461.

Liu, R., Guo, B., Wang, M., Li, W., Yang, T., Ling, H., & Chen, T. (2020). Isotopic fingerprinting of dissolved iron sources in the deep western Pacific since the late Miocene. *Science China Earth Sciences*, **63**, doi:10.1007/s11430-020-9648-6.

Liu, S. A., Wu, H., Shen, S. Z., Jiang, G., Zhang, S., Lv, Y., Zhang, H., & Li, S. (2017). Zinc isotope evidence for intensive magmatism immediately before the end-Permian mass extinction. *Geology*, **45**, 343–346.

Liu, X., & Millero, F. J. (2002). The solubility of iron in seawater. *Mar. Chem.*, **77**(1), 43-54.

Liu, Y., Li, X., Zeng, Z., Yu, H. M., Huang, F., Felis, T., & Shen, C. C. (2019). Annually-resolved coral skeletal $\delta^{138/134}$Ba records: A new proxy for oceanic Ba cycling. *Geochim. Cosmochim. Acta*, **247**, 27-39.

Lohan, M. C., Crawford, D. W., Purdie, D. A., & Statham, P. J. (2005). Iron and Zinc Enrichments in the Northeastern Subarctic Pacific : Ligand Production and Zinc Availability in Response to Phytoplankton Growth. *Limnol. Oceanogr.*, **50**, 1427–1437.

Lough, A. J. M., Klar, J. K., Homoky, W. B., Comer-Warner, S. A., Milton, J. A., Connelly, D. P., James, R. H., & Mills, R. A. (2017). Opposing authigenic controls on the isotopic signature of dissolved iron in hydrothermal plumes. *Geochim. Cosmochim. Acta*, **202**, 1-20.

Lv, Y., Liu, S. A., Wu, H., Hohl, S. V., Chen, S., & Li, S. (2018). Zn-Sr isotope records of the Ediacaran Doushantuo Formation in South China: diagenesis assessment and implications. *Geochim. Cosmochim. Acta*, *239*, 330-345.

Lyons, T. W., Anbar, A. D., Severmann, S., Scott, C., & Gill, B. C. (2009). Tracking Euxinia in the Ancient Ocean: A Multiproxy Perspective and Proterozoic Case Study. *Annu. Rev. Earth Planet. Sci.*, **37**, 507–534, doi:10.1146/annurev.earth.36.031207.124233.

Lyons, T. W., Severmann, S. (2006). A critical look at iron paleoredox proxies: New insights from modern euxinic marine basins. *Geochim. Cosmochim. Acta*, **70**(23), 5698-5722.

Ma, Z., Gray, E., Thomas, E., Murphy, B., Zachos, J., & Paytan, A. (2014). Carbon sequestration during the Palaeocene–Eocene Thermal Maximum by an efficient biological pump. *Nat. Geosci.*, **7**(5), 382.

Ma, Z., Ravelo, A. C., Liu, Z., Zhou, L., & Paytan, A. (2015). Export production fluctuations in the eastern equatorial Pacific during the Pliocene-Pleistocene: Reconstruction using barite accumulation rates. *Paleoceanography*, **30**(11), 1455-1469.

Mahaffey, C., Reynolds, S., Davis, C. E., & Lohan, M. C. (2014). Alkaline phosphatase activity in the subtropical ocean: insights from nutrient, dust and trace metal addition experiments. *Front. Mar. Sci.*, **1**, 1–13.

Maldonado, M. T., Allen, A. E., Chong, J. S., Lin, K., Leus, D., Karpenko, N., & Harris, S. L. (2006). Copper-dependent iron transport in coastal and oceanic diatoms. *Limnol. Oceanogr.* **51**, 1729–1743.

Maret, W. Zinc biochemistry, physiology, and homeostasis – recent insights and current trends. *Biometals* **14**, 187–190 (2001). https://doi.org/10.1023/A:1012945110820

Marchitto, T. M., Curry, W. B., & Oppo, D. W. (2000) Zinc concentrations in benthic foraminifera reflect seawater chemistry. *Paleoceanography*, **15**, 299–306.

Marcus, M. A., Edwards, K. J., Gueguen, B., Fakra, S. C., Horn, G., Jelinski, N. A., Rouxel, O., Sorensen, J., & Toner, B. M. (2015). Iron mineral structure, reactivity, and isotopic composition in a South Pacific Gyre ferromanganese nodule over 4 Ma. *Geochim. Cosmochim. Acta*, **171**, 61-79.

Maréchal, C. N., Nicolas, E., Douchet, C., & Albarède, F. (2000). Abundance of zinc isotopes as a marine biogeochemical tracer. *Geochem. Geophys. Geosyst.*, **1**, 1015, http://doi.wiley.com/10.1029/1999GC000029.

Marks, J. A., Perakis, S. S., King, E. K., & Pett-Ridge, J. (2015). Soil organic matter regulates molybdenum storage and mobility in forests. *Biogeochemistry*, **125**, 167–183, doi:10.1007/s10533-015-0121-4.

Marsay, C. M., Lam, P. J., Heller, M. I., Lee, J. M., & John, S. G. (2018). Distribution and isotopic signature of ligand-leachable particulate iron along the GEOTRACES GP16 East Pacific Zonal Transect. *Mar. Chem.*, **201**, 198-211.

Martin, J. H. (1990). Glacial-interglacial CO_2 change: the iron hypothesis. *Paleoceanography* **5**, 1-13.

Martin, J. H., & Fitzwater, S. E. (1988). Iron deficiency limits phytoplankton growth in the north-east Pacific subarctic. *Nature*, **331**(6154), 341-343.

Martin, J. H., Fitzwater, S. E., & Gordon, R. M. (1990). Iron deficiency limits phytoplankton growth in Antarctic waters. *Global Biogeochem. Cycles*, **4**(1), 5-12.

Martin, J. H., Knauer, G. A. and Gordon, R. M. (1983) Silver distributions and fluxes in north-east Pacific waters. *Nature*, **305**, 306-309.

Martin, J. M., & Thomas, A. J. (1994). The global insignificance of telluric input of dissolved trace metals (Cd, Cu, Ni and Zn) to ocean margins. *Mar. Chem.*, **46**(1-2), 165-178.

Martin, J. H., Knauer, G. A., Karl, D. M., & Broenkow, W. W. (1987). VERTEX: carbon cycling in the northeast Pacific. *Deep Sea Res. Part A*, **34**(2), 267-285.

Martínez-Garcia, A., Rosell-Melé, A., Jaccard, S. L., Geibert, W., Sigman, D. M., & Haug, G. H. (2011). Southern Ocean dust–climate coupling over the past four million years. *Nature*, **476**(7360), 312-315.

Martínez-Garcia, A., Sigman, D. M., Ren, H., Anderson, R. F., Straub, M., Hodell, D. A., et al. (2014). Iron fertilization of the Subantarctic Ocean during the last ice age. *Science*, **343**, 1347-1350, doi:10.1126/science.1246848.

Martinez-Ruiz, F., Paytan, A., Gonzalez-Muñoz, M. T., Jroundi, F., Abad, M. M., Lam, P. J., Bishop, J. K. B., Horner, T. J., Morton, P. L., & Kastner, M. (2019). Barite formation in the ocean: Origin of amorphous and crystalline precipitates. *Chem. Geol.*, **511**, 441-451.

Martínez Ruíz, F. C., Paytan, A., González Muñoz, M. T., Jroundi, F., Abad, M. D. M., Lam, P. J., Horner, T.J.,. & Kastner, M. (2020). Barite precipitation on suspended organic matter in the mesopelagic zone. *Front. Earth Sci.* **8**:567714. doi:10.3389/feart.2020.567714

Mathur, R., Arribas, A., Megaw, P., Wilson, M., Stroup, S., Meyer-Arrivillaga, D., & Arribas, I. (2018). Fractionation of silver isotopes in native silver explained by redox reactions. *Geochim. Cosmochim. Acta*, **224**, 313-326.

Mawji, E. et al. (2015). The GEOTRACES Intermediate Data Product 2014. *Mar. Chem.*, **177**, 1-8, doi:10.1016/j.marchem.2015.04.005.

Mayfield, K .K., Eisenhauer, A., Santiago Ramos, D., Higgins, J. A., Horner, T. J., Auro, M. E., Magna, T., Moosdorf, N., Charette, M. A., Gonneea, M. E., Brady, C. E., Komar, N., Peucker-Ehrenbrink, B., & Paytan, A. (2021) Groundwater discharge impacts marine isotope budgets of Li, Mg, Ca, Sr, and Ba. *Nat. Commun.* **12**, 148, doi:10.1038/s41467-020-20248-3.

McKay, J. L., & Pedersen, T. F. (2008). The accumulation of silver in marine sediments: A link to biogenic Ba and marine productivity. *Global Biogeochem. Cycles*, **22**, GB4010, doi:10.1029/2007GB003136

McManus, J., Berelson, W. M., Klinkhammer, G. P., Johnson, K. S., Coale, K. H., Anderson, R. F., Kumar, N., Burdige, D. J., Hammond, D. E., Brumsack, H. J., McCorkle, D. C., & Rushdi, A. (1998). Geochemistry of barium in marine sediments: Implications for its use as a paleoproxy. *Geochim. Cosmochim. Acta*, **62**(21-22), 3453-3473.

McManus, J., Dymond, J., Dunbar, R. B., & Collier, R. W. (2002). Particulate barium fluxes in the Ross Sea. *Mar. Geol.*, **184**(1-2), 1-15.

McManus, J., Berelson, W. M., Severmann, S., Poulson, R. L., Hammond, D. E., Klinkhammer, G. P., & Holm, C. (2006). Molybdenum and uranium geochemistry in continental margin sediments:

Paleoproxy potential. *Geochim. Cosmochim. Acta*, **70**, 4643–4662, doi:10.1016/j.gca.2006.06.1564.

Mead, C., Herckes, P., Majestic, B. J., & Anbar, A. D. (2013). Source apportionment of aerosol iron in the marine environment using iron isotope analysis. *Geophys. Res. Lett.*, **40**(21), 5722-5727.

Mendel, R. R., & Bittner, F. (2006) Cell biology of molybdenum. *Biochim. Biophys. Acta*, **1763**(7), 621-635, doi:10.1016/j.bbamcr.2006.03.013.

Middag, R., van Heuven, S. M., Bruland, K. W., & de Baar, H. J. (2018). The relationship between cadmium and phosphate in the Atlantic Ocean unraveled. *Earth Planet. Sci. Lett.*, **492**, 79-88.

Middag, R., de Baar, H. J. W., & Bruland, K. W. (2019). The relationships between dissolved zinc and major nutrients phosphate and silicate along the GEOTRACES GA02 transect in the west Atlantic Ocean. *Global Biogeochem. Cycles*, **33**, 63-84, doi:10.1029/2018GB006034.

Middleton, J. L., Langmuir, C. H., Mukhopadhyay, S., McManus, J. F., & Mitrovica, J. X. (2016). Hydrothermal iron flux variability following rapid sea level changes. *Geophys. Res. Lett.*, **43**, 3848-3856.

Miller, C. A., Peucker-Ehrenbrink, B., Walker, B. D., & Marcantonio, F. (2011). Re-assessing the surface cycling of molybdenum and rhenium. *Geochim. Cosmochim. Acta*, **75**, 7146–7179, doi:10.1016/j.gca.2011.09.005.

Miller, L. A., & Bruland, K. W. (1995). Organic speciation of silver in marine waters. *Environ. Sci. Technol.*, **29**, 2616-2621.

Milletto, M., Wang, X., Planavsky, N. J., Luther, G. W., Lyons, T. W., & Tebo, B. M. (2021). Marine microbial Mn(II) oxidation mediates Cr(III) oxidation and isotope fractionation. *Geochim. Cosmochim. Acta*, **297**, 101-119, doi:10.1016/j.gca.2021.01.008.

Misumi, K., Lindsay, K., Moore, J. K., Doney, S. C., Bryan, F. O., Tsumune, D., & Yoshida, Y. (2014). The iron budget in ocean surface waters in the 20th and 21st centuries: projections by the Community Earth System Model version. *Biogeosciences*, **11**, 33-55.

Mitra, R. Marchitto, T. M., Ge, Q., Zhong, B., Kanakiya, B., Cook, M. S., Fehrenbacher, J. S., Ortiz, J. D., Tripati, A., & Lobaton, E. (2019). Automated species-level identification of planktic foraminifera using convolutional neural networks, with comparison to human performance. *Mar. Micropaleontol.* **147**, 16-24.

Moeller, K., Schoenberg, R., Pedersen, R. B., Weiss, D., & Dong, S. (2012). Calibration of the new certified reference materials ERM-AE633 and ERM-AE647 for copper and IRMM-3702 for zinc isotope amount ratio determinations. *Geostan. Geoanal. Res.* **36**(2), 177-199.

Moffett, J. W., & Brand, L. E. (1996). Production of strong, extracellular Cu chelators by marine cyanobacteria in response to Cu stress. *Limnol. Oceanogr.* **41**, 388–395.

Moffett, J. W., & Dupont, C. (2007). Cu complexation by organic ligands in the sub-arctic NW Pacific and Bering Sea. *Deep. Res. Part I Oceanogr. Res. Pap.* **54**, 586–595.

Moffett, J. W., Zika, R. G., & Brand, L. E. (1990). Distribution and potential sources and sinks of copper chelators in the Sargasso Sea. *Deep Sea Res. Part A, Oceanogr. Res. Pap.* **37**, 27–36.

Monnin, C., Jeandel, C., Cattaldo, T., & Dehairs, F. (1999). The marine barite saturation state of the world's oceans. M*ar. Chem.*, **65**(3-4), 253-261.

Moore, C. M., Mills, M. M., Arrigo, K. R., Berman-Frank, I., Bopp, L., Boyd, P. W., Galbraith, E. D., Geider, R. J., Guieu, C., Jaccard, S. L., Jickells, T. D., La Roche, J., Lenton, T. M., Mahowald, N. M., Maranon, E., Marinov, I., Moore, J. K., Nakatsuka, T., Oschlies, A., Saito, M. A., Thingstad,

T. F., Tsuda, A., & Ulloa, O. (2013). Processes and patterns of oceanic nutrient limitation. *Nat. Geosci.* **6**, 701-710.

Moore, C. M. (2016). Diagnosing oceanic nutrient deficiency. *Philosophical Transactions of the Royal Society A: Mathematical, Physical and Engineering Sciences*, **374**(2081), 20150290.

Moos, S. B. & Boyle, E. A. (2019). Determination of accurate and precise chromium isotope ratios in seawater samples by MC-ICP-MS illustrated by analysis of SAFe Station in the North Pacific Ocean. *Chem. Geol.*, **511**, 481-493, doi:10.1016/j.chemgeo.2018.07.027.

Moos, S. B., Boyle, E. A., Altabet, M. A., & Bourbonnais, A. (2020). Investigating the cycling of chromium in the oxygen deficient waters of the Eastern Tropical North Pacific Ocean and the Santa Barbara Basin using stable isotopes. *Mar. Chem.*, **221**, 103756, doi:10.1016/j.marchem.2020.103756 .

Morel, F. M. M., & Price, N. M. (2003). The biogeochemical cycles of trace metals in the oceans. *Science*, **300**, 944-947, doi:10.1126/science.1083545.

Morel, F. M. M., Reinfelder, J. R., Roberts, S. B., Chamberlain, C. P., Lee, J. G., & Yee, D. (1994) Zinc and carbon co-limitation of marine phytoplankton. *Nature*, **369**, 740-742.

Morel, F. M., Lam, P. J., & Saito, M. A. (2020). Trace Metal Substitution in Marine Phytoplankton. *Annual Review of Earth and Planetary Sciences*, **48**.

Morford, J. L., Kalnejais, L. H., Helman, P., Yen, G., & Reinard, M. (2008). Geochemical cycling of silver in marine sediments along an offshore transect. *Mar. Chem.*, **110**, 77-88.

Morgan, J. L., Wasylenki, L. E., Nuester, J., & Anbar, A. D. (2010). Fe isotope fractionation during equilibration of Fe–organic complexes. *Environ. Sci. Technol.*, **44**(16), 6095-6101.

Morris, A. W. (1975). Dissolved molybdenum and vanadium in the northeast Atlantic Ocean. *Deep Sea Research and Oceanographic Abstracts*, **22**, 49–54, doi:10.1016/0011-7471(75)90018-2.

Moynier, F., Vance, D., Fujii, T., & Savage, P. (2017). The Isotope Geochemistry of Zinc and Copper. *Rev. Mineral. Geochemistry* **82**, 543–600.

Mulholland, D.S., Poitrasson, F., Boaventura, G.R., Allard, T., Vieira, L.C., Santos, R.V., Mancini, L. & Seyler, P. (2015). Insights into iron sources and pathways in the Amazon River provided by isotopic and spectroscopic studies. *Geochim. Cosmochim. Acta*, **150**, 142–159.

Murphy, K. L. (2016). *Isotopic studies in marine geochemistry* (Doctoral dissertation, Imperial College London), doi:10.25560/68270.

Murray, J. W., Spell, B., & Paul, B. (1983). The contrasting geochemistry of manganese and chromium in the eastern tropical Pacific Ocean. In: Wong C.S., Boyle E., Bruland K.W., Burton J.D., Goldberg E.D. (eds) *Trace Metals in Sea Water*. NATO Conference Series (IV Marine Sciences), 9. Springer, Boston, MA, p. 643-669.

Nägler, T. F., Neubert, N., Böttcher, M. E., Dellwig, O., & Schnetger, B. (2011). Molybdenum isotope fractionation in pelagic euxinia: Evidence from the modern Black and Baltic Seas. *Chem. Geol.*, **289**, 1–11, doi:10.1016/j.chemgeo.2011.07.001.

Nägler, T. F., Anbar, A. D., Archer, C., Goldberg, T., Gordon, G. W., Greber, N. D., Seibert, C., Sohrin, Y., & Vance, D. (2014). Proposal for an international molybdenum isotope measurement standard and data representation. *Geostand. Geoanal. Res.*, **38**(2), 149-151.

Nakagawa, Y., Takano, S., Firdaus, M. L., Norisuye, K., Hirata, T., Vance, D., & Sohrin, Y. (2012). The molybdenum isotopic composition of the modern ocean. *Geochemical Journal*, **46**, 131–141, doi:10.2343/geochemj.1.0158.

Nameroff, T. J., Calvert, S. E., & Murray, J. W. (2004). Glacial-interglacial variability in the eastern tropical North Pacific oxygen minimum zone recorded by redox-sensitive trace metals. *Paleoceanogr. Paleoclim.*, **19**(1), PA1010, doi:10.1029/2003PA000912.

Nan, X. Y., Yu, H. M., Rudnick, R. L., Gaschnig, R. M., Xu, J., Li, W.-Y., Zhang, Q., Jin, Z.-D., Li, X.-H., & Huang, F. (2018). Barium isotopic composition of the upper continental crust. *Geochim. Cosmochim. Acta*, **233**, 33-49.

Nasemann, P., Gault-Ringold, M., Stirling, C. H., Koschinsky, A., & Sander, S. G. (2018). Processes affecting the isotopic composition of dissolved iron in hydrothermal plumes: A case study from the Vanuatu back-arc. *Chem. Geol.*, **476**, 70-84. https://doi.org/10.1016/j.chemgeo.2017.11.005.

Nasemann, P., Janssen, D. J., Rickli, J., Grasse, P., Franck, M., & Jaccard, S. L. (2020). Chromium reduction and associated stable isotope fractionation restricted to anoxic shelf waters in the Peruvian Oxygen Minimum Zone. *Geochim. Cosmochim. Acta*, **285**, 207-224, doi:10.1016/j.gca.2020.06.027.

Navarrete, J. U., Borrok, D. M., Viveros, M., & Ellzey, J. T. (2011). Copper isotope fractionation during surface adsorption and intracellular incorporation by bacteria. *Geochim. Cosmochim. Acta*, **75**(3), 784-799.

Nishioka, J., Obata, H., Ogawa, H., Ono, K., Yamashita, Y., Lee, K., Takeda, S., & Yasuda, I. (2020). Subpolar marginal seas fuel the North Pacific through the intermediate water at the termination of the global ocean circulation. *Proc. Natl Acad. Sci. U. S. A.* **117**(23), 12665-12673 https://doi.org/10.1073/pnas.2000658117.

Ndung'u, K., Thomas, M.A., & Flegal, A.R. (2001). Silver in the western equatorial and South Atlantic Ocean. *Deep-Sea Research II*, **48**, 2933-2945.

Neubert, N., Nägler, T. F., and Böttcher, M. E. (2008). Sulfidity controls molybdenum isotope fractionation into euxinic sediments: Evidence from the modern Black Sea. *Geology*, **36**, 775–778, doi:10.1130/G24959A.1.

Nielsen, S. G., Wasylenki, L. E., Rehkämper, M., Peacock, C. L., Xue, Z., & Moon, E. M. (2013). Towards an understanding of thallium isotope fractionation during adsorption to manganese oxides. *Geochim. Cosmochim. Acta*, **117**, 252-265.

Noordmann, J., Weyer, S., Montoya-Pino, C., Dellwig, O., Neubert, N., Eckert, S., Paetzel, M., & Böttcher, M. E. (2015). Uranium and molybdenum isotope systematics in modern euxinic basins: Case studies from the central Baltic Sea and the Kyllaren fjord (Norway). *Chem. Geol.*, **396**, 182–195, doi:10.1016/j.chemgeo.2014.12.012.

Ohnemus, D. C., & Lam, P. J. (2015). Cycling of lithogenic marine particles in the US GEOTRACES North Atlantic transect. *Deep Sea Res. Pt. II*, **116**, 283-302.

Ohnemus, D. C., Rauschenberg, S., Cutter, G. A., Fitzsimmons, J. N., Sherrell, R. M., & Twining, B. S. (2017). Elevated trace metal content of prokaryotic communities associated with marine oxygen deficient zones. *Limnol. Oceanog.*, **62**(1), 3-25.

Ohnemus, D. C., Torrie, R., & Twining, B. S. (2019). Exposing the Distributions and Elemental Associations of Scavenged Particulate Phases in the Ocean Using Basin-Scale Multi-Element Data Sets. *Global Biogeochem. Cycles*, **33**(6), 725-748, doi:10.1029/2018GB006145.

Park, H., Song, B., & Morel, F. M. (2007). Diversity of the cadmium-containing carbonic anhydrase in marine diatoms and natural waters. *Environmental Microbiology*, **9**(2), 403-413.

Paytan, A. (2009). Ocean Paleoproductivity. In: Gornitz V. (eds) *Encyclopedia of Paleoclimatology and Ancient Environments*. Encyclopedia of Earth Sciences Series, Springer, Dordrecht.

Paytan, A., & Kastner, M. (1996). Benthic Ba fluxes in the central Equatorial Pacific, implications for the oceanic Ba cycle. *Earth Planet. Sci. Lett.*, **142**(3-4), 439-450.

Paytan, A., Kastner, M., & Chavez, F. P. (1996). Glacial to interglacial fluctuations in productivity in the equatorial Pacific as indicated by marine barite. *Science*, **274**(5291), 1355-1357.

Paytan, A., & Griffith, E. M. (2007). Marine barite: Recorder of variations in ocean export productivity. *Deep Sea Res. Pt. II*, **54**(5-7), 687-705.

Paytan, A., Mackey, K. R., Chen, Y., Lima, I. D., Doney, S. C., Mahowald, N., Labiosa, R., & Post, A. F. (2009). Toxicity of atmospheric aerosols on marine phytoplankton. *Proc. Natl. Acad. Sci.*, **106**(12), 4601-4605.

Peers, G., & Price, N. M. (2006). Copper-containing plastocyanin used for electron transport by an oceanic diatom. *Nature* **441**, 341–344.

Peers, G., Quesnel, S., & Price, N. M. (2005). Copper requirements for iron acquisition and growth of coastal and oceanic diatoms. *Limnol. Oceanogr.* **50**, 1149–1158.

Pereira, N. S., Vögelin, A. R., Paulukat, C., Sial, A. N., Ferreira, V. P., & Frei, R. (2016). Chromium-isotope signatures in scleractinian corals from the Rocas Atoll, Tropical South Atlantic. *Geobiology*, **14**, 54–67, doi:10.1111/gbi.12155.

Pettine, M., Millero, F. J., & La Noce, T. (1991). Chromium (III) interactions in seawater through its oxidation kinetics. *Mar. Chem.*, **34**(1-2), 29-46.

Pettine, M., D'Ottone, L., Campanella, L., Millero, F. J., & Passino, R. (1998). The reduction of chromium (VI) by iron (II) in aqueous solutions. *Geochim. Cosmochim. Acta*, **62**(9), 1509-1519.

Pichat, S., Douchet, C., & Albarède, F. (2003). Zinc isotope variations in deep-sea carbonates from the eastern equatorial Pacific over the last 175 ka. *Earth Planet. Sci. Lett.*, **210**, 167–178.

Pichevin, L. E., Ganeshram, R. S., Geibert, W., Thunell, R., & Hinton, R. (2014). Silica burial enhanced by iron limitation in oceanic upwelling margins. *Nat. Geosci.*, **7**(7), 541-546.

Pinedo-González, P., Hawco, N. J., Bundy, R. M., Virginia Armbrust, E., Follows, M. J., Cael, B. B., White, A. E., Ferrón, S., Karl, D. M., & John, S. G. (2020). Anthropogenic Asian aerosols provide Fe to the North Pacific Ocean. *Proc. Natl. Acad. Sci. USA*, **117**, 27862-27868, doi:10.1073/pnas.2010315117.

Plass, A., Schlosser, C., Sommer, S., Dale, A. W., Achterberg, E. P., & Scholz, F. (2020). The control of hydrogen sulfide on benthic iron and cadmium fluxes in the oxygen minimum zone off Peru. *Biogeosciences*, **17**(13), 3685-3704.

Poitrasson, F. (2006). On the iron isotope homogeneity level of the continental crust. *Chem. Geol.*, **235**(1-2), 195-200.

Poitrasson, F., Vieira, L. C., Seyler, P., dos Santos Pinheiro, G. M., Mulholland, D. S., Bonnet, M. P., Martinez, J.-M., Lima, B. A., Boaventura, G. R., Chmeleff, J., Dantas, E. L., Guyot, J.-L., Mancini, L., Pimentel, M. M., Santos, R. V., Sondag, F., & Vauchel, P. (2014). Iron isotope composition of the bulk waters and sediments from the Amazon River Basin. *Chem. Geol.*, **377**, 1-11.

Pokrovsky, O. S., Viers, J., Emnova, E. E., Kompantseva, E. I., & Freydier, R. (2008). Copper isotope fractionation during its interaction with soil and aquatic microorganisms and metal oxy (hydr) oxides: Possible structural control. *Geochim. Cosmochim. Acta*, **72**(7), 1742-1757.

Price, N. M., & Morel, F. M. M. (1990). Cadmium and cobalt substitution for zinc in a marine diatom. *Nature*, **344**(6267), 658.

Price, N. M., & Morel, F. M. M. (1991). Colimitation of phytoplankton growth by nickel and nitrogen. *Limnol. Oceanogr.* **50**, 1071-1077.

Quay, P., & Wu, J. (2015). Impact of end-member mixing on depth distributions of δ^{13}C, cadmium and nutrients in the N. Atlantic Ocean. *Deep Sea Res. Pt. II*, **116**, 107-116.

Radic, A., Lacan, F., & Murray, J. W. (2011). Iron isotopes in the seawater of the equatorial Pacific Ocean: New constraints for the oceanic iron cycle. *Earth Planet. Sci. Lett.*, **306**, 1-10.

Rafter, P. A., Sigman, D. M., & Mackey, K. R. (2017). Recycled iron fuels new production in the eastern equatorial Pacific Ocean. *Nat. Commun.*, **8**(1), 1100.

Ragsdale, S. W. (2009). Nickel-based enzyme systems. *J. Biol. Chem.* **284**, 18571–18575.

Ranville, M. A., & Flegal, A.R. (2005). Silver in the North Pacific Ocean. *Geochemistry, Geophysics, Geosystems*, **6**(3), doi:10.1029/2004GC000770

Ranville, M. A., Cutter, G. A., Buck, C. S., Landing, W. M., Cutter, L. S., Resing. J. A, & Flegal, A. R. (2010). Aeolian contamination of Se and Ag in the North Pacific from Asian fossil fuel combustion. *Environ. Sci. Tech*., **44**, 1587–1593.

Rehkämper, M., Wombacher, F., Horner, T. J., & Xue, Z. (2012). Natural and anthropogenic Cd isotope variations. In Baskaran, M. (Ed.) *Handbook of Environmental Isotope Geochemistry* (pp. 125-154). Springer, Berlin, Heidelberg, doi:10.1007/978-3-642-10637-8_8.

Reinhard, C. T., Planavsky, N. J., Robbins, L. J., Partin, C. A., Gill, B. C., Lalonde, S. V., Bekker, A., Konhauser, K. O., & Lyons, T. W. (2013). Proterozoic ocean redox and biogeochemical stasis. *Proc. Natl. Acad. Sci.*, **110**, 5357–5362, doi:10.1073/pnas.1208622110.

Reinhard, C. T., Planavsky, N. J., Wang, X., Fischer, W. W., Johnson, T. M., & Lyons, T. W. (2014). The isotopic composition of authigenic chromium in anoxic marine sediments: a case study from the Cariaco Basin. *Earth Planet. Sci. Lett.*, **407**, 9–18, doi:10.1016/j.epsl.2014.09.024.

Remmelzwaal, S. R. C., Sadekov, A. Y., Parkinson, I. J., Schmidt, D. N., Titelboim, D., Abramovich, S., Roepert, A., Kienhuis, M., Polerecky, L., Goring-Harford, H., et al. (2019). Post-depositional overprinting of chromium in foraminifera. *Earth Planet Sci Lett.*, **515**, 100-111, doi:10.1016/j.epsl.2019.03.001.

Resing, J. A., Sedwick, P. N., German, C. R., Jenkins, W. J., Moffett, J. W., Sohst, B. M., & Tagliabue, A. (2015). Basin-scale transport of hydrothermal dissolved metals across the South Pacific Ocean. *Nature*, **523**(7559), 200-203.

Revels, B. N., Zhang, R., Adkins, J. F., & John, S. G. (2015). Fractionation of iron isotopes during leaching of natural particles by acidic and circumneutral leaches and development of an optimal leach for marine particulate iron isotopes. *Geochim. Cosmochim. Acta*, **166**, 92–104.

Richon, C., & Tagliabue, A. (2019). Insights into the major processes driving the global distribution of copper in the ocean from a global model. *Global Biogeochem. Cycles*, *33*(12), 1594-1610.

Rickaby, R. E. M., & Elderfield, H. (1999). Planktonic foraminiferal Cd/Ca: paleonutrients or paleotemperature?. *Paleoceanography*, **14**(3), 293-303.

Rickli, J., Janssen, D. J., Hassler, C., Ellwood, M. J., & Jaccard, S. L. (2019). Chromium biogeochemistry and stable isotope distribution in the Southern Ocean. *Geochim. Cosmochim. Acta*, **262**, 188-206, doi:10.1016/j.gca.2019.07.033.

Ridge, P. G., Zhang, Y., & Gladyshev, V. N. (2008). Comparative genomic analyses of copper transporters and cuproproteomes reveal evolutionary dynamics of copper utilization and its link to oxygen. *PLoS One* **3**(1), https://doi.org/10.1371/journal.pone.0001378.

Rijkenberg, M. J. A., Middag, R., Laan, P., Gerringa, L. J., van Aken, H. M., Schoemann, V., de Jong, J. T. M., & de Baar, H. J. W. (2014). The distribution of dissolved iron in the West Atlantic Ocean. *PloS One*, **9**(6).

Ripperger, S., & Rehkämper, M. (2007). Precise determination of cadmium isotope fractionation in seawater by double spike MC-ICPMS. *Geochim. Cosmochim. Acta*, **71**(3), 631-642.

Ripperger, S., Rehkämper, M., Porcelli, D., & Halliday, A. N. (2007). Cadmium isotope fractionation in seawater—A signature of biological activity. *Earth Planet. Sci. Lett.*, **261**(3-4), 670-684.

Rivera-Duarte, I., Flegal, A. R., Sañudo-Wilhelmy, S. A., & Véron, A. J. (1999). Silver in the far North Atlantic Ocean. *Deep-Sea Research II*, **46**, 979-990.

Robinson, L. F., Adkins, J. F., Frank, N., Gagnon, A. C., Prouty, N. G., Roark, E. B., & van de Flierdt, T. (2014). The geochemistry of deep-sea coral skeletons: A review of vital effects and applications for palaeoceanography. *Deep. Res. Part II Top. Stud. Oceanogr.*, **99**, 184–198. http://dx.doi.org/10.1016/j.dsr2.2013.06.005.

Rohatgi, A. (2019) WebPlotDigitizer (version 4.2; April 2019). https://automeris.io/WebPlotDigitizer [accessed 2020-06-22].

Rolison, J. M., Stirling, C. H., Middag, R., Gault-Ringold, M., George, E., & Rijkenberg, M. J. A. (2018). Iron isotope fractionation during pyrite formation in a sulfidic Precambrian ocean analogue. *Earth Planet. Sci. Lett.*, **488**, 1-13. https://doi.org/10.1016/j.epsl.2018.02.006.

Roshan, S., & Wu, J. (2015a). The distribution of dissolved copper in the tropical-subtropical north Atlantic across the GEOTRACES GA03 transect. *Mar. Chem.*, **176**, 189-198, doi:10.1016/j.marchem.2015.09.006.

Roshan, S., & Wu, J. (2015b). Cadmium regeneration within the North Atlantic. *Global Biogeochem. Cycles*, **29**(12), 2082-2094.

Roshan, S., & Wu, J. (2018). Dissolved and colloidal copper in the tropical South Pacific. *Geochim. Cosmochim. Acta*, **233**, 81-94, doi:10.1016/j.gca.2018.05.008.

Roshan, S., DeVries, T., Wu, J., & Chen, G. (2018). The internal cycling of zinc in the ocean. *Global Biogeochem. Cycles*, **32**(12), 1833-1849, doi:10.1029/2018GB006045.

Roshan, S., DeVries, T., Wu, J., John, S., & Weber, T. (2020). Reversible scavenging traps hydrothermal iron in the deep ocean. Earth and Planetary Science Letters, 542, 116297.

Rouxel, O. J., Bekker, A., & Edwards, K. J. (2005). Iron isotope constraints on the Archean and Paleoproterozoic ocean redox state. *Science*, **307**(5712), 1088-1091.

Rouxel, O., Shanks III, W. C., Bach, W., & Edwards, K. J. (2008). Integrated Fe-and S-isotope study of seafloor hydrothermal vents at East Pacific Rise 9–10 N. *Chem. Geol.*, **252**(3-4), 214-227.

Rouxel, O., Toner, B. M., Manganini, S. J., & German, C. R. (2016). Geochemistry and iron isotope systematics of hydrothermal plume fall-out at East Pacific Rise 9°50′N. *Chem. Geol.* **441**, 212-234. https://doi.org/10.1016/j.chemgeo.2016.08.027.

Rouxel, O., Toner, B., Germain, Y., & Glazer, B. (2018). Geochemical and iron isotopic insights into hydrothermal iron oxyhydroxide deposit formation at Loihi Seamount. *Geochim. Cosmochim. Acta*, **220**, 449-482. https://doi.org/10.1016/j.gca.2017.09.050.

Rosenthal, Y., Lam, P., Boyle, E. A., & Thomson, J. (1995). Authigenic cadmium enrichments in suboxic sediments: Precipitation and postdepositional mobility. *Earth Planet. Sci. Lett.*, **132**(1-4), 99-111.

Rue, E. L., Smith, G. J., Cutter, G. A., & Bruland, K. W. (1997). The response of trace element redox couples to suboxic conditions in the water column. *Deep Sea Res. I.*, **44**(1), 113-134.

Rushdi, A. I., McManus, J., & Collier, R. W. (2000). Marine barite and celestite saturation in seawater. *Mar. Chem.*, **69**(1-2), 19-31.

Ryan, B. M., Kirby, J. K., Degryse, F., Scheiderich, K., & McLaughlin, M. J. (2014). Copper isotope fractionation during equilibration with natural and synthetic ligands. *Environ. Sci. Technol.*, **48**(15), 8620-8626.

Saito, M. A., Moffett, J. W., & DiTullio, G. R. (2004). Cobalt and nickel in the Peru upwelling region: A major flux of labile cobalt utilized as a micronutrient. *Global Biogeochem. Cycles* **18**, 1–14.

Saito, M. A., Bertrand, E. M., Dutkiewicz, S., Bulygin, V. V., Moran, D. M., Monteiro, F. M., Follows, M. J., Valois, F. W., & Waterbury, J. B. (2011). Iron conservation by reduction of metalloenzyme inventories in the marine diazotroph *Crocosphaera watsonii*. *Proc. Natl. Acad. Sci.*, **108**(6), 2184-2189.

Saito, M. A., Noble, A. E., Tagliabue, A., Goepfert, T. J., Lamborg, C. H., & Jenkins, W. J. (2013). Slow-spreading submarine ridges in the South Atlantic as a significant oceanic iron source. *Nat. Geosci.*, **6**(9), 775-779.

Samanta, M., Ellwood, M. J., Sinoir, M., & Hassler, C. S. (2017). Dissolved zinc isotope cycling in the Tasman Sea, SW Pacific Ocean. *Mar. Chem.,* **192**, 1–12. http://dx.doi.org/10.1016/j.marchem.2017.03.004.

Samanta, M., Ellwood, M. J., & Strzepek, R. F. (2018). Zinc isotope fractionation by *Emiliania huxleyi* cultured across a range of free zinc ion concentrations. *Limnol. Oceanogr.*, **63**, 660–671.

Sarmiento, J. L., & Gruber, M. (2006). Carbon Cycle. In *Ocean Biogeochemical Dynamics* (pp. 318-358). Princeton, NJ: Princeton University Press.

Sarmiento, J. L., Gruber, N., Brzezinski, M. A., & Dunne, J. P. (2004). High-latitude controls of thermocline nutrients and low latitude biological productivity. *Nature*, **427**(6969), 56-60.

Scheiderich, K., Amini, M., Holmden, C., & Francois, R. (2015) Global variability of chromium isotopes in seawater demonstrated by Pacific, Atlantic, and Arctic Ocean samples. *Earth Planet. Sci. Lett.*, **423**, 87–97, doi:10.1016/j.epsl.2015.04.030.

Schönbächler, M., Carlson, R. W., Horan, M. F., Mock, T. D., & Hauri, E. H. (2007). High precision Ag isotope measurements in geologic materials by multiple-collector ICPMS: An evaluation of dry versus wet plasma. *Intl J. Mass Spectrom.*, **261**(2-3), 183-191.

Sclater, F. R., Boyle, E., & Edmond, J. M. (1976). On the marine geochemistry of nickel. *Earth Planet. Sci. Lett.*, **31**(1), 119-128.

Sedwick, P. N., Church, T. M., Bowie, A.R., Marsay, C. M., Ussher, S. J., Achilles, K. M., Lethaby, P. J., Johnson, R. J., Sarin, M. M., McGillicuddy, D. J. (2005). Iron in the Sargasso Sea (Bermuda Atlantic Time-series Study region) during summer: Eolian imprint, spatiotemporal variability, and ecological implications. *Global Biogeochem. Cycles,* 19, GB4006. https://doi.org/10.1029/2004GB002445.

Semeniuk, D. M., Maldonado, M. T., & Jaccard, S. L. (2016). Chromium uptake and adsorption in marine phytoplankton - Implications for the marine chromium cycle. *Geochim. Cosmochim. Acta*, **184**, 41-54. doi:10.1016/j.gca.2016.04.021.

Sharma, M., Polizzotto, M., & Anbar, A. D. (2001). Iron isotopes in hot springs along the Juan de Fuca ridge. *Earth Planet. Sci. Lett.* **194**(1-2), 39-51. https://doi.org/10.1016/S0012-821X(01)00538-6.

Sherman, D. M. (2013). Equilibrium isotopic fractionation of copper during oxidation/reduction, aqueous complexation and ore-forming processes: Predictions from hybrid density functional theory. *Geochim. Cosmochim. Acta*, **118**, 85-97.

Sherman, D. M., Little, S. H., & Vance, D. (2015). Reply to comment on" Molecular controls on Cu and Zn isotopic fractionation in Fe-Mn crusts". *Earth Planet. Sci. Lett.*, **411**, 313-315.

Sherman, D. M., & Little, S. H. (2020). Isotopic disequilibrium of Cu in marine ferromanganese crusts: Evidence from ab initio predictions of Cu isotope fractionation on sorption to birnessite. *Earth Planet. Sci. Lett.*, **549**, 116540.

Sherman, D. M., & Peacock, C. L. (2010). Surface complexation of Cu on birnessite (δ-MnO2): Controls on Cu in the deep ocean. *Geochim. Cosmochim. Acta*, **74**(23), 6721-6730.

Schlitzer, R., et al. (2018). The GEOTRACES intermediate data product 2017. *Chem. Geol.*, **493**, 210-223.

Schlitzer, R. (2019) eGEOTRACES - Electronic Atlas of GEOTRACES Sections and Animated 3D Scenes, http://egeotraces.org [accessed 2020-08-31].

Schmitt, A. D., Galer, S. J., & Abouchami, W. (2009a). Mass-dependent cadmium isotopic variations in nature with emphasis on the marine environment. *Earth Planet. Sci. Lett.*, **277**(1-2), 262-272.

Schmitt, A. D., Galer, S. J., & Abouchami, W. (2009b). High-precision cadmium stable isotope measurements by double spike thermal ionisation mass spectrometry. *Journal of Analytical Atomic Spectrometry*, **24**(8), 1079-1088.

Schmitz, B. (1987). Barium, equatorial high productivity, and the northward wandering of the Indian continent. *Paleoceanography*, **2**(1), 63-77.

Schoenberg, R., Zink, S., Staubwasser, M., & von Blackenburg, F. (2008). The stable Cr isotope inventory of solid Earth reservoirs determined by double spike MC-ICP-MS. *Chem. Geol.*, **249**, 294-306, doi:10.1016/j.chemgeo.2008.01.009.

Scholz, F., McManus, J., & Sommer, S. (2013). The manganese and iron shuttle in a modern euxinic basin and implications for molybdenum cycling at euxinic ocean margins. *Chem. Geol.*, **355**, 56–68, doi:10.1016/j.chemgeo.2013.07.006.

Scholz, F., Siebert, C., Dale, A. W., & Frank, M. (2017). Intense molybdenum accumulation in sediments unearth a nitrogenous water column and implications for the reconstruction of paleo-redox conditions based on molybdenum isotopes. *Geochim. Cosmochim. Acta*, **213**, 400-417.

Schönbächler, M., Carlson, R. W., Horan, M. F., Mock, T. D., & Hauri, E. H. (2007). High precision Ag isotope measurements in geological materials by multiple-collector ICPMS: An evaluation of dry versus wet plasma. *Int. J. Mass Spectrom.*, **261**, 183-191.

Schulz, K. G., Zondervan, I., Gerringa, L. J. A, Timmermans, K. R., Veldhuis, M. J. W., & Riebesell, U. (2004). Effect of trace metal availability on coccolithophorid calcification. *Nature,* **430**, 673–676.

Scott, C., & Lyons, T. W. (2012). Contrasting molybdenum cycling and isotopic properties in euxinic versus non-euxinic sediments and sedimentary rocks: Refining the paleoproxies. *Chem. Geol.*, **324–325**, 19–27, doi:10.1016/j.chemgeo.2012.05.012.

Semeniuk, D. M., Cullen, J. T., Johnson, W. K., Gagnon, K., Ruth, T. J., & Maldonado, M. T. (2009). Plankton copper requirements and uptake in the subarctic Northeast Pacific Ocean. *Deep Sea Research Part I: Oceanographic Research Papers*, **56**(7), 1130-1142.

Semeniuk, D. M., Bundy, R. M., Payne, C. D., Barbeau, K. A., & Maldonado, M. T. (2015). Acquisition of organically complexed copper by marine phytoplankton and bacteria in the northeast subarctic Pacific Ocean. *Mar. Chem.* **173**, 222–233.

Serno, S., Winckler, G., Anderson, R. F., Hayes, C. T., Ren, H., Gersonde, R., & Haug, G. H. (2014). Using the natural spatial pattern of marine productivity in the Subarctic North Pacific to evaluate paleoproductivity proxies. *Paleoceanography*, **29**(5), 438-453.

Severmann, S., Johnson, C. M., Beard, B. L., German, C. R., Edmonds, H. N., Chiba, H., & Green, D. R. H. (2004). The effect of plume processes on the Fe isotope composition of hydrothermally derived Fe in the deep ocean as inferred from the Rainbow vent site, Mid-Atlantic Ridge, 36°14′ N. *Earth Planet. Sci. Lett.*, **225**(1-2), 63-76. https://doi.org/10.1016/j.epsl.2004.06.001.

Severmann, S., Johnson, C. M., Beard, B. L., & McManus, J. (2006). The effect of early diagenesis on the Fe isotope compositions of porewaters and authigenic minerals in continental margin sediments. *Geochim. Cosmochim. Acta*, **70**(8). 2006-2022. https://doi.org/10.1016/j.gca.2006.01.007.

Severmann, S., McManus, J., Berelson, W. M., & Hammond, D. E. (2010). The continental shelf benthic iron flux and its isotope composition. *Geochim. Cosmochim. Acta*, **74**(14), 3984-4004. https://doi.org/10.1016/j.gca.2010.04.022.

Shaked, Y., Xu, Y., Leblanc, K., & Morel, F. M. M. (2006) Zinc availability and alkaline phosphatase activity in Emiliania huxleyi: Implications for Zn-P co-limitation in the ocean. *Limnol. Oceanogr.*, **51**, 299–309.

Shemesh, A., Mortlock, R. A., Smith, R. J., & Froelich, P. N. (1988). Determination of Ge/Si in marine siliceous microfossils: Separation, cleaning and dissolution of diatoms and radiolaria. *Mar. Chem.* **25**, 305-323.

Shen, G. T., Boyle, E. A., & Lea, D. W. (1987). Cadmium in corals as a tracer of historical upwelling and industrial fallout. *Nature*, **328**(6133), 794.

Shiel, A. E., Weis, D., & Orians, K. J. (2010). Evaluation of zinc, cadmium and lead isotope fractionation during smelting and refining. *Science of the Total Environment*, **408**(11), 2357-2368.

Sieber, M., Conway, T. M., de Souza, G. F., Hassler, C. S., Ellwood, M. J., & Vance, D. (2019a). High-resolution Cd isotope systematics in multiple zones of the Southern Ocean from the Antarctic Circumnavigation Expedition. *Earth Planet. Sci. Lett.*, **527**, doi:10.1016/j.epsl.2019.115799.

Sieber, M., Conway, T. M., de Souza, G. F., Obata, H., Takano, S., Sohrin, Y., & Vance, D. (2019b). Physical and biogeochemical controls on the distribution of dissolved cadmium and its isotopes in the Southwest Pacific Ocean. *Chem. Geol.*, **511**, 494-509.

Sieber, M., Conway, T. M., de Souza, G. F., Hassler, C. S., Ellwood, M. J., & Vance, D. (2020). Cycling of zinc and its isotopes across multiple zones of the Southern Ocean: Insights from the Antarctic Circumnavigation Expedition. *Geochim. Cosmochim. Acta*, **268**, 310-324, doi:10.1016/j.gca.2019.09.039.

Sieber, M., Conway, T. M., de Souza, G. F., Hassler, C.S., Ellwood, M.J. and Vance, D. (2021). Isotopic fingerprinting of biogeochemical processes and iron sources in the iron-limited surface Southern Ocean. *Earth and Planetary Science Letters*. In Press.

Siebert, C., Nägler, T. F., von Blanckenburg, F., and Kramers, J. D. (2003). Molybdenum isotope records as a potential new proxy for paleoceanography. *Earth Planet. Sci. Lett.*, **211**, 159–171, doi:10.1016/S0012-821X(03)00189-4.

Siebert, C., Pett-Ridge, J. C., Opfergelt, S., Guicharnaud, R. A., Halliday, A. N., & Burton, K. W. (2015). Molybdenum isotope fractionation in soils: Influence of redox conditions, organic matter, and atmospheric inputs. *Geochim. Cosmochim. Acta*, **162**, 1–24, doi:10.1016/j.gca.2015.04.007.

Sigman, D. M., & Boyle, E. A. (2000). Glacial/interglacial variations in atmospheric carbon dioxide. *Nature*, **407**(6806), 859-869.

Sigman, D. M., & Hain, M. P. (2012). The Biological Productivity of the Ocean: Section 1, *Nature Education Knowledge*, **3**(10):21.

Sigman, D. M., Hain, M. P., & Haug, G. H. (2010). The polar ocean and glacial cycles in atmospheric CO_2 concentration, *Nature*, **466**, 47-55, doi:10.1038/nature09149.

Skulan, J. L., Beard, B. L., & Johnson, C. M. (2002). Kinetic and equilibrium Fe isotope fractionation between aqueous Fe (III) and hematite. *Geochim. Cosmochim. Acta*, **66**(17), 2995-3015.

Sinoir, M., Butler, E. C. V., Bowie, A. R., Mongin, M., Nesterenko, P. N., & Hassler, C. S. (2012). Zinc marine biogeochemistry in seawater: A review. *Mar. Freshw. Res.*, **63**, 644–657.

Sorensen, J. V., Gueguen, B., Stewart, B. D., Peña, J., Rouxel, O., & Toner, B. M. (2020). Large nickel isotope fractionation caused by surface complexation reactions with hexagonal birnessite. *Chem. Geol*., **537**, 119481.

Staubwasser, M., Schoenberg, R., von Blanckenburg, F., Krüger, S., & Pohl, C. (2013) Isotope fractionation between dissolved and suspended particulate Fe in the oxic and anoxic water column of the Baltic Sea. *Biogeosciences*, **10**, 233-245. doi:10.5194/bg-10-233-2013.

Sternberg, E., Jeandel, C., Robin, E., & Souhaut, M. (2008). Seasonal cycle of suspended barite in the Mediterranean sea. *Geochim. Cosmochim. Acta*, **72**(16), 4020-4034.

Stevenson, E. I., Fantle, M. S., Das, S. B., Williams, H. M., & Aciego, S. M. (2017). The iron isotopic composition of subglacial streams draining the Greenland ice sheet. *Geochim. Cosmochim. Acta*, **213**, 237-254.

Sun, W.-P., Hu, C.-Y., Han, Z.-B., Shen, C., & Pan, J.-M. (2016). Zn/Si records in diatom opal from Prydz Bay, East Antarctica. *Marine Geology* **381**, 34-41.

Sun, Z., Wang, X., & Planavsky, N. (2019). Cr isotope systematics in the Connecticut River estuary. *Chem. Geol.*, **506**, 29-39, doi:10.1016/j.chemgeo.2018.12.034.

Sunda, W. G. (2012). Feedback interactions between trace metal nutrients and phytoplankton in the ocean. *Front. Microbiol.*, **3**(204), doi:10.3389/fmicb.2012.00204.

Sunda, W. G., & Huntsman, S. A. (1995). Iron uptake and growth limitation in oceanic and coastal phytoplankton. *Mar. Chem.*, **50**, 189–206.

Sunda, W. G., & Huntsman, S. A. (2000). Effect of Zn, Mn, and Fe on Cd accumulation in phytoplankton: implications for oceanic Cd cycling. *Limnol. Oceanogr.*, **45**(7), 1501-1516.

Sweere, T. C., Dickson, A. J., Jenkyns, H. C., Porcelli, D., & Henderson, G. M. (2020). Zinc-and cadmium-isotope evidence for redox-driven perturbations to global micronutrient cycles during Oceanic Anoxic Event 2 (Late Cretaceous). *Earth Planet. Sci. Lett.*, **546**, 116427.

Sweere, T. C., Dickson, A. J., Jenkyns, H. C., Porcelli, D., Elrick, M., van den Boorn, S. H., & Henderson, G. M. (2018). Isotopic evidence for changes in the zinc cycle during Oceanic Anoxic Event 2 (Late Cretaceous). *Geology*, **46**(5), 463-466.

Tabouret, H., Pomerleau, S., Jolivet, A., Pécheyran, C., Riso, R., et al. (2012). Specific pathways for the incorporation of dissolved barium and molybdenum into the bivalve shell: An isotopic tracer approach in the juvenile Great Scallop (*Pecten maximus*). *Mar. Environ. Res.*, **78**, 15-25, doi:10.1016/j.marenvres.2012.03.006.

Tagliabue, A., Aumont, O., DeAth, R., Dunne, J. P., Dutkiewicz, S., Galbraith, E., Misumi, K., Moore, J. K., Ridgwell, A., Sherman, E., Stock, C., Vichi, M., Völker, C., & Yool, A. (2016). How well do global ocean biogeochemistry models simulate dissolved iron distributions?. *Global Biogeochem. Cycles*, **30**(2), 149-174.

Tagliabue, A., Bowie, A. R., Boyd, P. W., Buck, K. N., Johnson, K. S., & Saito, M. A. (2017). The integral role of iron in ocean biogeochemistry. *Nature*, **543**(7643), 51-59.

Tagliabue, A., Bowie, A. R., DeVries, T., Ellwood, M. J., Landing, W. M., Milne, A., Ohnemus, D. C., Twining, B. S., & Boyd, P. W. (2019). The interplay between regeneration and scavenging fluxes drives ocean iron cycling. *Nat. Commun.*, 10**(**1), 1-8.

Takano, S., Tanimizu, M., Hirata, T. , & Sohrin, Y. (2014). Isotopic constraints on biogeochemical cycling of copper in the ocean. *Nat. Commun.* **5**, 5663.

Takano, S., Tanimizu, M., Hirata, T., Shin, K. C., Fukami, Y., Suzuki, K., & Sohrin, Y. (2017). A simple and rapid method for isotopic analysis of nickel, copper, and zinc in seawater using chelating extraction and anion exchange. *Anal. Chim. Acta* **967**, 1–11.

Tang, Y., Elzinga, E. J., Lee, Y. J., & Reeder, R. J. (2007). Coprecipitation of chromate with calcite: batch experiments and X-ray absorption spectroscopy. *Geochim. Cosmochim. Acta*, **71**, 1480–1493, doi:10.1016/j.gca.2006.12.010.

Tankéré, S. P. C., Muller, F. L. L., Burton, J. D., Statham, P. J., Guieu, C., & Martin, J. M. (2001). Trace metal distributions in shelf waters of the northwestern Black Sea. *Cont. Shelf Res.* **21**, 1501–1532.

Tesoriero, A. J., & Pankow, J. F. (1996). Solid solution partitioning of Sr^{2+}, Ba^{2+}, and Cd^{2+} to calcite. *Geochim. Cosmochim. Acta*, **60**(6), 1053-1063.

Tessin, A., Chappaz, A., Hendy, I., & Sheldon, N. (2019). Molybdenum speciation as a paleo-redox proxy: A case study from Late Cretaceous Western Interior Seaway black shales. *Geology*, **47**, 59–62, doi:10.1130/G45785.1.

Thébault, J. Chauvaud, L. L'Helguen, S., Clavier, J., Barats, A., et al. (2009). Barium and molybdenum records in bivalve shells: Geochemical proxies for phytoplankton dynamics in coastal environments? *Limnol. Oceanogr.*, **54**(3), 1002-1014, doi:10.4319/lo.2009.54.3.1002.

Thibon, F., Blichert-Toft, J., Albarede, F., Foden, J., & Tsikos, H. (2019). A critical evaluation of copper isotopes in Precambrian Iron Formations as a paleoceanographic proxy. *Geochim. Cosmochim. Acta*, *264*, 130-140.

Thompson, C. M., & Ellwood, M. J. (2014). Dissolved copper isotope biogeochemistry in the Tasman Sea, SW Pacific Ocean. *Mar. Chem.* **165**, 1–9.

Torres, M. E., Brumsack, H. J., Bohrmann, G., & Emeis, K. C. (1996). Barite fronts in continental margin sediments: a new look at barium remobilization in the zone of sulfate reduction and formation of heavy barites in diagenetic fronts. *Chem. Geol.*, **127**(1-3), 125-139.

Tossell, J. A. (2005). Calculating the partitioning of the isotopes of Mo between oxidic and sulfidic species in aqueous solution. *Geochim. Cosmochim. Acta*, **69**, 2981–2993, doi:10.1016/j.gca.2005.01.016.

Tribovillard, N., Algeo, T. J., Lyons, T., & Riboulleau, A. (2006). Trace metals as paleoredox and paleoproductivity proxies: an update. *Chem. Geol.*, **232**(1-2), 12-32.

Turekian, K. K. (1968). Deep-sea deposition of barium, cobalt and silver. *Geochim. Cosmochim. Acta*, **32**(6), 603-612.

Turner, D. R., Whitfield, M., & Dickson, A. G. (1981). The equilibrium speciation of dissolved components in freshwater and sea water at 25°C and 1 atm pressure. *Geochim. Cosmochim. Acta*, **45**, 855–881.

Twining, B. S., & Baines, S. B. (2013). The trace metal composition of marine phytoplankton. *Annual Review of Marine Science*, **5**, 191-215.

Twining, B. S., Baines, S. B., & Fisher, N. S. (2004) Element stoichiometries of individual plankton cells collected during the Southern Ocean Iron Experiment (SOFeX). *Limnol. Oceanogr.,* **49**, 2115–2128.

Twining, B. S., Baines, S. B., Vogt, S., & Nelson, D. M. (2012) Role of diatoms in nickel biogeochemistry in the ocean. *Glob. Biogeochem. Cycles*, **26** (4), GB4001, doi:10.1029/2011GB004233.

Twining, B. S., Nodder, S. D., King, A. L., Hutchins, D. A., LeCleir, G. R., DeBruyn, J. M., Maas, E. W., Vogt, S., Wilhelm S. W.,. & Boyd, P. W. (2014). Differential remineralization of major and trace elements in sinking diatoms. *Limnol. Oceanogr.*, **59**(3), 689-704.

Urban Jr., E. R., Bowie, A. R., Boyd, P. W., Buck, K. N., Lohan, M. C., Sander, S. G., Schlitzer, R., Tagliabue, A. & Turner, D. (2020). The Importance of Bottom-Up Approaches to International Cooperation in Ocean Science. *Oceanography*. **33**(1), 11-15.

van der Weijden, C. H., & Reith, M. (1982). Chromium(III) - chromium(VI) interconversions in seawater. *Mar. Chem.*, **11**(6), 565-572.

van Geen, A., Luoma, S. N., Fuller, C. C., Anima, R., Clifton, H. E., & Trumbore, S. (1992). Evidence from Cd/Ca ratios in foraminifera for greater upwelling off California 4,000 years ago. *Nature*, **358**(6381), 54.

van Geen, A., McCorkle, D. C., & Klinkhammer, G. P. (1995). Sensitivity of the phosphate-cadmium-carbon isotope relation in the ocean to cadmium removal by suboxic sediments. *Paleoceanography*, **10**(2), 159-169.

van Helmond, N. A. G. M., Jilbert, T., & Slomp, C. P. (2018). Hypoxia in the Holocene Baltic Sea: Comparing modern versus past intervals using sedimentary trace metals. *Chem. Geol.*, **493**, 478-490, doi:10.1016/j.chemgeo.2018.06.028.

Vance, D., Archer, C., Bermin, J., Perkins, J., Statham, P. J., Lohan, M. C., Ellwood, M. J., & Mills, R. A. (2008). The copper isotope geochemistry of rivers and the oceans. *Earth Planet. Sci. Lett.* **274**, 204–213.

Vance, D., Little, S. H., Archer, C., Cameron, V., Andersen, M. B., Rijkenberg, M. J. A., & Lyons, T. W. (2016). The oceanic budgets of nickel and zinc isotopes: the importance of sulfidic environments as illustrated by the Black Sea. *Philos. Trans. R. Soc. A Math. Phys. Eng. Sci.* **374**, 20150294.

Vance, D., Little, S. H., de Souza, G. F., Khatiwala, S., Lohan, M. C., & Middag, R. (2017). Silicon and zinc biogeochemical cycles coupled through the Southern Ocean. *Nat. Geosci.*, **10**, 202–206.

Vance, D., de Souza, G. F., Zhao, Y., Cullen, J. T., & Lohan, M. C. (2019). The relationship between zinc, its isotopes, and the major nutrients in the North-East Pacific. *Earth Planet. Sci. Lett.*, **525**, doi:10.1016/j.epsl.2019.115748.

Velasquez, I. B., Ibisanmi, E., Maas, E. W., Boyd, P. W., Nodder, S., & Sander, S. G. (2016). Ferrioxamine Siderophores Detected amongst Iron Binding Ligands Produced during the Remineralization of Marine Particles. *Front. Mar. Sci.* **3**, 172. https://doi.org/10.3389/fmars.2016.00172.

Vihtakari, M., Ambrose Jr., W. G., Renaud, P. E., Locke V, W. L., Carroll, M. L., et al. (2017). A key to the past? Element ratios as environmental proxies in two Arctic bivalves. *Palaeogeogr. Palaeoclimatol. Palaeoecol.*, **465**, 316-332, doi:10.1016/j.palaeo.2016.10.020.

Voegelin, A. R., Nägler, T. F., Samankassou, E., & Villa, I. M. (2009). Molybdenum isotopic composition of modern and Carboniferous carbonates. *Chem. Geol.*, **265**, 488-498, doi:10.1016/j.chemgeo.2009.05.015.

Volk, T., & Hoffert, M. I. (1985). Ocean carbon pumps: Analysis of relative strengths and efficiencies in ocean-driven atmospheric CO_2 changes. *The carbon cycle and atmospheric* CO_2*: natural variations Archean to present*, **32**, 99-110.

Von Allmen, K., Böttcher, M. E., Samankassou, E., & Nägler, T. F. (2010). Barium isotope fractionation in the global barium cycle: First evidence from barium minerals and precipitation experiments. *Chem. Geol.*, **277**(1-2), 70-77.

Vorlicek, T. P., Chappaz, A., Groskreutz, L. M., Young, N., & Lyons, T. W. (2015). A new analytical approach to determining Mo and Re speciation in sulfidic waters. *Chem. Geol.*, **403**, 52–57, doi:10.1016/j.chemgeo.2015.03.003.

Vorlicek, T. P., Helz, G. R., Chappaz, A., Vue, P., Vezina, A., & Hunter, W. (2018). Molybdenum Burial Mechanism in Sulfidic Sediments: Iron-Sulfide Pathway. *ACS Earth and Space Chemistry*, **2**, 565–576, doi:10.1021/acsearthspacechem.8b00016.

Waeles, M., Baker, A. R., Jickells, T., & Hoogewerff, J. (2007). Global dust teleconnections: aerosol iron solubility and stable isotope composition. *Environmental Chemistry*, **4**(4), 233-237.

Wagner, M. E. (2013). *Silver as a novel tracer for Late Quaternary Southern Ocean biological and geophysical processes*. PhD thesis, University of Michigan, 189p.

Wagner, M., Hendy, I. L., McKay, J. L., & Pedersen, T.F. (2013). Influence of biological productivity on silver and redox-sensitive trace metal accumulation in Southern Ocean surface sediments, Pacific sector. *Earth Planet. Sci. Lett.*, **380**, 31-40.

Wagner, M., Chappaz, A., & Lyons, T.W. (2017). Molybdenum speciation and burial pathway in weakly sulfidic environments: Insights from XAFS. *Geochim. Cosmochim. Acta*, **206**, 18–29, doi:10.1016/j.gca.2017.02.018.

Waldron, K. J., & Robinson, N. J. (2009). How do bacterial cells ensure that metalloproteins get the correct metal? *Nature Reviews Microbiology*, **7**(1), 25.

Walker, J. C. (1983). Possible limits on the composition of the Archaean ocean. *Nature*, **302**(5908), 518-520.

Wang, W. X., Griscom, S. B., & Fisher, N. S. (1997). Bioavailability of Cr(III) and Cr(VI) to Marine Mussels from Solute and Particulate Pathways. *Environ. Sci. Technol.*, **31**(2), 603-611.

Wang, D., Xia, W., Lu, S., Wang, G., Liu, Q., Moore, W. S., and Arthur Chen, C. T. (2016). The nonconservative property of dissolved molybdenum in the western Taiwan Strait: Relevance of submarine groundwater discharges and biological utilization. *Geochemistry, Geophysics, Geosystems*, **17**, 28–43, doi:10.1002/2014GC005708.

Wang, R. M., Archer, C., Bowie, A. R., & Vance, D. (2019a). Zinc and nickel isotopes in seawater from the Indian Sector of the Southern Ocean: The impact of natural iron fertilization versus Southern Ocean hydrography and biogeochemistry. *Chem. Geol.*, **511**, 452-464.

Wang, Z., Li, J., Wei, G., Deng, W., Chen, X., Zeng, T., Wang, X., Ma, J., Zhang, L., Tu, X., Wang, Q., & McCulloch, M. (2019b). Biologically controlled Mo isotope fractionation in coral reef systems. *Geochim. Cosmochim. Acta*, **262**, 128-142, doi:10.1016/j.gca.2019.07.037.

Wang, S.-J., Rudnick, R. L., Gaschnig, R. M., Wang, H., & Wasylenki, L. E. (2019c). Methanogenesis sustained by sulfide weathering during the Great Oxidation Event. *Nat. Geosci.*, **12**, 296-300, doi:10.1038/s41561-019-0320-z.

Wang, C., Reinhard, C. T., Rybacki, K. S., Hardisty, D. S., Ossa, F. O., Wang, X., Hofmann, A., Asael, D., Robbins, L. J., Zhang, L., & Planavsky, N. J. (2021). Chromium isotope systematics and the diagenesis of marine carbonates. *Earth Planet. Sci. Lett.*, **562**, 116824, doi:10.1016/j.epsl.2021.116824.

Wanner, C., & Sonnenthal, E. L. (2013). Assessing the control on the effective kinetic Cr isotope fractionation factor: A reactive transport modeling approach. *Chem. Geol.*, **337-338**, 88-98. doi:10.1016/j.chemgeo.2012.11.008.

Wasylenki, L. E., Anbar, A. D., Liermann, L. J., Mathur, R., Gordon, G. W., & Brantley, S. L. (2007). Isotope fractionation during microbial metal uptake measured by MC-ICP-MS. *J. Anal. At. Spectrom.*, **22**, 905-910, doi:10.1039/b705476a.

Wasylenki, L. E., Rolfe, B. A., Weeks, C. L., Spiro, T. G., and Anbar, A. D. (2008). Experimental investigation of the effects of temperature and ionic strength on Mo isotope fractionation during adsorption to manganese oxides. *Geochim. Cosmochim. Acta*, **72**, 5997–6005, doi:10.1016/j.gca.2008.08.027.

Wasylenki, L. E., Swihart, J. W., & Romaniello, S. J. (2014). Cadmium isotope fractionation during adsorption to Mn oxyhydroxide at low and high ionic strength. *Geochim. Cosmochim. Acta*, **140**, 212-226.

Weber, T., John, S. G., Tagliabue, A., & DeVries, T. (2018). Biological uptake and reversible scavenging of zinc in the global ocean. *Science*, **361**, 72–76.

Wefing, A. M., Arps, J., Blaser, P., Wienberg, C., Hebbeln, D., & Frank, N. (2017). High precision U-series dating of scleractinian cold-water corals using an automated chromatographic U and Th extraction. *Chem. Geol.*, **475**, 140-148.

Wei, W., & Algeo, T. J. (2020). Secular variation in the elemental composition of marine shales since 840 Ma: Tectonic and seawater influences. *Geochim. Cosmochim. Acta*, **287**, 367-390.

Wei, W., Frei, R., Chen, T., Klaebe, R. Wei, G., Li, D., & Ling, H. (2020). Marine ferromaaganese oxide: a potentially important sink of light chromium isotopes? *Chem. Geol.*, **495**, 90-103, doi:10.1016/j.chemgeo.2018.08.006.

Wei, W., Klaebe, R. Ling, H. F., Huang, F., & Frei, R. (2020). Biogeochemical cycle of chromium isotopes at the modern Earth's surface and its applications as a paleo-environment proxy. *Chem. Geol.*, **541**, 119570, doi:10.1016/j.chemgeo.2020.119570.

Welch, S. A., Beard, B. L., Johnson, C. M., & Braterman, P. S. (2003). Kinetic and equilibrium Fe isotope fractionation between aqueous Fe(II) and Fe(III). *Geochim. Cosmochim. Acta*, **67**, 4231-4250. https://doi.org/10.1016/S0016-7037(03)00266-7.

Wichard, T., Mishra, B., Myneni, S. C. B., Bellenger, J. P., & Kraepiel, A. M. L. (2009). Storage and bioavailability of molybdenum in soils increased by organic matter complexation. *Nat. Geosci.*, **2**, 625–630, doi:10.1038/ngeo589.

Willbold, M., & Elliott, T. (2017). Molybdenum isotope variations in magmatic rocks. *Chem. Geol.*, **449**, 253-268.

Winckler, G., Anderson, R. F., Jaccard, S. L., & Marcantonio, F. (2016). Ocean dynamics, not dust, have controlled equatorial Pacific productivity over the past 500,000 years. *Proceedings of the National Academy of Sciences*, **113**(22), 6119-6124.

Wolgemuth, K., & Broecker, W. S. (1970). Barium in sea water. *Earth Planet. Sci. Lett.*, **8**(5), 372-378.

Wong, P. T. S., & Trevors J. T. (1988). Chromium toxicity to algae and bacteria. In *Chromium in the Natural and Human Environments* (eds. O. J. Nriagru and E. Nieboer). John Wiley and Sons, New York, pp. 305–315.

Woodland, S. J., Rehkämper, M., Halliday, A. N., Lee, D.-C., Hatterndorf, B., & Günther, D. (2005) Accurate measurement of silver isotopic compositions in geological materials including lowPd/Ag meteorites. *Geochim. Cosmochim. Acta*, **69**(8). doi:10.1016/j.gca.2004.10.012.

Wuttig, K., Townsend, A. T., van der Merwe, P., Gault-Ringold, M., Holmes, T., Schallenberg, C., Latour, P., Tonnard, M., Rijkenberg, M. J. A., Lannuzel, D., & Bowie, A. R. (2019). Critical evaluation of a seaFAST system for the analysis of trace metals in marine samples. *Talanta*, **197**, 653-668.

Xiao, H., Deng, W., Wei, G., Chen, J., Zheng, X., Shi, T., Chen, X., Wang, C., Liu, X., Zeng, T., 2020. A pilot study on zinc isotopic compositions in shallow water coral skeletons. *Geochem. Geophys.* **21**(11): e2020GC009430**.,** https://doi.org/10.1029/2020gc009430

Xie, R. C., Galer, S. J., Abouchami, W., Rijkenberg, M. J., De Baar, H. J., De Jong, J., & Andreae, M. O. (2017). Non-Rayleigh control of upper-ocean Cd isotope fractionation in the western South Atlantic. *Earth Planet. Sci. Lett.*, **471**, 94-103.

Xie, R. C., Galer, S. J. G., Abouchami, W., & Frank, M. (2019a) Limited impact of eolian and riveringe sources on the biogeochemical cycling of Cd in the tropical Atlantic. *Chem. Geol.* **511**, 371-379. https://doi.org/10.1016/j.chemgeo.2018.10.018.

Xie, R., C., Rehkämper, M., Grasse, P., van de Flierdt, T., Frank, M., & Xue, Z. (2019b). Isotopic evidence for complex biogeochemical cycling of Cd in the eastern tropical South Pacific. *Earth Planet. Sci. Lett.* **512**, 134-146. https://doi.org/10.1016/j.epsl.2019.02.001.

Xu, Y., Feng, L., Jeffrey, P. D., Shi, Y., & Morel, F. M. (2008). Structure and metal exchange in the cadmium carbonic anhydrase of marine diatoms. *Nature*, **452**(7183), 56.

Xue, Z., Rehkämper, M., Schönbächler, M., Statham, P. J., & Coles, B. J. (2012). A new methodology for precise cadmium isotope analyses of seawater. *Analytical and Bioanalytical Chemistry*, **402**(2), 883-893.

Xue, Z., Rehkämper, M., Horner, T. J., Abouchami, W., Middag, R., van de Flierd, T., & de Baar, H. J. (2013). Cadmium isotope variations in the Southern Ocean. *Earth Planet. Sci. Lett.*, **382**, 161-172.

Yang, S.-C., Lee, D.-L., & Ho, T.-Y. (2012). The isotopic composition of Cadmium in the water column of the South China Sea. *Geochim. Cosmochim. Acta*, **98**, 66-77. https://doi.org/10.1016/j.gca.2012.09.022.

Yang, S.-C., Lee, D.-L., Ho, T.-Y., Wen, L.-S., & Yang, H.-H. (2014). The isotopic composition of dissolved cadmium in the water column of the West Philippine Sea. *Front. Mar. Sci.* **1**(61). https://doi.org/10.3389/fmars.2014.00061

Yang, S.-C., Lee, D.-C., & Ho, T.-Y. (2015). Cd isotopic composition in the suspended and sinking particles of the surface water of the South China Sea: The effects of biotic activities. *Earth Planet. Sci. Lett.*, **428**, 63-72.

Yang, S.-C., Zhang, J., Sohrin, Y., & Ho, T.-Y. (2018). Cadmium cycling in the water column of the Kuroshio-Oyashio Extension region: Insights from dissolved and particulate isotopic composition. *Geochim. Cosmochim. Acta*, **233**, 66-80.

Yang, S.-C., Hawco, N. J., Pinedo-González, P., Bian, X., Huang, K.-F., & John, S. G. (2020). A new purification method for Ni and Cu stable isotopes in seawater provides evidence for widespread Ni isotope fractionation by phytoplankton in the North Pacific. *Chem. Geol.* **547**, 119662. https://doi.org/10.1016/j.chemgeo.2020.119662.

Yang, T., Chen, Y. Zhou, S., & Li, H. (2019). Impacts of aerosol copper on marine phytoplankton: A review. *Atmosphere*, **10**(7), 414, doi:10.3390/atmos10070414.

Yee, D., & Morel, F. M. M. (1996). In vivo substitution in carbonic of zinc by cobalt of a marine anhydrase diatom. *Limnol. Oceanogr.*, **41**, 573–577.

Zhang, R., John, S. G., Zhang, J., Ren, J., Wu, y., Zhu, Z., Liu, S., Zhu, X., Marsay, C. M., & Wenger, F. (2015). Transport and reaction of iron and iron stable isotopes in glacial meltwaters on Svalbard near Kongsfjorden: From rivers to estuary to ocean. *Earth Planet. Sci. Lett.*, **424**, 201-211. https://doi.org/10.1016/j.epsl.2015.05.031.

Zhang, R., Jensen, L. T., Fitzsimmons, J. N., Sherrell, R. M., & John, S. (2019). Dissolved cadmium and cadmium stable isotopes in the western Arctic Ocean. *Geochim. Cosmochim. Acta*, **258**, 258-273, https://doi.org/10.1016/j.gca.2019.05.028.

Zhang, Y., Amakawa, H., & Nozaki, Y. (2001). Oceanic profiles of dissolved silver: precise measurements in the basins of western North Pacific, Sea of Okhotsk, and the Japan Sea. *Marine Chemistry*, **75**, 151-163.

Zhang, Y., Obata, H., & Nozaki, Y. (2004). Silver in the Pacific Ocean and the Bering Sea. *Geochemical Journal*, **38**, 623-633.

Zhao, Y., Vance, D., Abouchami, W., & de Baar, H. J. W. (2014). Biogeochemical cycling of zinc and its isotopes in the Southern Ocean. *Geochim. Cosmochim. Acta*, **125**, 653–672. http://dx.doi.org/10.1016/j.gca.2013.07.045.

Zhu, X. K., O'Nions, R. K., Guo, Y., & Reynolds, B. C. (2000). Secular variation of iron isotopes in North Atlantic deep water. *Science*, **287**(5460).

Zink, S., Schoenberg, R., & Staubwasser, M. (2010). Isotopic fractionation and reaction kinetics between Cr(III) and Cr(VI) in aqueous media. *Geochim. Cosmochim. Acta*, **74**, 5729-5745, doi:10.1016/j.gca.2010.07.015.

Zirino, A., & Yamamoto, S. (1972). A pH-dependent model for the chemical speciation of copper, zinc, cadmium, and lead in seawater. *Limnol. Oceanogr.* **17**, 661–671.